AD_____

AWARD NUMBER: W81XWH-05-1-0470

TITLE: Genomic Instability and Breast Cancer

PRINCIPAL INVESTIGATOR: Junjie Chen, Ph.D.

CONTRACTING ORGANIZATION: Yale University
New Haven, CT 06520

REPORT DATE: October 2009

TYPE OF REPORT: Annual

PREPARED FOR: U.S. Army Medical Research and Materiel Command
Fort Detrick, Maryland 21702-5012

REPORT DOCUMENTATION PAGE

Form Approved
OMB No. 0704-0188

1. REPORT DATE	2. REPORT TYPE	3. DATES COVERED
1 October 2009	Annual	5 Sep 2008 – 4 Sep 2009

4. TITLE AND SUBTITLE

Genomic Instability and Breast Cancer

5a. CONTRACT NUMBER

5b. GRANT NUMBER
W81XWH-05-1-0470

5c. PROGRAM ELEMENT NUMBER

6. AUTHOR(S)

Junjie Chen, Ph.D.

E-Mail: jchen8@mdanderson.org

5d. PROJECT NUMBER

5e. TASK NUMBER

5f. WORK UNIT NUMBER

7. PERFORMING ORGANIZATION NAME(S) AND ADDRESS(ES)

Yale University
New Haven, CT 06520

8. PERFORMING ORGANIZATION REPORT NUMBER

9. SPONSORING / MONITORING AGENCY NAME(S) AND ADDRESS(ES)
U.S. Army Medical Research and Materiel Command
Fort Detrick, Maryland 21702-5012

10. SPONSOR/MONITOR'S ACRONYM(S)

11. SPONSOR/MONITOR'S REPORT NUMBER(S)

12. DISTRIBUTION / AVAILABILITY STATEMENT
Approved for Public Release; Distribution Unlimited

13. SUPPLEMENTARY NOTES

14. ABSTRACT

We are investigating the regulation of genomic stability and how the disruption of such regulation contributes to breast cancer development. We have performed in-depth studies of BRCA1 and the DNA damage response, which allow us to propose a new model of DNA damage signaling pathways and how it functions to ensure genomic stability in response to DNA damage. In addition, we are continuing our purification of protein complexes for the study of cell cycle and DNA damage networks involved in breast cancer development. We have identified several new components involved in DNA damage repair or mitotic progression. While some of these studies are still ongoing, we have already made several exciting findings and published some of them recently. We hope that these studies will help us to understand breast cancer etiology and discover new targets for cancer treatment.

15. SUBJECT TERMS
Tumor suppressor, Oncology, Cell signaling, DNA repair, cell biology

16. SECURITY CLASSIFICATION OF:			17. LIMITATION OF ABSTRACT	18. NUMBER OF PAGES	19a. NAME OF RESPONSIBLE PERSON
a. REPORT	b. ABSTRACT	c. THIS PAGE			USAMRMC
U	U	U	UU	124	19b. TELEPHONE NUMBER *(include area code)*

Standard Form 298 (Rev. 8-98)
Prescribed by ANSI Std. Z39.18

Table of Contents

Introduction:

Our genetic material is continuously challenged by genotoxic stress. DNA damage can arise during normal cellular metabolic processes such as DNA replication, from endogenous sources like free radicals, or from exogenous agents such as UV light and ionizing radiation. To ensure genome stability, the cell has evolved the ability to sense DNA damage, activate cell cycle checkpoint and initiate DNA repair. Failure to properly repair damaged DNA contributes to tumorigenesis. Similarly, improper or unable to activate mitotic checkpoints also leads to chromosomal instability and increased neoplastic transformation. The importance of cell cycle checkpoint control in tumorigenesis is exemplified by numerous cancer-predisposing clinical syndromes that are attributed to mutations in components involved in these cellular processes that prevent genomic instability. The main interest of my research program is to understand the signaling networks that govern genomic integrity in humans and how the dysregulation of these pathways result in tumorigenesis.

Body:

The specific Aims are:

Specific Aim 1: Develop biomarkers for early detection of breast cancers.

The objective of this specific aim is to understand early genetic alternations that would eventually lead to the development of malignant breast cancers.

We are continuing our studies of DNA damage response (DDR) pathways. Activation of DDR has recently been proposed to be a general protective mechanism during early tumorigenesis, and that inactivating mutations of this anti-cancer barrier correlate with genome instability and tumor progression (Bartkova et al., 2005; Gorgoulis et al., 2005). In the last two to three years, we and others in the field have elucidated a DNA damage signal transduction cascade that initiates from H2AX phosphorylation, relays to an ubiquitination-dependent signaling pathway that involves two E3 ubiquitin ligases RNF8 and RNF168, which eventually results in the stable accumulation of BRCA1 and 53BP1 at DNA damage sites (Doil et al., 2009; Huen et al., 2007; Kolas et al., 2007; Mailand et al., 2007; Stewart et al., 2009; Wang and Elledge, 2007).

We reasoned that this signaling cascade is likely to regulate the accumulation of many other DNA damage repair proteins besides BRCA1 and 53BP1. Indeed, we recently demonstrated that two other DNA damage repair proteins or protein complexes, PTIP/PA1 and RAD18, also localize to DNA damage foci in a manner that requires H2AX phosphorylation and the damage-induced ubiquitination-dependent signaling pathway. We showed that the proper localization of the PTIP/PA1 complex to DNA damage sites is important for cell survival following DNA damage (Gong et al., 2009). However, we do not yet know exactly how this protein complex is recruited to DNA damage sites via the damage-induced ubiquitin chains, since neither PTIP nor PA1 binds to ubiquitin *in vitro* or *in vivo*.

As for RAD18, we now understand precisely how it is recruited to DNA damage sites. RAD18 contains an UBZ domain (ubiquitin-binding zinc finger domain). We showed that RAD18 UBZ domain binds to ubiquitin *in vitro* and this UBZ domain is also required for the recruitment of RAD18 to sites of DNA double-strand breaks *in vivo*. While RAD18 is best known for its function in promoting PCNA mono-ubiquitination following UV radiation, we discovered that RAD18 also has a role in response to DNA double-strand breaks. In the later case, RAD18 serves as an adaptor protein, which mediates the recruitment of RAD51 paralogs to sites of DNA breaks and therefore facilitates homologous recombination repair. This study was recently published in Nature Cell Biology (Huang et al., 2009b).

Early studies from us and others have suggested that RAP80 and CCDC98/Abraxis are involved in the recruitment of BRCA1 via the above mentioned ubiquitination-dependent signaling pathway (Kim et al., 2007a; Kim et al., 2007b; Liu et al., 2007; Petrini, 2007; Sobhian et al., 2007; Wang et al., 2007). Recently, we and two other groups successfully isolated RAP80/CCDC98 complex and identified several additional components in this complex, BRE/BRCC45, BRCC36 and MERIT40/NBA1 (Feng et al., 2009; Shao et al., 2009; Wang et al., 2009). We showed that these five proteins form a stable complex. Each subunit in this complex is required for the stability of the whole complex and the proper localization of BRCA1 following DNA damage. We are currently studying the precise role of each component in this five-protein complex and how they may regulate BRCA1 activity and function following DNA damage.

Although the H2AX/MDC1/RNF8-dependent DNA damage signaling pathway is required for the stable accumulation of many DNA damage repair proteins as I summarized above, we also know for sometime that the depletion of these components only resulted in relatively milder phenotypes when compared to BRCA1 or 53BP1 depletion. These observations suggest the existence of a H2AX-indpendent pathway for the recruitment of BRCA1 and 53BP1 to DNA damage sites, which was also raised by a previous study (Celeste et al., 2003). We now know that this H2AX-independent pathway also functions in MDC1 or RNF8 deficient cells (**Figure 1**). Moreover, we demonstrated that this H2AX-independent pathway requires the Mre11/Rad50/Nbs1 complex (**Figure 2**).

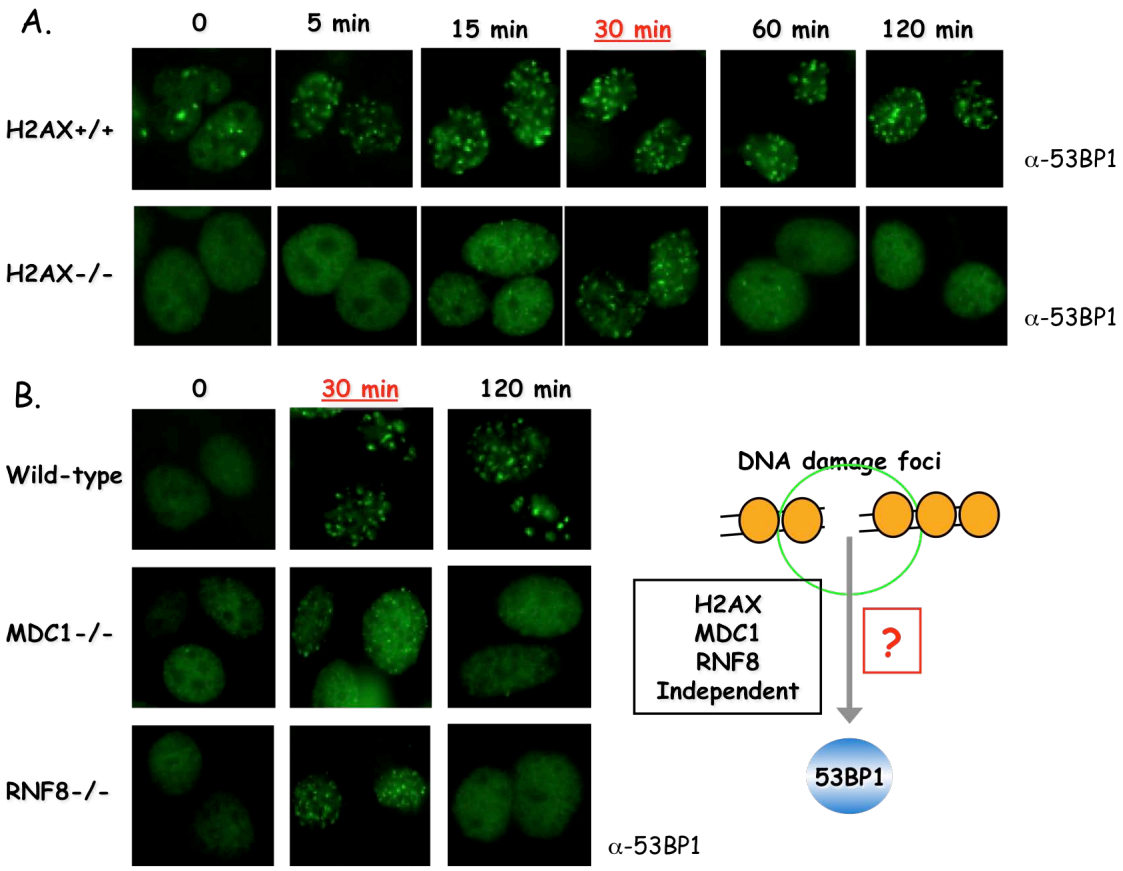

Figure 1. The initial recruitment of 53BP1 to sites of DNA double-strand breaks (DSBs) can occur independently of H2AX, MDC1 or RNF8. (**A**) 53BP1 transiently localizes to focus structure after IR treatment in H2AX-/- cells. H2AX+/+ and H2AX-/- were irradiated (3 Gy) and fixed at various time points after IR. Cells were immunostained with 53BP1 antibody (green). (**B**) Transient recruitment of 53BP1 upon DNA damage still occur in RNF8-/- and MDC1-/- MEFs.

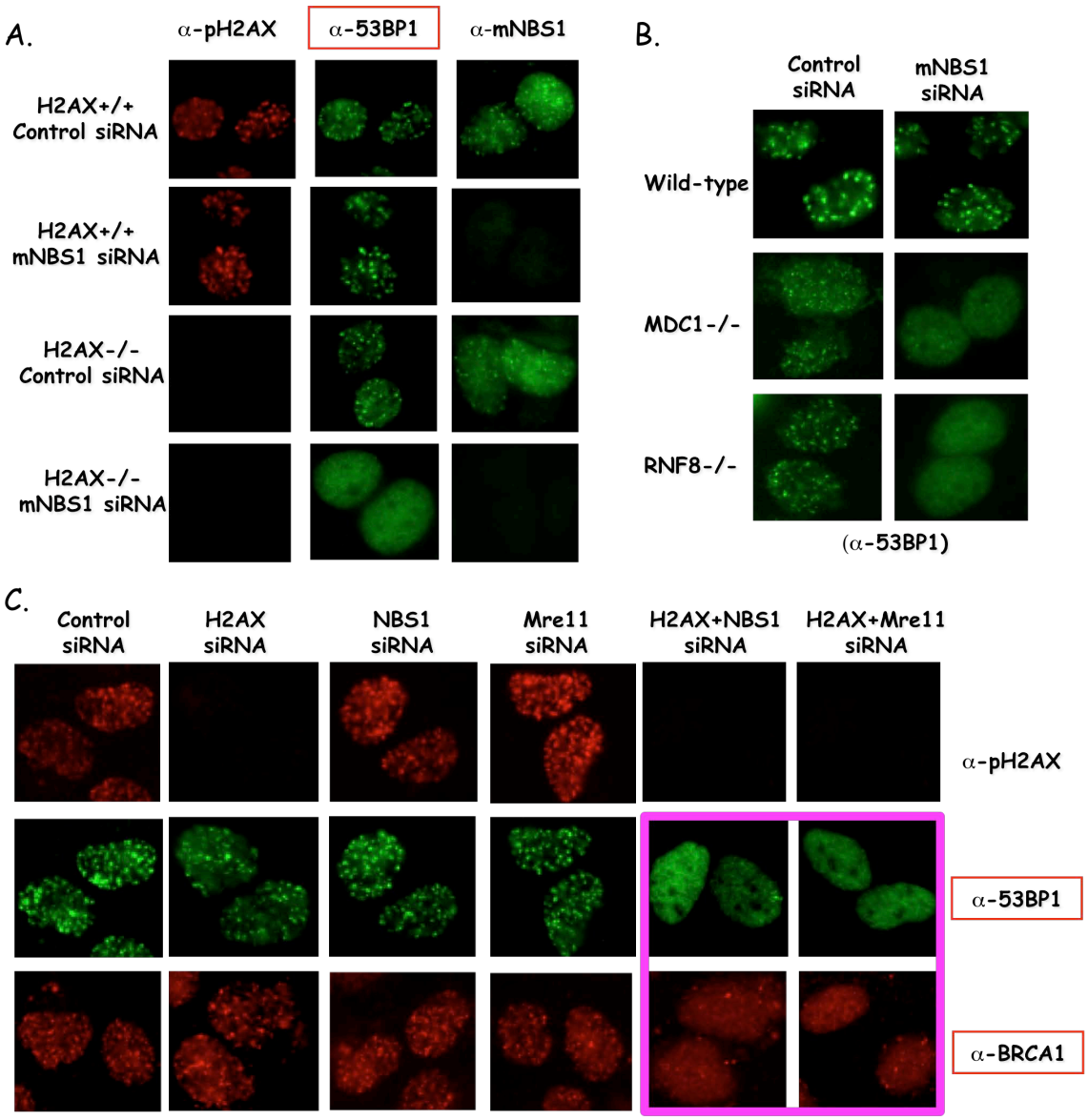

Figure 2. The MRN complex is responsible for the initial recruitment of repair and signaling proteins to sites of DNA double-strand breaks (DSBs). (**A**) The initial 53BP1 foci formation observed in H2AX-/- cells depends on NBS1. H2AX+/+ and H2AX-/- were transfected with control siRNA or siRNA specifically targeting mouse NBS1 (simNBS1). 72 hours later, cells were irradiated (3 Gy) and fixed at 30 minutes or 4 hours after IR. Immunostaining was carried out with anti-pH2AX, anti-53BP1 or anti-mouse NBS1 antibodies. (**B**) The transient recruitment of 53BP1 upon DNA damage was abolished by NBS1 depletion in RNF8-/- and MDC1-/- MEFs. Cells with or without siRNA transfection were irradiated and fixed 30 minutes after IR. (**C**) The initial focus localization of 53BP1 and BRCA1 requires MRN complex. Double depletion of H2AX and NBS1, or H2AX and MRE11 was performed in U2OS cells. Following siRNA transfection, cells were irradiated (5 Gy) and fixed 30 minutes later. Immunostaining was carried out using the indicated antibodies.

Based on these studies, we modified our working model of DNA damage signal transduction network and proposed that two independent pathways can occur simultaneously at the sites of DNA damage for the recruitment of additional DNA damage repair proteins to facilitate DNA damage checkpoint acivation and DNA repair (**Figure 3**).

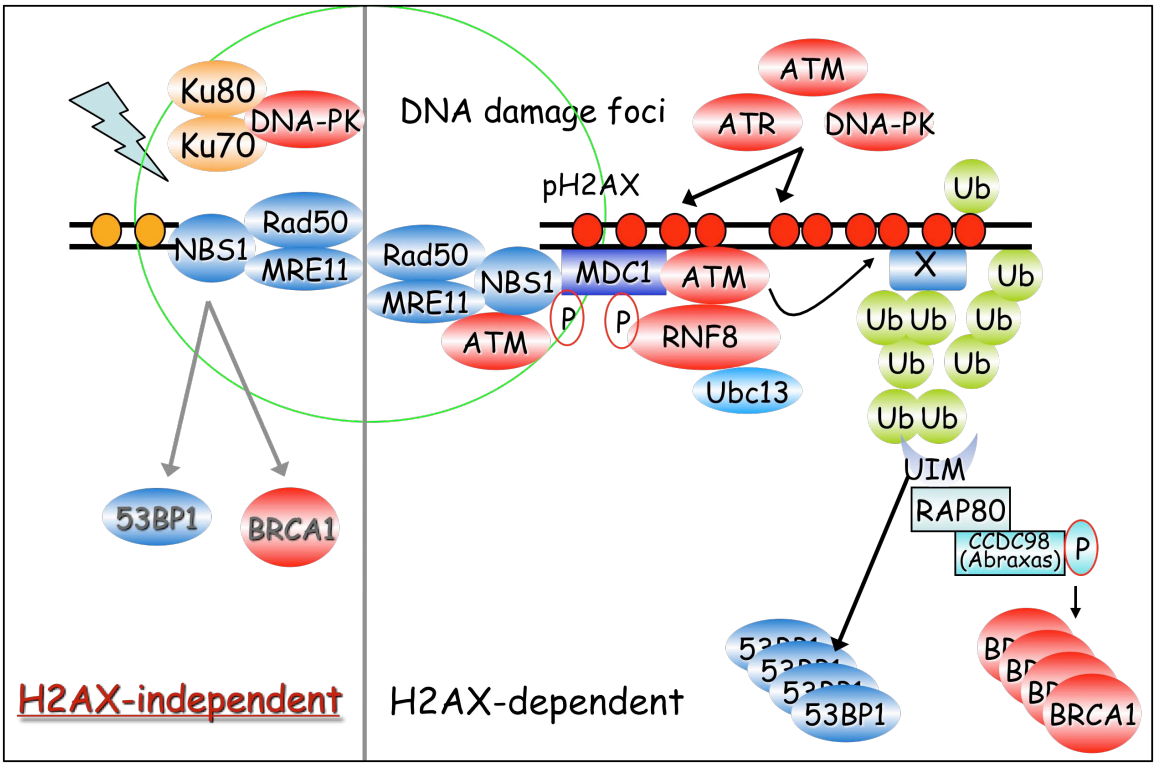

Figure 3. A proposed working model for the recruitment of DNA damage repair proteins at sites of DNA double-strand breaks.

In our previous annual report, we described the identification of PALB2 as the protein that bridges the BRCA1/BRCA2 interaction. I am glad to report here that the manuscript on this subject was recently published by PNAS (Sy et al., 2009b). We also expanded our analysis on PALB2. We showed that the N-terminus of PALB2 carries out multiple functions, e.g. association with BRCA1, association with chromatin and oligomerization. All of these functions are important for PALB2 function in promoting homologous recombination repair (Sy et al., 2009c). In addition, we identified a new PALB2-interacting protein as MRG15. We showed that this interaction is mediated by a conserved motif on PALB2. While the deletion of this conserved motif did not reduce the homologous recombination efficiency, it resulted in an increase of sister chromatin exchange (SCE), suggesting that PALB2 not only regulate the efficiency of HR repair, but also dictate the template usage during HR repair (Sy et al., 2009a). This series of studies highlighted the critical role of PALB2 in directing homologous recombination repair, which we will further investigate.

We previously described the establishment of a tandem affinity protocol for the purification of protein complexes in mammalian cells. We proposed to focus on a group of proteins involved in cell cycle regulation and/or DNA damage response to gain a better understanding of the DDR pathways in mammalian cells. Besides the above studies, we also successfully identified two new hSSB-containing heterotrimeric complexes. Replication protein A (RPA) is a heterotrimeric protein complex that has long been suggested to be the major single-strand DNA binding protein in high eukaryotes. Indeed, RPA is essential for all cellular functions that involve single-strand DNA. These include DNA replication, recombination and repair. However, a recent study reported the identification of a new human single-strand DNA binding protein, hSSB1 (Richard et al., 2008). Unlike RPA, hSSB1 is not required for DNA replication, but it seems that it has a specific function in DNA repair (Richard et al., 2008). Using our tandem affinity purification approach, we were able to show that hSSB also forms heterotrimeric complexes *in vivo*, which we named as SOSS complexes (Sensor Of Single-Strand DNA). The SOSS complexes consist of human SSB homologs hSSB1/2 (SOSS-B1/2), INTS3 (SOSS-A) and a previously uncharacterized protein C9orf80 (SOSS-C). We have shown that SOSS-A serves as a central adaptor required not only for SOSS complex assembly and stability, but also for facilitating the accumulation of SOSS complex to DNA ends. Moreover, SOSS-depleted cells display increased ionizing radiation sensitivity, defective G2/M checkpoint, and impaired homologous recombination repair. Thus, our study defines a pathway involving the sensing of ssDNA by SOSS complex and suggests that these SOSS complexes are likely involved in the maintenance of genome stability (Huang et al., 2009a).

Specific Aim 2: Explore Chfr/Aurora pathway for breast cancer development and treatment.

Besides DNA damage responsive pathways, we also study mitotic progression especially how the dyregulation of proper mitotic control would lead to chromosomal instability and tumorigenesis. We have previously published that an E3 ligase Chfr is mitotic checkpoint protein that negatively regulates Aurora A expression *in vivo* (Yu et al., 2005). Since Chfr is an E3 ubiquitin ligase, we speculate that Chfr may regulate a number of substrates besides Aurora A. We reported last year that using the tandem affinity purification approach, we uncovered a new Chfr-associated protein Kid/Kif22. Kif22 is a chromokinesin that binds to both DNA and microtubules. We demonstrated that Kif22 is a novel substrate of Chfr. Chfr-mediated Kif22 downregulation is critical for early mitotic checkpoint control and the maintenance of chromosome stability. This study was published this year (Maddika et al., 2009). In addition, we are studying another Chfr-associated protein TOPK. TOPK is a mitotic specific kinase (Abe et al., 2007; Matsumoto et al., 2004). Just like Kif22, we showed that TOPK is also a substrate of Chfr (**Figure 4A**). TOPK levels reversely correlate with Chfr expression in cells (**Figure 4B**), suggesting that TOPK indeed is a bone fide *in vivo* substrate of Chfr. We are currently studying the functional significance of TOPK overexpression in Chfr deficient cells. We believe that these studies will allow us to understand how Chfr may control the expression of multiple mitotic regulators and thus ensure genome integrity especially during mitotic transitions.

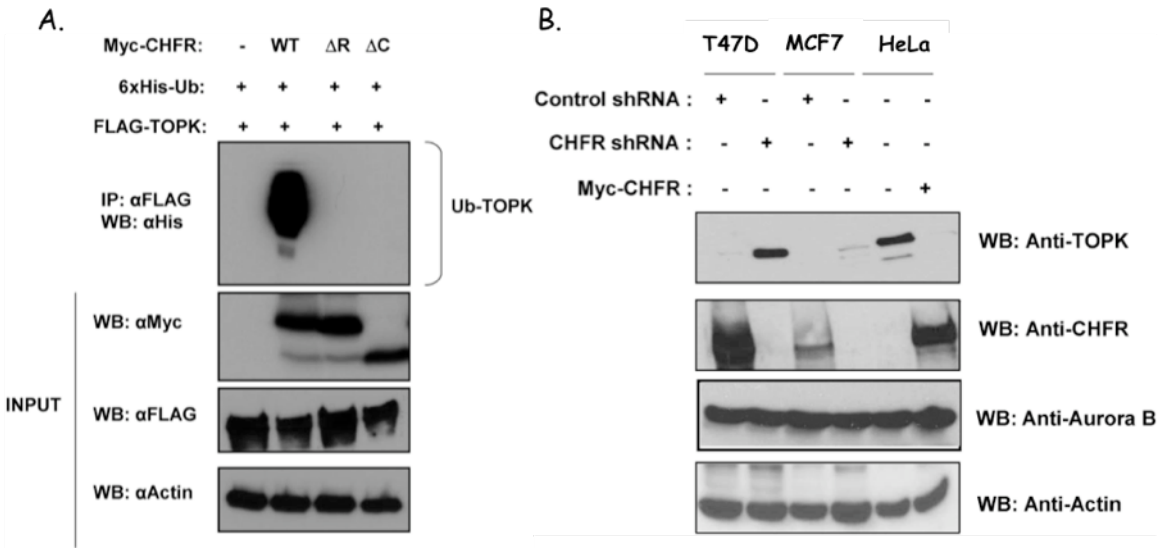

Figure 4. Chfr ubiquitinates TOPK and promotes its degradation. (**A**) Myc-tagged full-length, ΔRING or ΔCys-rich domain mutants of Chfr were expressed in HeLa cells along with Flag-TOPK and His-Ub. The levels of TOPK ubiquitination were evaluated by anti-His immunoblotting following immunoprecipitation of TOPK. (**B**) T47D and MCF7 cells were stably transfected with either control shRNA or Chfr shRNA. The control HeLa cells lacking endogenous Chfr expression were stably transfected with plasmids encoding Myc-Chfr. Protein levels of TOPK, Chfr, Aurora B and Actin were detected by immunoblotting with their respective antibodies.

Specific Aim 3: Identify novel druggable targets for the development of anti-cancer agents.

As we reported last year, we would like to establish a large panel of tagged protein kinases purified from human cells for *in vivo* and *in vitro* studies. These reagents will not only help our studies of kinase functions *in vivo*, but also provide essential tools for developing and validating any specific kinase inhibitors in the future. One of the exciting projects we developed during this endeavor is the demonstration that a protein kinase DYRK2 has an unexpected role as a molecular assembler of an E3-ubiquitin ligase complex. We showed that DYRK2 is not only involved in the formation of this E3 ligase complex, its kinase activity is required for the phosphorylation and subsequent degradation of its downstream substrate, Katanin p60. This interesting story, which underscores a novel function of protein kinases, was recently published by Nature Cell Biology (Maddika and Chen, 2009).

We are continuing these studies of protein kinases. Because of our recently developed interests in protein ubiquitination, we have also included some E3 ligases and deubiquitinating enzymes in our analyses. Interesting, while we are studying the JAMM domain-containing deubiquitinating enzymes BRCC36, which is involved in BRCA1 regulation, we found that a portion of this protein localized to cytoplasm (data not shown). Further tandem affinity purification revealed the existence of two BRCC36 containing complexes (**Figure 5A**). One is the nuclear complex that contains RAP80, CCDC98/Abraxas, BRCC45/BRE and MERIT40/NBA1 (Feng et al., 2009; Shao et al.,

2009; Wang et al., 2009). The cytoplasmic complex also contains BRCC45/BRE and MERIT40/NBA1, however it includes a new component Kiaa0157 (**Figure 5B** and data not shown), a protein that shares significant similarity with CCDC98/Abraxas. Interestingly, we also identified several HECT domain-containing proteins including ITCH, WWP1 and WWP2 in the cytoplasmic BRCC36 complex. These HECT domain E3 ligases associate specifically with a PY motif on Kiaa0157, but they do not bind to CCDC98 (**Figure** 5C and data not shown).

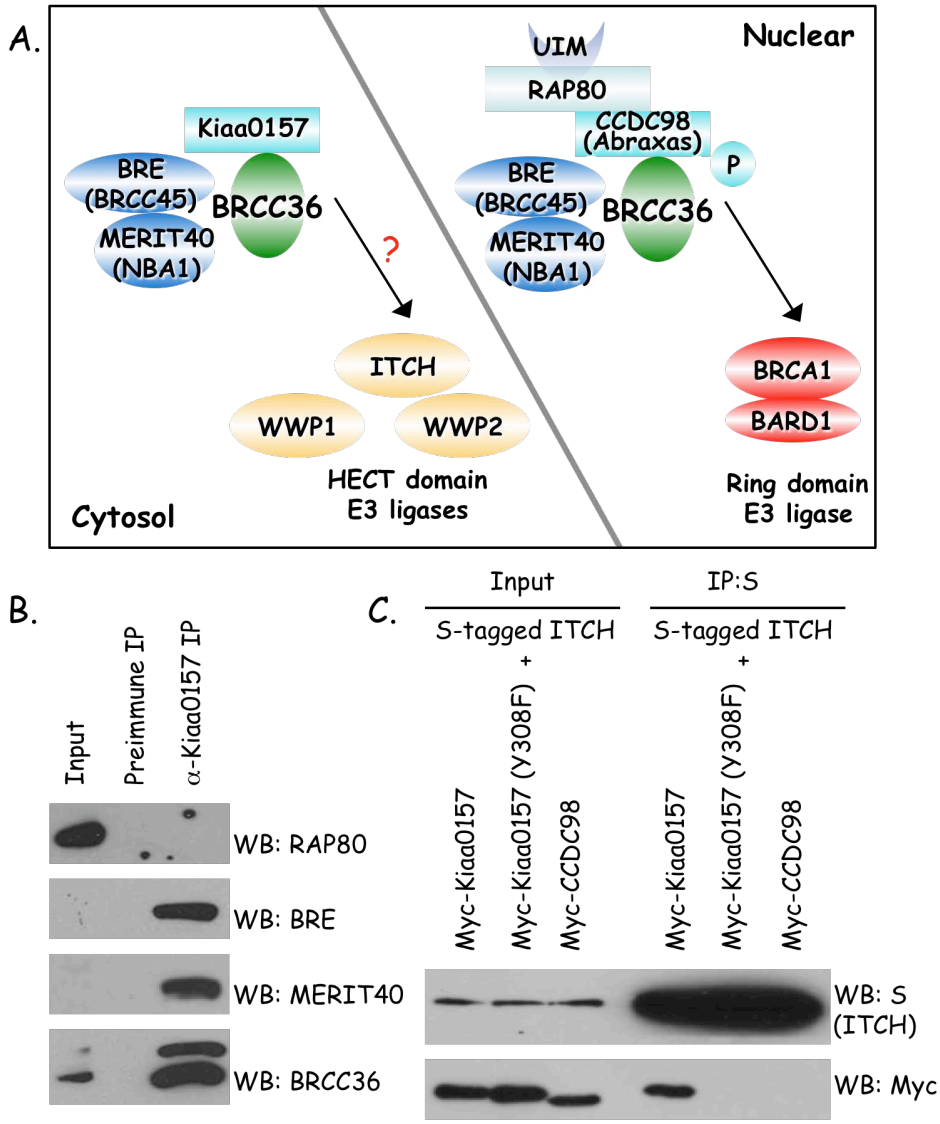

Figure 5. (**A**) A model of two BRCC36-containing complexes and their potential functions *in vivo*. (**B**) Kiaa0157 associates with BRE, MERIT40 and BRCC36, but not RAP80. Extracts were immunoprecipitated using control or anti-Kiaa0157 antibodies and immunoblotted with antibodies as indicated. (**C**) A PY motif within Kiaa0157 is specifically required for its interaction with ITCH. Myc-tagged CCDC98, Kiaa0157 were expressed along with S-tagged ITCH. S beads pull down were immunoblotted with anti-S or anti-Myc antibodies.

Since the HECT domain E3 ligases exist in sub-stoichiometric amount in the cytoplasmic BRCC36 complex, we reasoned that the four proteins BRCC36, Kiaa0157, BRCC45/BRE, MERIT40/NBA1 form a stable core complex in cytosol. This complex may interact with these HECT domain proteins and regulate their activities or functions, in a manner similar to the regulation of BRCA1 by the nuclear BRCC36-containing complex. The analyses of these protein complexes are ongoing in my laboratory.

Training potential for the PI:

This training award allows us to carry out research with great flexibility. While we are and will continue to conduct mechanism-based studies of individual proteins and pathways, we have initiated several large-scale studies. These studies have already provided new insight and information for the understanding of breast cancer etiology and treatment.

This award also gives me the flexibility to train junior scientists and permit them to develop their own careers in a number of breast cancer research fields. Over the past four years, I have successfully trained six junior faculty, who left my laboratory and established their own research teams in the United States (Drs. Zhenkou Lou and Xiaochun Yu), Korea (Drs. Hongtae Kim and Ja-Eun Kim), HongKong (Dr. Michael Huen) and India (Dr. Reddy Maddika). While all of them are continuing breast cancer related projects, their research topics range from DNA damage response, mitotic regulation, SIRT1 function to critical cell survival kinases. This diversity gives them a chance to further develop their own research program and contribute to various aspects of breast cancer research.

Key Research Accomplishments:

- We have shown that the H2AX/MDC1/RNF8-dependent DNA damage-signaling cascade not only is required for BRCA1 and 53BP1 localization following DNA damage, but also plays an important role in the regulation of PTIP/PA1 and RAD18 focus formation following DNA damage. Collectively, these studies suggest that the same signaling pathway is involved in the recruitment of multiple downstream DNA damage checkpoint and repair proteins and thus contribute to the overall cellular DNA damage response.

- We have identified a five-subunit protein complex that is involved in the localization of BRCA1 following DNA damage. This complex contains two previously identified subunits, but also includes three new subunits. We are further studying the functional importance of these subunits in BRCA1 regulation and/or other cellular processes.

- We are very excited about the discovery of a H2AX-independent mechanism that is required for the localization of DNA damage repair proteins at DSB sites. We showed that this pathway involves the Mre11/Rad50/Nbs1 complex and thus underline a new function of the MRN complex in DNA damage response.

-Our studies on PALB2 allowed us to identify its critical functions in mediating BRCA1/BRCA2 interaction and promoting efficient homologous recombination repair. In addition, our detailed analysis of PALB2 also revealed a new function for PALB2, namely in dictating the choice of template usage during HR repair.

- We are making progress in our purification of protein complexes involved in cell cycle regulation and DNA damage repair. We have successfully identified new ssDNA-binding protein complexes, which we believe will yield significant insights into the regulation of DNA damage repair in the near future.

- We have finished and published the functional analysis of a new Chfr substrate Kif22/Kid. We have identified another Chfr substrate as TOPK. We will further study the role of TOPK overexpression in mitotic progression and chromosomal instability.

- We finished the DYRK2 study and showed that a new function for protein kinase as an adaptor protein required for the formation of E3 ubiquitin ligase complexes. We continue to develop a panel of cell lines that we can use to produce active enzymes for functional studies and also for future screening of anti-cancer inhibitors.

Reportable Outcomes:

Gong, Z., Cho, Y.W., Kim, J.E., Ge, K. and **Chen, J.** Accumulation of Pax2 transactivation domain interaction protein (PTIP) at sites of DNA breaks via RNF8-dependent pathway is required for cell survival after DNA damage. J Biol Chem. 284(11):7284-93, 2009.

Feng, L., Huang, J. and **Chen, J.** MERIT40 facilitates BRCA1 localization and DNA damage repair. Genes Dev. 23(6):719-28, 2009.

Maddika, S and **Chen, J.** Protein kinase DYRK2 is an E3-ligase specific molecular assembler. Nature Cell Biol., 11(4):409-19, 2009.

Maddika, S., Sy, S.M. and **Chen, J.** Functional interaction between Chfr and Kif22 controls genomic stability. J Biol Chem., 284(19):12998-3003, 2009.

Sy, S.M., Huen, M.S. and **Chen, J.** PALB2 is an integral component of the BRCA complex required for homologous recombination repair. Proc Natl Acad Sci U S A., 106(17):7155-60, 2009.

Huang, J., Huen, M.S., Kim, H., Leung, C.C., Glover, J.N., Yu, X. and **Chen, J.** RAD18 transmits DNA damage signalling to elicit homologous recombination repair. Nature Cell Biol. 11(5):592-603, 2009.

Sy, S.M., Huen, M.S., Zhu, Y. and **Chen, J.** PALB2 regulates recombinational repair through chromatin association and oligomerization. J. Biol. Chem. 284(27):18302-10, 2009.

Sy, S.M., Huen, M.S. and **Chen, J.** MRG15 Is a Novel PALB2-interacting Factor Involved in Homologous Recombination. J Biol Chem. 284(32):21127-31, 2009.

Huang, J., Gong, Z, Ghosal, G. and **Chen, J.** SOSS complexes participate in the maintenance of genomic stability. Mol Cell 35(3):384-93, 2009.

Conclusions:

We are conducting the experiments proposed in our application. We have already published many of our findings in leading biomedical journals. We anticipate that the continuation of this research effort will allow us to make new discoveries and test our hypotheses both *in vitro* and *in vivo*.

References:

Abe, Y., Takeuchi, T., Kagawa-Miki, L., Ueda, N., Shigemoto, K., Yasukawa, M., and Kito, K. (2007). A mitotic kinase TOPK enhances Cdk1/cyclin B1-dependent phosphorylation of PRC1 and promotes cytokinesis. J Mol Biol *370*, 231-245.

Bartkova, J., Horejsi, Z., Koed, K., Kramer, A., Tort, F., Zieger, K., Guldberg, P., Sehested, M., Nesland, J.M., Lukas, C.*, et al.* (2005). DNA damage response as a candidate anti-cancer barrier in early human tumorigenesis. Nature *434*, 864-870.

Celeste, A., Fernandez-Capetillo, O., Kruhlak, M.J., Pilch, D.R., Staudt, D.W., Lee, A., Bonner, R.F., Bonner, W.M., and Nussenzweig, A. (2003). Histone H2AX phosphorylation is dispensable for the initial recognition of DNA breaks. Nat Cell Biol *5*, 675-679.

Doil, C., Mailand, N., Bekker-Jensen, S., Menard, P., Larsen, D.H., Pepperkok, R., Ellenberg, J., Panier, S., Durocher, D., Bartek, J.*, et al.* (2009). RNF168 binds and amplifies ubiquitin conjugates on damaged chromosomes to allow accumulation of repair proteins. Cell *136*, 435-446.

Feng, L., Huang, J., and Chen, J. (2009). MERIT40 facilitates BRCA1 localization and DNA damage repair. Genes Dev *23*, 719-728.

Gong, Z., Cho, Y.W., Kim, J.E., Ge, K., and Chen, J. (2009). Accumulation of Pax2 transactivation domain interaction protein (PTIP) at sites of DNA breaks via RNF8-dependent pathway is required for cell survival after DNA damage. J Biol Chem *284*, 7284-7293.

Gorgoulis, V.G., Vassiliou, L.V., Karakaidos, P., Zacharatos, P., Kotsinas, A., Liloglou, T., Venere, M., Ditullio, R.A., Jr., Kastrinakis, N.G., Levy, B.*, et al.* (2005). Activation of the DNA damage checkpoint and genomic instability in human precancerous lesions. Nature *434*, 907-913.

Huang, J., Gong, Z., Ghosal, G., and Chen, J. (2009a). SOSS complexes participate in the maintenance of genomic stability. Mol Cell *35*, 384-393.

Huang, J., Huen, M.S., Kim, H., Leung, C.C., Glover, J.N., Yu, X., and Chen, J. (2009b). RAD18 transmits DNA damage signalling to elicit homologous recombination repair. Nat Cell Biol *11*, 592-603.

Huen, M.S., Grant, R., Manke, I., Minn, K., Yu, X., Yaffe, M.B., and Chen, J. (2007). RNF8 transduces the DNA-damage signal via histone ubiquitylation and checkpoint protein assembly. Cell *131*, 901-914.

Kim, H., Chen, J., and Yu, X. (2007a). Ubiquitin-binding protein RAP80 mediates BRCA1-dependent DNA damage response. Science *316*, 1202-1205.
Kim, H., Huang, J., and Chen, J. (2007b). CCDC98 is a BRCA1-BRCT domain-binding protein involved in the DNA damage response. Nat Struct Mol Biol *14*, 710-715.
Kolas, N.K., Chapman, J.R., Nakada, S., Ylanko, J., Chahwan, R., Sweeney, F.D., Panier, S., Mendez, M., Wildenhain, J., Thomson, T.M.*, et al.* (2007). Orchestration of the DNA-damage response by the RNF8 ubiquitin ligase. Science *318*, 1637-1640.
Liu, Z., Wu, J., and Yu, X. (2007). CCDC98 targets BRCA1 to DNA damage sites. Nat Struct Mol Biol *14*, 716-720.
Maddika, S., and Chen, J. (2009). Protein kinase DYRK2 is a scaffold that facilitates assembly of an E3 ligase. Nat Cell Biol *11*, 409-419.
Maddika, S., Sy, S.M., and Chen, J. (2009). Functional interaction between Chfr and Kif22 controls genomic stability. J Biol Chem *284*, 12998-13003.
Mailand, N., Bekker-Jensen, S., Faustrup, H., Melander, F., Bartek, J., Lukas, C., and Lukas, J. (2007). RNF8 ubiquitylates histones at DNA double-strand breaks and promotes assembly of repair proteins. Cell *131*, 887-900.
Matsumoto, S., Abe, Y., Fujibuchi, T., Takeuchi, T., Kito, K., Ueda, N., Shigemoto, K., and Gyo, K. (2004). Characterization of a MAPKK-like protein kinase TOPK. Biochem Biophys Res Commun *325*, 997-1004.
Petrini, J.H. (2007). Cell signaling. A touching response to damage. Science *316*, 1138-1139.
Richard, D.J., Bolderson, E., Cubeddu, L., Wadsworth, R.I., Savage, K., Sharma, G.G., Nicolette, M.L., Tsvetanov, S., McIlwraith, M.J., Pandita, R.K.*, et al.* (2008). Single-stranded DNA-binding protein hSSB1 is critical for genomic stability. Nature *453*, 677-681.
Shao, G., Patterson-Fortin, J., Messick, T.E., Feng, D., Shanbhag, N., Wang, Y., and Greenberg, R.A. (2009). MERIT40 controls BRCA1-Rap80 complex integrity and recruitment to DNA double-strand breaks. Genes Dev *23*, 740-754.
Sobhian, B., Shao, G., Lilli, D.R., Culhane, A.C., Moreau, L.A., Xia, B., Livingston, D.M., and Greenberg, R.A. (2007). RAP80 targets BRCA1 to specific ubiquitin structures at DNA damage sites. Science *316*, 1198-1202.
Stewart, G.S., Panier, S., Townsend, K., Al-Hakim, A.K., Kolas, N.K., Miller, E.S., Nakada, S., Ylanko, J., Olivarius, S., Mendez, M.*, et al.* (2009). The RIDDLE syndrome protein mediates a ubiquitin-dependent signaling cascade at sites of DNA damage. Cell *136*, 420-434.
Sy, S.M., Huen, M.S., and Chen, J. (2009a). MRG15 is a novel PALB2-interacting factor involved in homologous recombination. J Biol Chem *284*, 21127-21131.
Sy, S.M., Huen, M.S., and Chen, J. (2009b). PALB2 is an integral component of the BRCA complex required for homologous recombination repair. Proc Natl Acad Sci U S A *106*, 7155-7160.
Sy, S.M., Huen, M.S., Zhu, Y., and Chen, J. (2009c). PALB2 Regulates Recombinational Repair through Chromatin Association and Oligomerization. J Biol Chem *284*, 18302-18310.
Wang, B., and Elledge, S.J. (2007). Ubc13/Rnf8 ubiquitin ligases control foci formation of the Rap80/Abraxas/Brca1/Brcc36 complex in response to DNA damage. Proc Natl Acad Sci U S A *104*, 20759-20763.

Wang, B., Hurov, K., Hofmann, K., and Elledge, S.J. (2009). NBA1, a new player in the Brca1 A complex, is required for DNA damage resistance and checkpoint control. Genes Dev *23*, 729-739.
Wang, B., Matsuoka, S., Ballif, B.A., Zhang, D., Smogorzewska, A., Gygi, S.P., and Elledge, S.J. (2007). Abraxas and RAP80 form a BRCA1 protein complex required for the DNA damage response. Science *316*, 1194-1198.
Yu, X., Minter-Dykhouse, K., Malureanu, L., Zhao, W.M., Zhang, D., Merkle, C.J., Ward, I.M., Saya, H., Fang, G., van Deursen, J.*, et al.* (2005). Chfr is required for tumor suppression and Aurora A regulation. Nat Genet *37*, 401-406.

Appendices:

Manuscript 1 Gong, Z., Cho, Y.W., Kim, J.E., Ge, K. and **Chen, J.** Accumulation of Pax2 transactivation domain interaction protein (PTIP) at sites of DNA breaks via RNF8-dependent pathway is required for cell survival after DNA damage. J Biol Chem. 284(11):7284-93, 2009.

Manuscript 2 Feng, L., Huang, J. and **Chen, J.** MERIT40 facilitates BRCA1 localization and DNA damage repair. Genes Dev. 23(6):719-28, 2009.

Manuscript 3 Maddika, S and **Chen, J.** Protein kinase DYRK2 is an E3-ligase specific molecular assembler. Nature Cell Biol., 11(4):409-19, 2009.

Manuscript 4 Maddika, S., Sy, S.M. and **Chen, J.** Functional interaction between Chfr and Kif22 controls genomic stability. J Biol Chem., 284(19):12998-3003, 2009.

Manuscript 5 Sy, S.M., Huen, M.S. and **Chen, J.** PALB2 is an integral component of the BRCA complex required for homologous recombination repair. Proc Natl Acad Sci U S A., 106(17):7155-60, 2009.

Manuscript 6 Huang, J., Huen, M.S., Kim, H., Leung, C.C., Glover, J.N., Yu, X. and **Chen, J.** RAD18 transmits DNA damage signalling to elicit homologous recombination repair. Nature Cell Biol. 11(5):592-603, 2009.

Manuscript 7 Sy, S.M., Huen, M.S., Zhu, Y. and **Chen, J.** PALB2 regulates recombinational repair through chromatin association and oligomerization. J. Biol. Chem. 284(27):18302-10, 2009.

Manuscript 8 Sy, S.M., Huen, M.S. and **Chen, J.** MRG15 Is a Novel PALB2-interacting Factor Involved in Homologous Recombination. J Biol Chem. 284(32):21127-31, 2009.

Manuscript 9 Huang, J., Gong, Z, Ghosal, G. and **Chen, J.** SOSS complexes participate in the maintenance of genomic stability. Mol Cell 35(3):384-93, 2009.

THE JOURNAL OF BIOLOGICAL CHEMISTRY VOL. 284, NO. 11, pp. 7284–7293, March 13, 2009
Printed in the U.S.A.

Accumulation of Pax2 Transactivation Domain Interaction Protein (PTIP) at Sites of DNA Breaks via RNF8-dependent Pathway Is Required for Cell Survival after DNA Damage*[S]

Received for publication, December 4, 2008, and in revised form, January 5, 2009 Published, JBC Papers in Press, January 5, 2009, DOI 10.1074/jbc.M809158200

Zihua Gong[‡], Young-Wook Cho[§], Ja-Eun Kim[‡¶], Kai Ge[§], and Junjie Chen[‡1]

From the [‡]Department of Therapeutic Radiology, Yale University School of Medicine, New Haven, Connecticut 06520, the [§]Nuclear Receptor Biology Section, Clinical Endocrinology Branch, NIDDK, National Institutes of Health, Bethesda, Maryland 20892, and the [¶]Department of Pharmacology, Kyung Hee University School of Medicine, Hoegi-Dong, Dongdaemun-Gu, Seoul 130-701, Korea

Genomic stability in eukaryotic cells is maintained by the coordination of multiple cellular events including cell cycle checkpoint, DNA repair, transcription, and apoptosis after DNA damage. Pax2 transactivation domain interaction protein (PTIP), a protein that contains six BRCT domains, has been implicated in DNA damage response. In this study we showed that recruitment of PTIP to damaged chromatin depends on DNA damage signaling proteins γH2AX·MDC1·RNF8, which in turn facilitates sustained localization of PA1 (PTIP-associated protein 1) to sites of DNA break. Similar to PTIP, depletion of PA1 increases cellular sensitivity to ionizing radiation. Furthermore, we demonstrated that the N-terminal PA1 binding domain and the C-terminal focus-localization domain of PTIP are critical for PTIP function in DNA damage repair. Interestingly, although PTIP and PA1 associate with MLL (mixed lineage leukemia) complexes and participate in transcriptional regulation, this function of PTIP·PA1 in DNA damage response is likely to be independent of the MLL complexes. Taken together, we propose that a subset of PTIP·PA1 complex is recruited to DNA damage sites via the RNF8-dependent pathway and is required for cell survival in response to DNA damage.

The genome of all living cells constantly suffers a variety of genomic insults, which if not fixed would lead to genomic instability. Therefore, in response to DNA damage, cells elicit an elaborated signaling network, which is collectively known as the DNA damage response pathway (1). Through a cascade of sensors, transducers, and effectors, the DNA damage response pathway coordinates a process that include cell cycle checkpoints, DNA repair, cellular senescence, and apoptosis (2, 3).

The regulation of this pathway is best studied after ionizing radiation (IR).[2] In response to IR, the histone variant H2AX is phosphorylated by ATM or ATR (4) and serves as a platform for the recruitment of MDC1, which further facilitates the loading of many checkpoint and repair proteins to sites of DNA damage to form IR-induced foci (IRIF) (5, 6). More recent studies revealed that phosphorylation of MDC1 binds directly to and accumulates the E3 ubiquitin ligase complex, RNF8·Ubc13 at DNA damage sites, which ubiquitinates H2AX, H2A, and possibly additional proteins and allows the recruitment of 53BP1 and the ubiquitin-interacting motif domain-containing protein RAP80 at sites of breaks after DNA damage (7–13). Although RAP80 specifically recruits BRCA1 to sites of DNA break, it remains to be determined how 53BP1 localizes to DNA damage sites via this ubiquitination-dependent cascade and whether additional DNA damage checkpoint and repair proteins would localize to sites of DNA break through the same or a similar mechanism.

PTIP was originally identified as Pax2 transactivation domain interaction protein in a yeast two-hybrid screen (14). Subsequently, several studies suggest that PTIP is an essential component of histone H3K4 methyltransferase complexes, which may be involved in the regulation of gene expression through modulation of H3K4 methylation (15, 16). The importance of PTIP functions *in vivo* is revealed by the observations that PTIP null embryos die at E9.5 due to widespread cell death (17). In addition, PTIP null cells show a very high number of DNA breaks during S-phase and an inability to progress through mitosis, suggesting a defect in DNA repair (17). A possible function of PTIP in DNA damage repair is also suggested by the presence of six BRCT domains in PTIP, as BRCT domains are phosphoprotein binding domains that preferentially bind to Ser(P)/Thr(P) motifs, especially those generated by ATM and ATR (18). Indeed, PTIP has been shown to interact with 53BP1 in response to DNA damage, and this interaction requires ATM-

* This work was supported, in whole or in part, by National Institutes of Health Grants CA089239, CA092312, and CA100109 (to J. C.). The costs of publication of this article were defrayed in part by the payment of page charges. This article must therefore be hereby marked "*advertisement*" in accordance with 18 U.S.C. Section 1734 solely to indicate this fact.

[S] The on-line version of this article (available at http://www.jbc.org) contains supplemental Table 1 and Figs. S1–S3.

[1] Recipient of an Era of Hope Scholar award from the Department of Defense and a member of the Mayo Clinic Breast SPORE program. To whom correspondence should be addressed. Tel.: 203-785-3758; Fax: 203-785-7482; E-mail: Junjie.chen@yale.edu.

[2] The abbreviations used are: IR, ionizing radiation; IRIF, IR-induced foci; PTIP, Pax2 transactivation domain interaction protein; PA1, PTIP-associated protein 1; siRNA, small interfering RNAs; MLL, mixed lineage leukemia; DAPI, 4′,6-diamidino-2-phenylindole; MEF, mouse embryonic fibroblast; HA, hemagglutinin; Gy, gray; UTX, ubiquitously transcribed tetratricopeptide repeat, X chromosome; ATM, ataxia telangiectasia mutated; ATR, ataxia telangiectasia and Rad3related; BRCT, BRCA1 carboxyl termini; FANCN, Fanconi anemia, complementation group N; DSB, double strand break.

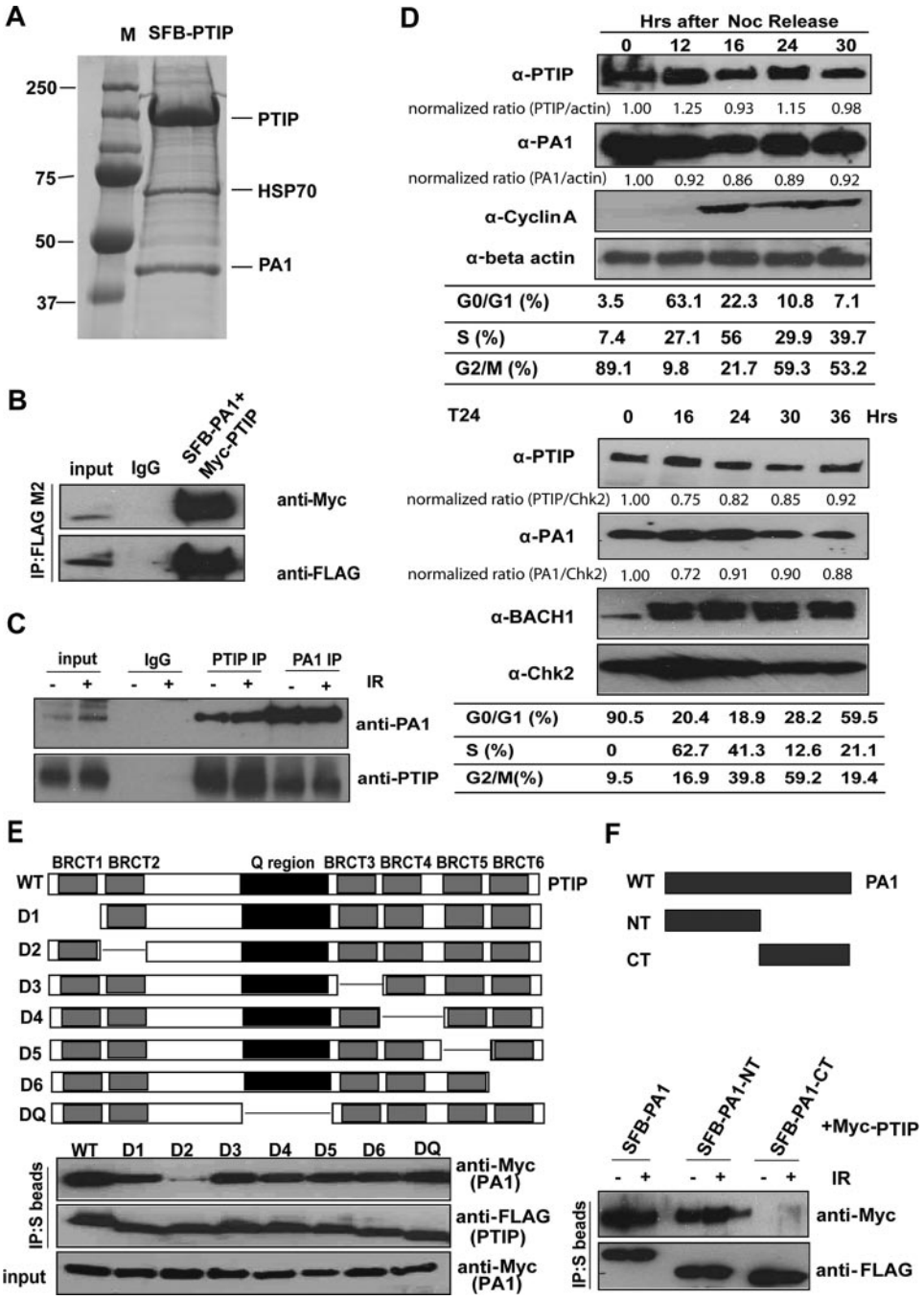

FIGURE 1. **PTIP interacts with PA1.** *A*, Coomassie Blue staining of affinity-purified PTIP-containing protein complexes. Cell extracts prepared from 293T cells stably expressing SFB-PTIP were subjected to tandem affinity purification. The final eluent was subjected to SDS-PAGE and visualized by Coomassie Blue staining. Proteins were identified by matrix-assisted laser desorption ionization time-of-flight mass spectrometry analysis and summarized in supplemental Table 1. Lines indicate protein bands corresponding to PTIP and PA1. *M*, molecular mass standards. *B*, 293T cells were transfected with plasmids encoding SFB-tagged PTIP together with plasmids encoding Myc-tagged PA1. Immunoprecipitation (*IP*) reactions were performed using S-protein beads and then subjected to Western blot analyses using indicated antibodies. *C*, endogenous interaction between PTIP and PA1 in the absence or presence of IR. For a control, anti-PTIP or anti-PA1 immunoprecipitates were immunoblotted with indicated antibodies. *D*, cell cycle-independent expression of PTIP and PA1. HeLa cells were arrested overnight with 0.5 μg/ml nocodazole (*Noc*). Mitotic cells were "shaken off" and then released into normal media (*upper*). T24 cells were allowed to grow to confluency for 96 h and then trypsinized and released into fresh media (*lower*). Samples were taken at the indicated time points and analyzed by fluorescence-activated cell sorting and Western blotting. *E* and *F*, mapping of the corresponding regions required for PTIP·PA1 interaction. Immunoprecipitation reactions were performed using S-protein beads and then subjected to Western blot analyses using antibodies as indicated. Schematic diagrams of wild-type (*WT*) and deletion mutants of PTIP (*E*) and PA1 (*F*) used in this study are also included. *NT*, N terminus; *CT*, C terminus.

dependent phosphorylation of 53BP1 (18, 19). The four C-terminal BRCT domains of PTIP are required for its foci formation after IR and its interaction with 53BP1 via 53BP1 Ser-25 phosphorylation (19). However, the exact function of PTIP in the DNA damage-responsive pathway and where it fits in the well defined DNA damage-signaling cascade remain elusive.

Here we report that PTIP acts downstream of γH2AX·MDC1·RNF8 in the DNA damage signal transduction cascade. In addition, we showed that PTIP forms a stable complex with PTIP-associated protein 1 (PA1), and this complex is required for cell survival after IR.

MATERIALS AND METHODS

Cell Culture and Plasmids—HeLa, 293T, and U2OS cells were maintained in RPMI 1640 supplemented with 10% fetal bovine serum and 1% penicillin/streptomycin at 37 °C in a humidified incubator with 5% CO_2 (v/v). Mouse embryonic fibroblast (MEF) cells were cultivated in Dulbecco's modified Eagle's medium supplemented with 10% fetal bovine serum and 1% penicillin/streptomycin at 37 °C in 5% CO_2 (v/v). SV40T-immortalized $PTIP^{flox/flox}$ MEFs (15) were infected with adenovirus expressing Cre to permanently delete *PTIP* gene. After serial dilution, single colonies were isolated, and deletion of the *PTIP* gene was confirmed by real time PCR. $H2AX^{-/-}$ MEFs, $H2AX^{-/-}$ MEFs reconstituted with wild type H2AX, $MDC1^{-/-}$, $53BP1^{-/-}$, $RNF8^{-/-}$, $UBC13^{-/-}$, $PTIP^{-/-}$, and their respective wild-type MEFs, NBS1-deficient ILB1 cells and its derivative cells reconstituted with wild-type NBS1, ATM-deficient (FT169A), and reconstituted (YZ5) cells, and HCC1937 and HCC1937-BRCA1, FANCD2-reconstituted and -deficient cells were previously reported (6, 7, 20–22). $RAD18^{+/+}$ and $RAD18^{-/-}$ MEFs were a generous gift of Masaru Yamaizumi at Kumamoto Univer-

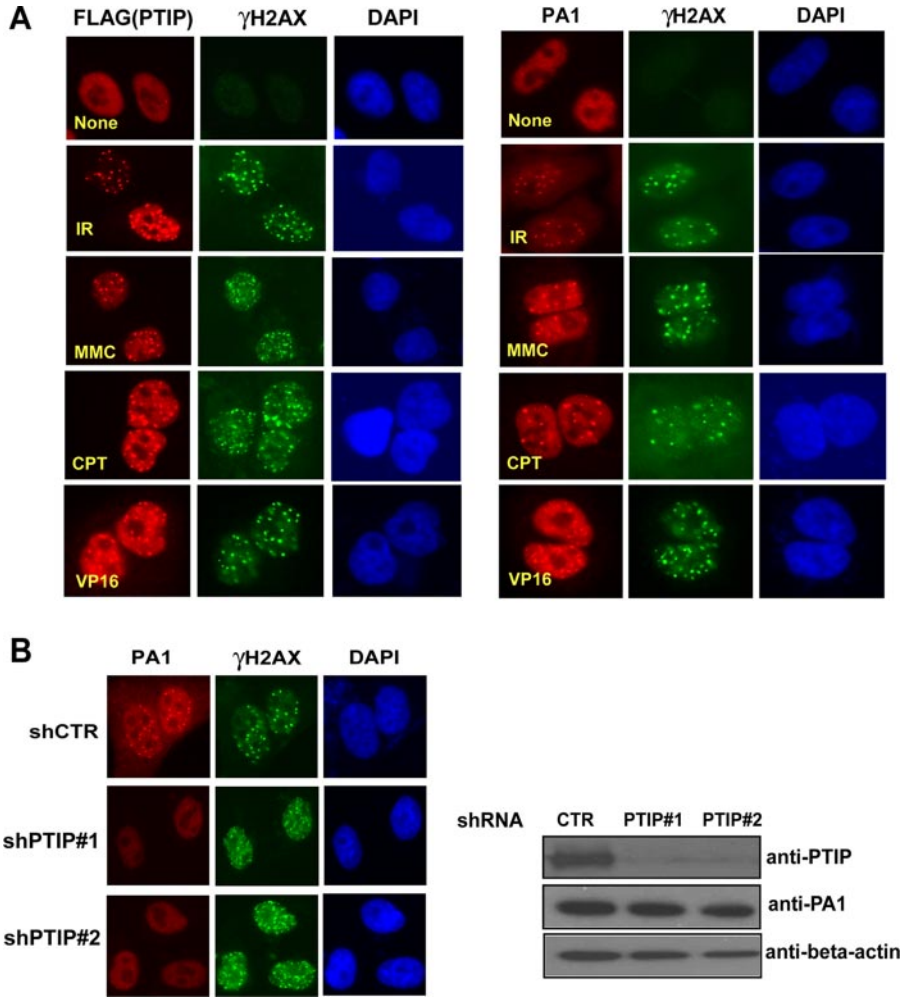

FIGURE 2. **PTIP accumulates PA1 at DNA damage sites.** *A*, PTIP and PA1 form foci after DNA damage. SFB-PTIP 293T stable cell lines or U2OS cells grown on coverslips were treated with 10 Gy IR, 100 μg/ml mitomycin (*MMC*), 25 nM camptothecin (*CPT*), or 2.5 μM VP16. 8 h later cells were fixed, and immunostaining was carried out using indicated antibodies. *B*, U2OS cells with PTIP knockdown (shPTIP#1, shPTIP#2) or transfected with control vector (*shCTR*) were irradiated (10 Gy), allowed to recover for 6 h, fixed, and immunostained using antibodies as indicated. Western blot analysis was performed to verify the stable knockdown of PTIP (*right panel*).

sity. FANCN-deficient VU1341F cells were provided by Dr. de Winter.

Mouse PTIP cDNA was subcloned into pDONR201 entry vector and then transferred to destination vectors containing N-terminal triple-epitope tag SFB (S protein, FLAG, and streptavidin binding peptide tag) or HA- or Myc-epitope tag using the gateway system (Invitrogen). All deletion mutants were generated by site-directed mutagenesis (Stratagene) and verified by sequencing. Transfections were performed using FuGENE 6 or Lipofectamine according to the manufacturer's instructions.

Antibodies—Rabbit polyclonal anti-PA1 antibodies were raised by immunizing rabbits with glutathione *S*-transferase-fused PA1 recombinant protein. The antibody was affinity-purified using AminoLink Plus Immobilization and a purification kit (Pierce). Phospho-H2AX, MDC1, RNF8, MLL3 antibodies were described previously (6, 7, 15, 23). Both monoclonal anti-FLAG M2 and anti-β-actin antibodies were purchased from Sigma.

Retrovirus Production and Infection—Full-length PTIP was cloned into pEF1A-HA-FLAG retroviral vector using the gateway system. Virus-containing supernatant was collected 48 and 72 h after co-transfection of pEF1A-HA-FLAG PTIP and pcl-ampho into BOSC23 packaging cells and were used to infect MEF cells in the presence of Polybrene. Two days later MEF cells were either irradiated as indicated or cultured in medium containing puromycin for the selection of stable clones. The clones stably expressing HA-FLAG-tagged PTIP were identified and verified by Western blotting and immunostaining using anti-FLAG antibodies.

Immunofluorescence Staining—Cells grown on coverslips were mock-treated or irradiated with a JL Shepherd Cs137 source (10 Gy) and allowed to recover for 6 h. Cells were fixed in 3% paraformaldehyde solution for 10 min and then permeabilized in 0.5% Triton X-100-containing solution for 5 min at room temperature. Cells were incubated with primary antibodies diluted in 5% goat serum at 37 °C for 30 min. After washing with phosphate-buffered saline twice, cells were incubated either with fluorescein isothiocyanate-conjugated or rhodamine-conjugated secondary antibodies for 20 min at 37 °C. Nuclei were counterstained with 4′,6-diamidino-2-phenylindole (DAPI) and then mounted onto glass slides with anti-Fade solution. Images were taken with a Nikon Eclipse E800 fluorescence microscope.

Co-immunoprecipitation and Western Blotting—Cells were lysed with NTEN buffer (20 mM Tris-HCl, pH 8.0, 100 mM NaCl, 1 mM EDTA, 0.5% Nonidet P-40) containing 20 mM NaF and 1 μg/ml of pepstatin A and aprotinin on ice for 20 min. After removal of cell debris by centrifugation, the soluble fractions were collected and incubated with either protein A-agarose beads coupled with anti-PTIP, PA1 antibodies, or streptavidin-Sepharose beads (Amersham Biosciences) for 3 h at 4 °C. The precipitates were then washed 4 times with NTEN buffer and boiled in 2× SDS loading buffer. Samples were resolved on SDS-PAGE and transferred to polyvinylidene difluoride membranes, and immunoblotting was carried out with antibodies as indicated.

Fluorescence-activated Cell Sorting—For cell cycle analysis, cells were washed twice with phosphate-buffered saline, resuspended in 300 μl of phosphate-buffered saline, and then fixed

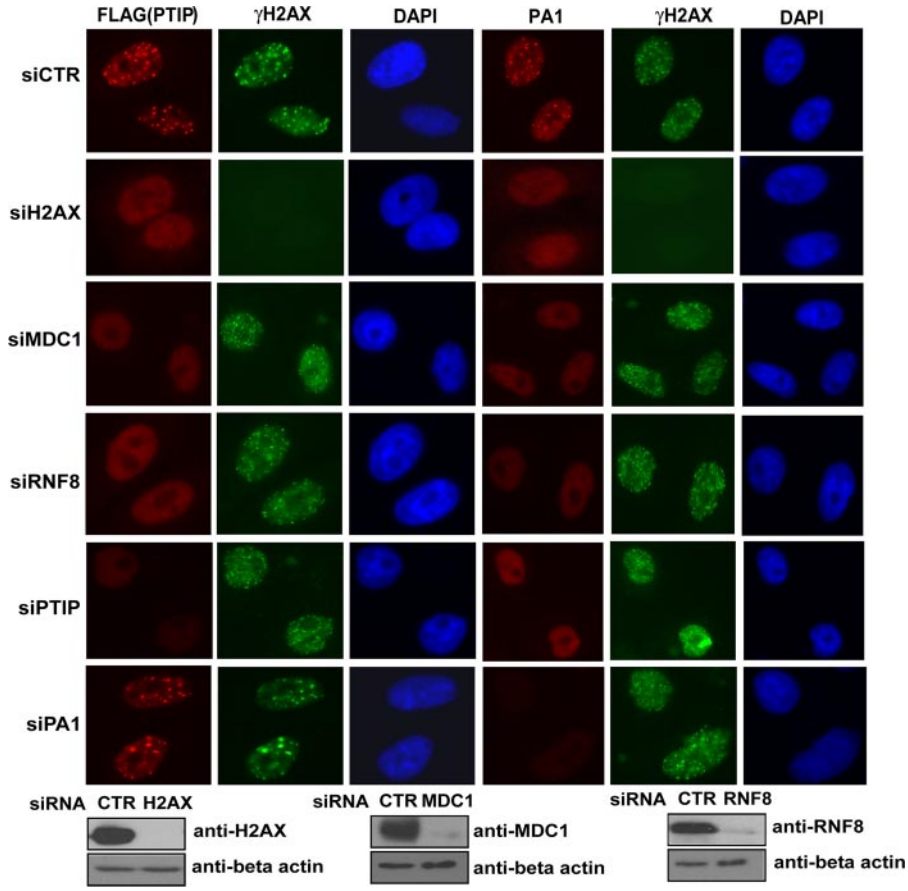

FIGURE 3. **PTIP·PA1 localization depends on a signaling cascade involves H2AX, MDC1, and RNF8.** HeLa cells or HeLa cells stably expressing HA-FLAG-PTIP were transfected with control siRNA or H2AX-, MDC1-, RNF8-, PTIP-, PA1-specific siRNAs. Cells were irradiated (10 Gy), fixed, and immunostained with anti-FLAG, anti-PA1, and pH2AX antibodies. Western blot analysis was carried out to verify the knockdown of H2AX, MDC1, and RNF8 (*lower panel*).

with the addition of 700 μl of 100% ethanol. After being stored at −20 °C overnight, fixed cells were washed and incubated in sodium citrate buffer containing RNase A for 30 min and then stained with propidium iodide for 30 min. Cells were then run on a FACScan, and cell cycle analysis was performed.

Tandem Affinity Purification—293T cells stably expressing SFB-PTIP were used for tandem affinity purification. The SFB-PTIP stable cells were lysed with NETN buffer (see above) on ice for 20 min. After removal of cell debris by centrifugation, crude lysates were incubated with streptavidin-Sepharose beads for 1 h at 4 °C. The bead-bound proteins were washed 3 times with NETN buffer and eluted with 2 mg/ml biotin (Sigma) for 1 h twice at 4 °C. The eluates were further incubated with S-protein-agarose (Novagen) for 1 h at 4 °C and washed 3 times with NETN buffer. The proteins bound to S-protein-agarose beads were subjected to SDS-PAGE and visualized by Coomassie Blue staining. The identities of eluted proteins were revealed by mass spectrometry analysis, performed by the Taplin Biological Mass Spectrometry Facility (Harvard University).

RNA Interference—Small interfering RNAs (siRNAs) against human PTIP or PA1 were purchased from Dharmacon, Inc. A non-targeting siRNA was used as control. The sequences of PA1 siRNA#1 and siRNA#2 are CUGAUUGACCGGAGACGCAUU and AUGAGGAGCCGGAGGCCAAUU, respectively. Sequences of siRNA#1 and siRNA#2 against PTIP are ACACUGAGGAAUAUUACUAdTdT and UGUUUGCAAUUGCGGAUUAUU, respectively. The sequences of MLL3 siRNA#1 and siRNA#2 are GCAAUGGUCUUUCUGGAUAUU and CCAGGUCAAUCAACAGUUAUU, respectively. The sequence of H2AX siRNA is CAACAAGAAGACGCGAAUCdTdT. The sequences for MDC1 and RNF8 siRNA were previously described (7). The sequence of control siRNA is UUCAAUAAAUUCUUGAGGUUU. HeLa cells were transfected twice at 24-h time intervals with the indicated siRNAs using Oligofectamine (Invitrogen) to achieve efficient siRNA-mediated down-regulation of their target genes.

Clonogenic Survival Assays—IR sensitivity assays were carried out as described previously (24). Briefly, cells were seeded onto 60-mm dish in triplicate and treated with ionizing radiation with indicated doses. Cells were left for 14 days to allow colonies to form. Colonies were fixed and stained with Coomassie Blue and then counted using a GelDoc with Quantity One software (Bio-Rad). Results were the averages of data obtained from three independent experiments.

G_2/M Checkpoint Assay—PTIP MEFs, siRNA knockdown PTIP, or siRNA knockdown PA1 U2OS cells were seeded onto 10-cm dishes, irradiated with 3 Gy of ionizing radiation, and incubated for 1 h before collection. G_2/M checkpoint assay were performed as described previously (24).

RESULTS

PA1 Is a Major PTIP-associated Protein—In an attempt to understand PTIP functions in DNA damage response, we established a 293T derivative cell line stably expressing a triple-tagged (S-protein, FLAG, and streptavidin binding peptide) PTIP for the identification of potential PTIP binding partners. After tandem affinity purification, the identities of PTIP-associated proteins were revealed by mass spectrometry analysis (supplemental Table 1). In agreement with our recent report (15), we reproducibly identified PA1 as a major PTIP-associated protein (Fig. 1*A*). We performed co-immunoprecipitation experiments and were able to confirm an interaction not only between overexpressed PTIP and PA1 (Fig. 1*B*) but also between endogenous proteins (Fig. 1*C*), suggesting that these two proteins indeed associate with each other *in vivo*. Moreover, the binding of PA1 to PTIP was not changed after cells were exposed to IR (Fig. 1*C*).

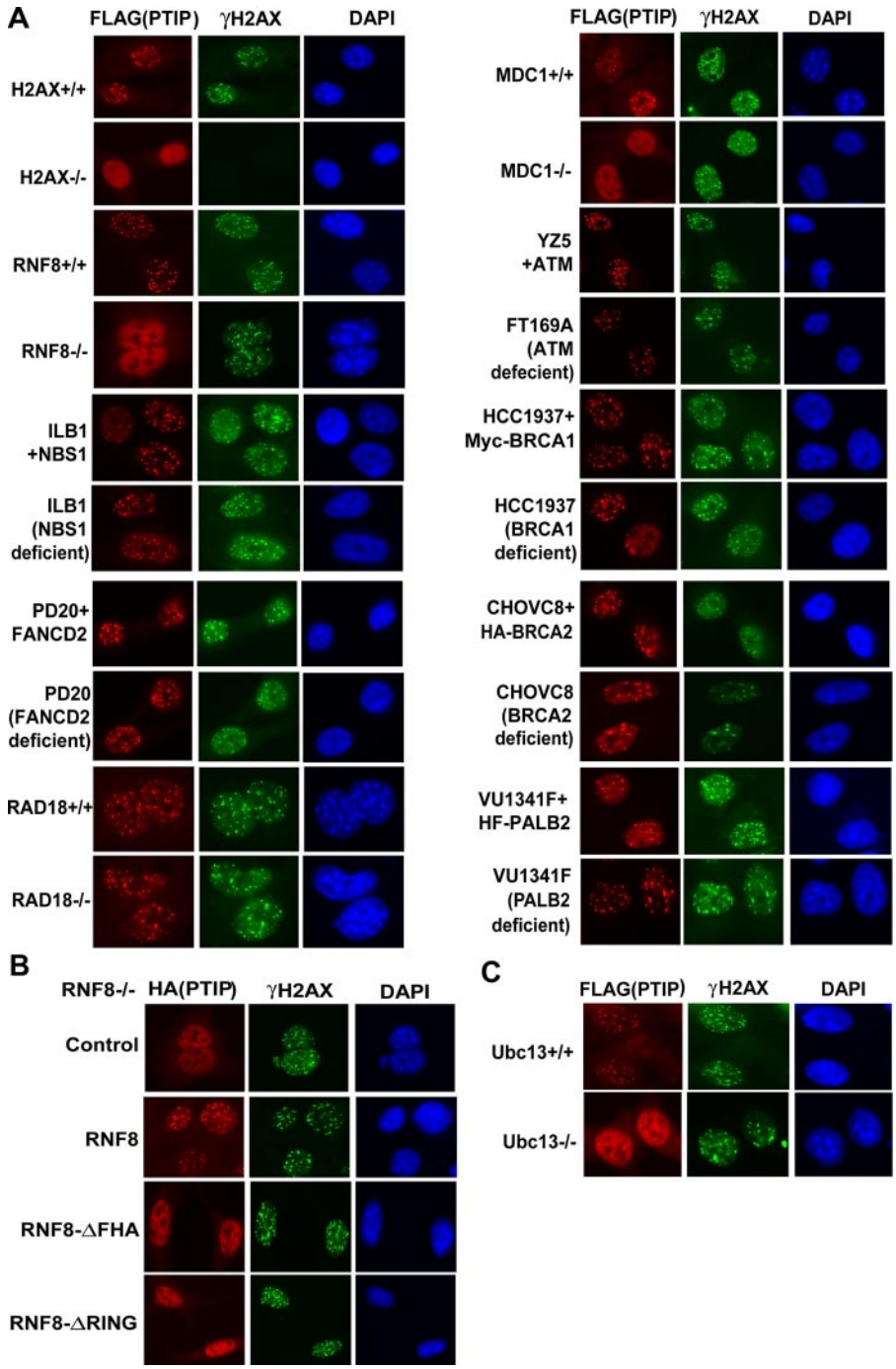

FIGURE 4. **PTIP foci formation depends on γH2AX·MDC1·RNF8 but not other DNA damage checkpoint or repair proteins.** *A*, PTIP acts downstream of H2AX·MDC1·RNF8 signaling pathway in response to DNA damage. Cells deficient for various DNA damage checkpoint or repair proteins and their respective wild-type counterparts or reconstituted cells were infected with retrovirus expressing FLAG-tagged PTIP. Cells were then irradiated (10 Gy), and immunostaining experiments were performed using anti-FLAG and anti-γH2AX antibodies 6 h later. *B*, both the FHA domain and RING domain of RNF8 are required for PTIP IRIF formation. RNF8$^{-/-}$ MEFs stably expressing HA-tagged PTIP were infected with retroviruses expressing SFB-RNF8, SFB-RNF8-ΔFHA, or SFB-RNF8-ΔRING mutants. Immunostaining experiments were performed using anti-γH2AX and anti-HA antibodies. *C*, UBC13 is required for PTIP localization at or near the sites of DNA breaks. Wild-type or UBC13$^{-/-}$ MEFs were infected with retroviruses expressing SFB-PTIP. Cells were irradiated (10 Gy), fixed, and immunostained with anti-FLAG and pH2AX antibodies.

To understand how these two proteins may function together, we examined whether PTIP and PA1 expression would be coordinately regulated in cells. We carried out mitotic "shake off" experiments using HeLa cells. In addition, we also arrested T24 cells in G_0 phase by contact inhibition. In both cases we allowed these synchronized cells to enter the cell cycle by changing them into fresh media at appropriate density. As shown in Fig. 1*D*, the levels of PTIP and PA1 only varied slightly, indicating that both PTIP and PA1 are ubiquitously expressed throughout cell cycle.

To identify the region(s) on PTIP required for its interaction with PA1, we co-expressed a series of internal deletion mutants of PTIP (Fig. 1*E*) with Myc-tagged PA1 in 293T cells. Results revealed that the interaction between PTIP and PA1 was dramatically decreased by the deletion of the second BRCT domain of PTIP, suggesting that this N-terminal BRCT2 domain of PTIP is involved in its interaction with PA1 (Fig. 1*E*). Conversely, we found that the N terminus of PA1, but not its C terminus, is critical for PA1-PTIP interaction (Fig. 1*F*). Using bacterially expressed and purified proteins, we showed that PA1 binds directly to PTIP BRCT1/2, but not to PTIP BRCT3/4 or PTIP BRCT5/6 (supplemental Fig. S1). This result indicates that although PTIP·PA1 interaction requires the BRCT2 domain of PTIP, this interaction occurs in a phosphorylation-independent manner.

PTIP Targets PA1 to Sites of DNA Damage—Previous studies suggested that PTIP forms nuclear foci in response to ionizing radiation (19). Because of the limited sensitivity of our anti-PTIP antibodies, we repeated these experiments using 293T cells stably expressing SFB-tagged PTIP. Indeed, damage-induced PTIP foci formation was readily detected after ionizing radiation (Fig. 2*A*). We also observed PTIP foci formation in cells treated with various agents leading to DNA damage, including camptothecin (*CPT*), mitomycin C (*MMC*), and etoposide (VP16) (Fig. 2*A*), suggesting that PTIP responds to a variety of DNA-damaging agents. Similarly, we detected PA1 foci formation in cells treated with the same agents that induce DNA damage (Fig. 2*A*). The fact that DNA damage-induced PTIP and PA1 foci co-localized with those containing γH2AX (Fig.

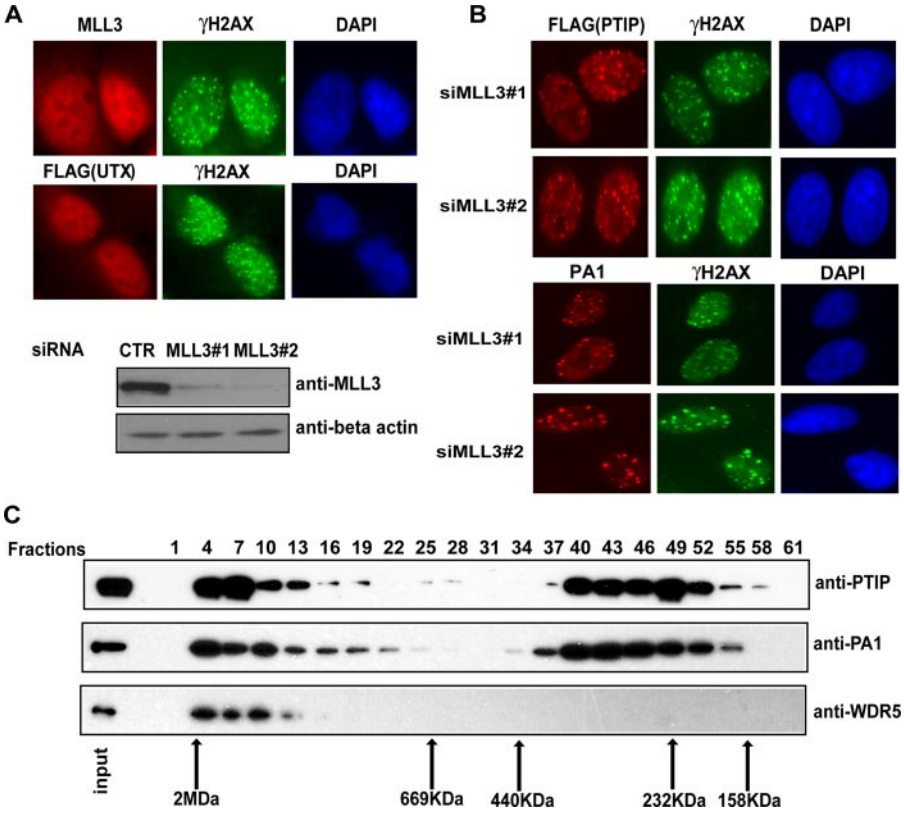

FIGURE 5. **MLL3 complex may not be involved in DNA damage response.** *A*, MLL3 and UTX do not form IRIF. U2OS cells were transfected with plasmids encoding SFB-tagged UTX. Immunostaining was carried out with anti-MLL3, anti-FLAG, and anti-γH2AX antibodies 6 h after cells exposed to IR (10 Gy). *CTR*, control. *B*, PTIP or PA1 IRIF formation occurs independently of MLL3. HeLa cells or HeLa cells stably expressing HA-FLAG-PTIP were transfected with control siRNA or MLL3 specific siRNAs (*siMLL3#1* and *siMLL3#2*). Cells were irradiated (10 Gy), fixed, and immunostained with anti-FLAG, anti-PA1, and pH2AX antibodies. Western blot analysis was carried out to verify the knockdown of MLL3 (*left panel*). *C*, FLAG-PTIP-associated proteins isolated from HeLa S cell nuclear extracts were fractionated on Superose 6 gel filtration column (Amersham Biosciences) as described in Ref. 15. Fractions were analyzed by Western blot with indicated antibodies. Positions of protein molecular weight standards are indicated at the *bottom*.

2*A*) indicates that both PTIP and PA1 relocate to sites of DNA breaks.

IR-induced PA1 foci formation was reduced in U2OS cells with PTIP knockdown (Fig. 2*B*), whereas PTIP IRIF remained the same in cells with or without PA1 knockdown (Fig. 3). These data suggest that PTIP targets PA1 to sites of DNA damage. We further confirmed these results using overexpressed PA1 and PTIP. Ectopically expressed PA1 (FLAG-PA1-NLS) localized to nuclei but could not form visible DNA damage-induced foci (supplemental Fig. S2). However, when co-expressed with PTIP, PA1 foci were readily detected after IR (supplemental Fig. S2). This PTIP-dependent localization of exogenously expressed PA1 also requires the intact PA1/PTIP interaction, as PTIP deleted of its N-terminal BRCT2 domain, which has reduced PA1 binding activity, failed to target PA1 to damage-induced foci (supplemental Fig. S2), again supporting that a direct interaction between PTIP and PA1 is required for PTIP ability to target PA1 to sites of DNA breaks.

PTIP Acts Downstream of the H2AX·MDC1·RNF8-signaling Pathway in Response to DNA Damage—Having established that PTIP is required for PA1 localization after DNA damage, we next explored what would be the upstream signaling molecules that facilitate PTIP localization to DNA damage sites. We performed experiments using siRNA knockdown in HeLa cells. PTIP and PA1 IRIF were abolished in cells with H2AX, MDC1, or RNF8 knockdown (Fig. 3). We also used a panel of cell lines defective in various components known to be involved in DNA damage checkpoint response. As shown in Fig. 4*A*, in contrast to their respective wild type counterparts, PTIP foci formation was abolished in H2AX$^{-/-}$, MDC1$^{-/-}$, and RNF8$^{-/-}$ MEFs, indicating that the damage-induced focus localization of PTIP depends on a signaling cascade involves H2AX, MDC1, and RNF8. On the other hand, we observed normal PTIP localization in ATM-deficient FT169A cells (Fig. 4*A*), suggesting that ATM is not essential for PTIP localization after DNA damage. Similarly, there is no evident difference of PTIP foci formation in BRCA1-deficient HCC1937 cells or NBS1-deficient ILB1 fibroblast cells when compared with the same cells reconstituted with wild-type BRCA1 or NBS1 (Fig. 4*A*). Collectively, these data establish that PTIP acts downstream of H2AX, MDC1, and RNF8 but is independent of BRCA1 or NBS1 in the DNA damage-signaling cascade.

We next examined whether PTIP foci formation would depend on several DNA repair proteins. We employed RAD18$^{-/-}$ MEFs, FANCD2-deficient PD20 cells, BRCA2-deficient CHOVC8 cells, PALB2/FANCN-deficient VU1341F cells, and their wild-type counterpart or reconstituted cells. As shown in Fig. 4*A*, PTIP IRIF formed normally in all these cells, implying that PTIP foci formation is independent of these repair proteins after IR.

Given that PTIP IRIF requires RNF8, we next determined whether RNF8-dependent ubiquitination events are instrumental for PTIP accumulation at sites of DNA breaks. Because we do not have any anti-mouse PTIP antibody that works for immunostaining, we established RNF8$^{-/-}$ MEF cells stably expressly HA-epitope-tagged PTIP. Interestingly, relocalization of PTIP to DNA damage sites was observed only in RNF8$^{-/-}$ cells when these cells were reconstituted with wild-type RNF8 but not when they were reconstituted with RNF8 FHA or RING domain deletion mutants (Fig. 4*B*), indicating that appropriate loading of RNF8 and its subsequent ability to promote protein ubiquitination at the vicinity of double-strand breaks are pre-requisite events for sustained accumulation of PTIP.

UBC13 was recently proposed to function with RNF8 in a DNA damage-signaling pathway to mediate focal accumulation

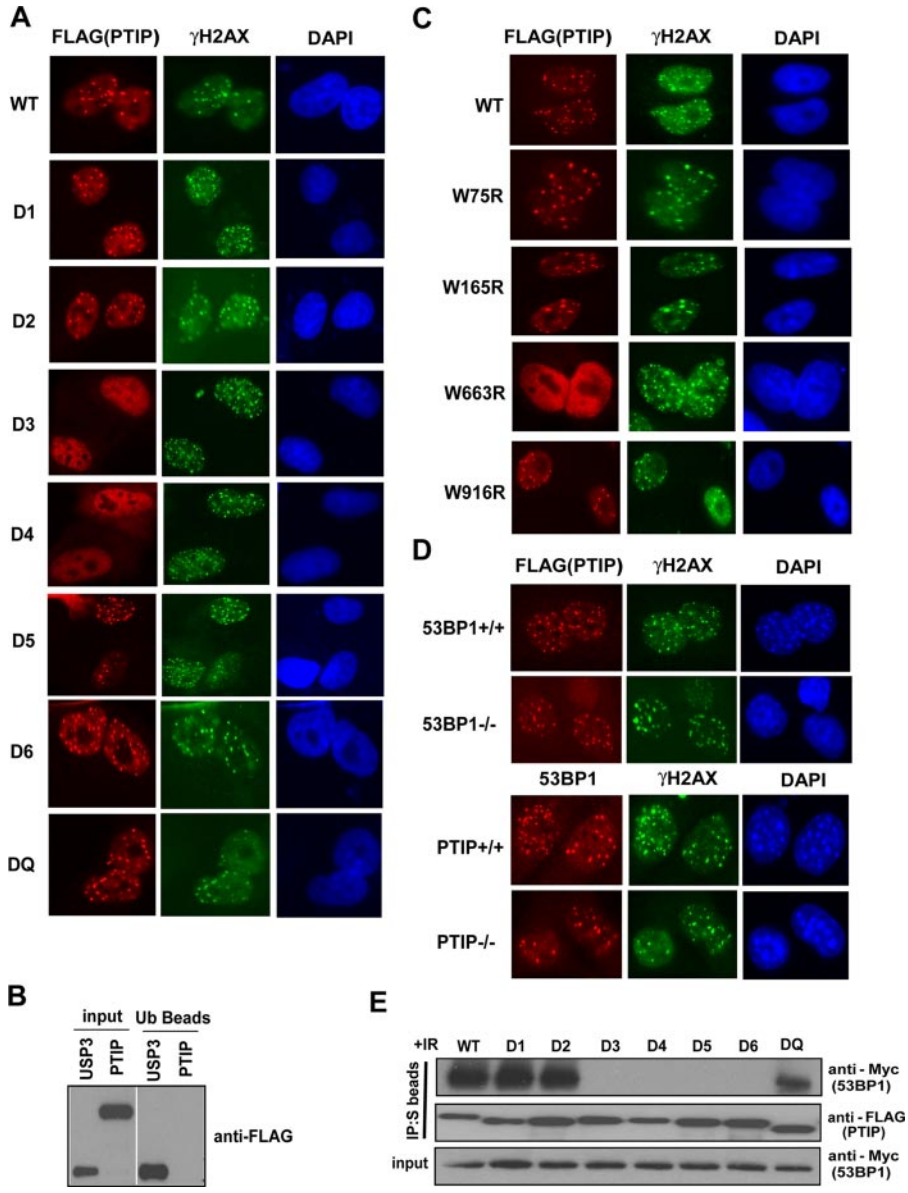

FIGURE 6. **Distinct C-terminal BRCT domains are involved in PTIP foci formation and PTIP/53BP1 interaction.** *A*, PTIP foci formation requires its BRCT3 and BRCT4 domains. U2OS cells transfected with plasmids encoding SFB-tagged wild-type (*WT*) or deletion mutants of PTIP were exposed to 10 Gy of ionizing radiation. Cells were fixed and immunostained with anti-FLAG and anti-γH2AX antibodies. *B*, U2OS cells were transfected with plasmids encoding SFB-tagged wild-type (*WT*) or mutant PTIP. Immunostaining was carried out with anti-FLAG and anti-γH2AX antibodies 6 h after cells were exposed to IR (10 Gy). *C*, PTIP does not bind to ubiquitin. Ubiquitin-agarose beads were incubated lysates containing either SFB-PTIP or SFB-USP3 (positive control) for 2 h, and proteins associated with ubiquitin were subjected to Western blotting with anti-FLAG antibody. *D*, PTIP and 53BP1 form foci independent of each other. Wild-type, 53BP1$^{-/-}$, or PTIP$^{-/-}$ MEFs were irradiated, fixed, and immunostained with antibodies as indicated. *E*, binding to 53BP1 requires all four C-terminal BRCT domains of PTIP. 293T cells were transfected with plasmids encoding Myc-tagged 53BP1 together with plasmids encoding wild-type or deletion mutants of SFB-tagged PTIP. Cells were irradiated and immunoprecipitation (*IP*) reactions were conducted using S protein beads and then subjected to Western blotting using antibodies as indicated.

of a number of checkpoint proteins at sites of DNA breaks (7, 12). Consistent with this notion, we noticed that PTIP foci formation was abrogated in UBC13$^{-/-}$ MEFs (Fig. 4*C*). Thus, RNF8/UBC13 act together and are required for the concentration of PTIP at or near the sites of DNA breaks.

MLL Complexes May Not Be Involved in DNA Damage Response Together with PTIP·PA1—Recent reports have shown that PTIP associates physically with the mixed lineage leukemia 3 (MLL3)-, and MLL4-containing histone methyltransferases complexes (15, 25) and raised the possibility that similar to PTIP, these MLL complexes might also participate in DNA damage response. To explore a role for MLL complexes in DNA damage response, we first examined whether MLL3 protein or other MLL components would be able to form IRIF. As shown in Fig. 5*A*, neither MLL3 nor UTX, one of component of MLL3 complex, could localize to IRIF. In addition, knockdown of endogenous MLL3 has no effect on PTIP or PA1 IRIF formation (Fig. 5*B*). Moreover, using a gel filtration assay and a common MLL subunit WDR5 as a marker, we detected a distinct subcomplex of PTIP and PA1 that is not associated with MLL complexes (Fig. 5*C*), indicating that separate PTIP pools with different functions are present in the cell. Taken together, we conclude that PTIP participates in DNA damage response in a manner that is largely independent of the MLL protein complexes.

Targeting PTIP to DNA Damage Sites Requires Its BRCT3 and BRCT4 Domains—Previous report have documented that the C-terminal BRCT domains of PTIP are important for its localization to double-strand breaks (19). To fine map the focus localization region of PTIP, we used a series of internal deletion mutants of PTIP. Deletion of the N-terminal BRCT domains (BRCT1 and BRCT2) and the very C-terminal BRCT domains (BRCT5 and BRCT6) as well as the poly glutamine region of PTIP had no effect on PTIP foci formation, whereas deletion of BRCT3 domain or BRCT4 domain abolished PTIP focus localization after IR (Fig. 6*A*). These observations suggest that this pair of BRCT domains, BRCT 3 and BRCT4, is essential for PTIP localization to DNA breaks.

The dependence of PTIP localization on RNF8/UBC13 implies the involvement of an ubiquitin-binding protein in the localization of PTIP. Using ubiquitin-agarose pulldown assay, we showed that PTIP could not bind to ubiquitin (Fig. 6*B*). A previous study has already shown that the tandem BRCT domain (BRCT3/4) of PTIP has phosphopeptide binding activ-

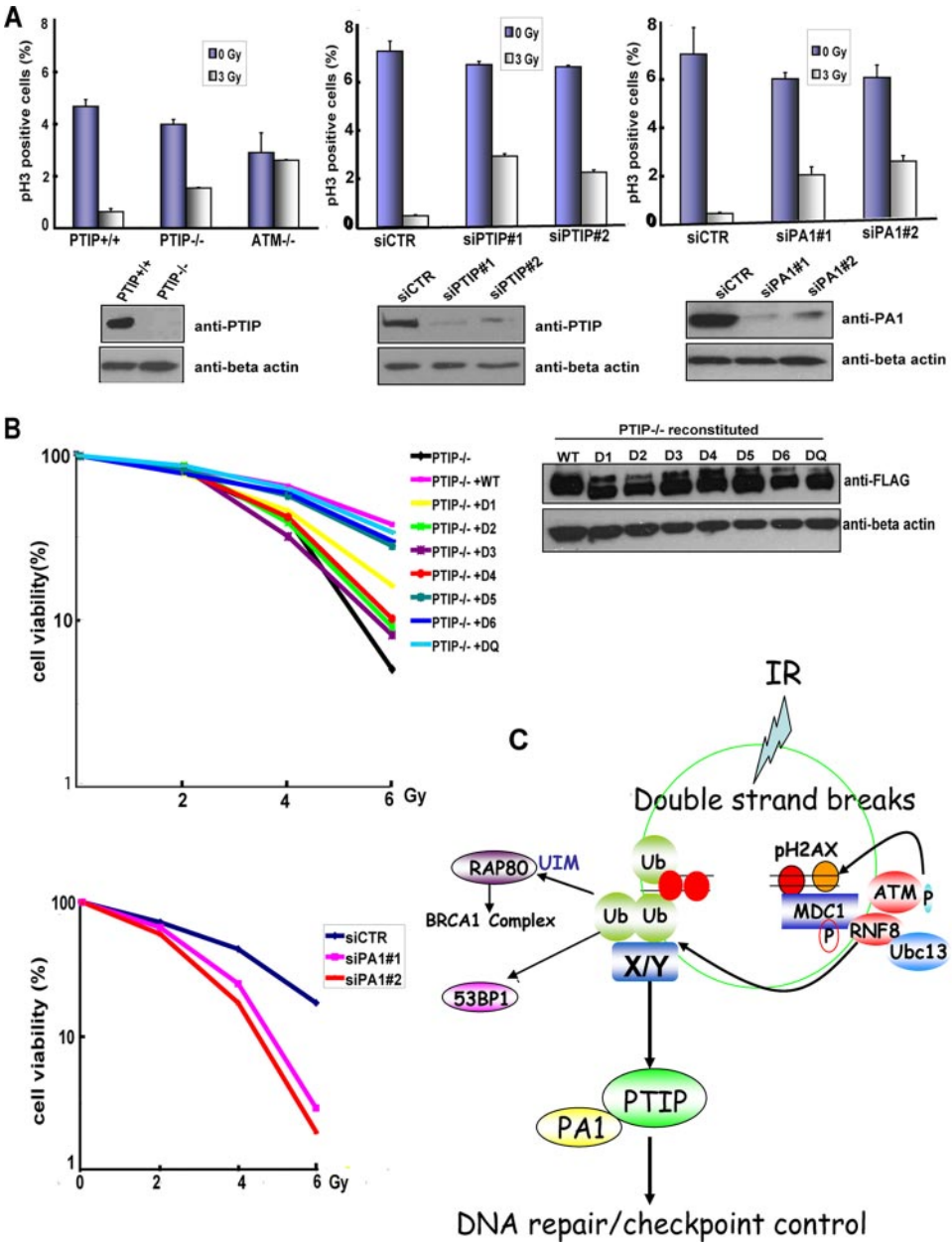

FIGURE 7. **PTIP is important for proper DNA damage response after ionizing radiation.** *A*, PTIP and PA1 play a minor role in G_2/M checkpoint control after DNA damage. $PTIP^{+/+}$, or $PTIP^{-/-}$, and $ATM^{-/-}$ MEFs were mock-treated or irradiated (3 Gy). Similarly, U2OS cells transfected with control siRNA (*siCTR*), PTIP specific siRNAs (*siPTIP#1* and *siPTIP#2*), or PA1-specific siRNAs (*siPA1#1* and *siPA1#2*) were also mock-treated or irradiated. Cells were harvested 1 h later, and a G_2/M checkpoint assay was carried out (see "Materials and Methods"). The percentages of cells stained with phospho-H3 antibody before and after IR treatment were obtained from three individual experiments. *Error bars* indicate S.D. *B*, PTIP and PA1 are required for cell survival after ionizing radiation. $PTIP^{-/-}$ cells were reconstituted with wild-type or various PTIP deletion mutants. Cell survival after irradiation was measured by clonogenic assay according to the "Materials and Methods." The expression of PTIP or its deletion mutants in these cells were confirmed by Western blotting using indicated antibodies (*lower panel*). Similarly, U2OS cells were treated with control or PA1 specific siRNAs. Cell survival after IR was measured by clonogenic assay (*upper panel*), and Western blot analysis was performed to verify the depletion of PA1 after siRNA transfection (*right panel*). *WT*, wild type. *C*, a proposed model of the DNA damage responsive pathway involving PTIP. See "Discussion" for details.

ity (18), suggesting that an unknown phosphorylated protein may be required for PTIP localization after DNA damage. To further confirm that the integrity of this tandem BRCT domain is required for PTIP IRIF formation, we mutated the highly conserved Trp residue on the α3 helix of BRCT domain. We observed normal focus localization of W75R (mutation in BRCT1), W165R (mutation in BRCT2), and W916R (mutation in BRCT6) mutants of PTIP but failed to detect foci formation of PTIP W663R mutant (mutation in BRCT3) after DNA damage (Fig. 6*C*). This is consistent with our deletion analysis and supports that the intact BRCT3/4 pair of PTIP is required for PTIP focus localization in response to DNA damage. Furthermore, in agreement with our hypothesis that PTIP is required for PA1 foci formation, PTIP mutant with deletion of either its BRCT3 or BRCT4 domain failed to target exogenously expressed PA1 to IRIF (supplemental Fig. S2), suggesting that PTIP localization to sites of DNA break is a prerequisite for the damage-induced focus localization of PA1.

Accumulation of PTIP and 53BP1 at DNA Damage Sites Occurs Independently of Each Other—It is well established that PTIP interacts with 53BP1 after IR (18, 19, 26). Because the C-terminal BRCT domains of PTIP have been shown to mediate its interaction with 53BP1 as well as its localization after DNA damage (18, 19, 26), we examined whether PTIP localization would depend on 53BP1. As shown in Fig. 6*D*, PTIP foci formation was similar in $53BP1^{-/-}$ and wild-type MEFs. Likewise, we also found typical 53BP1 localization after IR in $PTIP^{-/-}$ cells, suggesting that although both act downstream of RNF8/UBC13, these two proteins are recruited to DNA damage sites through independent mechanisms.

Using a series of internal deletion mutants of PTIP, we showed that the interaction between PTIP and 53BP1 was abolished by deletion of any of the four C-terminal BRCT domains of PTIP (Fig. 6*E*), suggesting that all four C-terminal BRCT domains of PTIP are indispensable for its interaction with 53BP1. Thus, the requirement for 53BP1 binding is distinctly different from its focus formation, which only requires BRCT3 and BRCT4.

PTIP and PA1 Are Required for Cell Survival after Double-strand Breaks—Although PTIP is clearly involved in DNA damage response, its function in this process remains to be determined. We first examined the role of PTIP in IR-induced

G_2/M checkpoint control. As a control, $ATM^{-/-}$ MEFs displayed a clear defect in IR-induced G_2/M checkpoint (Fig. 7*A*). However, $PTIP^{-/-}$ cells showed modest G_2/M checkpoint deficiency. PTIP knockdown in human cells also led to a partial defect in G_2/M checkpoint control, which is very similar to those observed in cells with PA1 knockdown (Fig. 7*A*), indicating that PTIP and PA1 may play a minor role in this G_2/M checkpoint control after DNA damage.

Next we examined whether PTIP would be required for cell survival after IR. We established $PTIP^{-/-}$ MEF cells that stably express wild-type or various deletion mutants of PTIP as indicated (Fig. 7*B*). Although $PTIP^{-/-}$ cells reconstituted with wild-type PTIP was able to restore cell survival after IR similar to wild-type cells or $PTIP^{-/-}$ cells reconstituted with the BRCT1, BRCT5, BRCT6, or glutamine region deletion mutants of PTIP, $PTIP^{-/-}$ cells reconstituted with the BRCT2, BRCT3, or BRCT4 domain deletion mutants failed to do so (Fig. 7*B*). These results suggest that PTIP is required for cell survival after IR and that the N-terminal BRCT2 domain and C-terminal tandem BRCT3 or BRCT4 domains are critical for this function of PTIP. Similar to PTIP, depletion of PA1 increased IR sensitivity, suggesting that the PTIP·PA1 complex is required for cell survival in response to DNA damage.

DISCUSSION

PTIP is known to be involved in DNA damage response (19, 26). In this study we demonstrated that PTIP acts downstream of the well defined γH2AX·MDC1·RNF8 DNA damage signaling pathway (Fig. 7*C*). The loading of PTIP at DNA damage foci relies on the RNF8/UBC13-dependent protein ubiquitination events. Once at the sites of DNA breaks, PTIP can further load its binding partner PA1 via a direct interaction between PTIP and PA1. Moreover, we showed that the PTIP·PA1 complex is required for cell survival and optimal G_2/M checkpoint control after IR. These studies firmly establish a role of PTIP in the known DNA damage-signaling cascade.

Our study also demonstrated that PTIP is required for cell survival and G_2/M checkpoint control after ionizing radiation, albeit its role in G_2/M checkpoint is limited. Moreover, we show that the focus-localization of PTIP is critical for its function in promoting cell survival following IR and re-enforces a notion that sustained accumulation of DNA damage checkpoint and repair proteins at sites of DNA breaks are important for optimal DNA repair after DNA damage. Currently, we do not know exactly how PTIP accumulates at DNA damage sites. Early studies suggest that RNF8-dependent ubiquitin chains formed at DNA damage sites can serve as docking sites for the recruitment of downstream proteins or protein complexes (7, 11, 12). For instance, ubiquitin-interacting motif-containing protein RAP80 can be recruited to DNA damage sites via its ability to bind to ubiquitin chains and itself serves as an "adaptor" for the further recruitment of BRCA1 (8–10, 13). The focus localization region of PTIP is mapped to a tandem BRCT domain, which is best known for its ability to bind to phosphorylated proteins (18). It is unlikely that this tandem BRCT domain of PTIP would interact directly with ubiquitin chains formed at DNA damage sites. Indeed, we failed to obtain any ubiquitin binding activity of PTIP (Fig. 6*B*). We suspect that PTIP recruitment may be very similar to the recruitment of BRCA1 as discussed above. There is another yet-to-be identified mediator protein that has ubiquitin binding capability similar to RAP80, which allows its own localization to DNA damage sites. This unidentified protein may be phosphorylated and, therefore, recruit PTIP through a direct protein-protein interaction via the PTIP BRCT3/4 domains. The goal in the near future is to identify this and other specific ubiquitin-binding proteins and elucidate how these proteins facilitate DNA damage signal transduction and regulate proteins including PTIP in the DNA damage response.

Besides binding to PA1, PTIP also interacts with 53BP1. In this study we showed that although PTIP and 53BP1 associate with each other (18, 19, 26) and both position downstream of RNF8 in the DNA damage-signaling cascade (7, 11, 12), they localize to sites of DNA damage independently. We speculate that their interaction at DNA damage sites may be important for certain DNA repair process. However, we did not observe an obvious defect in cell survival after ionizing radiation in cells expressing PTIP mutants specifically defective in 53BP1-binding (*e.g.* PTIP BRCT5 or BRCT6 deletion mutants). This could suggest that an interaction between PTIP and 53BP1 may only be essential for a particular repair process (for example, class-switch recombination), and thus, its functional significance cannot be revealed by IR sensitivity assay used here, which measures combined capacity of multiple DNA repair pathways. Indeed, we examined whether PTIP or PA1 would be involved in a particular DNA repair pathway, for example homologous recombination repair. As shown in supplemental Fig. S3, we observed normal damage-induced replication protein A foci formation, Rad51 foci formation, and gene conversion in PTIP- or PA1-depleted cells, suggesting that this complex may not play a major role in homologous recombination repair. We speculate that similar to 53BP1, PTIP·PA1 complex may participate in certain aspect of NHEJ. Further studies using PTIP conditional knock-out mice will reveal whether similar to 53BP1, PTIP (and the PTIP/53BP1 interaction) would be involved in class-switch recombination and/or other specific DNA repair processes.

Acknowledgments—We thank all colleagues in the Chen laboratory, especially Dr. Jun Huang for insightful discussion and technical assistance. We also thank Dr. Michael S. Y. Huen for proofreading the manuscript and the Harvard Taplin Biological Mass Spectrometry Facility for mass spectrometry analysis.

REFERENCES

1. Harper, J. W., and Elledge, S. J. (2007) *Mol. Cell* **28,** 739–745
2. Sancar, A., Lindsey-Boltz, L. A., Unsal-Kacmaz, K., and Linn, S. (2004) *Annu. Rev. Biochem.* **73,** 39–85
3. Zhou, B. B., and Elledge, S. J. (2000) *Nature* **408,** 433–439
4. Rogakou, E. P., Pilch, D. R., Orr, A. H., Ivanova, V. S., and Bonner, W. M. (1998) *J. Biol. Chem.* **273,** 5858–5868
5. Stucki, M., and Jackson, S. P. (2006) *DNA Repair* (*Amst*) **5,** 534–543
6. Lou, Z., Minter-Dykhouse, K., Franco, S., Gostissa, M., Rivera, M. A., Celeste, A., Manis, J. P., van Deursen, J., Nussenzweig, A., Paull, T. T., Alt, F. W., and Chen, J. (2006) *Mol. Cell* **21,** 187–200
7. Huen, M. S., Grant, R., Manke, I., Minn, K., Yu, X., Yaffe, M. B., and Chen,

J. (2007) *Cell* **131,** 901–914
8. Kim, H., Chen, J., and Yu, X. (2007) *Science* **316,** 1202–1205
9. Wang, B., and Elledge, S. J. (2007) *Proc. Natl. Acad. Sci. U. S. A.* **104,** 20759–20763
10. Wang, B., Matsuoka, S., Ballif, B. A., Zhang, D., Smogorzewska, A., Gygi, S. P., and Elledge, S. J. (2007) *Science* **316,** 1194–1198
11. Mailand, N., Bekker-Jensen, S., Faustrup, H., Melander, F., Bartek, J., Lukas, C., and Lukas, J. (2007) *Cell* **131,** 887–900
12. Kolas, N. K., Chapman, J. R., Nakada, S., Ylanko, J., Chahwan, R., Sweeney, F. D., Panier, S., Mendez, M., Wildenhain, J., Thomson, T. M., Pelletier, L., Jackson, S. P., and Durocher, D. (2007) *Science* **318,** 1637–1640
13. Sobhian, B., Shao, G., Lilli, D. R., Culhane, A. C., Moreau, L. A., Xia, B., Livingston, D. M., and Greenberg, R. A. (2007) *Science* **316,** 1198–1202
14. Lechner, M. S., Levitan, I., and Dressler, G. R. (2000) *Nucleic Acids Res.* **28,** 2741–2751
15. Cho, Y. W., Hong, T., Hong, S., Guo, H., Yu, H., Kim, D., Guszczynski, T., Dressler, G. R., Copeland, T. D., Kalkum, M., and Ge, K. (2007) *J. Biol. Chem.* **282,** 20395–20406
16. Patel, S. R., Kim, D., Levitan, I., and Dressler, G. R. (2007) *Dev. Cell* **13,** 580–592
17. Cho, E. A., Prindle, M. J., and Dressler, G. R. (2003) *Mol. Cell Biol.* **23,** 1666–1673
18. Manke, I. A., Lowery, D. M., Nguyen, A., and Yaffe, M. B. (2003) *Science* **302,** 636–639
19. Jowsey, P. A., Doherty, A. J., and Rouse, J. (2004) *J. Biol. Chem.* **279,** 55562–55569
20. Maser, R. S., Zinkel, R., and Petrini, J. H. (2001) *Nat. Genet.* **27,** 417–421
21. Yu, X., Fu, S., Lai, M., Baer, R., and Chen, J. (2006) *Genes Dev.* **20,** 1721–1726
22. Rappold, I., Iwabuchi, K., Date, T., and Chen, J. (2001) *J. Cell Biol.* **153,** 613–620
23. Chini, C. C., Wood, J., and Chen, J. (2006) *Oncogene* **25,** 4165–4171
24. Lou, Z., Minter-Dykhouse, K., Wu, X., and Chen, J. (2003) *Nature* **421,** 957–961
25. Issaeva, I., Zonis, Y., Rozovskaia, T., Orlovsky, K., Croce, C. M., Nakamura, T., Mazo, A., Eisenbach, L., and Canaani, E. (2007) *Mol. Cell. Biol.* **27,** 1889–1903
26. Munoz, I. M., Jowsey, P. A., Toth, R., and Rouse, J. (2007) *Nucleic Acids Res.* **35,** 5312–5322

MERIT40 facilitates BRCA1 localization and DNA damage repair

Lin Feng, Jun Huang and Junjie Chen

Genes Dev. 2009 23: 719-728 originally published online March 4, 2009
Access the most recent version at doi:10.1101/gad.1770609

MERIT40 facilitates BRCA1 localization and DNA damage repair

Lin Feng, Jun Huang, and Junjie Chen[1]

Department of Therapeutic Radiology, Yale University School of Medicine, New Haven, Connecticut 06520, USA

The product of breast cancer susceptibility gene 1, BRCA1, plays pivotal roles in the maintenance of genomic integrity. Mounting evidence indicates that BRCA1 associates with many proteins or protein complexes to regulate diverse processes important for the cellular response to DNA damage. One of these complexes, which mediates the accumulation of BRCA1 at sites of DNA breaks, involves the ubiquitin-binding motif (UIM)-containing protein RAP80, a coiled-coil domain protein CCDC98/Abraxas, and a deubiquitinating enzyme BRCC36. Here we describe the characterization of a novel component of this complex, MERIT40 (Mediator of Rap80 Interactions and Targeting 40 kd), which together with an adaptor protein BRE/BRCC45, enforces the BRCA1-dependent DNA damage response. MERIT40 is assembled into this RAP80/CCDC98-containing complex via its direct interaction with BRE/BRCC45. Importantly, MERIT40 regulates BRCA1 retention at DNA breaks and checkpoint function primarily via a role in maintaining the stability of BRE and this five-subunit protein complex at sites of DNA damage. Together, our study reveals that a stable complex containing MERIT40 acts early in DNA damage response and regulates damage-dependent BRCA1 localization.

[*Keywords:* MERIT40; RAP80; CCDC98/Abraxas; BRE/BRCC45; BRCC36; BRCA1]

Supplemental material is available at http://www.genesdev.org.

Received December 8, 2008; revised version accepted February 2, 2009.

The breast cancer susceptible gene 1 (BRCA1) is a tumor suppressor that plays critical roles in diverse cellular processes that include DNA damage repair, ubiquitination, and transcriptional regulation, and dysregulation of which predisposes women to early onset familial breast and ovarian cancers (Boulton 2006; Mullan et al. 2006; Greenberg 2008; Venkitaraman 2009). Emerging evidence indicates that BRCA1 participates in various tumor-suppressing functions through its ability to form distinct protein complexes in the cell, supporting a multifactorial model in which the concerted actions of these BRCA1 complexes play instrumental roles in the maintenance of genomic stability through regulation of checkpoint activation, DNA repair, and/or other cellular functions.

The BRCA1 protein contains two well-characterized functional domains, namely, its N-terminal RING finger domain, which encodes for its ubiquitin ligase activity (Joazeiro and Weissman 2000; Hashizume et al. 2001; Baer and Ludwig 2002), and a C-terminal tandem BRCT repeat. Importantly, patient mutations have been found within these domains, implicating their importance for BRCA1 function. Notably, its BRCT domain, which constitutes a phosphopeptide recognition domain that binds specifically to phospho-SXXF motifs (Manke et al. 2003; Yu et al. 2003), has been documented to associate with a list of interacting partners. Through this BRCT domain, BRCA1 was recently reported to exist in at least three distinct protein complexes. Our previous work demonstrated that BRCA1 associates with BACH1 (BRCA1-associated C-terminal helicase) (Cantor et al. 2001) in a phosphorylation-dependent manner to mediate S-phase checkpoint control (Manke et al. 2003; Yu et al. 2003). Subsequent studies revealed that the association of BRCA1 with CtIP (CtBP-interacting protein) (Yu et al. 1998; Li et al. 1999) is also phosphorylation-dependent and is important for the BRCA1-dependent G2/M checkpoint control (Yu and Chen 2004). More recently, a coiled-coil domain-containing protein CCDC98/Abraxas was also found to interact with BRCA1, which again is mediated by the binding of BRCA1 BRCT domains with a phosphorylated SXXF motif on CCDC98/Abraxas (Kim et al. 2007b; Liu et al. 2007; Wang et al. 2007). The current working hypothesis is that BACH1 and CtIP are likely to act downstream from or in parallel with BRCA1, and thus they do not contribute to proper BRCA1 localization at DNA damage sites (Greenberg et al. 2006). On the other hand, CCDC98 and its associated proteins RAP80 and BRCC36 are all involved in the recruitment of BRCA1 to DNA damage sites (Chen et al. 2006; Kim et al. 2007a; Sobhian et al. 2007; Wang et al. 2007). This recruitment is controlled by protein ubiquitination at sites of DNA breaks (Polanowska et al. 2006; Zhao et al. 2007) and

[1]**Corresponding author.**
E-MAIL Junjie.chen@yale.edu; FAX (203) 785-7482.
Article published online ahead of print. Article and publication date are online at http://www.genesdev.org/cgi/doi/10.1101/gad.1770609.

relies on a recently identified signaling pathway from pH2AX/MDC1 to an E3 ubiquitin ligase RNF8 (Huen et al. 2007; Kolas et al. 2007; Mailand et al. 2007; Bennett and Harper 2008).

Since RAP80 contains tandem ubiquitin-binding motifs (UIMs), which is required for its localization at DNA damage sites, it is now generally accepted that RAP80 recognizes the ubiquitinated proteins at sites of DNA breaks, which in turn facilitates the recruitment of BRCA1 via a direct interaction between BRCA1 and CCDC98 (Kim et al. 2007a; Sobhian et al. 2007; Wang et al. 2007). In this study, we isolated a multiprotein complex containing RAP80, CCDC98, BRCC36, and BRCA1. We described the identification and characterization of a novel component in this complex, Hspc142 (C19orf62), which participates in RAP80 complex formation and is required for BRCA1 localization, cell cycle checkpoint control, and cell survival following DNA damage. To better reflect its cellular function, we named Hspc142 as MERIT40 (Mediator of Rap80 Interactions and Targeting 40 kd) in the text.

Results

MERIT40 is a novel component of RAP80/CCDC98 complex

Previous studies have reported association between RAP80, CCDC98/Abraxas, BRCC36, and BRCA1 (Kim et al. 2007a; Sobhian et al. 2007; Wang and Elledge 2007; Wang et al. 2007). However, exactly how this complex is assembled in vivo remains elusive. To better understand how the RAP80/CCDC98/BRCC36 protein complex is assembled in the cell, we generated 293T derivative cell lines stably expressing triple-tagged (S-Flag-Streptavidin-binding peptide) RAP80, CCDC98, or BRCC36 with an aim to identify additional components important for the complex formation. Following a tandem affinity purification (TAP) scheme, proteins associated with RAP80, CCDC98, or BRCC36 were identified by mass spectrometry analyses (Fig. 1A, top panel). Interestingly, beside RAP80, CCDC98, and BRCC36, we also identified BRE (brain and reproductive organ-expressed protein) (Li et al. 1995), also known as BRCC45 (Dong et al. 2003)] and an uncharacterized protein, Hspc142 (C19orf62), among the three purified protein complexes. As indicated above, we renamed this protein Hspc142/C19orf62 as MERIT40. To further confirm that MERIT40 and BRE exist in the same complex with RAP80, CCDC98, and BRCC36, we generated stable cells expressing triple-tagged MERIT40 and BRE, respectively. Notably, mass spectrometry analyses of MERIT40 or BRE-associated proteins revealed peptides that corresponded to RAP80, CCDC98, and BRCC36 (Fig. 1A; bottom panel), suggesting that these five proteins likely form a stable complex in vivo.

BRE was previously identified as a subunit in the BRCA1/BRCA2-containing protein complex (Dong et al. 2003), whereas MERIT40 is a 329-amino-acid protein with unknown function. Neither BRE nor MERIT40 has any known functional motif. To verify the association among MERIT40, BRE, BRCC36, and RAP80, we performed coimmunoprecipitation (co-IP) experiments and found that endogenous MERIT40 immunoprecipitated RAP80, BRE, and BRCC36 (Fig. 1B), suggesting that these proteins indeed form a complex in vivo. Because the molecular weight of CCDC98 (~50 KDa) is similar to the immunoglobulin heavy chain, we did not include it in our co-IP experiments. Taken together, our data reveal the presence of a stable RAP80-containing protein complex in the cell and suggest that MERIT40 is a novel component that resides in this complex.

Next, we sought to determine how this complex is assembled in vivo. Ectopically expressed MERIT40 interacted strongly with BRE, but only weakly with other components in co-overexpression experiments (Fig. 1C), indicating that MERIT40 may interact directly with BRE. This observation is consistent with the data obtained from several independent large-scale studies of protein–protein interactions, which suggest that BRE binds to MERIT40 (Rual et al. 2005; Ewing et al. 2007). To determine the region on BRE responsible for its interaction with MERIT40, we generated two BRE truncation mutants. Similar to that between full-length BRE and MERIT40, we observed a robust interaction between the C terminus of BRE (residues 201–383) with MERIT40 (Fig. 1D). Interestingly, while the N terminus (residues 1–200) of BRE is not required for its binding to MERIT40, it is essential for the association of BRE with CCDC98 and BRCC36 (Fig. 1D), suggesting that BRE interacts with MERIT40 and CCDC98/BRCC36 via different regions.

Next, we generated a series of MERIT40 internal deletion mutants to map the BRE-binding domain on MERIT40. Although the very N terminus of MERIT40 is dispensable for the MERIT40/BRE interaction, we found that the C-terminal three-quarters of MERIT40 all seem to be involved in its interaction with BRE (Fig. 1E, top panel), albeit the expression of these C-terminal deletion mutants of MERIT40 is lower than that of wild-type MERIT40 or the N-terminal deletion mutant (Fig. 1E, middle panel). Surprisingly, coexpression of MERIT40 with BRE also stabilized BRE in the cell and this stabilization effect of MERIT40 on BRE correlates with the interaction between the two proteins (Fig. 1E, middle panel). Conversely, MERIT40 stability does not depend on BRE (see also Fig. 3A, below; data not shown).

Interestingly, MERIT40 mutations that disrupted its binding with BRE also abolished the MERIT40–CCDC98 interaction (Fig. 1E, middle panel), which coincided with the regions required for MERIT40 foci formation (Fig. 1E, bottom panel). Together, these data suggest that MERIT40 may be assembled into the RAP80/CCDC98 complex through its association with BRE.

BRE bridges the interaction between MERIT40 and RAP80/CCDC98/BRCC36

Earlier reports have shown that BRCC36 interacts with CCDC98 through the coiled-coil domain of the latter (Wang and Elledge 2007). RAP80 associates with a large region containing N-terminal three-fourths of CCDC98

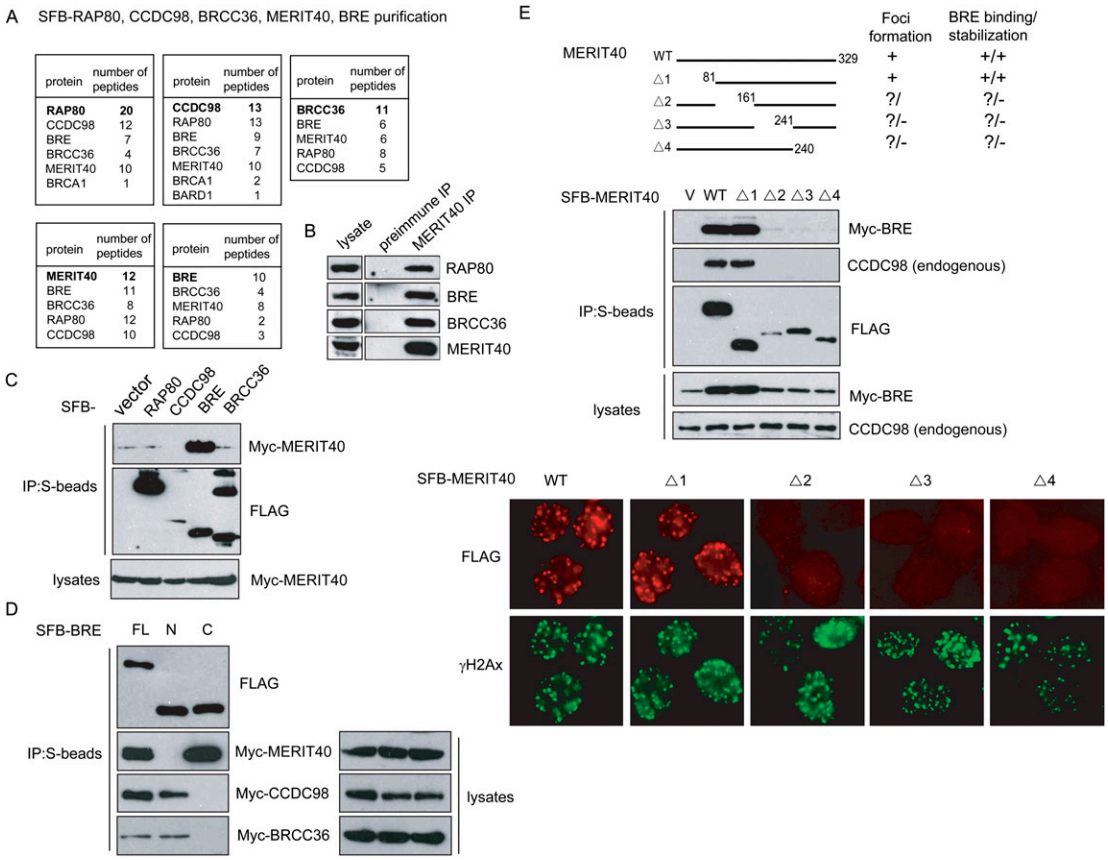

Figure 1. Identification of MERIT40 as a new component in the RAP80/CCDC98 protein complex. (*A*) 293T cells stably expressing SFB-tagged (S-tag, Flag epitope tag, and streptavidin-binding peptide tag)-RAP80, CCDC98, BRCC36, MERIT40, or BRE were used for TAP of protein complexes specifically from chromatin fractions isolated from irradiated cells. Tables are summaries of proteins identified by Mass spectrometry analysis. Letters in bold indicate the bait proteins. (*B*) Immunoprecipitations were performed using preimmune serum or anti-MERIT40 antibodies. Interactions between endogenous MERIT40 and RAP80, BRE, or BRCC36 were assessed by immunoblotting using antibodies as indicated. (*C*) Myc-tagged MERIT40 interacted strongly with SFB-tagged BRE. 293T cells were transiently transfected with plasmids encoding SFB-tagged RAP80, CCDC98, BRE, BRCC36, or empty vector together with plasmids encoding myc-tagged MERIT40. Cell lysates were precipitated with S-protein beads and immunoblotted with indicated antibodies. (*D*) CCDC98, BRCC36, or MERIT40 binds to different regions on BRE. 293T cells were transfected with plasmids encoding SFB-tagged full-length (FL), N-terminal part (N; residues 1–200), or C-terminal part (C; residues 201–383) of BRE, together with plasmids encoding Myc-tagged CCDC98, BRCC36, or BRE. Cell lysates were subjected to precipitation (IP) using S-protein beads, and immunoblotting was conducted using antibodies as indicated. (*E*) MERIT40 associates with BRE and forms IRIF. (*Top* panel) 293T cells were transfected with plasmids encoding SFB-tagged wild-type MERIT40 or its deletion mutants (Δ1–Δ4) together with plasmids encoding Myc-tagged BRE. Co-IP experiments were performed as described in *C*. (*Bottom* panel) 293T cells stably expressing SFB-tagged wild-type (WT) or deletion mutants (Δ1–Δ4) of MERIT40 were irradiated with 10 Gy, allowed to recove for 4 h before fixation and immunostaining with anti-Flag (red) and anti-γH2AX (green) antibodies.

(Kim et al. 2007b; Wang and Elledge 2007), while BRCA1 binds directly to the C-terminal SPTF motif of CCDC98 in a phosphorylation-dependent manner (Kim et al. 2007b; Liu et al. 2007; Wang et al. 2007). Thus, it appears that CCDC98 is at the center of this protein complex. Indeed, the interaction between MERIT40 and CCDC98 seems to correlate with its interaction with BRE (Fig. 1E, middle panel), implying that BRE may bind directly to CCDC98. Therefore, we used a series of CCDC98 mutants to examine how CCDC98 mediates this complex formation (Fig. 2A).

While wild-type CCDC98 binds strongly to BRE, mutations in CCDC98, Δ1, and Δ2 resulted in a loss of the interaction between CCDC98 and BRE/MERIT40 (Fig. 2A). Importantly, although BRE and BRCC36 bound to different regions on CCDC98, both of these regions overlapped with the RAP80-binding domain on CCDC98 (Fig. 2A). We thus investigated whether RAP80 could exist in a single protein complex containing not only CCDC98, but also BRCC36, BRE, and MERIT40. As shown in Figure 2B, all four of these proteins coimmunoprecipited with wild-type RAP80 and RAP80 UIM deletion mutant (Δ1). However, they failed to interact with RAP80Δ3 mutant, which lacks the CCDC98-interacting region (Fig. 2B). These data support the hypothesis that all five of these proteins exist in one protein complex. While

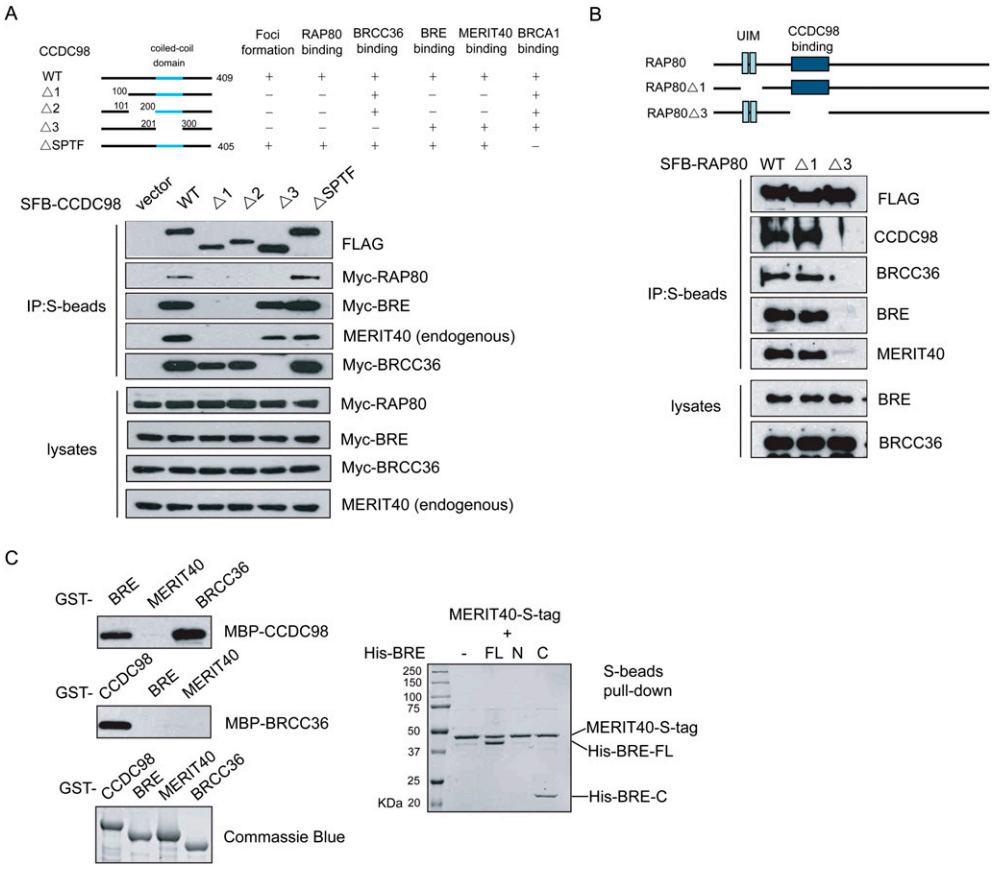

Figure 2. BRE mediates the interaction between MERIT40 and CCDC98. (*A*) RAP80, BRE, and BRCC36 bind to different regions on CCDC98. 293T cells were transfected with plasmids encoding SFB-tagged wild-type or internal deletion mutants of CCDC98 together with plasmids encoding Myc-tagged RAP80, BRE, or BRCC36. Cell lysates were prepared, precipitated with S-protein beads, and immnoblotted with indicated antibodies. (*B*) The CCDC98-interacting region, but not the UIM domains of RAP80 is required for the interaction between RAP80 and BRE, BRCC36, or MERIT40. 293T cells were transiently transfected with plasmids encoding SFB-tagged wild-type RAP80 (WT), UIM deletion mutant (Δ1), or CCDC98-interacting region deletion mutant (Δ3) of RAP80. Cell lysates were subjected to precipitation (IP) with S-protein beads and immunoblotting with indicated antibodies. (*C*, *left* panels) BRE and BRCC36 bind directly to CCDC98 in vitro. Bacterially expressed MBP-tagged CCDC98, BRE, MERIT40, or BRCC36 were incubated with GST fusion proteins as indicated. Proteins bound to the beads were eluted by boiling in SDS sample buffer, separated by SDS-PAGE, and immunoblotted with anti-MBP antibody. GST fusion proteins used in these pull-down assays were analyzed by Commassie blue staining. (*Right* panels) BRE associates with MERIT40 in vitro. S-tagged MERIT40 was coexpressed with His-tagged wild-type or deletion mutants of BRE using bicistronic vectors in BL21 cells. Proteins bound to S-beads were eluted and visualized by Commassie blue staining.

RAP80, BRE, and BRCC36 seem to share overlapping binding regions on CCDC98, they associate with each other in a nonexclusive manner to form a single entity.

Next, we used pull-down assays to further confirm the direct interactions among these proteins. Bacterially expressed and purified MBP-CCDC98 bound directly to GST-BRE and GST-BRCC36, but not to GST-MERIT40 (Fig. 2C). Similarly, GST-CCDC98 was also able to pull down MBP-BRE or MBP-BRCC36 (Fig. 2C), but not MBP-MERIT40 (data not shown), which agrees with our in vivo interaction data. In addition, when BRE and MERIT40 were coexpressed in *Escherichia coli*, they formed a stable complex (Fig. 2C). The association between BRE and MERIT40 in bacteria requires the C terminus of BRE (Fig. 2C), which again confirms our in vivo study (Fig. 1D). These data indicate that MERIT40 binds directly to BRE.

MERIT40 and BRE are required for maintaining the integrity of RAP80/CCDC98 complex

A multicomponent protein complex sometimes relies on one or several of its components for the stability of the protein complex. Therefore, we depleted each one of these subunits in the RAP80/CCDC98 protein complex and examined the stability of other components and also the complex formation under these situations. As shown in Figure 3A, depletion of RAP80, CCDC98, BRE, or BRCC36 did not affect the stability of the remaining four components in this complex. However, while depletion of MERIT40 by siRNA did not affect the steady levels of RAP80, CCDC98, or BRCC36, it led to a dramatic decrease in BRE protein level (Fig. 3A). This suggests that BRE is normally stabilized in vivo by MERIT40, which is

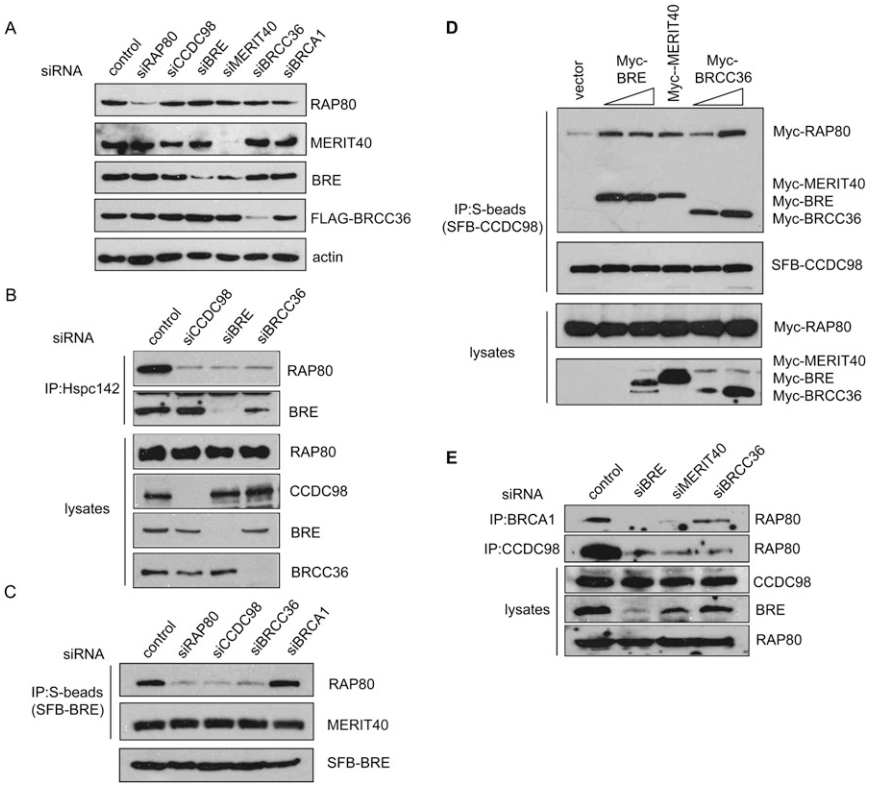

Figure 3. MERIT40 is critical for maintaining the integrity of RAP80/CCDC98-containing protein complex. (*A*) U2OS cells were transfected with a scrambled control siRNA or siRNAs specific for the indicated genes. Cell lysates were prepared and immunoblotted with indicated antibodies. (*B*) CCDC98, BRE, and BRCC36 are required for the association of MERIT40 with RAP80. HeLa cells were transfected with control siRNA or siRNAs targeting CCDC98, BRE, or BRCC36. Cell lysates were immunoprecipitated with antibody against MERIT40, and immunoblotting experiments were carried out using antibodies as indicated. (*C*) CCDC98 and BRCC36 are required for the binding of BRE to RAP80, but are dispensable for BRE/MERIT40 interaction. 293T cells stably expressing SFB-BRE were transfected with control siRNA or siRNAs targeting RAP80, CCDC98, BRCC36, or BRCA1. Cell lysates were immunoprecipitated using anti-MERIT40 antibodies. Immunoblots were performed using antibodies as indicated. (*D*) Overexpression of BRE, MERIT40, or BRCC36 promotes RAP80/CCDC98 interaction. 293T cells were transfected with plasmids encoding SFB-tagged CCDC98 and Myc-tagged RAP80, together with empty vector or variables amount of plasmids encoding Myc-tagged BRE, MERIT40, or BRCC36 as indicated. Cell lysates were prepared, immunoprecipitated with S-protein beads, and immnoblotted with indicated antibodies. (*E*) Depletion of BRE, MERIT40, or BRCC36 impaired endogenous RAP80/CCDC98 or RAP80/BRCA1 interaction. HeLa cells were transfected with control siRNA or siRNAs targeting BRE, MERIT40, or BRCC36. Cell lysates were immunoprecipitated using anti-BRCA1 or anti-CCDC98 antibodies, and immunoblotting was carried out using indicated antibodies.

entirely consistent with our overexpression results shown in Figure 1E.

To further investigate the nature of this complex formation, we immunoprecipitated endogenous MERIT40 from control cells or cells depleted of CCDC98, BRE, or BRCC36. Knockdown of CCDC98 dramatically decreased endogenous RAP80 and MERIT40 interaction (Fig. 3B). In addition, when BRE was depleted, the binding of MERIT40 to RAP80 was also greatly diminished (Fig. 3B), further supporting the hypothesis that MERIT40 is assembled into the RAP80/CCDC98 complex through its interaction with BRE. Strikingly, depletion of BRCC36 also reduced the interaction between MERIT40 and RAP80 (Fig. 3B). Likewise, knockdown of CCDC98 or BRCC36 by siRNAs in 293T cells stably expressing SFB-BRE also led to decreased binding between RAP80 and SFB-BRE, without any detectable change in BRE/MERIT40 association (Fig. 3C). In addition, knockdown of BRE or BRCC36 also led to decreased interaction between SFB-MERIT40 with RAP80 or CCDC98 (Supplemental Fig. 1A). These data imply that the interactions of CCDC98 with BRE/MERIT40 or with BRCC36 influence the whole complex formation.

This notion is supported by the observations that the regions on CCDC98 responsible for BRE and BRCC36 binding overlap with the region required for RAP80 binding (Fig. 2A). It is possible that all of these proteins bind to CCDC98 in a cooperative manner. To test this idea, we determined the complex formation between Myc-RAP80 and SFB-CCDC98 in the absence or the presence of overexpressed BRE, Hpsc142, or BRCC36. Interestingly, overexpression of any of these three proteins (BRE, MERIT40, and BRCC36) resulted in an increased RAP80/CCDC98 interaction (Fig. 3D). Furthermore, knockdown of endogenous BRE, MERIT40, or BRCC36 weakened the interaction between endogenous RAP80 and endogenous CCDC98 or BRCA1 (Fig. 3E), thereby demonstrating that these proteins bind cooperatively to maintain the assembly of a stable protein complex in vivo.

RAP80/CCDC98/BRCC36/BRE/MERIT40 depend on each other for their focus localization following DNA damage

RAP80, CCDC98, BRCC36, and BRCA1 all localize to sites of DNA breaks in cells exposed to ionizing radiation (IR) (Scully et al. 1997; Kim et al. 2007a,b; Liu et al. 2007; Sobhian et al. 2007; Wang et al. 2007). Given that MERIT40 and BRE exist in the RAP80/CCDC98 complex

and that MERIT40 also localizes to damage-induced foci (Fig. 1E), we would like to examine how they influence each other's IR-induced foci (IRIF) formation. As shown in Figure 4, A and B, both endogenous MERIT40 and ectopically expressed BRE formed IRIF, which colocialized with those of the DNA damage marker γH2AX (Fig. 4A,B; Paull et al. 2000), indicating that MERIT40 and BRE indeed localize to DSB sites. As shown in Figure 4, IRIF of BRCC36, RAP80, CCDC98 were significantly decreased in BRE or MERIT40-depleted cells and vice versa, suggesting RAP80/CCDC98/BRCC36/BRE/MERIT40 depend on each other for their IRIF formation. Interestingly, depletion of BRCA1 did not affect the focus formation of any of the four components in the protein complex (Fig. 4), which agrees with previous reports that BRCA1 acts downstream from the RAP80/CCDC98 complex (Kim et al. 2007a,b; Liu et al. 2007; Sobhian et al. 2007; Wang et al. 2007) and that BRCA1 is not a stable component of this protein complex (Fig. 1A).

A stable protein complex consisting of RAP80/CCDC98/BRCC36/BRE/MERIT40 is required for efficient BRCA1 localization and function following DNA damage

RAP80/CCDC98 and BRCC36 are all known to act upstream of BRCA1 and are required for targeting BRCA1 to DNA damage foci (Chen et al. 2006; Kim et al. 2007a,b; Liu et al. 2007; Sobhian et al. 2007; Wang and Elledge 2007; Wang et al. 2007). Since MERIT40 and BRE are components of this five-subunit protein complex and are required for the overall stability and the focus formation of this protein complex following DNA damage, we speculated that MERIT40 and BRE might also be required for BRCA1 foci formation. As shown in Figure 5A, similar to RAP80-, CCDC98-, or BRCC36-depleted cells, BRCA1 IRIF formation was compromised in cells transfected with MERIT40 or BRE siRNAs, suggesting that this protein complex containing MERIT40 and BRE acts

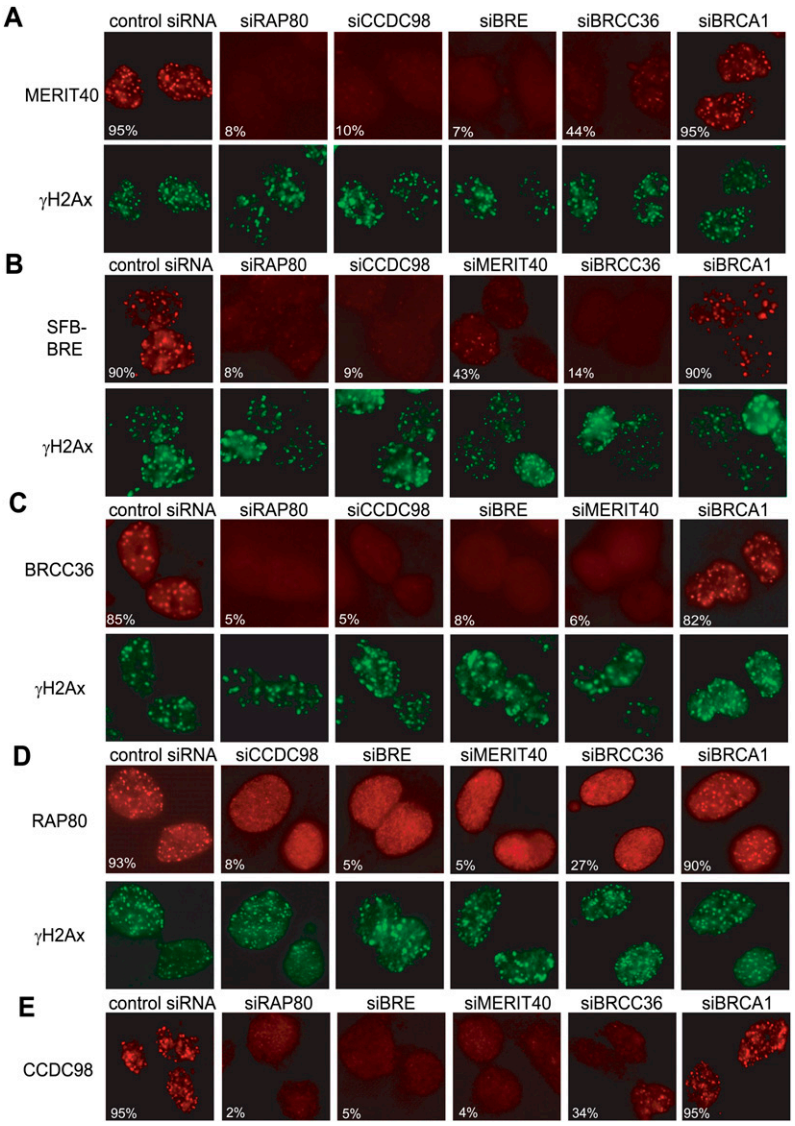

Figure 4. IRIF formation of RAP80, CCDC98, BRCC36, BRE, and MERIT40 requires all four other components in this protein complex. (*A*,*C*–*E*) U2OS cells or 293T cells stably expressing SFB-tagged BRE (*B*) were transfected with control siRNAs or siRNAs specifically targeting indicated genes. Cells were irradiated, fixed, and immunostained with anti-MERIT40 (*A*), anti-Flag (BRE) (*B*), anti-BRCC36 (*C*), anti-RAP80 (*D*), or anti-CCDC98 (*E*) antibodies with or without costaining with anti-γH2AX antibodies. More than 200 cells were counted to determine the percentages of foci-forming cells in each sample.

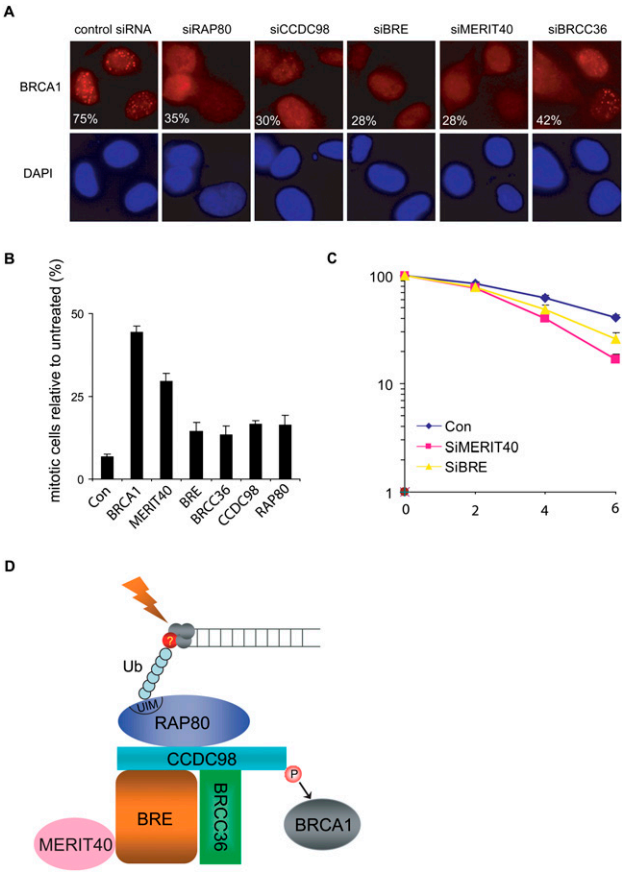

Figure 5. MERIT40 and BRE participate in IR-induced DNA damage response. (*A*) Defective BRCA1 foci formation was observed in RAP80-, CCDC98-, BRE-, MERIT40-, or BRCC36-depleted cells. U2OS cells were transfected with different siRNAs as indicated. Cells were irradiated, fixed, and immunostained with anti-BRCA1 antibody. More than 200 cells were counted to determine the percentages of cells containing BRCA1 foci. Two independent siRNAs were used for the depletion of CCDC98, BRE, BRCC36, or MERIT40, and similar results were obtained (data not shown). (*B*) IR-induced G2/M checkpoint is defective in cells depleted of MERIT40, BRE, or other components in the RAP80/CCDC98 complex. HeLa cells were transfected with indicated siRNAs and percentages of mitotic cells before and after radiation were determined by FACS analysis as described in the Materials and Methods. The figure represents the value obtained from three separate experiments. Error bars indicate standard deviations. (*C*) Cells depleted of MERIT40 or BRE display increased radiation sensitivity. HeLa cells were transfected with control siRNAs or siRNAs specifically targeting indicated genes. Cells were irradiated with various doses of IR. Percentages of surviving colonies were determined 11 d later. Experiments were done in triplicate. Results shown are averages of two or three independent experiments at each dose, and error bars indicate standard deviation. (*D*) A model describing the assembly of the RAP80/CCDC98/BRCC36/BRE/MERIT40 complex at sites of DNA breaks. See the text for details.

upstream of BRCA1 in the DNA damage response pathway. We used a second MERIT40 siRNA and observed similar reduction of RAP80 and BRCA1 foci formation following DNA damage (Supplemental Fig. 1B). In addition, MERIT40 or BRE depletion led to a defective G2/M checkpoint control (Fig. 5B) and reduced cell survival following IR (Fig. 5C; also see Supplemental Fig. 1C), highlighting the importance of these subunits in regulating BRCA1 and cellular response to DNA damage.

Discussion

In this study, we adopted the TAP approach to isolate RAP80/CCDC98-containing protein complex and identified a novel component, MERIT40, in this complex. Similar to RAP80 and CCDC98, MERIT40 localizes to sites of DNA break, participates in G2/M checkpoint control, and promotes cell survival following DNA damage, suggesting that MERIT40 is an important factor within the RAP80 complex that plays crucial roles in the DNA damage response. More importantly, we analyzed the RAP80/CCDC98 protein complex in great detail. Our data suggest that this RAP80/CCDC98 complex consists of five core subunits (Fig. 5D), with CCDC98 as the central component that facilitates the assembly of this protein complex. CCDC98 binds to RAP80 via a large N-terminal region (Kim et al. 2007b; Wang and Elledge 2007) and interacts with the DUB BRCC36 through its C-terminal coiled-coil domain (Wang and Elledge 2007). CCDC98 also directly interacts with BRE/BRCC45 via its N terminus. While MERIT40 does not associate directly with CCDC98, it is brought into this complex through its interaction with BRE. We were able to reconstitute this five-protein complex in vitro using baculovirus expression system (Supplemental Fig. 1D). Interestingly, we showed that a stable complex formation among these five subunits is not only required for their own IRIF formation, but is also involved in the recruitment of BRCA1 to the sites of DNA breaks. Previous studies indicated that the very C terminus of CCDC98 is phosphorylated and directly recruits BRCA1 (Kim et al. 2007b; Liu et al. 2007; Wang et al. 2007). Here, we showed that in the absence of MERIT40, BRE, or BRCC36, we also observed a significant reduction in BRCA1 foci formation. This is mediated by the destabilization of this protein complex, especially by the reduced interaction between RAP80 and CCDC98 in cells missing any one of these components (Fig. 3).

Early studies have already suggested that the localization of this RAP80/CCDC98-containing protein complex to DNA damage sites requires the interaction between the RAP80 UIM domain and ubiquitin chains formed at the sites of DNA breaks (Kim et al. 2007a,b; Liu et al. 2007; Sobhian et al. 2007; Wang and Elledge 2007; Wang et al. 2007). Intriguingly, we observed that depletion of any one of the four other components beside RAP80 also greatly reduced RAP80 focus formation (Fig. 4), a phenomenon that was also noticed in an early study in cells with CCDC98 depletion (Wang and Elledge 2007). Exactly how these proteins, of which their IRIF formation all depend on RAP80, can also feedback and influence RAP80 DSB localization is still elusive. One plausible explanation is that the stable complex formation among

these proteins may lead to important conformational changes that enhance the interaction between RAP80 and the ubiquitination chains formed at the sites of DNA breaks. An alternative but not exclusive explanation could be that there is a second chromatin-binding protein that exists in this complex that may facilitate the stable accumulation of the entire complex at or near the sites of DNA breaks. Another interesting phenomenon is that while RAP80 IRIF can be easily detected, we have to use a pre-extraction method to visualize BRE/MERIT40 and BRCC36 foci formation. This implies that only a fraction of cellular BRE/MERIT40 and BRCC36 localizes to the sites of DNA breaks, raising the possibility that BRE/MERIT40 and BRCC36 may also have other functions in the cell.

A prominent feature of the recently advanced DNA damage signaling pathway that involves BRCA1 is the presence of many ubiquitination and presumably deubiquitination events. Several groups, including ourselves, have shown that an E3 ligase RNF8 localizes to DNA damage sites and probably initiates K63-linked ubiquitin chains at the vicinity of DNA breaks (Bennett and Harper 2008; Yan and Jetten 2008). This initiation ubiquitination event is believed to lead to the accumulation of a RAP80-containing complex to the sites of DNA damage, at least in part, via a direct interaction between protein ubiquitination chains and the RAP80 UIM domains. There are several additional ubiquitination-related events after that. First, the BRCA1/BARD1 heterodimer is a ubiquitin ligase that promotes K6-linked protein ubiquitination and has a number of substrates including CtIP involved in DNA damage response (Morris and Solomon 2004; Yu et al. 2006). Second, BRCC36 is a deubiquitinating enzyme that specifically hydrolyzes K63-linked polyubiquitination chains, but not K48-linked polyubiquitin chains (Sobhian et al. 2007). Third, an early study has also suggested that BRCC36 may facilitate BRCA1 ubiquitin ligase activity (Dong et al. 2003). Putting these together, an attractive model is that there may be a ubiquitin-editing event that occurs at or near the sites of DNA breaks, which could be similar to the case of A20 in the NF-κB pathway (Wertz et al. 2004; Balakirev and Wilkinson 2008). Such editing activity may be mediated by BRCC36 and thus convert the initial K63-linked polyubiquitination chains to BRCA1-dependent, K6-linked polyubiquitination chains for subsequent accumulation of yet-to-be-identified DNA damage checkpoint and repair proteins. Future studies will be conducted to test this hypothesis.

It is also noteworthy to mention that checkpoint defect or IR sensitivity observed in cells that are deficient of RAP80 or any other component in this five-subunit protein complex are usually not as severe as those observed in BRCA1-deficient cells. In addition, incomplete BRCA1 localization at laser-induced DSBs still occurs in the absence of RAP80 (Sobhian et al. 2007). This agrees with an early study suggesting that transient BRCA1 localization at DNA damage sites can occur in the absence of H2AX (Celeste et al. 2003). All of these point out that the possibility of a parallel pathway that acts cooperatively with the H2AX/MDC1/RNF8/RAP80 pathway to regulate the localization and function of BRCA1 in response to DNA damage.

Materials and methods

Cell culture and IR

U2OS, 293T, and HeLa cells were maintained in RMPI 1640 supplemented with 10% fetal bovine serum. Cells were irradiated using JL Spepherd ^{137}Cs radiation source at indicated doses. Irradiated cells were then returned to culture conditions and maintained for the indicated periods of time specified in the figure legends.

TAP

293T cells were transfected with plasmids encoding SFB-tagged RAP80, CCDC98, MERIT40, BRE, or BRCC36, respectively, to establish stable cell lines expressing their corresponding tagged proteins. Cells were irradiated (10 Gy) and harvested 4 h later. Cells were lysed in NETN buffer (20 mM Tris-Hcl at pH 8.0, 100 mM NaCl, 1 mM EDTA, 0.5% Nonidet P-40) containing 50 mM β-glycerophosphate, 10 mM NaF, and 1 μg/mL each of pepstatin A and aprotinin. Following centrifugation, the pellet was sonicated for 40 sec in high-salt solution (20 mM HEPES at pH 7.8, 0.4 M NaCl, 1 mM EDTA, 1 mM EGTA, protease inhibitor) to extract chromatin-bound proteins fractions. The supernatants were cleared at 14,000 rpm to remove debris and then incubated with streptavidin-conjugated beads (Amersham) for 1 h at 4°C. The immunocomplexes were washed three times with NETN buffer and then bead-bound proteins were eluted with NETN buffer containing 2 mg/mL biotin (Sigma). The elutes were incubated with S protein beads (Novagen). After three washes, the immunocomplexes were analyzed by SDS-PAGE, and Mass spectrometry analyses were performed by the Harvard Medical School Taplin Biological Mass Spectrometry facility.

SiRNA, transfection and immunoprecipitation

All siRNAs were synthesized by Dharmacon, Inc. The siRNAs were 21 base pairs and sequences are as follows: MERIT40 siRNA, CAGAGAACGUGCAGACGAUdTdT; BRCC45 siRNA, GAGGAUAACUGACUUAAAAdTdT; BRCC36 siRNA, CAUAAUGGCUCAGUGUUUAdTdT; RAP80 siRNA, GAAGGAUGUGGAAACUACCdTdT; CCDC98 siRNA, ACACAAGACAAACGAUCUAUU; BRCA1 siRNA, UCACAGUGUCCUUUAUGUAdTdT; and control siRNA, UUCAAUAAAUUCUUGAGGUdTdT.

Plasmid transfection was performed using Lipofectamine2000 (Invitrogen). Oligofectamine (Invitrogen) was used for siRNA transfection. U2OS or HeLa cells were transfected with siRNA duplexes twice at 24-h intervals, while 293T cells were transfected with siRNAs three times at 24-h intervals. Twenty-four hours after the last transfection, cells were collected or irradiated.

Cell lysates and immunoprecipitation were performed similar to that described previously (Kim et al. 2007b), except that cell extracts were prepared using NETN buffer containing higher salt concentration (400 mM NaCl).

Antibodies

Anti-Flag and anti-actin antibodies were purchased from Sigma. Anti-phospho-H3 antibody was purchased from Upstate Biotechnologies. Anti-Myc monoclonal antibody, anti-MBP antibody, and anti-BRCC36 polyclonal antibody were obtained from Santa

Cruz Biotechnologies, New England Biolabs, and ProSci, Inc., respectively. RAP80, CCDC98, and BRCA1 polyclonal antibodies have been described previously (Kim et al. 2007b). Rabbit anti-MERIT40 and anti-BRE antisera were raised by immunizing rabbits, respectively, with GST-MERIT40 (residues 130–329) and GST-BRE (residues 1–200) fusion proteins expressed and purified from *E. coli*. Antisera were affinity-purified using AminoLink Plus Immobilization and Purification Kit (Pierce).

Pull-down assay

GST- or MBP-fused CCDC98, BRE, MERIT40, and BRCC36 were expressed in BL21 cells (Novagen). GST fusion proteins were purified with glutathione Sepharose beads (Amersham Biosciences) according to the manufacturer's instructions. MBP fusion proteins were purified with Amylose beads (New England Biolabs) according to the manufacturer's instructions. For pull-down assay, 1 μg of maltose-eluted MBP fusion proteins were incubated with GST fusion proteins in NETN buffer for 2 h at 4°C. Beads were washed five times with NETN buffer. Proteins bound to the beads were separated by SDS-PAGE and analyzed by Western blotting or Coomassie Blue staining as indicated in the figure legends. For coexpression of MERIT40 with wild-type or deletion mutants of BRE, the corresponding coding sequences were cloned into pETduet-1 vector (Novagen). Bacterial expression and purification were performed according to the manufacturer's instructions (Novagen).

Immunofluorescent staining

Cells grown on coverslips were fixed with 3% paraformaldehyde at room temperature for 20 min and then permeabilized with PBS containing 0.5% Triton X-100 for 5 min at room temperature. The coverslips were blocked with PBS containing 5% goat serum for 30 min at room temperature before incubation with indicated primary antibodies for 1 h at room temperature. After extensive washing at least three times with PBS, cells were incubated with secondary antibodies (FITC-conjugated goat anti-mouse IgG, rhodamine-conjugated goat anti-rabbit IgG, or rhodamine-conjugated goat anti-mouse IgG; Jackson Immuno-Reserach Laboratories, Inc.) for 1 h at room temperature. DAPI (4, 6-diamidino-2-phenylindole) was used to counterstain the nuclei. After a final wash with PBS, coverslips were mounted with glycerin containing p-phenylenediamine. All images were obtained with a Nikon ECLIPSE E800 fluorescence microscope.

G2/M checkpoint assay

HeLa cells in a 35-mm plate were transfected twice with control siRNA or siRNAs specifically targeting RAP80, CCDC98, BRCC45, BRCC36, MERIT40, or BRCA1 at 24-h intervals. Twenty-four hours after the second siRNA transfection, cells were transferred into 100-mm dishes. Cells were incubated for another 24 h before they were mock treated or irradiated using a JL Spepherd 137Cs radiation source at indicated doses. One hour after irradiation, cells were fixed with 70% ethanol for 24 h at −20°C. Cells were then stained with rabbit anti-phosphohistone H3 antibody (pH3), followed by incubation with FITC-conjugated goat anti-rabbit immunoglobulin secondary antibody. The stained cells were treated with RNaseA, incubated with propidium iodide, and then analyzed by flow cytometry to determine the percentages of mitotic cells.

Colony-forming assay

HeLa cells in a 35-mm plate were transfected twice with control siRNA or siRNAs specifically targeting RAP80, CCDC98, BRCC45, BRCC36, MERIT40, or BRCA1, similar to that mentioned above. Twenty-four hours after the second transfection, cells were split and transferred into 60-mm dishes. Cells were incubated for 24 h before they were irradiated using a JL Spepherd ^{137}Cs radiation source at various doses. Eleven days after irradiation, cells were washed with PBS, fixed, and stained with 2% methylene blue, and the numbers of colonies were determined.

Acknowledgments

We thank all colleagues in J.C.'s laboratory, especially Dr. Michael S.Y. Huen, for insightful discussion, technical assistance, and proofreading of this manuscript. We also thank Dr. Roger Greenberg at the University of Pennsylvania for sharing unpublished observations. This work was supported in part by grants from the National Institutes of Health (CA089239 and CA092312 to J.C.). J.C is a recipient of an Era of Hope Scholar award from the Department of Defense and is a member of the Mayo Clinic Breast SPORE program.

References

Baer, R. and Ludwig, T. 2002. The BRCA1/BARD1 heterodimer, a tumor suppressor complex with ubiquitin E3 ligase activity. *Curr. Opin. Genet. Dev.* **12:** 86–91.

Balakirev, M.Y. and Wilkinson, K.D. 2008. OTU takes the chains OUT. *Nat. Chem. Biol.* **4:** 227–228.

Bennett, E.J. and Harper, J.W. 2008. DNA damage: Ubiquitin marks the spot. *Nat. Struct. Mol. Biol.* **15:** 20–22.

Boulton, S.J. 2006. BRCA1-mediated ubiquitylation. *Cell Cycle* **5:** 1481–1486.

Cantor, S.B., Bell, D.W., Ganesan, S., Kass, E.M., Drapkin, R., Grossman, S., Wahrer, D.C., Sgroi, D.C., Lane, W.S., Haber, D.A., et al. 2001. BACH1, a novel helicase-like protein, interacts directly with BRCA1 and contributes to its DNA repair function. *Cell* **105:** 149–160.

Celeste, A., Fernandez-Capetillo, O., Kruhlak, M.J., Pilch, D.R., Staudt, D.W., Lee, A., Bonner, R.F., Bonner, W.M., and Nussenzweig, A. 2003. Histone H2AX phosphorylation is dispensable for the initial recognition of DNA breaks. *Nat. Cell Biol.* **5:** 675–679.

Chen, X., Arciero, C.A., Wang, C., Broccoli, D., and Godwin, A.K. 2006. BRCC36 is essential for ionizing radiation-induced BRCA1 phosphorylation and nuclear foci formation. *Cancer Res.* **66:** 5039–5046.

Dong, Y., Hakimi, M.A., Chen, X., Kumaraswamy, E., Cooch, N.S., Godwin, A.K., and Shiekhattar, R. 2003. Regulation of BRCC, a holoenzyme complex containing BRCA1 and BRCA2, by a signalosome-like subunit and its role in DNA repair. *Mol. Cell* **12:** 1087–1099.

Ewing, R.M., Chu, P., Elisma, F., Li, H., Taylor, P., Climie, S., McBroom-Cerajewski, L., Robinson, M.D., O'Connor, L., Li, M., et al. 2007. Large-scale mapping of human protein–protein interactions by mass spectrometry. *Mol. Syst. Biol.* **3:** 89. doi: 10.1038/msb4100134.

Greenberg, R.A. 2008. Recognition of DNA double strand breaks by the BRCA1 tumor suppressor network. *Chromosoma* **117:** 305–317.

Greenberg, R.A., Sobhian, B., Pathania, S., Cantor, S.B., Nakatani, Y., and Livingston, D.M. 2006. Multifactorial contributions to an acute DNA damage response by BRCA1/BARD1-containing complexes. *Genes & Dev.* **20:** 34–46.

Hashizume, R., Fukuda, M., Maeda, I., Nishikawa, H., Oyake, D., Yabuki, Y., Ogata, H., and Ohta, T. 2001. The RING heterodimer BRCA1-BARD1 is a ubiquitin ligase inactivated

by a breast cancer-derived mutation. *J. Biol. Chem.* **276:** 14537–14540.

Huen, M.S., Grant, R., Manke, I., Minn, K., Yu, X., Yaffe, M.B., and Chen, J. 2007. RNF8 transduces the DNA-damage signal via histone ubiquitylation and checkpoint protein assembly. *Cell* **131:** 901–914.

Joazeiro, C.A. and Weissman, A.M. 2000. RING finger proteins: Mediators of ubiquitin ligase activity. *Cell* **102:** 549–552.

Kim, H., Chen, J., and Yu, X. 2007a. Ubiquitin-binding protein RAP80 mediates BRCA1-dependent DNA damage response. *Science* **316:** 1202–1205.

Kim, H., Huang, J., and Chen, J. 2007b. CCDC98 is a BRCA1–BRCT domain-binding protein involved in the DNA damage response. *Nat. Struct. Mol. Biol.* **14:** 710–715.

Kolas, N.K., Chapman, J.R., Nakada, S., Ylanko, J., Chahwan, R., Sweeney, F.D., Panier, S., Mendez, M., Wildenhain, J., Thomson, T.M., et al. 2007. Orchestration of the DNA-damage response by the RNF8 ubiquitin ligase. *Science* **318:** 1637–1640.

Li, L., Yoo, H., Becker, F.F., Ali-Osman, F., and Chan, J.Y. 1995. Identification of a brain- and reproductive-organs-specific gene responsive to DNA damage and retinoic acid. *Biochem. Biophys. Res. Commun.* **206:** 764–774.

Li, S., Chen, P.L., Subramanian, T., Chinnadurai, G., Tomlinson, G., Osborne, C.K., Sharp, Z.D., and Lee, W.H. 1999. Binding of CtIP to the BRCT repeats of BRCA1 involved in the transcription regulation of p21 is disrupted upon DNA damage. *J. Biol. Chem.* **274:** 11334–11338.

Liu, Z., Wu, J., and Yu, X. 2007. CCDC98 targets BRCA1 to DNA damage sites. *Nat. Struct. Mol. Biol.* **14:** 716–720.

Mailand, N., Bekker-Jensen, S., Faustrup, H., Melander, F., Bartek, J., Lukas, C., and Lukas, J. 2007. RNF8 ubiquitylates histones at DNA double-strand breaks and promotes assembly of repair proteins. *Cell* **131:** 887–900.

Manke, I.A., Lowery, D.M., Nguyen, A., and Yaffe, M.B. 2003. BRCT repeats as phosphopeptide-binding modules involved in protein targeting. *Science* **302:** 636–639.

Morris, J.R. and Solomon, E. 2004. BRCA1: BARD1 induces the formation of conjugated ubiquitin structures, dependent on K6 of ubiquitin, in cells during DNA replication and repair. *Hum. Mol. Genet.* **13:** 807–817.

Mullan, P.B., Quinn, J.E., and Harkin, D.P. 2006. The role of BRCA1 in transcriptional regulation and cell cycle control. *Oncogene* **25:** 5854–5863.

Paull, T.T., Rogakou, E.P., Yamazaki, V., Kirchgessner, C.U., Gellert, M., and Bonner, W.M. 2000. A critical role for histone H2AX in recruitment of repair factors to nuclear foci after DNA damage. *Curr. Biol.* **10:** 886–895.

Polanowska, J., Martin, J.S., Garcia-Muse, T., Petalcorin, M.I., and Boulton, S.J. 2006. A conserved pathway to activate BRCA1-dependent ubiquitylation at DNA damage sites. *EMBO J.* **25:** 2178–2188.

Rual, J.F., Venkatesan, K., Hao, T., Hirozane-Kishikawa, T., Dricot, A., Li, N., Berriz, G.F., Gibbons, F.D., Dreze, M., Ayivi-Guedehoussou, N., et al. 2005. Towards a proteome-scale map of the human protein–protein interaction network. *Nature* **437:** 1173–1178.

Scully, R., Chen, J., Ochs, R.L., Keegan, K., Hoekstra, M., Feunteun, J., and Livingston, D.M. 1997. Dynamic changes of BRCA1 subnuclear location and phosphorylation state are initiated by DNA damage. *Cell* **90:** 425–435.

Sobhian, B., Shao, G., Lilli, D.R., Culhane, A.C., Moreau, L.A., Xia, B., Livingston, D.M., and Greenberg, R.A. 2007. RAP80 targets BRCA1 to specific ubiquitin structures at DNA damage sites. *Science* **316:** 1198–1202.

Venkitaraman, A.R. 2009. Linking the cellular functions of *BRCA* genes to cancer pathogenesis and treatment. *Annu. Rev. Pathol.* **4:** 461–487.

Wang, B. and Elledge, S.J. 2007. Ubc13/Rnf8 ubiquitin ligases control foci formation of the Rap80/Abraxas/Brca1/Brcc36 complex in response to DNA damage. *Proc. Natl. Acad. Sci.* **104:** 20759–20763.

Wang, B., Matsuoka, S., Ballif, B.A., Zhang, D., Smogorzewska, A., Gygi, S.P., and Elledge, S.J. 2007. Abraxas and RAP80 form a BRCA1 protein complex required for the DNA damage response. *Science* **316:** 1194–1198.

Wertz, I.E., O'Rourke, K.M., Zhou, H., Eby, M., Aravind, L., Seshagiri, S., Wu, P., Wiesmann, C., Baker, R., Boone, D.L., et al. 2004. De-ubiquitination and ubiquitin ligase domains of A20 downregulate NF-κB signalling. *Nature* **430:** 694–699.

Yan, J. and Jetten, A.M. 2008. RAP80 and RNF8, key players in the recruitment of repair proteins to DNA damage sites. *Cancer Lett.* **271:** 179–190.

Yu, X. and Chen, J. 2004. DNA damage-induced cell cycle checkpoint control requires CtIP, a phosphorylation-dependent binding partner of BRCA1 C-terminal domains. *Mol. Cell. Biol.* **24:** 9478–9486.

Yu, X., Wu, L.C., Bowcock, A.M., Aronheim, A., and Baer, R. 1998. The C-terminal (BRCT) domains of BRCA1 interact in vivo with CtIP, a protein implicated in the CtBP pathway of transcriptional repression. *J. Biol. Chem.* **273:** 25388–25392.

Yu, X., Chini, C.C., He, M., Mer, G., and Chen, J. 2003. The BRCT domain is a phospho-protein binding domain. *Science* **302:** 639–642.

Yu, X., Fu, S., Lai, M., Baer, R., and Chen, J. 2006. BRCA1 ubiquitinates its phosphorylation-dependent binding partner CtIP. *Genes & Dev.* **20:** 1721–1726.

Zhao, G.Y., Sonoda, E., Barber, L.J., Oka, H., Murakawa, Y., Yamada, K., Ikura, T., Wang, X., Kobayashi, M., Yamamoto, K., et al. 2007. A critical role for the ubiquitin-conjugating enzyme Ubc13 in initiating homologous recombination. *Mol. Cell* **25:** 663–675.

nature cell biology

Protein kinase DYRK2 is a scaffold that facilitates assembly of an E3 ligase

Subbareddy Maddika[1] and Junjie Chen[1,2]

Protein kinases have central functions in various cellular signal transduction pathways through their substrate phosphorylation. Here we show that a protein kinase, DYRK2, has unexpected role as a scaffold for an E3 ubiquitin ligase complex. DYRK2 associates with an E3 ligase complex containing EDD, DDB1 and VPRBP proteins (EDVP complex). Strikingly, DYRK2 serves as a scaffold for the EDVP complex, because small-interfering-RNA-mediated depletion of DYRK2 disrupts the formation of the EDD–DDB1–VPRBP complex. Although the kinase activity of DYRK2 is dispensable for its ability to mediate EDVP complex formation, it is required for the phosphorylation and subsequent degradation of its downstream substrate, katanin p60. Collectively, our results reveal a new type of E3-ubiquitin ligase complex in humans that depends on a protein kinase for complex formation as well as for the subsequent phosphorylation, ubiquitylation and degradation of their substrates.

DYRK2 is a member of an evolutionarily conserved family of dual-specificity tyrosine-phosphorylation-regulated kinases (DYRKs) that belongs to the CMGC group of protein kinases[1,2]. During protein synthesis, DYRK2 autophosphorylates a tyrosine residue in its own activation loop. Once autophosphorylated at this tyrosine residue, DYRK2 loses its tyrosine kinase activity and functions only as a serine/threonine kinase[3]. DYRK2 phosphorylates a very limited number of substrates such as NFAT[4], eIFB[5], Glycogen synthase[6], Oma-1 (ref. 7), MEI-1 (ref. 8) and the chromatin remodelling factors SNR1 and TRX[9], thus regulating calcium signalling, protein synthesis, glucose metabolism, developmental processes and gene expression. Recently, DYRK2 has also been suggested to function in the DNA damage signalling pathway by phosphorylating p53 at serine 46 in the nucleus and promoting cellular apoptosis after genotoxic stress[10]. In addition to its role in cellular responses and developmental processes, DYRK2 is a potential oncogene[11], because DYRK2 amplification and overexpression have been reported in adenocarcinomas of the oesophagus and lung[12]. However, the exact mechanism of DYRK2 in tumorigenesis remains to be clarified.

RESULTS

DYRK2 associates with EDVP E3 ligase complex

In an attempt to elucidate DYRK2 function further, we established 293T derivative cell line stably expressing a triple-epitope (S-protein, Flag and streptavidin-binding peptide)-tagged version of DYRK2 (SFB–DYRK2). Tandem affinity purification with streptavadin-agarose beads and S-protein-agarose beads followed by mass spectrometry analysis allowed us to discover several proteins that interacted with DYRK2 (Fig. 1a and Supplementary Information, Table S1). Among them we repeatedly identified EDD, DDB1 and VPRBP as major DYRK2-associated proteins (Fig. 1a). EDD (also known as UBR5, hHYD or KIAA0896) is an E3 ligase with a distinct amino-terminal UBA domain, a UBR box and a carboxy-terminal HECT domain that mediates ubiquitin-dependent protein degradation[13,14]. EDD is likely to be involved in tumorigenesis, because an allelic imbalance at the EDD locus has been reported in several cancers[15,16]. DDB1 (DNA-damage binding protein 1)[17] is an adaptor subunit of the Cul4–Roc1 E3 ligase complex[18] that mediates the ubiquitin-dependent degradation of various substrates including Cdt1, $p21^{Cip1/WAF1}$ and c-Jun. VPRBP (also known as DCAF1)[19,20], a WD40-domain-containing protein, is a substrate recognition subunit of the DDB1–Cul4A–Roc1 complex.

By transient overexpression of SFB–DYRK2 in 293T cells, we confirmed the interaction of DYRK2 *in vivo* with EDD, DDB1 and VPRBP (Fig. 1b). Although DDB1 and VPRBP have been discovered recently as key components in the Cul4–Roc1 E3 ligase complex[18,21,22], surprisingly we did not identify either Cul4 or Roc1 in our purification. Indeed, we could not detect any interaction of overexpressed DYRK2 with either Cul4A or Roc1 (Fig. 1b), confirming that Cul4 and Roc1 are not components of this novel complex, which contains DYRK2, EDD, DDB1 and VPRBP. We further confirmed the existence of this complex *in vivo* by demonstrating that endogenous DYRK2 co-immunoprecipitated with EDD, DDB1 and VPRBP (Fig. 1c). In contrast, Cul4A–Roc1 components were not seen in EDD immunoprecipitates (Fig. 1c). However, neither EDD nor DYRK2 was seen in Cul4A immunoprecipitates, supporting the notion that the presence of the EDVP complex is independent of the Cul4A–Roc1 complex (Fig. 1c). The interactions between EDD, DDB1 and VPRBP with DYRK2 are specific, because we could only observe

[1]Department of Therapeutic Radiology, Yale University School of Medicine, PO Box 208040, New Haven, Connecticut 06520, USA.
[2]Correspondence should be addressed to J.C. (e-mail: junjie.chen@yale.edu)

Received 22 October 2008; accepted 4 December 2008; published online 15 March 2009; DOI:10.1038/ncb1848

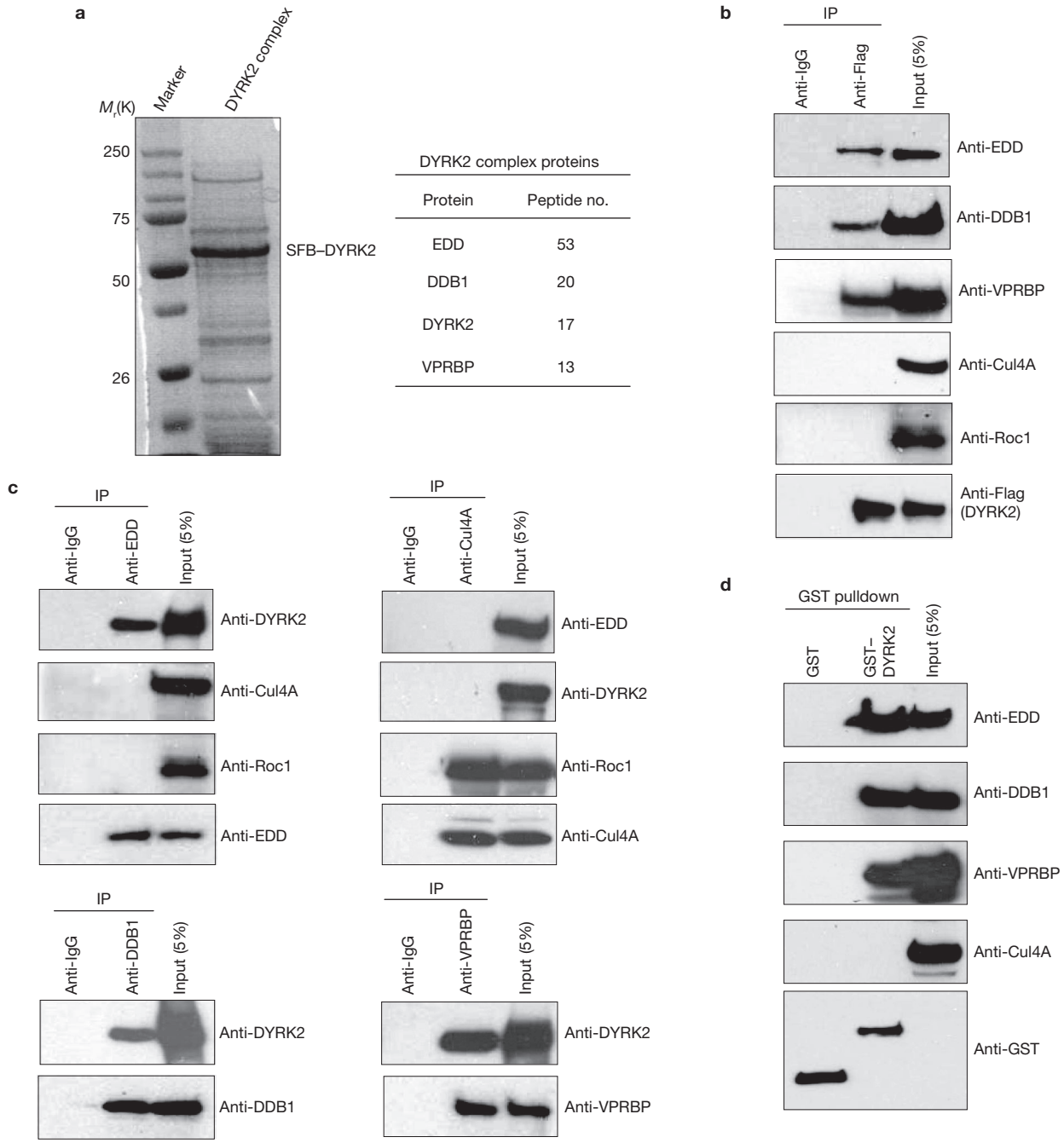

Figure 1 Identification of EDD–DDB1–VPRBP as DYRK2-associated proteins. **(a)** Tandem affinity purification of DYRK2-containing protein complexes was conducted with 293T cells stably expressing triple-tagged DYRK2. Associated proteins were separated by SDS–PAGE and revealed by staining with Coomassie blue. The proteins and the number of peptides identified by mass spectrometry analysis are shown in the table at the right and also in Supplementary Information, Table S1. **(b)** Immunoprecipitation (IP) with control IgG or anti-Flag (DYRK2) antibody were performed with extracts prepared from 293T derivative cells stably expressing Flag-tagged DYRK2. The presence of EDD, DDB1, VPRBP, Cul4A or Roc1 in these immunoprecipitates was evaluated by immunoblotting with their respective antibodies. **(c)** Reverse co-immunoprecipitation experiments were performed with anti-EDD, anti-Cul4A, anti-DDB1 and anti-VPRBP antibodies and the associated endogenous DYRK2 and other indicated proteins was identified by western blotting with their respective antibodies. **(d)** A GST pulldown assay was performed with immobilized control GST or GST–DYRK2 fusion proteins on agarose beads, followed by incubation with extracts prepared from 293T cells. The interaction of EDD, DDB1, VPRBP or Cul4A with DYRK2 was assessed by immunoblotting with their respective antibodies. Uncropped images of blots are shown in Supplementary Information, Fig. S4.

these associations in cells transfected with control small interfering RNA (siRNA) but not in cells after transfection with DYRK2-specific siRNA (Supplementary Information, Fig. S1a). In addition, exogenously expressed Myc–EDD interacted only with Flag–DYRK2 but not with another DYRK family member, DYRK1B (Supplementary Information, Fig. S1b, c), underlining the specificity of the interaction between DYRK2

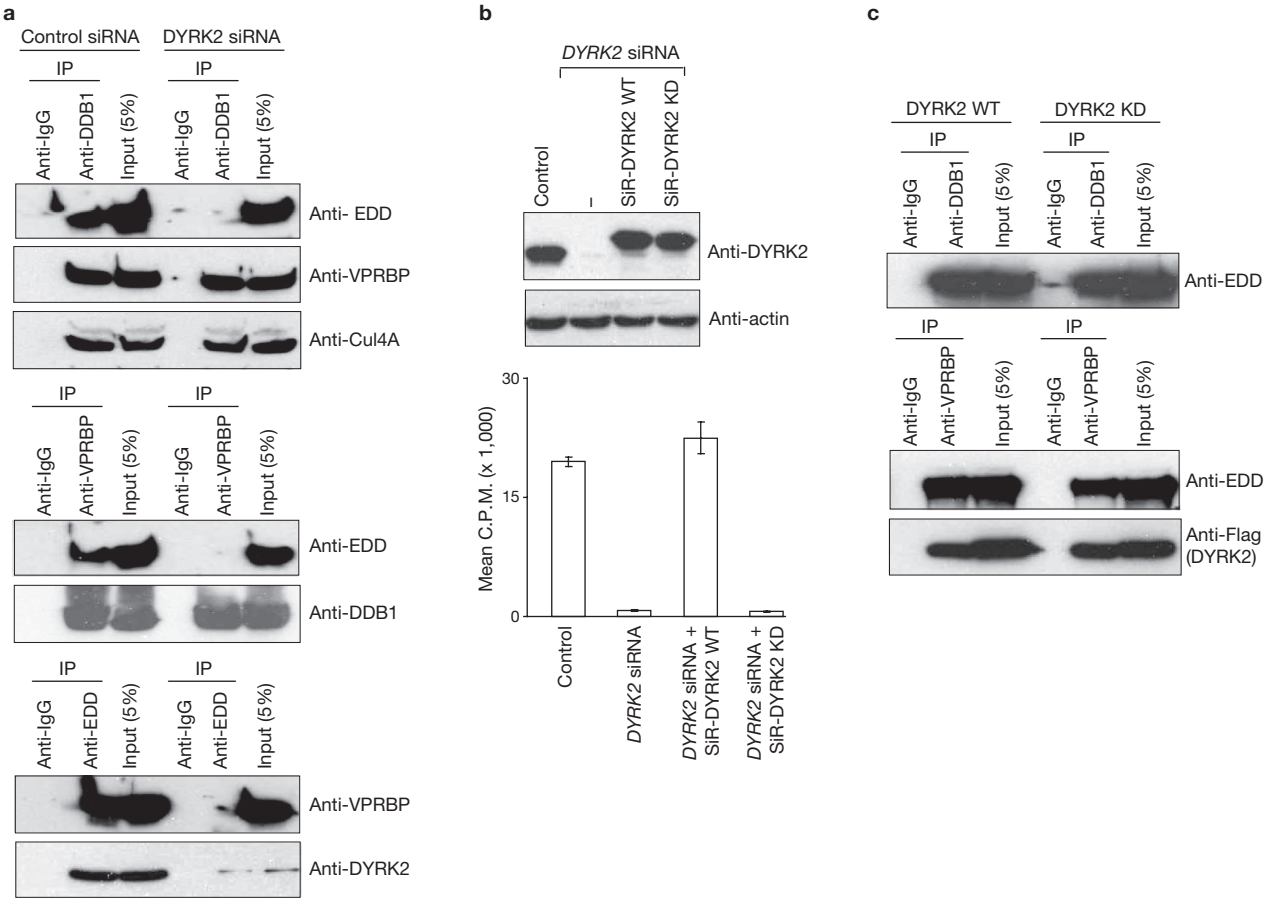

Figure 2 DYRK2 functions as an adaptor in the EDVP E3 ligase complex. **(a)** HeLa cells were transfected with control siRNA or DYRK2-specific siRNA and immunoprecipitation (IP) was performed with anti-DDB1 (top panel), anti-VPRBP (middle panel) or anti-EDD (bottom panel) antibodies. The presence of associated proteins in the immunoprecipitated complexes was assessed by immunoblotting with antibodies as indicated. **(b)** HeLa cells transfected with DYRK2 specific siRNA were retransfected with either siRNA-resistant wild-type DYRK2 (SiR-DYRK2 WT) or kinase-dead DYRK2 (SiR-DYRK2 KD). The expression of endogenous DYRK2 and the transfected siRNA-resistant DYRK2 was assessed by immunoblotting with anti-DYRK2 antibody. Actin was used as a loading control. The graph represents DYRK2 kinase activity measured after performing an *in vitro* kinase assay with DYRK2 immunoprecipitates prepared from the indicated cell lysates, with Woodtide peptide as a substrate (means ± s.d., $n = 3$). **(c)** HeLa cells transfected with DYRK2-specific siRNA were retransfected with either siRNA-resistant wild-type (WT) DYRK2 or kinase-dead (KD) DYRK2. Lysates prepared from these cells were used to immunoprecipitate DDB1 or VPRBP with their respective antibodies. The associated EDD in these immunoprecipitates was assessed by immunoblotting with anti-EDD antibody. Uncropped images of blots are shown in Supplementary Information, Fig. S4.

and EDD. Bacterially expressed glutathione *S*-transferase (GST)-tagged DYRK2 pulled down EDD, DDB1 and VPRBP, but not Cul4A from cell extracts (Fig. 1d), again arguing that DYRK2 forms a distinct complex with EDD, DDB1 and VPRBP. The formation of a DYRK2–EDD–DDB1–VPRBP complex might not be strictly regulated by the cell cycle, because we observed an interaction of DYRK2 with the other components of the complex independently of cell cycle phases, although the levels of EDD and VPRBP interacting with DYRK2 vary and are proportional to their protein levels at specific phases of the cell cycle (Supplementary Information, Fig. S2c).

EDD is a known HECT-domain-containing E3 ligase that regulates the ubiquitin-dependent degradation of its substrates[14]. We named this E3 ligase complex containing EDD, DDB1 and VPRBP proteins the EDVP complex, to distinguish it from the previously identified Cul4–Roc1–DDB1–VPRBP E3 ligase complex. To assess the significance of the interaction between DYRK2 and this new EDVP E3 ligase complex, we checked DYRK2 protein levels in cells depleted of EDD, DDB1 or VPRBP. We found no difference between the DYRK2 protein levels in any of the knockdown cells in comparison with control-siRNA-transfected cells (Supplementary Information, Fig. S2a). We also checked the protein levels of DYRK2, EDD and VPRBP at different phases of the cell cycle. Whereas the levels of EDD and VPRBP fluctuated during the cell cycle, DYRK2 levels remained constant (Supplementary Information, Fig. S2b), thus ruling out the possibility that DYRK2 may be a target for proteasomal degradation mediated by the EDVP ligase complex.

DYRK2 acts as an adaptor in the EDVP complex

Several Kelch-motif-containing proteins were shown previously to act as E3 ligase adaptors for specific substrates[23–25]. A preliminary analysis of the DYRK2 protein sequence revealed the presence of a Kelch motif (amino-acid residues 390–433) within its protein kinase catalytic domain (Supplementary Information, Fig. S3), so we next investigated whether DYRK2 functions as a molecular adaptor in the EDVP ligase complex. We depleted DYRK2 with siRNA and checked for complex formation

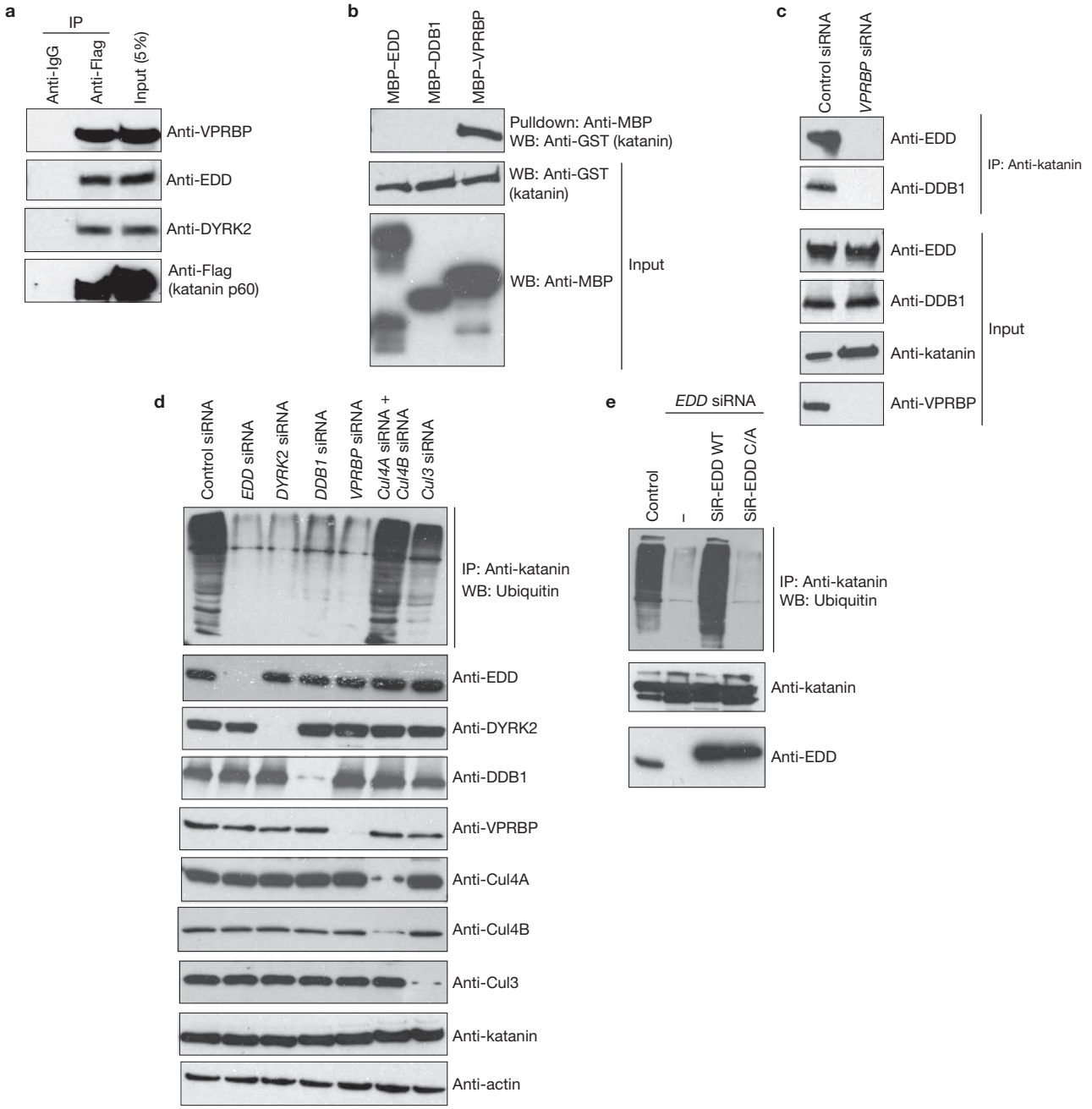

Figure 3 Katanin p60 is the ubiquitylation substrate for EDVP E3 ligase complex. **(a)** Control (IgG) or anti-Flag immunoprecipitates (IP) were prepared from 293T cells transfected with plasmid encoding a triple-tagged katanin. Western blotting (WB) was performed with the indicated antibodies to show a specific interaction between the DYRK2–EDVP complex and katanin p60. **(b)** Bacterially expressed recombinant MBP-tagged EDD, DDB1 or VPRBP bound to amylase-Sepharose beads was incubated with recombinant GST–katanin, and the association of katanin was detected by western blotting with anti-GST antibody. The expression of MBP fusion proteins was detected by anti-MBP antibody. **(c)** HeLa cells were transfected with either control siRNA or VPRBP siRNA, and the association of EDD and DDB1 with katanin was assessed by immunoblotting with their respective antibodies after immunoprecipitation with anti-katanin antibody. **(d)** HeLa cells were transfected with different siRNAs as indicated. Cell lysates prepared after 5 h of treatment with 10 μM MG132 were subjected to immunoprecipitation with anti-katanin antibodies. The ubiquitylated katanin was detected with anti-ubiquitin antibody. The protein expression and the specificity of different siRNAs were confirmed by immunoblotting of cell extracts with antibodies as indicated. **(e)** HeLa cells transfected with EDD-specific siRNA were retransfected with either siRNA-resistant wild-type EDD (SiR-EDD WT) or catalytically inactive EDD (SiR-EDD C/A). Ubiquitylation of katanin was assessed by immunoblotting with anti-ubiquitin antibody after immunoprecipitation with anti-katanin antibody. The expression of endogenous EDD and the transfected siRNA resistant EDD was assessed by immunoblotting with anti-EDD antibody. Uncropped images of blots are shown in Supplementary Information, Fig. S4.

of EDD, DDB1 and VPRBP. The interaction of EDD with DDB1 and VPRBP was seen only in the presence of intact DYRK2, whereas the knockdown of DYRK2 led to a loss of the interaction between EDD and DDB1 or VPRBP (Fig. 2a). Neither the interaction of DDB1 with VPRBP nor the association of Cul4A with DDB1–VPRBP was affected by the absence of DYRK2 (Fig. 2a). These experiments suggest that

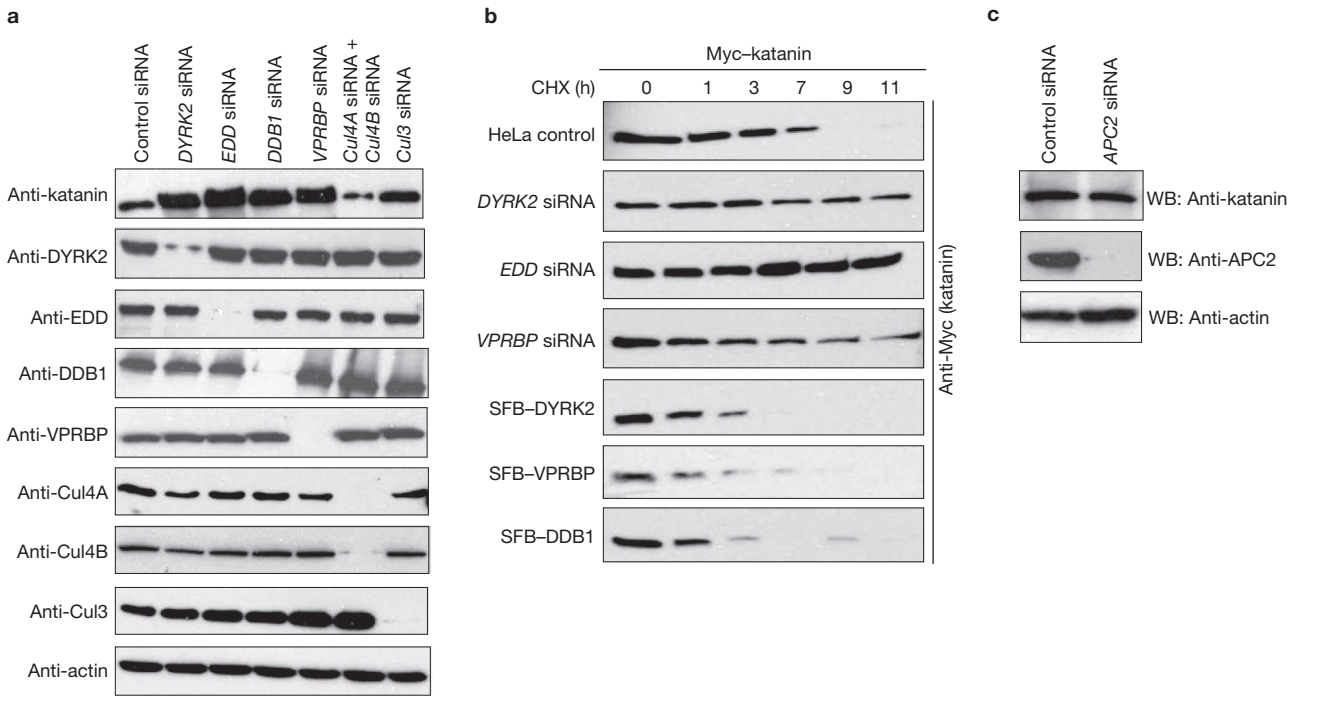

Figure 4 EDVP E3 ligase complex regulates katanin p60 protein levels. **(a)** HeLa cells were transfected with control siRNA or siRNAs against DYRK2, EDD, DDB1, VPRBP, Cul4A/Cul4B or Cul3. The protein levels of katanin were assessed by immunoblotting with anti-katanin antibody, and the efficiency of different siRNAs was shown by immunoblotting with the indicated antibodies. **(b)** HeLa cells transiently expressing Myc-tagged katanin were either transfected with siRNAs against DYRK2, EDD or VPRBP or with plasmids encoding SFB-tagged DYRK2, VPRBP or DDB1. At 12 h after transfection, cells were treated with cycloheximide (CHX) and collected at the indicated times afterwards. The protein levels of katanin were determined by anti-Myc immunoblotting. **(c)** Cells transfected with either control siRNA or APC2 siRNA were lysed, and the expression of katanin and APC2 was detected by western blotting (WB) with their respective antibodies. Actin is used as a loading control. Uncropped images of blots are shown in Supplementary Information, Fig. S4.

DYRK2 functions as a scaffold, required for the specific recruitment of EDD to DDB1–VPRBP, thus forming a novel EDVP E3 ligase complex. Surprisingly, DYRK2 kinase activity is dispensable as an scaffold for this E3 ligase complex, since the transfection of either siRNA-resistant wild-type DYRK2 or kinase-inactive DYRK2 (each of which was validated by both expression and kinase activity with a synthetic peptide; Fig. 2b), into DYRK2-depleted cells was able to restore the association of EDD with the DDB1–VPRBP complex (Fig. 2c).

EDVP–DYRK2 complex regulates katanin p60 ubiquitylation

We next examined the likely substrates of this new E3 ligase complex. Previously, MBK-2, the *Caenorhabditis elegans* homologue of mammalian DYRK2, was shown to phosphorylate and regulate MEI-1 during meiotic maturation in *C. elegans*[8]. MEI-1 (a *C. elegans* homologue of katanin p60) is an AAA-ATPase that associates with MEI-2 and functions as a microtubule-severing enzyme. When the *C. elegans* embryo enters the first mitotic division after exiting from the meiosis, MBK2 phosphorylates MEI-1, which is then degraded through a ubiquitin-dependent mechanism by binding to MEL-26, a BTB-domain-containing substrate adaptor protein complexed with Cul3 (ref. 24). The ubiquitin-mediated degradation of MEI-1/katanin was further regulated by a series of neddylation and deneddylation of Cul3 mediated by COP9/signalosome[26]. In higher eukaryotes, it is not yet known whether DYRK2 regulates katanin p60. We therefore first tested and showed that katanin p60 readily associated with the DYRK2–EDVP complex *in vivo* (Fig. 3a). To identify the direct katanin-binding subunit of the EDD–DDB1–VPRBP complex, we performed an *in vitro* binding assay using bacterially expressed recombinant maltose-binding protein (MBP)-tagged EDD, DDB1 and VPRBP along with GST-tagged katanin. Recombinant katanin directly binds VPRBP but not EDD and DDB1 *in vitro* (Fig. 3b). In addition, katanin interacts with EDD and DDB1 only in the presence of intact VPRBP but not in VPRBP knockdown cells, thus confirming VPRBP as the substrate-binding receptor subunit in the EDVP complex (Fig. 3c). We further examined whether the associated katanin p60 is a substrate of the DYRK2–EDVP E3 ligase complex. We evaluated endogenous katanin ubiquitylation in cells transfected with either control siRNA or siRNAs specific for different components of the DYRK2–EDVP complex in the presence of MG132, a proteasomal inhibitor. Katanin p60 was polyubiquitylated in the presence of the intact DYRK2–EDVP, but its ubiquitylation was severely decreased by the depletion of DYRK2, EDD, DDB1 or VPRBP (Fig. 3d). In contrast, katanin polyubiquitylation was unaffected in cells transfected with siRNAs against Cul4A and Cul4B. Previously, it was shown that Cul3/MEL26 also has a function in the degradation of MEI-1 (a *C. elegans* homologue of katanin p60) during meiotic maturation of *C. elegans*[24,26]. We therefore tested whether a similar mechanism for katanin regulation occurs in humans. Interestingly, knocking down Cul3 does lead to a modest decrease in katanin polyubiquitylation, although the severity of this decrease is not comparable with those observed in cells with knockdown of subunits of the EDVP complex (Fig. 3d). It is therefore likely that the EDVP complex has a primary function, whereas Cul3 is of secondary importance in promoting katanin polyubiquitylation in

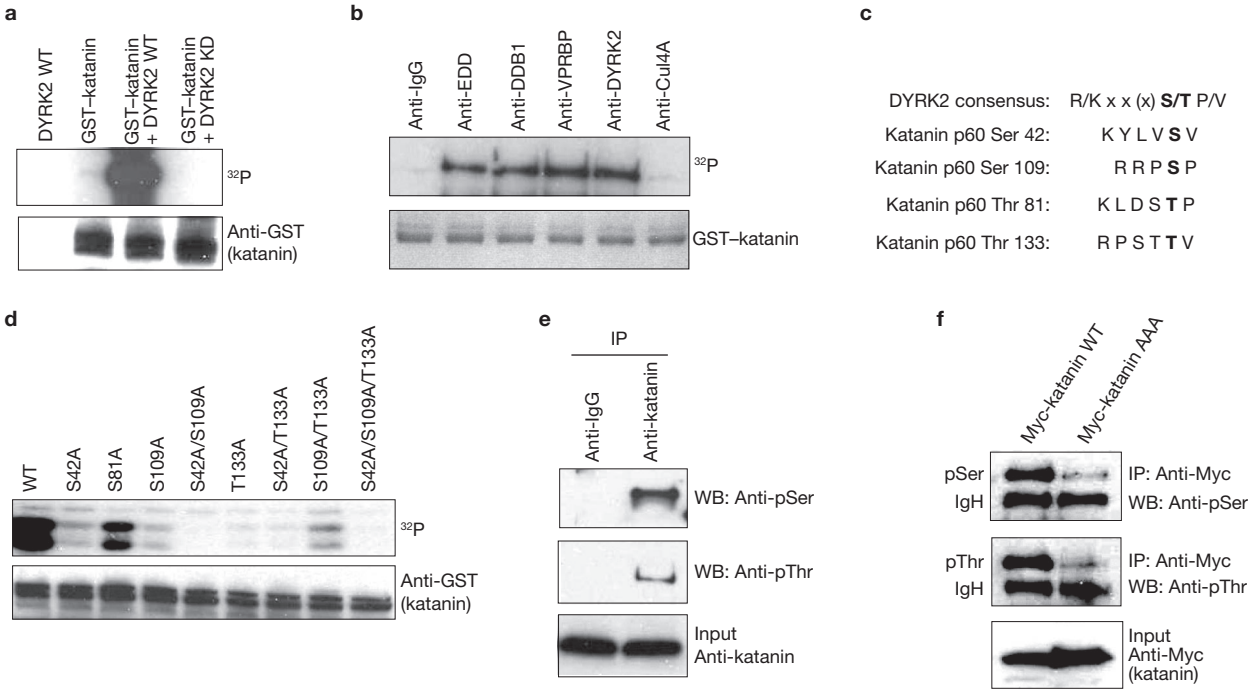

Figure 5 DYRK2 phosphorylates katanin. **(a)** An *in vitro* kinase assay was performed with a bacterially expressed GST–katanin and immunoprecipitated wild-type or kinase-inactive DYRK2. **(b)** An *in vitro* kinase assay was performed with a bacterially expressed GST–katanin with immunoprecipitates prepared by using antibodies against EDD, DDB1, VPRBP, DYRK2 and Cul4A. **(c)** The alignment of potential katanin phosphorylation sites with DYRK2 consensus sequence is presented. Bold lettering indicates the phosphorylated residue. **(d)** *In vitro* DYRK2 kinase assays were conducted with different bacterially expressed GST–katanin phosphorylation-site mutants as indicated. **(e)** The *in vivo* phosphorylation of katanin was detected by immunoblotting (WB) with anti-phosphoserine-specific or anti-phosphothreonine-specific antibodies after immunoprecipitation (IP) with control IgG or katanin antibodies. **(f)** The *in vivo* phosphorylation of wild-type katanin and the triple phospho-mutant of katanin (AAA) was assessed by immunoblotting with phosphoserine-specific or phosphothreonine-specific antibodies after anti-Myc immunoprecipitation of extracts prepared from 293T cells expressing Myc-tagged wild-type or mutant katanin. IgH indicates IgG heavy chain. Uncropped images of blots are shown in Supplementary Information, Fig. S4.

human cells. We also investigated whether EDD is the functional E3 ligase in the EDVP complex. Knockdown of EDD with siRNA severely affected katanin polyubiquitylation. This defect in katanin ubiquitylation was fully rescued by the expression of siRNA-resistant wild-type EDD, but not by the expression of a catalytically inactive HECT-domain mutant of EDD (Fig. 3e). EDD is therefore the catalytic subunit in this E3 ligase complex.

Polyubiquitylation of katanin by the DYRK2–EDVP complex is likely to be required for katanin degradation, as knockdown of DYRK2, EDD, DDB1 or VPRBP, but not that of Cul4A and Cul4B, increased the steady-state levels of katanin protein (Fig. 4a). Knockdown of Cul3 also resulted in a small increase in katanin protein levels, again suggesting a secondary role of the Cul3 complex in katanin degradation. In addition, in a cycloheximide chase experiment, Myc-tagged katanin was stabilized in cells depleted of DYRK2, EDD or VPRBP in comparison with cells transfected with control siRNAs. In sharp contrast, overexpression of DYRK2, DDB1 or VPRBP along with katanin led to diminished katanin stability (Fig. 4b). Taken together, these data suggest that katanin is a substrate of the DYRK2–EDVP E3 ligase complex. Because anaphase-promoting complex (APC) was also shown to work with MBK-2 and regulate the degradation of *C. elegans* katanin p60 in a Cul3 redundant pathway[8], we knocked down APC2, a critical subunit of APC, in human cells. However, we did not observe any change in katanin protein levels (Fig. 4c) and therefore concluded that APC may not be involved in katanin degradation in humans.

DYRK2-mediated phosphorylation is required for katanin p60 degradation

MBK2/DYRK2 is known to phosphorylate the katanin homologue MEI-1 in *C. elegans*[27]. We next investigated whether DYRK2 would phosphorylate katanin and be required for katanin ubiquitylation by the EDVP complex. *In vitro* kinase assays revealed that immunoprecipitated wild-type DYRK2, but not kinase-inactive DYRK2, could phosphorylate bacterially expressed GST–katanin (Fig. 5a). We also tested whether DYRK2 in the EDVP complex could phosphorylate katanin by performing immunoprecipitation of the EDVP complex followed by an *in vitro* kinase assay. Immunoprecipitates of EDD, DDB1 and VPRBP, but not of Cul4A, showed intrinsic kinase activity towards katanin (Fig. 5b), suggesting that DYRK2 in the EDVP complex is still capable of phosphorylating its substrate. Katanin contains several consensus DYRK2 phosphorylation sites[28] (Fig. 5c). We mutated katanin at these serine or threonine residues individually or in combination and examined whether any of these residues were potential DYRK2 phosphorylation sites *in vitro*. Serine 42, serine 109 and threonine 133 are likely to be the major DYRK2 phosphorylation sites, because single mutations at these sites showed decreased phosphorylation by DYRK2, and the triple mutant showed almost no DYRK2-mediated phosphorylation (Fig. 5d). Furthermore, we detected the presence of phosphoserine and phosphothreonine residues in the immunoprecipitated wild-type katanin (Fig. 5e), indicating that katanin is phosphorylated *in vivo*. However, these phosphorylations

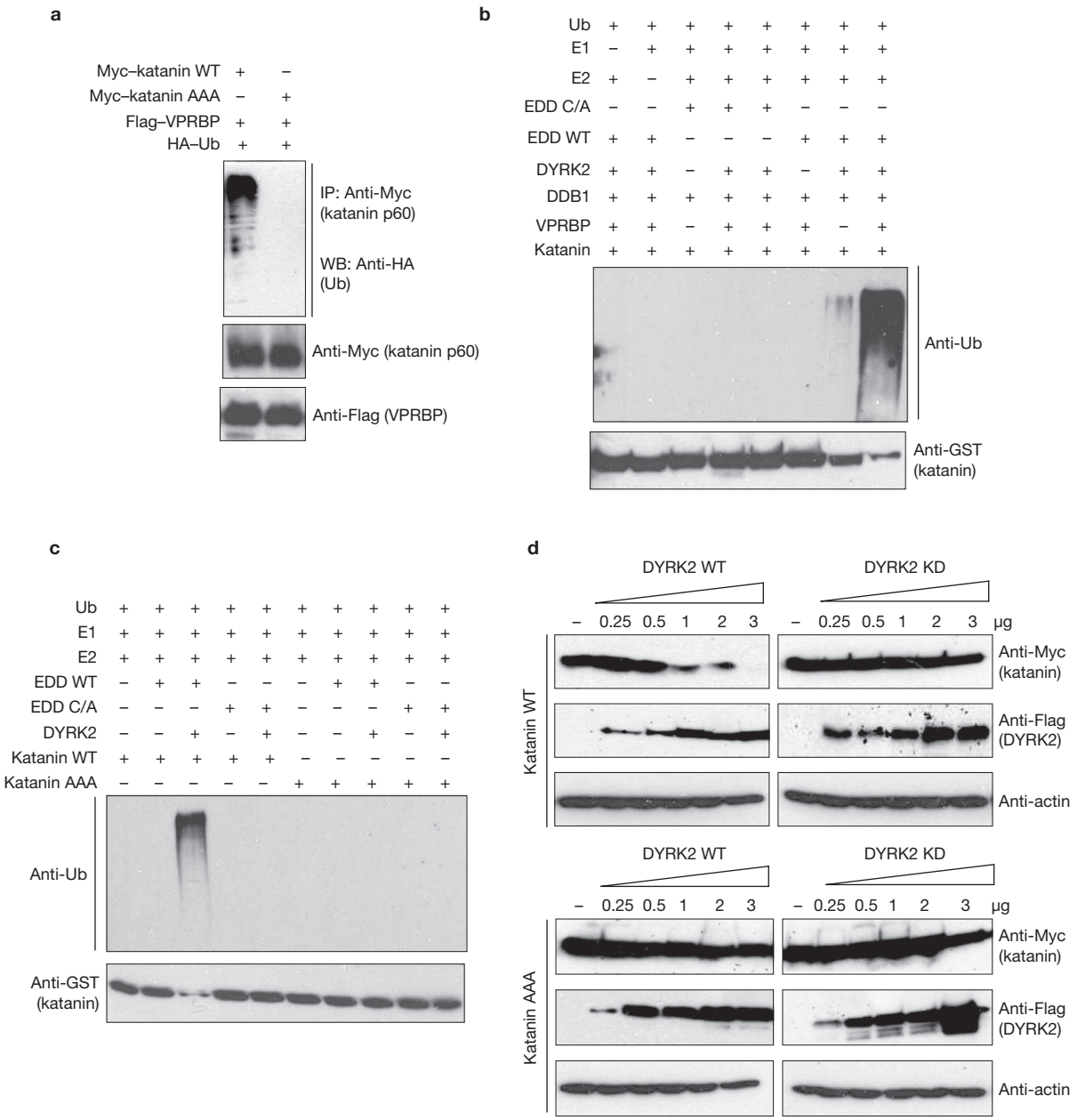

Figure 6 DYRK2 kinase activity is required for the regulation of katanin degradation. **(a)** Myc-tagged wild-type (WT) katanin or the triple phospho-mutant of katanin (AAA) was expressed in HeLa cells along with Flag–VPRBP and HA-tagged ubiquitin (HA–Ub). Levels of katanin ubiquitylation were evaluated by anti-HA immunoblotting (WB) after immunoprecipitation (IP) of katanin from the cell extracts. **(b)** *In vitro* reconstitution experiments were performed with GST–katanin as a substrate in the presence of recombinant ubiquitin, E1 (UBE1), E2 (UbcH5), MBP-tagged EDD, EDD C/A, DDB1, VPRBP and DYRK2 in various combinations as indicated. Ubiquitylated species of katanin and GST–katanin were detected by immunoblotting with anti-ubiquitin and anti-GST antibodies, respectively. **(c)** *In vitro* reconstitution experiments were performed as in **b**, using either wild-type GST–katanin or the AAA mutant of katanin as a substrate in the presence of various recombinant proteins as indicated. Ubiquitylated species of katanin and GST–katanin were detected by immunoblotting with anti-ubiquitin and anti-GST antibodies, respectively. **(d)** The effect of DYRK2 kinase activity and katanin phosphorylation on the regulation of katanin protein levels was assessed by transient transfection experiments. 293T cells were transfected with the indicated expression vectors for DYRK2 and katanin, and the protein levels were estimated by immunoblotting 24 h after transfection. Uncropped images of blots are shown in Supplementary Information, Fig. S4.

were greatly diminished in the triple phospho-mutant (AAA mutant) of katanin (Fig. 5f), suggesting that these residues are indeed major phosphorylation sites *in vivo*.

We further investigated whether the DYRK2-mediated phosphorylation of katanin is required for its ubiquitylation *in vivo*. Ubiquitylation of Myc-tagged wild-type katanin was easily detected, whereas the ubiquitylation of the AAA mutant of katanin was severely diminished (Fig. 6a). To further support the idea that the intact DYRK2–EDVP complex mediates the ubiquitylation of phosphorylated katanin, we performed *in vitro* reconstitution assays with GST–katanin as the ubiquitylation substrate. As shown in Fig. 6b, only the intact EDVP complex containing wild-type EDD (but not mutant EDD) resulted in robust

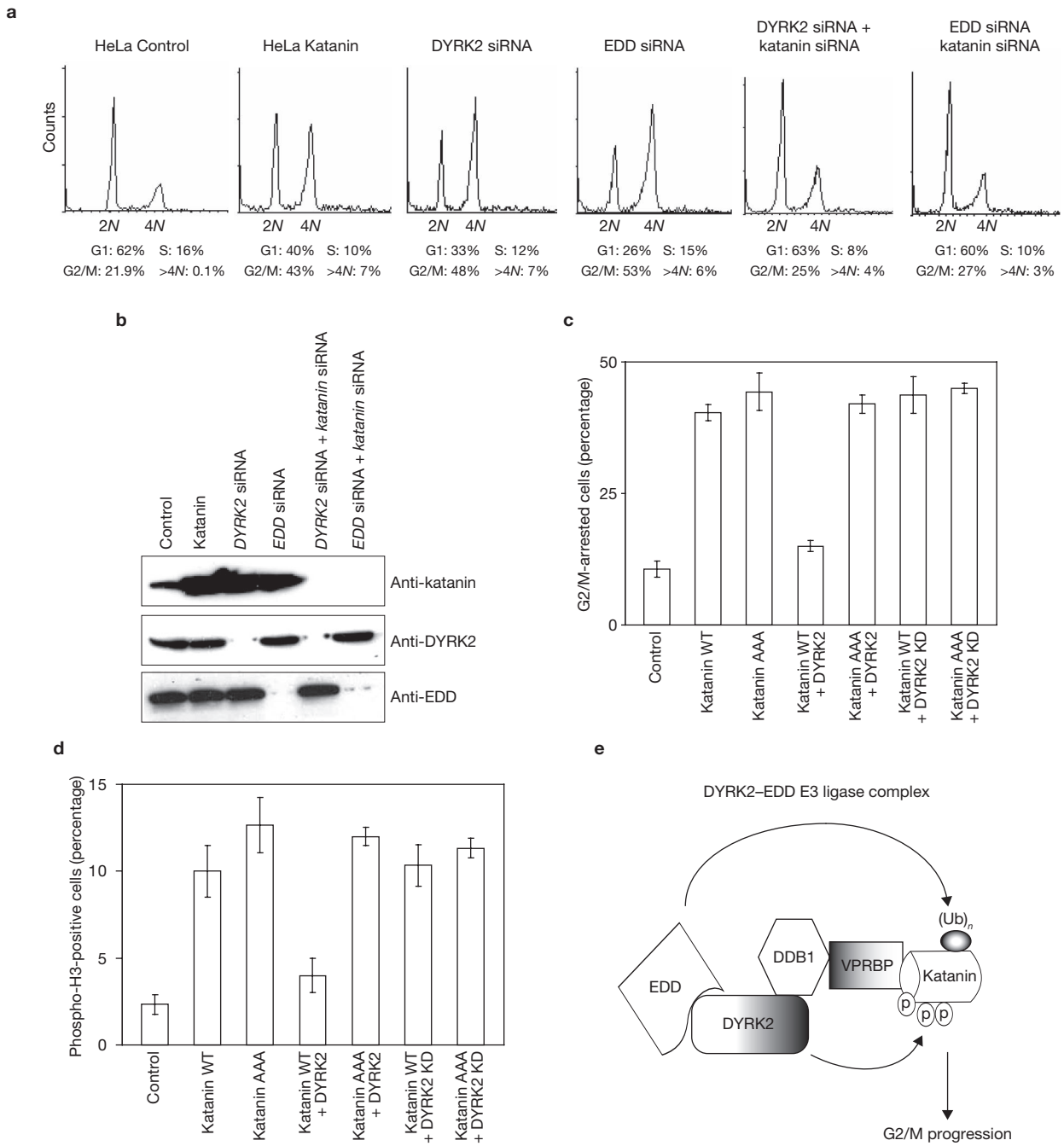

Figure 7 DYRK2 regulates mitotic progression by means of its adaptor and kinase function. **(a)** HeLa cells were transfected with plasmids encoding katanin or with different siRNAs as indicated, and the cell cycle profiles were determined by propidium iodide staining followed by flow cytometric analysis. **(b)** The protein levels of katanin, DYRK2 and EDD in HeLa cells transfected with plasmids encoding katanin or different siRNA combinations were determined by western blotting with the indicated antibodies. **(c)** HeLa cells were transfected with plasmids encoding wild-type katanin or the triple phospho-mutant of katanin (AAA) along with plasmids encoding wild-type (WT) or kinase-dead (KD) DYRK2. The percentage of cells in G2/M was determined by fluorescence-activated cell sorting analysis. Data are presented as mean ± SD for three different experiments. **(d)** The percentages of mitotic cells as measured by positive phospho-H3 staining were determined in HeLa cells transfected with the indicated constructs. Data are presented as mean ± SD for three different experiments. **(e)** Model for a novel DYRK2–EDD E3 ligase complex demonstrates that DYRK2 functions as both an adaptor and a kinase and regulates G2/M cell cycle progression. Uncropped images of blots are shown in Supplementary Information, Fig. S4.

katanin polyubiquitylation. Previous phosphorylation of katanin is essential for katanin ubiquitylation: only wild-type katanin, but not its AAA mutant, could be readily ubiquitylated by the EDVP complex *in vitro* (Fig. 6c). These data suggest that DYRK2-dependent katanin phosphorylation is a prerequisite for katanin ubiquitylation, indicating that DYRK2 kinase activity is critical for the function of the DYRK2–EDVP E3 ligase complex. The phosphorylation-dependent degradation of katanin was substantiated by co-transfection experiments. Co-transfection of wild-type DYRK2, but not kinase-inactive DYRK2, along with katanin decreased the steady-state levels of katanin protein (Fig. 6d). In contrast,

the protein levels of the AAA katanin mutant remained largely unaffected (Fig. 6d), suggesting that DYRK2-mediated phosphorylation is a priming event required for katanin ubiquitylation and degradation.

EDVP–DYRK2 complex controls mitotic transition

Previous studies have reported that katanin is a microtubule AAA-ATPase that is important in mitosis[29,30]. Katanin is required for severing microtubules at the mitotic spindles when disassembly of the microtubules is required for the segregation of sister chromatids during anaphase. Both DYRK2 (ref. 7) and EDD[31] have also been suggested to function during mitosis. To establish a functional link between the DYRK2–EDVP ligase complex and katanin degradation, we checked the cell cycle profile of HeLa cells transiently transfected with katanin. Overexpression of katanin led to the accumulation of a 4*N* population and polyploid (>4*N*) cells (Fig. 7a). Similarly, siRNA-mediated downregulation of either DYRK2 or EDD, which led to an upregulation of katanin (Fig. 7b), also resulted in the accumulation of cells with a 4*N* DNA content (Fig. 7a). This abnormal accumulation of 4*N* cells after depletion of DRYK2 or EDD could be rescued by the simultaneous depletion of katanin by siRNA (Fig. 7a). In addition, DYRK2-mediated katanin phosphorylation is required for proper cell cycle progression: co-expression of DYRK2 with the katanin AAA mutant but not wild-type katanin led to an increase in cells with a 4*N* DNA content (Fig. 7c). This increase in the 4*N* population is attributed to defective mitotic progression, because we observed an increased number of phospho-H3-positive cells when wild-type or non-phosphorylatable katanin was overexpressed (Fig. 7d). Co-expression of wild-type DYRK2 but not the kinase-dead version with wild-type katanin decreased the number of mitotic cells to normal levels, whereas co-expression of DYRK2 with the katanin AAA mutant failed to rescue this mitotic defect (Fig. 7d). Collectively, these results suggest that an active DYRK2–EDVP ligase complex regulates mitotic transition through the modulation of katanin protein levels.

DISCUSSION

Protein kinases regulate a variety of biological processes, including cell proliferation, apoptosis, development and tumorigenesis by phosphorylating their respective downstream substrates[32]. In this study we have uncovered a novel role for protein kinase; for example, it functions as an assembly factor for an E3 ubiquitin ligase complex. In particular, we have shown that DYRK2 has dual roles in this E3 ligase complex. Not only is it required for the assembly of the complex, but it also phosphorylates its substrate and primes the substrate for degradation. Phosphorylation-dependent protein degradation is a common mechanism for regulating protein stability in a cell-cycle-dependent or stimulus-dependent manner. This often occurs as a two-step process[33], in which initially a kinase phosphorylates the substrate. Once phosphorylated, the substrate is recognized by F-box-containing or BC-box substrate receptor proteins and targeted to E3 ligase complexes for degradation. Here we provide evidence for the integral presence of a kinase, DYRK2, within the EDD–DDB1–VPRBP (EDVP) E3 ligase complex, which merges the functional properties of a protein kinase and an E3 ligase into a single unit that can recognize, phosphorylate and degrade substrates in concert. It is currently unclear how DYRK2-mediated phosphorylation of katanin promotes its ubiquitylation, but it is possible that phosphorylation of katanin leads to a conformational change that exposes some of the substrate residues for efficient ubiquitylation by EDD. Our functional studies further suggest that the DYRK2–EDVP E3 ligase complex has a crucial function in regulating normal mitotic progression. Because overexpression of both DYRK2 (refs 11, 12) and EDD[15,16] is frequently reported in cancers, it is tempting to speculate that aberrant mitosis and altered cell cycle progression through the hyperactivation of the DYRK2–EDVP E3 ligase complex might be a key mechanism in promoting neoplastic transformation. Future studies with animal models will reveal the role of this DYRK2–EDVP complex in cancer development and progression. □

METHODS

Plasmids. Full-length DYRK2, DYRK1B, EDD, DDB1, VPRBP, Cul4A, katanin and DYRK2-KD were cloned into a S-protein–Flag–SBP (streptavidin-binding protein) triple tagged destination vector with the Gateway cloning system (Invitrogen). Full-length EDD, katanin and katanin AAA mutant were also cloned to a Myc-tagged destination vector. GST-tagged DYRK2, MBP-tagged EDD, catalytically inactive EDD (EDD C/A), DDB1 and VPRBP bacterial expression vectors were generated by transferring their coding sequences into destination vectors with the Gateway system. Various deletion and point mutants for katanin p60 and the kinase-dead version of DYRK2 were generated by PCR-based site-directed mutagenesis. Wild-type katanin and mutants of katanin were also cloned to a GST-tagged vector. Constructs of Myc-tagged ubiquitin and haemagglutinin (HA)-tagged ubiquitin were used in ubiquitylation assays *in vivo*. siRNA-resistant wild-type DYRK2, kinase-dead DYRK2, wild-type EDD and EDD C/A mutant constructs were generated by introducing silent mutations into their respective triple-tagged vectors by using site-directed mutagenesis; the constructs were verified by sequencing.

Antibodies. Rabbit anti-katanin antibodies were raised by immunizing rabbits with GST–katanin p60 fusion protein (residues 30–240). Antisera were affinity-purified with the AminoLink Plus Immobilization and Purification Kit (Pierce). Anti-DYRK2 (Abcam), anti-EDD, anti-DDB1, anti-VPRBP, anti-Cul4A, anti-Cul3 (all from Bethyl Laboratories), anti-FBX22 (Novus Biologicals), anti-PBK (Cell Signaling Technology), anti-Flag, anti-(maltose-binding protein); Clone 17, anti-actin, anti-Cul4B (Sigma), anti-Roc1 (Invitrogen), anti-GST, anti-Myc; Clone 9E10 (Santa Cruz Biotechnologies), anti-phosphoserine H3, anti-phosphothreonine (Cell Signaling Technology) and anti-phosphoserine, anti-ubiquitin (Millipore) antibodies were used in this study.

Tandem affinity purification. 293T cells were transfected with S-protein-Flag-SBP triple-tagged DYRK2; three weeks later, puromycin-resistant colonies were selected and screened for DYRK2 expression. The DYRK2-positive stable cells were then maintained in RPMI medium supplemented with fetal bovine serum and 2 μg ml^{-1} puromycin. The SFB–DYRK2 stable cells were lysed with NETN buffer (20 mM Tris-HCl pH 8.0, 100 mM NaCl, 1 mM EDTA, 0.5% Nonidet P40) containing 50 mM β-glycerophosphate, 10 mM NaF, 1 μg ml^{-1} pepstatin A and 1 μg ml^{-1} aprotinin on ice for 20 min. After removal of cell debris by centrifugation, crude cell lysates were incubated with streptavidin-Sepharose beads (Amersham Biosciences) for 1 h at 4 °C. The bound proteins were washed three times with NETN buffer and then eluted twice with 2 mg ml^{-1} biotin (Sigma) for 30 min at 4 °C. The eluates were incubated with S-protein-agarose beads (Novagen) for 1 h at 4 °C and then washed three times with NETN buffer. The proteins bound to S-protein-agarose beads were resolved by SDS–PAGE and revealed by staining with Coomassie blue. The identities of eluted proteins were revealed by mass spectrometry analysis performed at the Taplin Biological Mass Spectrometry Facility, Harvard University.

Cell transfections, immunoprecipitation and immunoblotting. 293T cells or HeLa cells were transfected with various plasmids by using Lipofectamine (Invitrogen) in accordance with the manufacturer's protocol. For immunoprecipitation assays, cells were lysed with NETN buffer as described above. The whole-cell lysates obtained by centrifugation were incubated with 2 μg of specified antibody bound to either protein A-Sepharose or protein G-Sepharose beads (Amersham Biosciences) for 1 h at 4 °C. The immunocomplexes were then washed with NETN buffer four times and subjected to SDS–PAGE. Immunoblotting was performed with standard protocols.

GST pulldown and *in vitro* binding assays. Bacterially expressed GST–DYRK2 or control GST bound to glutathione-Sepharose beads (Amersham) was incubated with 293T cell lysates for 1 h at 4 °C, and the washed complexes were eluted by boiling in SDS sample buffer and then separated by SDS–PAGE; the interactions were analysed by western blotting. For *in vitro* binding assays, bacterially expressed MBP–EDD, MBP–DDB1 or MBP–VPRBP bound to amylase-Sepharose beads were incubated with bacterially purified GST–katanin for 1 h at 4 °C; the washed complexes were eluted by boiling in SDS sample buffer and separated by SDS–PAGE, and the interactions were analysed by western blotting with the indicated antibodies.

RNA interference. Control siRNA and the smart-pool siRNAs against DDB1, Cul4A, Cul4B, Cul3, APC2 and katanin and the on-target plus individual siRNAs against DYRK2, EDD and VPRBP were purchased from Dharmacon Inc. Transfection was performed twice, 30 h apart, with 200 nM siRNA using Oligofectamine reagent in accordance with the manufacturer's protocol (Invitrogen). The following target sequences were used.

Individual siRNA sequences: DYRK2 siRNA, 5′-GGUGCUAUCACAUCUAUAU-3′;

EDD siRNA, 5′-CAACUUAGAUCUCCUGAAA-3′; DDB1 siRNA, 5′-ACACUUUGGUGCUCUCUU-3′; VPRBP siRNA, 5′-GAUGGCGGAUGCUUUGAUA-3′.

Pooled siRNA sequences: Cul4A siRNA, 5′-GCACAGAUCCUUCCGUUUA-3′, 5′-GAACAGCGAUCGUAAUCAA-3′, 5′-GCAUGUGGAUUCAAAGUUA-3′ and 5′-GCGAGUACAUCAAGACUUU-3′; Cul4B siRNA, 5′-GCUAUUGGCCGACAUAUGU-3′, 5′-CAGAAGUCAUUAAUUGCUA-3′, 5′-CAAACGGCCUAGCCAAAUC-3′ and 5′-CGGAAAGAGUGCAUCUGUA-3′; Cul3 siRNA, 5′-CCGAACAUCUCAUAAAUAA-3′, 5′-GAGAAGAUGUACUAAAUUC-3′, 5′-GAGAUCAAGUUGUACGUUA-3′ and 5′-GCGGAAAGGAGAAGUCGUA-3′; APC2 siRNA, 5′-GAGAUGAUCCAGCGUCUGU-3′, 5′-GACAUCAUCACCCUCUAUA-3′, 5′-GAUCGUAUCUACAACAUGC-3′ and 5′-GAGAAGAAGUCCACACUAU-3′; katanin siRNA, 5′-GGGAGGAGCUAUUACGAAU-3′, 5′-GCUGUUCGUUGUCGUGAAA-3′, 5′-GGAUCAUGCUAACUCGAGA-3′ and 5′-CAUUGAAAGAUACGAGAAA-3′.

***In vitro* kinase assay.** Wild-type DYRK2 and kinase-inactive DYRK2, which were expressed in 293T cells, were immunoprecipitated with Flag-agarose beads and used as a kinase source. GST-tagged katanin and its mutant proteins, expressed in *Escherichia coli* strain BL21, were purified with glutathione-Sepharose beads and used as substrates. The kinase (DYRK2) and substrates (katanin) were incubated in kinase assay buffer (10 mM HEPES pH 7.5, 50 mM NaCl, 10 nM $MgCl_2$, 10 mM $MnCl_2$, 1 mM EGTA, 1 mM dithiothreitol, 5 μM ATP, 10 mM NaF, 50 mM glycerophosphate) along with 10 μCi of [γ-^{32}P] ATP) for 30 min at 30 °C. Reactions were stopped by the addition of SDS sample buffer. Then samples were boiled for 5 min at 100 °C followed by SDS–PAGE and autoradiography. The validation of siRNA-resistant wild-type DYRK2 and kinase-dead DYRK2 was performed by DYRK2 immunoprecipitation followed by a kinase assay with a synthetic Woodtide peptide (KKISGRLSPIMTEQ) as a substrate (purchased from Millipore).

***In vivo* ubiquitylation assay.** HeLa cells were transfected with various combinations of plasmids as indicated in Figs 2d and 3f along with either Myc-tagged ubiquitin or HA-tagged ubiquitin. At 24 h after transfection, cells were treated with MG132 (4 μM) for 6 h and the whole-cell extracts prepared by lysis in NETN buffer were subjected to immunoprecipitation of the substrate protein. Analysis of ubiquitylation was performed by immunoblotting with either anti-Myc or anti-HA antibodies.

***In vitro* reconstitution assay.** The reactions were performed at 30 °C for 15 min in 25 μl of ubiquitylation reaction buffer (40 mM Tris-HCl pH 7.6, 2 mM dithiothreitol, 5 mM $MgCl_2$, 0.1 M NaCl, 2 mM ATP) containing the following components: 100 μM ubiquitin, 20 nM E1 (UBE1) and 100 nM UbcH5b (all from Boston Biochem). Various combinations of EDVP E3 ligase components (25 ng of EDD or EDD C/A, plus DDB1, VPRBP and DYRK2) as indicated were added to the reaction. Either wild-type GST–katanin or the AAA mutant bound to glutathione-Sepharose beads was used as a substrate in the reaction. After ubiquitylation reaction, the glutathione-Sepharose beads were washed five times with NETN buffer and boiled with SDS–PAGE loading buffer; the ubiquitylation of katanin was monitored by western blotting with anti-ubiquitin antibody.

Cell cycle analysis. HeLa cells transfected with the desired expression vectors and siRNA were harvested, washed with phosphate-buffered saline and fixed with ice-cold 70% ethanol for at least 1 h. Cells were washed twice in PBS and treated for 30 min at 37 °C with RNase A (5 μg ml^{-1}) and propidium iodide (50 μg ml^{-1}), then analysed on a FACScan flow cytometer (Becton Dickinson). The percentage of cells in different cell cycle phases was calculated with Flowjo analysis software.

Immunofluorescence staining. Cells grown on coverslips were fixed with 3% paraformaldehyde solution in PBS containing 50 mM sucrose at 25 °C for 15 min. After permeabilization at room temperature with 0.5% Triton X-100 buffer containing 20 mM HEPES pH 7.4, 50 mM NaCl, 3 mM $MgCl_2$ and 300 mM sucrose for 5 min, cells were incubated with a primary phosphoserine H3 antibody at 37 °C for 20 min. After being washed with PBS, cells were incubated with rhodamine-conjugated secondary antibody at 37 °C for 20 min. Nuclei were counterstained with DAPI (4,6-diamidino-2-phenylindole). After a final wash with PBS, coverslips were mounted in glycerine containing *p*-phenylenediamine.

Note: Supplementary Information is available on the Nature Cell Biology website.

ACKNOWLEDGEMENTS

We thank Jamie Wood for critical reading of the manuscript and for providing valuable suggestions. We thank Amanda Russell for providing EDD expression vectors. This work was supported in part by grants from the National Institutes of Health (to J.C.). J.C. is a recipient of an Era of Hope Scholars award from the Department of Defense and is a member of Mayo Clinic Breast SPORE programme.

AUTHOR CONTRIBUTIONS

S.M. performed all the experiments. S.M. and J.C. designed the experiments, analysed the data and wrote the manuscript.

COMPETING FINANCIAL INTERESTS

The authors declare that they have no competing financial interests.

Published online at http://www.nature.com/naturecellbiology
Reprints and permissions information is available online at http://npg.nature.com/reprintsandpermissions/

1. Becker, W. *et al.* Sequence characteristics, subcellular localization, and substrate specificity of DYRK-related kinases, a novel family of dual specificity protein kinases. *J. Biol. Chem.* **273,** 25893–25902 (1998).
2. Kannan, N. & Neuwald, A. F. Evolutionary constraints associated with functional specificity of the CMGC protein kinases MAPK, CDK, GSK, SRPK, DYRK, and CK2α. *Protein Sci.* **13,** 2059–2077 (2004).
3. Lochhead, P. A., Sibbet, G., Morrice, N. & Cleghon, V. Activation-loop autophosphorylation is mediated by a novel transitional intermediate form of DYRKs. *Cell* **121,** 925–936 (2005).
4. Gwack, Y. *et al.* A genome-wide *Drosophila* RNAi screen identifies DYRK-family kinases as regulators of NFAT. *Nature* **441,** 646–650 (2006).
5. Woods, Y. L. *et al.* The kinase DYRK phosphorylates protein-synthesis initiation factor eIF2Bε at Ser^{539} and the microtubule-associated protein tau at Thr^{212}: potential role for DYRK as a glycogen synthase kinase 3-priming kinase. *Biochem. J.* **355,** 609–615 (2001).
6. Skurat, A. V. & Dietrich, A. D. Phosphorylation of Ser^{640} in muscle glycogen synthase by DYRK family protein kinases. *J. Biol. Chem.* **279,** 2490–2498 (2004).
7. Nishi, Y. & Lin, R. DYRK2 and GSK-3 phosphorylate and promote the timely degradation of OMA-1, a key regulator of the oocyte-to-embryo transition in *C. elegans*. *Dev. Biol.* **288,** 139–149 (2005).
8. Lu, C. & Mains, P. E. The *C. elegans* anaphase promoting complex and MBK-2/DYRK kinase act redundantly with CUL-3/MEL-26 ubiquitin ligase to degrade MEI-1 microtubule-severing activity after meiosis. *Dev. Biol.* **302,** 438–447 (2007).
9. Kinstrie, R., Lochhead, P. A., Sibbet, G., Morrice, N. & Cleghon, V. dDYRK2 and Minibrain interact with the chromatin remodelling factors SNR1 and TRX. *Biochem. J.* **398,** 45–54 (2006).
10. Taira, N., Nihira, K., Yamaguchi, T., Miki, Y. & Yoshida, K. DYRK2 is targeted to the nucleus and controls p53 via Ser46 phosphorylation in the apoptotic response to DNA damage. *Mol. Cell* **25,** 725–738 (2007).
11. Gorringe, K. L., Boussioutas, A. & Bowtell, D. D. Novel regions of chromosomal amplification at 6p21, 5p13, and 12q14 in gastric cancer identified by array comparative genomic hybridization. *Genes Chromosomes Cancer* **42,** 247–259 (2005).
12. Miller, C. T. *et al.* Amplification and overexpression of the dual-specificity tyrosine-(Y)-phosphorylation regulated kinase 2 (DYRK2) gene in esophageal and lung adenocarcinomas. *Cancer Res.* **63,** 4136–4143 (2003).

13. Callaghan, M. J. *et al.* Identification of a human HECT family protein with homology to the *Drosophila* tumor suppressor gene hyperplastic discs. *Oncogene* **17,** 3479–3491 (1998).
14. Honda, Y. *et al.* Cooperation of HECT-domain ubiquitin ligase hHYD and DNA topoisomerase II-binding protein for DNA damage response. *J. Biol. Chem.* **277,** 3599–3605 (2002).
15. Clancy, J. L. *et al.* EDD, the human orthologue of the *hyperplastic discs* tumour suppressor gene, is amplified and overexpressed in cancer. *Oncogene* **22,** 5070–5081 (2003).
16. O'Brien, P. M. *et al.* The E3 ubiquitin ligase EDD is an adverse prognostic factor for serous epithelial ovarian cancer and modulates cisplatin resistance *in vitro*. *Br. J. Cancer* **98,** 1085–1093 (2008).
17. Chu, G. & Chang, E. Xeroderma pigmentosum group E cells lack a nuclear factor that binds to damaged DNA. *Science* **242,** 564–567 (1988).
18. Angers, S. *et al.* Molecular architecture and assembly of the DDB1–CUL4A ubiquitin ligase machinery. *Nature* **443,** 590–593 (2006).
19. Lee, J. & Zhou, P. DCAFs, the missing link of the CUL4-DDB1 ubiquitin ligase. *Mol. Cell* **26,** 775–780 (2007).
20. Jin, J., Arias, E. E., Chen, J., Harper, J. W. & Walter, J. C. A family of diverse Cul4-Ddb1-interacting proteins includes Cdt2, which is required for S phase destruction of the replication factor Cdt1. *Mol. Cell* **23,** 709–721 (2006).
21. He, Y. J., McCall, C. M., Hu, J., Zeng, Y. & Xiong, Y. DDB1 functions as a linker to recruit receptor WD40 proteins to CUL4–ROC1 ubiquitin ligases. *Genes Dev.* **20,** 2949–2954 (2006).
22. Higa, L. A. *et al.* CUL4–DDB1 ubiquitin ligase interacts with multiple WD40-repeat proteins and regulates histone methylation. *Nature Cell Biol.* **8,** 1277–1283 (2006).
23. Cullinan, S. B., Gordan, J. D., Jin, J., Harper, J. W. & Diehl, J. A. The Keap1-BTB protein is an adaptor that bridges Nrf2 to a Cul3-based E3 ligase: oxidative stress sensing by a Cul3-Keap1 ligase. *Mol. Cell. Biol.* **24,** 8477–8486 (2004).
24. Xu, L. *et al.* BTB proteins are substrate-specific adaptors in an SCF-like modular ubiquitin ligase containing CUL-3. *Nature* **425,** 316–321 (2003).
25. Salinas, G. D. *et al.* Actinfilin is a Cul3 substrate adaptor, linking GluR6 kainate receptor subunits to the ubiquitin–proteasome pathway. *J. Biol. Chem.* **281,** 40164–40173 (2006).
26. Pintard, L. *et al.* Neddylation and deneddylation of CUL-3 is required to target MEI-1/Katanin for degradation at the meiosis-to-mitosis transition in *C. elegans*. *Curr. Biol.* **13,** 911–921 (2003).
27. Stitzel, M. L., Pellettieri, J. & Seydoux, G. The *C. elegans* DYRK Kinase MBK-2 marks oocyte proteins for degradation in response to meiotic maturation. *Curr. Biol.* **16,** 56–62 (2006).
28. Campbell, L. E. & Proud, C. G. Differing substrate specificities of members of the DYRK family of arginine-directed protein kinases. *FEBS Lett.* **510,** 31–36 (2002).
29. McNally, F. J. & Thomas, S. Katanin is responsible for the M-phase microtubule-severing activity in *Xenopus* eggs. *Mol. Biol. Cell* **9,** 1847–1861 (1998).
30. McNally, K., Audhya, A., Oegema, K. & McNally, F. J. Katanin controls mitotic and meiotic spindle length. *J. Cell Biol.* **175,** 881–891 (2006).
31. Munoz, M. A. *et al.* The E3 ubiquitin ligase EDD regulates S-phase and G_2/M DNA damage checkpoints. *Cell Cycle* **6,** 3070–3077 (2007).
32. Manning, G., Whyte, D. B., Martinez, R., Hunter, T. & Sudarsanam, S. The protein kinase complement of the human genome. *Science* **298,** 1912–1934 (2002).
33. Hunter, T. The age of crosstalk: phosphorylation, ubiquitylation, and beyond. *Mol. Cell* **28,** 730–738 (2007).

nature cell biology

DOI: 10.1038/ncb1848

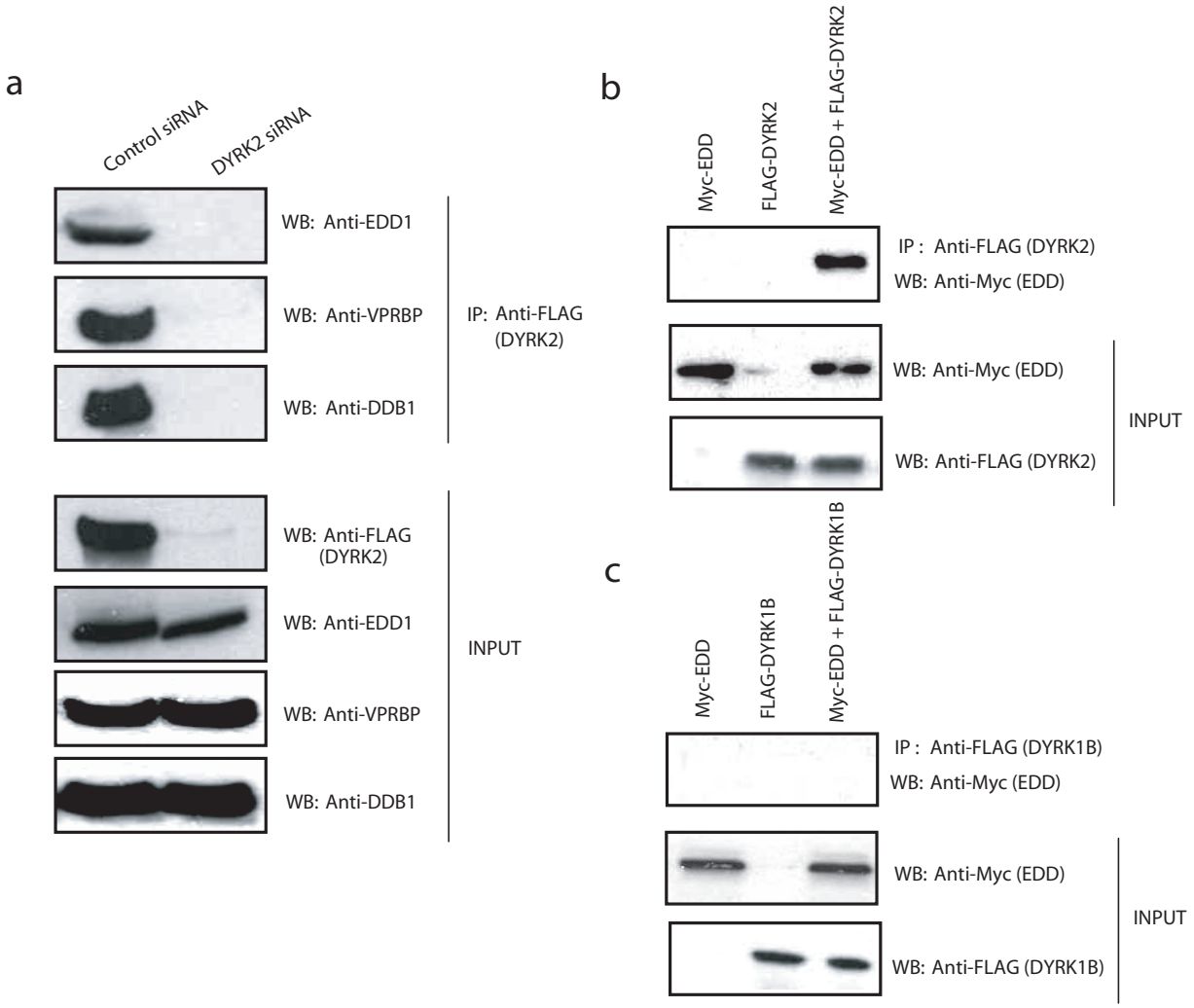

Figure S1 DYRK2 interacts specifically with EDD complex. (A) 293T cells stably expressing SFB tagged DYRK2 were transfected with control siRNA or DYRK2 specific siRNA. Cell lysates prepared 72 hours post transfection were used for immunoprecipitation with anti-FLAG antibody. The association of EDD, DDB1 and VPRBP with DYRK2 was detected by immunoblotting with their respective antibodies. (B) 293T cells were transfected with plasmids encoding FLAG-DYRK2 or (C) FLAG-DYRK1B alone or in combination with plasmid encoding Myc-EDD. Cell lysates were prepared and immunoprecipitated with anti-FLAG antibody. The interaction of EDD with DYRK2 or DYRK1B was evaluated by immunoblotting with anti-Myc antibody.

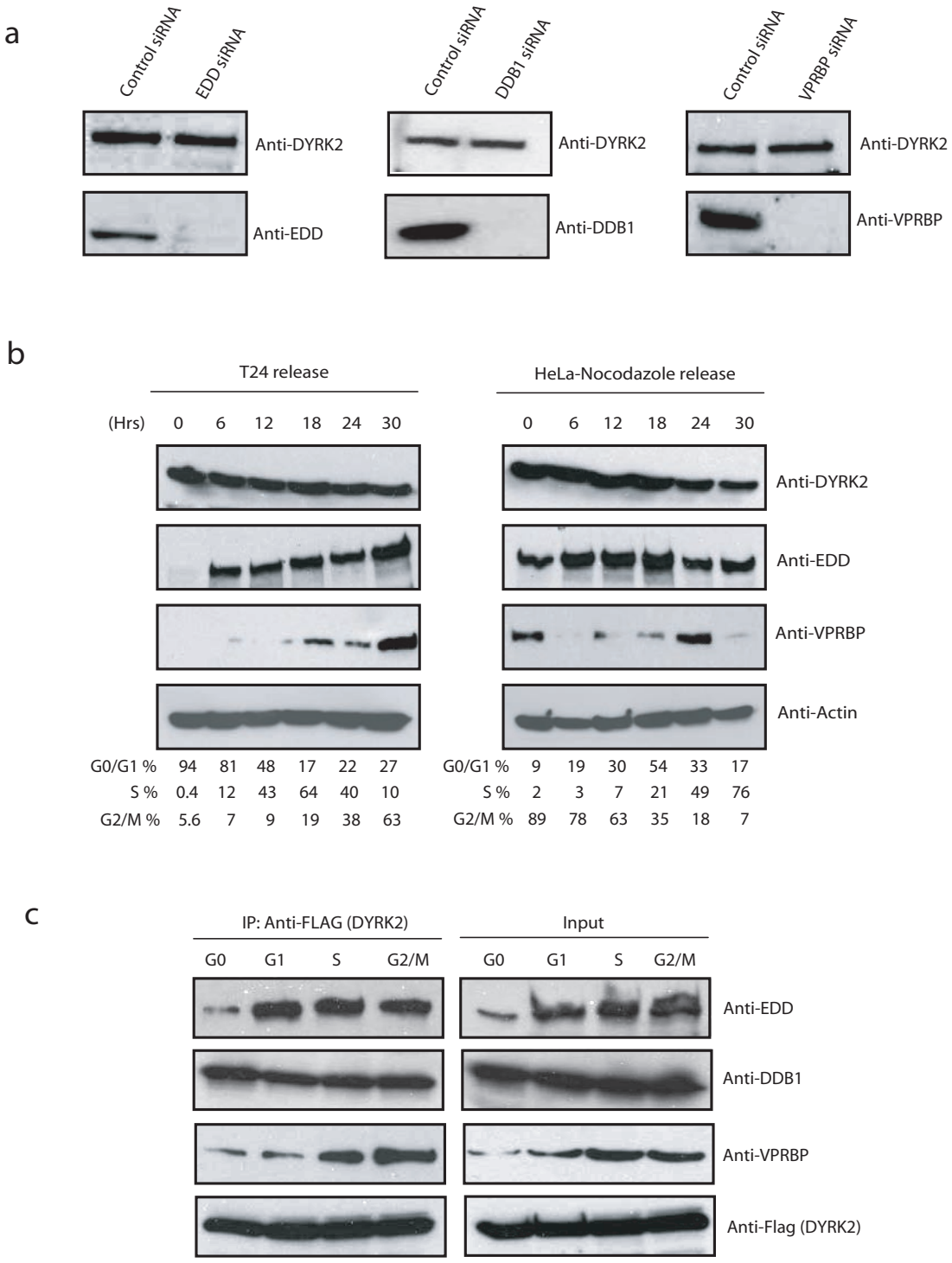

Figure S2 DYRK2 protein levels are not regulated by EDD-DDB1-VPRBP complex. (A) DYRK2 protein levels were assessed by anti-DYRK2 immunoblotting using extracts prepared from HeLa cells transfected with control siRNA, EDD siRNA, DDB1 siRNA or VPRBP siRNA. (B) DYRK2 levels are not cell cycle regulated. T24 cells were arrested in G0 phase by contact inhibition (left panel) and HeLa cells were synchronized in mitosis by nocodazole treatment (right panel). Lysates were prepared from cells collected at different times of post release as indicated. The expression levels of DYRK2, EDD, and VPRBP were analyzed by immunoblotting with their respective antibodies. Anti-Actin immunoblotting was included as a loading control. (C) T24 cells transfected with Flag-tagged DYRK2 were arrested in G0 phase by contact inhibition and further released into different phases of the cell cycle. Lysates were prepared from cells collected at 0h (G0), 6h (G1), 18h (S) and 30 hours (G2/M) of post release and subjected to immunoprecipitation with anti-Flag antibody. The interaction of EDD, DDB1 or VPRBP with DYRK2 was assessed by Western blotting with their respective antibodies.

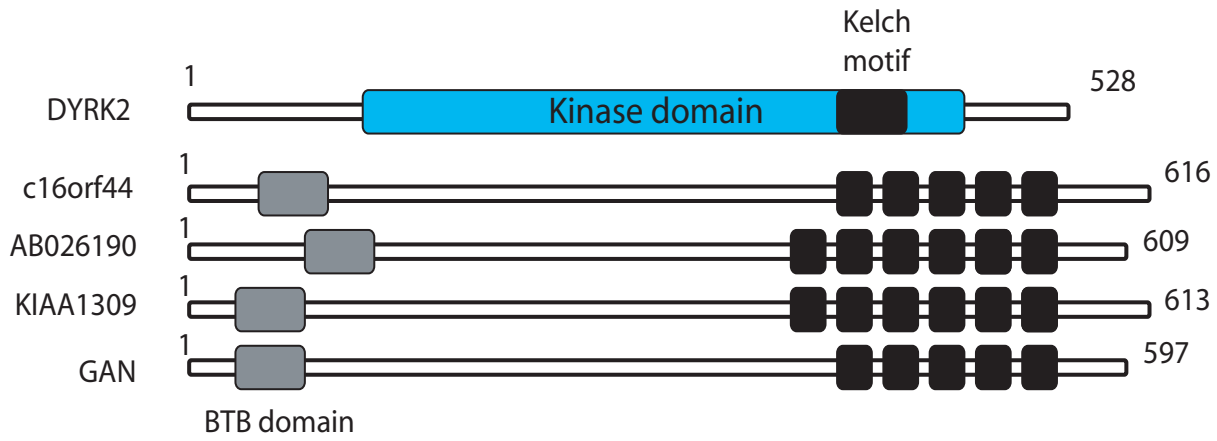

Figure S3 Schematic representation of DYRK2 along with known Kelch motif containing proteins. The kelch motif (aminoacids 390-433) in DYRK2 is positioned within the c-terminus of kinase catalytic domain. Other proteins aligned with DYRK2 contain kelch repeat. These proteins are known to function as E3-ubiquitin ligase adaptors.

Figure 1b

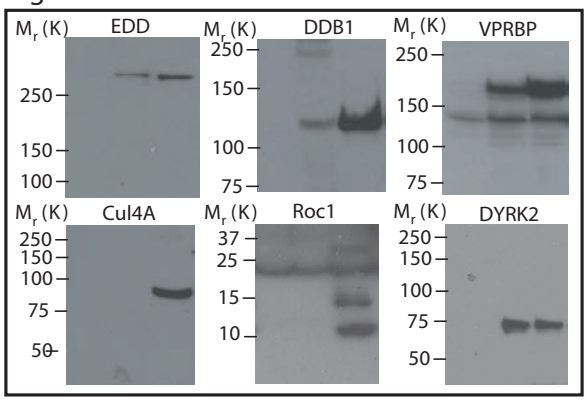

Figure 1c (top right)

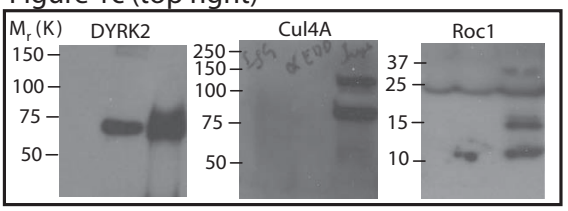

Figure 1c (top left)

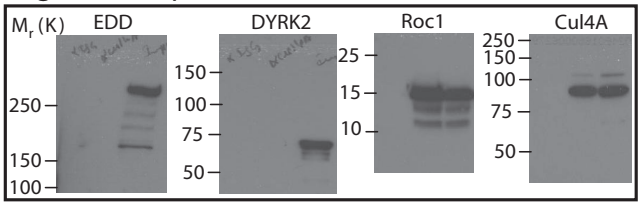

Figure 1d

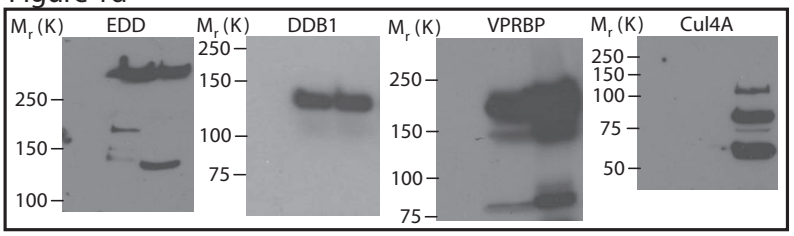

Figure 2c

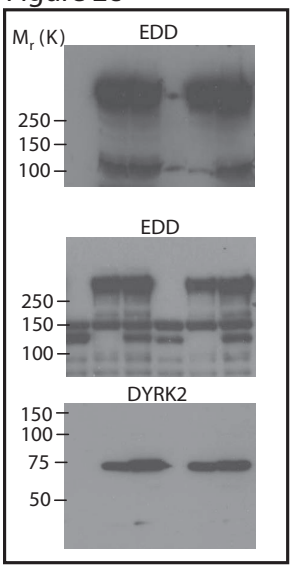

Figure 2a

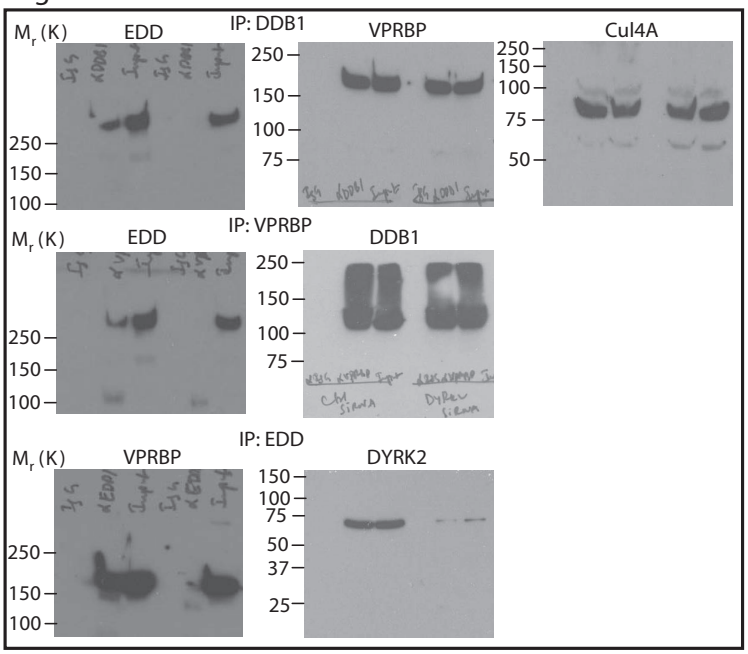

Figure 3b

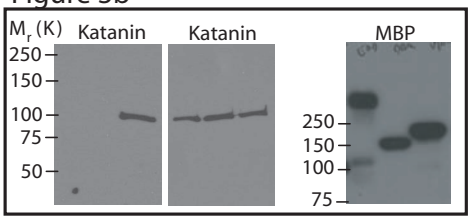

Figure 3c

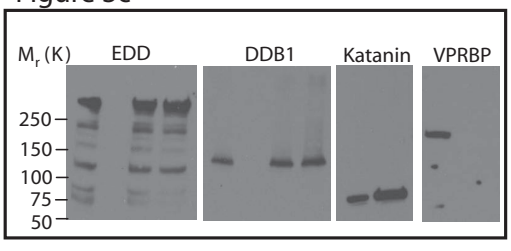

Figure 3a

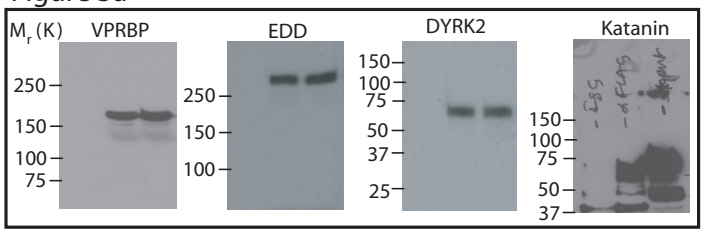

Figure S4 Full scans of key immunoblots shown in the manuscript.

Figure 3d

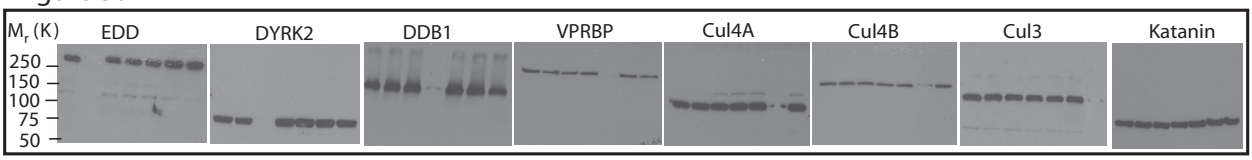

Figure 4a

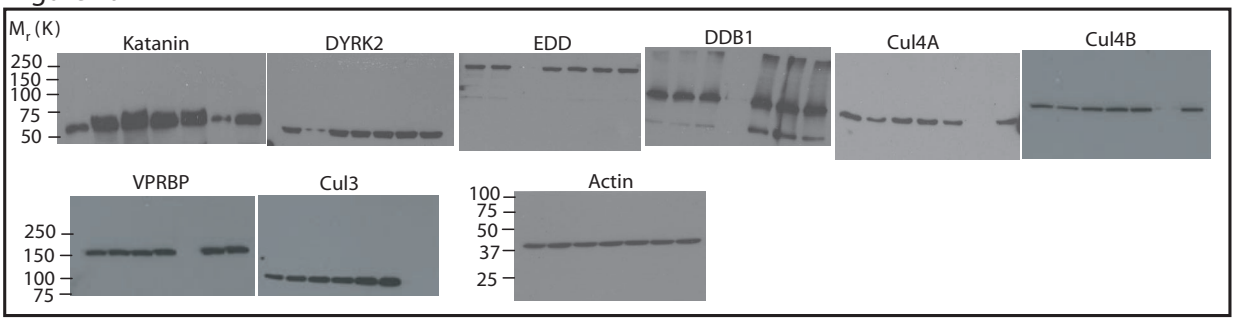

Figure 4b

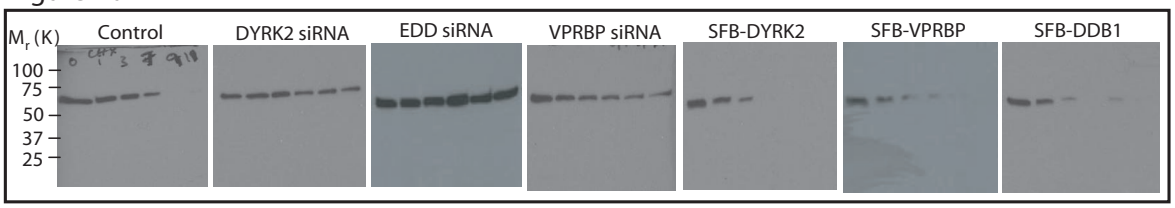

Figure 5

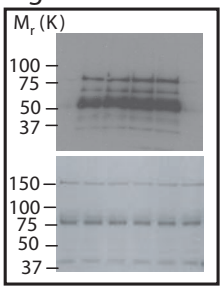

Figure 5d

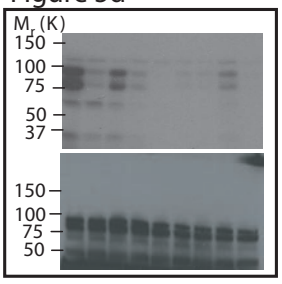

Figure 5e

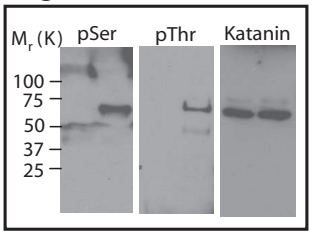

Figure 5f

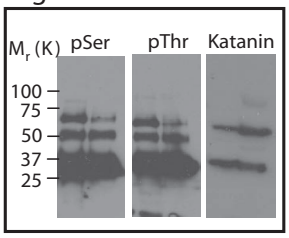

Figure 6a

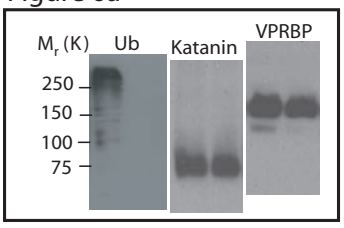

Figure 6b

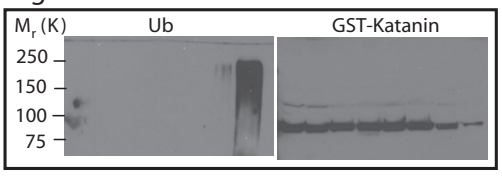

Figure 6c

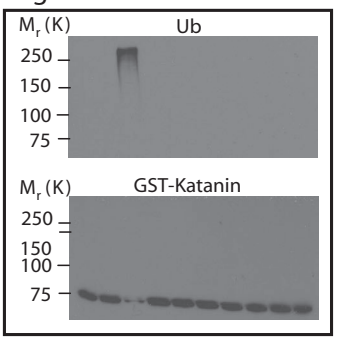

Figure 7b

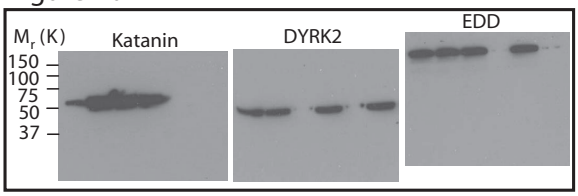

Figure S4 continued

Supplementary table 1:

Complete list of DYRK2 associated proteins identified by Mass spectrometric analysis:

Protein	No. of Peptides
Ubiquitin protein ligase EDD	53
Damage specific DNA binding protein (DDB1)	20
Dual specificity tyrosine-phosphorylation-regulated kinase 2 (DYRK2)	17
kiaa0800 protein (VPRBP)	13
78 kda glucose-regulated protein precursor (grp 78)	7
heat shock 70 kda protein 1 (hsp70.1)	6
heat shock 70 kda protein 1l (heat shock 70 kda protein 1-like)	6
heat shock cognate 71 kda protein (heat shock 70 kda protein 8)	3
dihydrolipoamide succinyltransferase	3
loc63929 protein	2
40s ribosomal protein s2 (s4) (llrep3 protein)	2
pyruvate dehydrogenase e1 component subunit beta	2
60s ribosomal protein l7	2
60s ribosomal protein l4	2
heterogeneous nuclear ribonucleoprotein u (hnrnp u)	1
dna-binding protein a	1
tubulin alpha-6 chain	1
60s acidic ribosomal protein p0 (l10e)	1
nucleophosmin (npm) (nucleolar phosphoprotein b23)	1
eukaryotic translation elongation factor 1 alpha-like 3	1
phosphate carrier protein, mitochondrial precursor (ptp)	1
60s ribosomal protein l7a (surfeit locus protein 3)	1
heat shock protein hsp 90-alpha (hsp 86)	1
mitochondrial 28s ribosomal protein s29 (s29mt)	1
wd repeat protein 22 (breakpoint cluster region protein 2)	1
tubulin alpha-2 chain	1
heterogeneous nuclear ribonucleoprotein g (hnrnp g)	1

replication protein a 70 kda dna-binding subunit (rp-a)	1
protein-beta-aspartate methyltransferase (pimt)	1
heat shock 70 kda protein 6	1
60s ribosomal protein l18	1

THE JOURNAL OF BIOLOGICAL CHEMISTRY VOL. 284, NO. 19, pp. 12998–13003, May 8, 2009

Functional Interaction between Chfr and Kif22 Controls Genomic Stability*[S]

Received for publication, January 16, 2009, and in revised form, March 25, 2009 Published, JBC Papers in Press, March 25, 2009, DOI 10.1074/jbc.M900333200

Subbareddy Maddika, Shirley M.-H. Sy[1], and Junjie Chen[2]

From the Department of Therapeutic Radiology, Yale University School of Medicine, New Haven, Connecticut 06520

Proper activation of checkpoint during mitotic stress is an important mechanism to prevent genomic instability. Chfr (Check point protein with FHA (Forkhead-associated domain) and RING domains) is a ubiquitin-protein isopeptide ligase (E3) that is important for the control of an early mitotic checkpoint, which delays entry into metaphase in response to mitotic stress. Because several lines of evidence indicate that Chfr is a potential tumor suppressor, it is critically important for us to identify Chfr substrates and understand how Chfr may regulate these substrates, control mitotic transitions, and thus, act as a tumor suppressor *in vivo*. Here, we report the discovery of a new Chfr-associated protein Kif22, a chromokinesin that binds to both DNA and microtubules. We demonstrated that Kif22 is a novel substrate of Chfr. We showed that Chfr-mediated Kif22 down-regulation is critical for the maintenance of chromosome stability. Collectively, our results reveal a new substrate of Chfr that plays a role in the maintenance of genome integrity.

Chfr (Check point protein with FHA and RING domains) is an early mitotic checkpoint protein that delays entry into metaphase in response to mitotic stress (1, 2). The checkpoint function of Chfr requires both of its FHA[3] and RING domains. The exact role of FHA domain in Chfr function is largely unknown. Chfr via its RING domain transfers both lysine 48-linked and lysine 63-linked polyubiquitin chains to its target proteins, which either promotes the degradation of target proteins or alters their function (3, 4). Recently, a PAR-binding zinc finger motif, which binds directly to polyADP-ribosylated substrates catalyzed by PARP1, was identified at the C-terminal region of Chfr (5). This PAR-binding zinc finger motif was reported to be required for Chfr function in antephase checkpoint (2, 5).

Chfr delays the cell cycle progression at mitosis by inactivating cyclin B1-bound Cdc2 and then exporting them from nucleus (6). Further, mechanistic studies have suggested that the inactivation of Cdc2 may be due to a negative regulation of Plk1 by Chfr (3). Polyubiquitination of Plk1 by Chfr negatively regulates the Plk1 protein levels, which delay the inactivation of Cdc2 inhibitory Wee1 kinase and the activation of Cdc25 phosphatase and thus maintain Cdc2 at its inactive state.

Several lines of evidence indicate that Chfr is a potential tumor suppressor. Loss or down-regulation of Chfr has been reported in several types of cancers including primary breast, lung, esophagus, colon, and gastric carcinomas (1, 7, 8). To investigate directly whether Chfr loss contributes to tumorigenesis, our laboratory has generated Chfr knock-out mice, which were cancer-prone and developed spontaneous tumors (9). The increased tumor incidence in Chfr null mice is likely due to a failure in maintaining chromosomal stability, which occurs at least partially due to the overexpression of a key mitotic kinase Aurora A (9). Chfr physically interacts with Aurora A and promotes its ubiquitination and degradation; thus, higher protein levels of Aurora A in Chfr null mice may contribute to chromosomal instability and eventually tumorigenesis. Therefore, our current hypothesis is that Chfr may regulate the stability of several of its substrates including Aurora A, and thus, control mitotic progression and prevent chromosomal instability. In this study, we reported the identification of another Chfr substrate as chromokinesin protein Kif22 and revealed that Kif22 overexpression also contributes to chromosomal instability observed in Chfr-deficient cells.

EXPERIMENTAL PROCEDURES

Plasmids—Full-length Chfr and Kif22 were cloned into an S-protein/FLAG/SBP (streptavidin-binding protein) triple-tagged destination vector using the Gateway cloning system (Invitrogen). Various Kif22 deletions (D1–D8), Chfr deletions (ΔFHA, ΔRING, and ΔCys), and point mutations were generated by PCR-based site-directed mutagenesis and verified by DNA sequencing. Full-length Chfr and Kif22 were also cloned to Myc-tagged mammalian expression destination vector and GST-tagged and MBP-tagged bacterial expression vector. An HA-tagged ubiquitin construct was used in *in vivo* ubiquitination assays.

Cell Culture—HeLa and 293T cells were maintained in RPMI medium supplemented with 10% fetal bovine serum and 1% penicillin and streptomycin. Human mammary epithelial cells (HMEC) were maintained in MEGM complete medium supplemented with bovine pituitary extract. 293T-Chfr, 293T-Kif22, MCF7-control shRNA, MCF7-Chfr shRNA, T47D-control shRNA, and T47D-Chfr shRNA stable cell lines were maintained in complete RPMI medium supplemented with 2 μg/ml puromycin. HeLa-Myc Chfr stable cell lines were maintained in

* This work was supported, in whole or in part, by National Institutes of Health Grant CA113381 (to J. C).
[S] The on-line version of this article (available at http://www.jbc.org) contains a supplemental table and a supplemental figure.
[1] A recipient of a postdoctoral fellowship from the Croucher Foundation.
[2] A recipient of an Era of Hope Scholars award from Department of Defense and a member of the Mayo Clinic Breast SPORE program. To whom correspondence should be addressed: Dept. of Therapeutic Radiology, Yale University School of Medicine, P. O. Box 208040, New Haven, CT 06520. Tel.: 203-785-3758; Fax: 203-785-7482; E-mail: Junjie.chen@yale.edu.
[3] The abbreviations used are: FHA, Forkhead-associated domain; PAR, poly(ADP-ribose); GST, glutathione *S*-transferase; MBP, myelin basic protein; HA, hemagglutinin; shRNA, short hairpin RNA; siRNA, small interfering RNA; DBD, DNA-binding domain; PBS, phosphate-buffered saline; HMEC, human mammary epithelial cells.

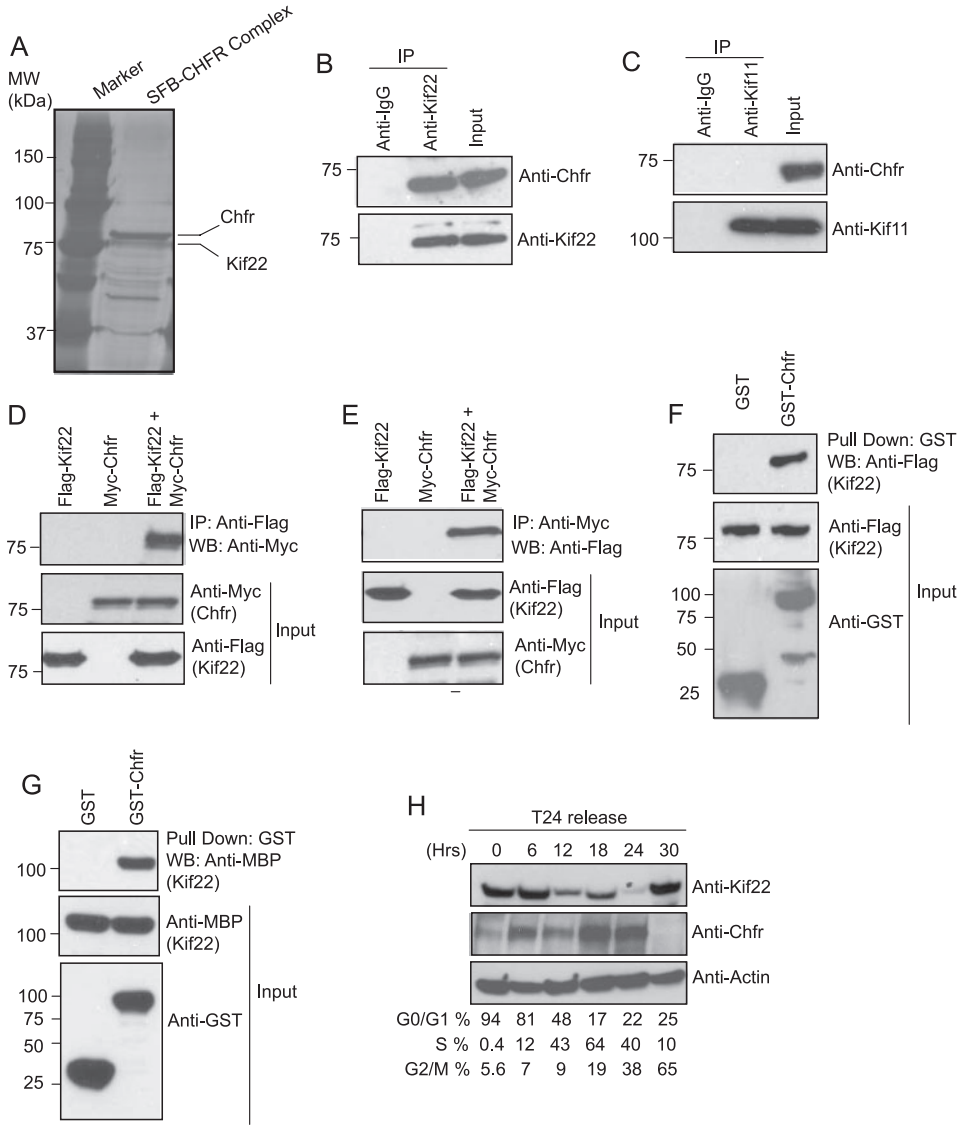

FIGURE 1. **Chfr interacts with Kif22.** *A*, 293T cells stably expressing triple-tagged Chfr (*SFB-Chfr*) were used in tandem affinity purification, and the associated proteins in the Chfr complex were separated by SDS-PAGE and visualized by Coomassie staining. The presence of Kif22 in the Chfr complex identified by mass spectrometry analysis was indicated. *MW*, molecular mass standards. *B* and *C*, immunoprecipitation (*IP*) using control IgG or Kif22 (*B*) or Kif11 antibody (*C*) was performed using 293T extracts, and the association of endogenous Chfr was evaluated by immunoblotting. *D*, 293T cells were transfected with plasmids encoding FLAG-tagged Kif22 or Myc-tagged Chfr alone or in combination. The immunoprecipitation was performed using anti-FLAG antibodies, and the associated Chfr was identified by Western blotting (*WB*) using anti-Myc antibody. *E*, reverse co-immunoprecipitation was performed using anti-Myc antibody, and the presence of Kif22 in Chfr immunocomplex was examined by Western blotting using anti-FLAG antibody. *F*, either control GST or GST-Chfr fusion proteins immobilized on agarose beads were incubated with extracts prepared from 293T cells expressing FLAG-tagged Kif22, and the interaction of Kif22 with Chfr was assessed by immunoblotting. *G*, either control GST or GST-Chfr fusion proteins immobilized on agarose beads were incubated with bacterially expressed recombinant MBP-Kif22, and the interaction of Kif22 with Chfr was assessed by immunoblotting with anti-MBP antibody. *H*, T24 cells were allowed to grow to confluency for 96 h and then trypsinized and released into fresh medium. Samples were taken at the indicated time points and analyzed by fluorescence-activated cell sorter and Western blotting.

RPMI medium with G418. All the cell lines described were maintained in humidified incubator at 37 °C with 5% CO_2.

Antibodies—Anti-Kif22 (Cytoskeleton Inc.), anti-HA (Covance), anti-GST, anti-Myc (Santa Cruz Biotechnology Inc.), anti-FLAG, anti-MBP, anti-actin, anti-α tubulin, anti-γ tubulin (all from Sigma), anti-CENPA (AbCam), and anti-phospho histone H3 serine 10 antibodies were used in this study. Mouse monoclonal anti-Chfr antibodies were produced by hybridoma fusions. Rabbit anti-Aurora B antibodies were raised previously in the laboratory by immunizing rabbits with GST-Aurora B fusion protein. Antisera were affinity-purified using AminoLink plus immobilization and purification kit (Pierce).

Tandem Affinity Purification—293T cells were transfected with plasmid encoding triple-tagged Chfr, and 3 weeks later, puromycin-resistant colonies were selected and screened for Chfr expression. Chfr stable cells were lysed with NETN buffer (20 mM Tris-HCl, pH 8.0, 100 mM NaCl, 1 mM EDTA, 0.5% Nonidet P-40) containing 50 mM β-glycerophosphate, 10 mM NaF, 1 μg/ml of pepstatin A and aprotinin (10 μg/ml) on ice for 20 min. Cell lysates were incubated with streptavidin-Sepharose beads (Amersham Biosciences) for 1 h at 4 °C. The bound proteins were washed three times with NETN and then eluted twice with 2 mg/ml biotin (Sigma) for 30 min at 4 °C. The eluates were incubated with S-protein-agarose (Novagen) for 1 h at 4 °C and then washed three times with NETN. The proteins bound to S-protein-agarose beads were resolved by SDS-PAGE and visualized by Coomassie Blue staining. The identities of eluted proteins were revealed by mass spectrometry analysis performed by the Taplin Biological Mass Spectrometry Facility at Harvard.

Transfection, Immunoprecipitation, and Immunoblotting—293T cells and HeLa cells were transfected with various plasmids using Lipofectamine (Invitrogen) according to the manufacturer's protocol. For immunoprecipitation assays, whole cell lysates were incubated with 2 μg of specified antibody bound to either protein A-Sepharose beads or protein G-Sepharose beads (Amersham Biosciences) for 1 h at 4 °C. The immunocomplexes were then washed with NETN buffer four times and applied to SDS-PAGE. Immunoblotting was performed following standard protocols.

In Vivo Ubiquitination Assay—HeLa Cells were transfected with various combinations of plasmids as shown in Fig. 3, *A* and *B*, along with HA-tagged ubiquitin. At 24 h after transfection, cells were treated with MG132 (4 μM) for 6 h, and whole cell

extracts prepared by NETN lysis were used to immunoprecipitate the substrate protein. The analysis of ubiquitination was performed by immunoblotting using anti-HA antibodies.

GST Pulldown Assays—GST-tagged Chfr or control GST bound to glutathione-Sepharose beads (Amersham Biosciences) were incubated with 293T cell lysates expressing FLAG-tagged Kif22 or a bacterially expressed recombinant MBP-Kif22 for 1 h at 4 °C, and the washed complexes were eluted by boiling in SDS sample buffer, separated by SDS-PAGE, and the interactions were analyzed by Western blotting.

RNA Interference—Control small interfering RNA (siRNA) and the smart pool siRNAs against Kif22 and Chfr were purchased from Dharmacon Inc. Transfection was performed twice 30 h apart with 200 nM siRNA using Oligofectamine reagent according to the manufacturer's protocol (Invitrogen), and the protein expression was analyzed by immunoblotting 72 h after transfection. Control shRNA and Chfr shRNA target sets were purchased from Open Biosystems, and stable clones of MCF-7 and T47D cells were made by transfecting with Lipofectamine followed by puromycin selection for 3 weeks.

Immunoflouroscence Staining—Cells grown on coverslips were fixed with 3% paraformaldehyde solution in phosphate-buffered saline (PBS) containing 50 mM sucrose at room temperature for 15 min. After permeabilization with 0.5% Triton X-100 buffer containing 20 mM HEPES, pH 7.4, 50 mM NaCl, 3 mM $MgCl_2$, and 300 mM sucrose at room temperature for 5 min, cells were incubated with a primary antibody (α-tubulin, CENPA, γ-tubulin, Chfr, and Kif22) at 37 °C for 20 min. After washing with PBS, cells were incubated with either fluorescein isothiocyanate-conjugated or rhodamine-conjugated secondary antibody at 37 °C for 20 min. Nuclei were counterstained with 4′6-diamidino-2-phenylindole. After a final wash with PBS, coverslips were mounted with glycerin containing paraphenylenediamine. Images were acquired by using a Nikon ECLIPSE E800 microscope.

Cell Cycle Analysis—T24 cells were arrested in G_0 phase by contact inhibition and were released into fresh medium. At the indicated time points, cells were lysed, and the levels of Chfr and Kif22 during different phases of the cell cycle were analyzed by Western blotting. Cell cycle progression was monitored by fluorescence-activated cell sorter analysis.

Metaphase Spreads—Metaphase chromosome spreads were performed as described before (9). Briefly, cells treated with colcemid for 8 h were collected, washed with PBS, and treated with 75 mM KCl at room temperature for 15 min. The treated cells were then fixed in fresh methanol:acetonic acid (3:1) solution and dropped onto glass slides. Cells were allowed to air dry and were stained with Giemsa (5%) and visualized under the microscope.

RESULTS

Kif22 Is a Chfr-associated Protein—In an attempt to better understand the molecular mechanisms underlying the tumor suppressor function of Chfr, we established a 293T derivative cell line stably expressing a triple epitope (S-protein, FLAG, and streptavidin-binding peptide)-tagged version of Chfr (SFB-Chfr). A two-step affinity purification using streptavidin-Sepharose beads and S-protein-agarose beads followed by mass

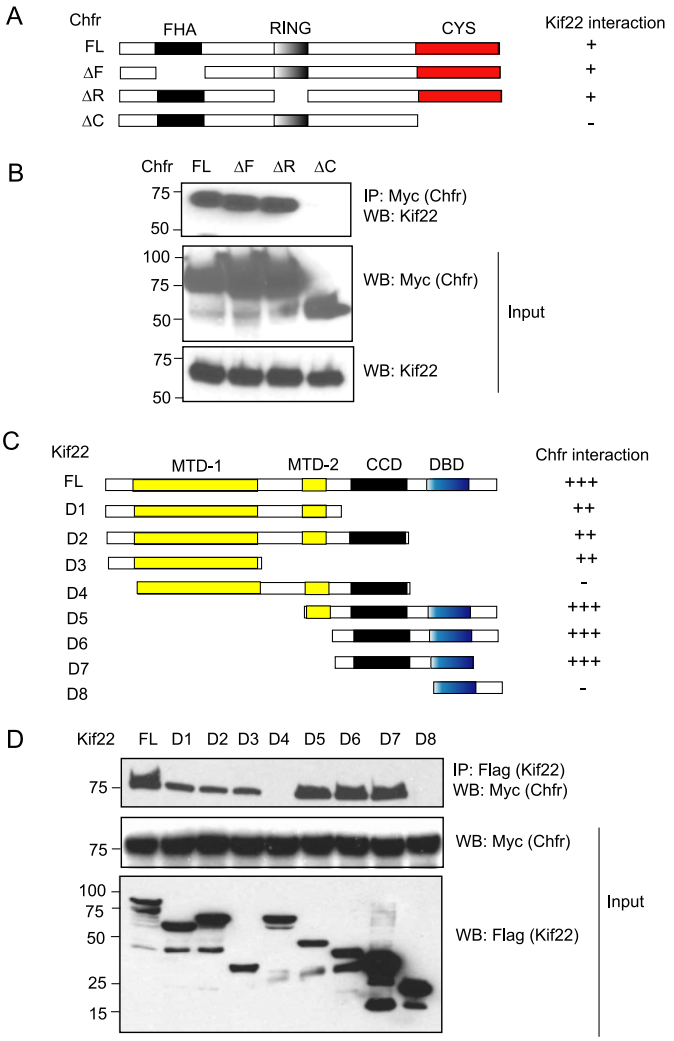

FIGURE 2. **Mapping the binding regions on Chfr and Kif22.** *A*, schematic representation of N-terminal Myc-tagged Chfr full-length (*FL*), ΔFHA (Δ*F*), ΔRING (Δ*R*), and Δcysteine-rich (Δ*C*) domain constructs used in this study. *B*, 293T cells were transfected with the indicated Myc-tagged Chfr constructs, and the interaction domain of Chfr with Kif22 was determined by immunoprecipitation (*IP*) followed by immunoblotting with the indicated antibodies. *WB*, Western blot. *C*, schematic representation of N-terminal FLAG-tagged Kif22 full-length, along with its various deletion mutants (*MTD*, motor domain; *CCD*, coiled-coil domain) used in this study. *D*, 293T cells were co-transfected with the indicated FLAG-tagged Kif22 constructs along with Myc-tagged Chfr, and the interaction region of Kif22 with Chfr was determined by immunoprecipitation and immunoblotting with the indicated antibodies.

spectrometry analysis allowed us to identify several Chfr-interacting proteins (Fig. 1*A* and supplemental Table 1). Among them, we repeatedly isolated Kif22 as a major associated protein in the purified Chfr complex. Kif22 (also known as hKid) is a mitotic motor protein with both DNA and microtubule binding activities and thus plays a positive role during spindle assembly and proper chromosome segregation in mitosis (10–12). We first confirmed that endogenous Kif22 but not Kif11 specifically associates with Chfr (Fig. 1, *B* and *C*). Co-immunoprecipitation (Fig. 1, *D* and *E*) and GST pulldown assays (Fig. 1, *F* and *G*) further confirmed a direct interaction between these two proteins. Further, immunostaining of Chfr and Kif22 revealed overlapping localization of both proteins during interphase and early mitotic phases, but they appear to localize differently during late mitotic phases (supplemental Fig. S1). To further

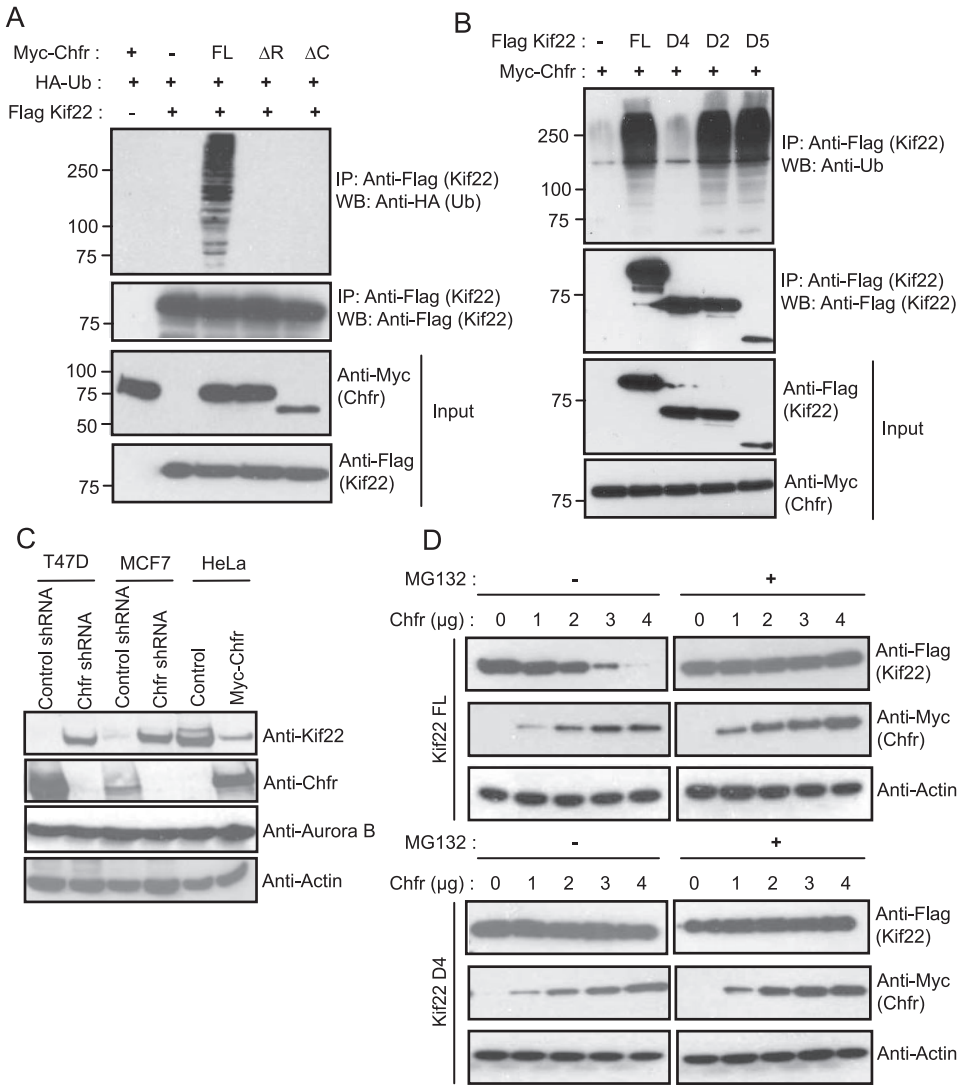

FIGURE 3. **Chfr ubiquitinates Kif22 and promotes its degradation.** *A*, Myc-tagged full-length (*FL*), ΔRING (Δ*R*), or ΔCys-rich (Δ*C*) domain mutants of Chfr were expressed in HeLa cells along with FLAG-Kif22 and HA-ubiquitin (*HA-Ub*). The levels of Kif22 ubiquitination were evaluated by anti-HA immunoblotting (*WB*) following immunoprecipitation (*IP*) of Kif22. Δ*F*, ΔFHA. *B*, HeLa cells were transfected with plasmids encoding FLAG-tagged full-length Kif22, a Chfr binding-defective mutant D4, an N-terminal mutant D2, or a C-terminal mutant D5 of Kif22 along with Myc-Chfr. The levels of Kif22 ubiquitination were evaluated by anti-ubiquitin immunoblotting following immunoprecipitation of Kif22. *C*, T47D and MCF7 cells were stably transfected with either control shRNA or Chfr shRNA. The control HeLa cells lacking endogenous Chfr expression were stably transfected with plasmids encoding Myc-Chfr. Protein levels of Kif22, Chfr, Aurora B, and actin were detected by immunoblotting with their respective antibodies. *D*, 293T cells were transiently transfected with the Kif22 FL or D4 mutant expression vector along with various indicated amounts of plasmids encoding full-length Chfr in the absence or presence of MG132. The levels of indicated proteins were estimated by immunoblotting 24 h after transfection.

understand how these two proteins may function together, we examined whether Chfr and Kif22 expression would be coordinately regulated during cell cycle. T24 cells were arrested in G_0 phase by contact inhibition, and the synchronized cells were allowed to reenter the cell cycle by releasing them into fresh medium at the appropriate density. As shown in Fig. 1*H*, the levels of Kif22 and Chfr were tightly regulated and inversely correlated during different phases of the cell cycle, suggesting a potential functional link between these two proteins.

Chfr contains N-terminal FHA, a middle RING, and C-terminal cysteine-rich domains (1). The FHA domain, known to be a phospho-peptide-binding motif, is important for Chfr checkpoint function in response to mitotic stress (1, 13, 14), but the identities of the proteins interacting with Chfr FHA domain are still unknown. The RING finger domain, a characteristic domain of ubiquitin-protein isopeptide ligase (E3), also plays a crucial role in Chfr function via its ability to ubiquitinate substrates such as Aurora A and Plk1 (3, 9, 15). The C-terminal cysteine-rich domain of Chfr is required for its binding to substrates and therefore targeting its substrates for degradation (9). To map the Kif22-binding region on Chfr, we used Myc epitope-tagged wild-type and a series of Chfr deletion mutants (Fig. 2*A*). Immunoprecipitation with anti-Myc antibody revealed that endogenous Kif22 interacted with full-length Chfr, ΔFHA, and ΔRING Chfr mutants but not with the Δcysteine-rich domain mutant of Chfr (Fig. 2*B*), suggesting that the C-terminal cysteine-rich domain of Chfr is essential for mediating its interaction with Kif22.

On the other hand, Kif22 also has several functional domains that are critically important for its mitotic function during spindle assembly and proper chromosome alignment in metaphase (11, 16). We generated expression constructs for FLAG-tagged Kif22 and a series of N-terminal or C-terminal deletion mutants that lack different Kif22 functional domains (Fig. 2*C*). To map the Chfr-binding region on Kif22, we co-expressed these constructs along with full-length Myc-tagged Chfr. The immunoprecipitation results suggest that Chfr interacts with Kif22 through both the N termini and the C termini because only a deletion mutant (D4) that lacks both termini of Kif22 failed to bind to Chfr (Fig. 2*D*). The interaction of Chfr with the N terminus of Kif22 appears to be weaker than its binding to the C terminus of Kif22 (Fig. 2*D*).

Kif22 Is a Novel Substrate of Chfr—At least in the case of Aurora A, we know that Chfr uses its C-terminal cysteine-rich domain as a substrate recognition domain, which recruits substrates for ubiquitination and degradation (9). Because Kif22 interacts with Chfr via its cysteine-rich domain, we reasoned that Kif22 might be a Chfr substrate. Kif22 was polyubiquitinated in the presence of the full-length Chfr but not ΔRING or Δcysteine-rich

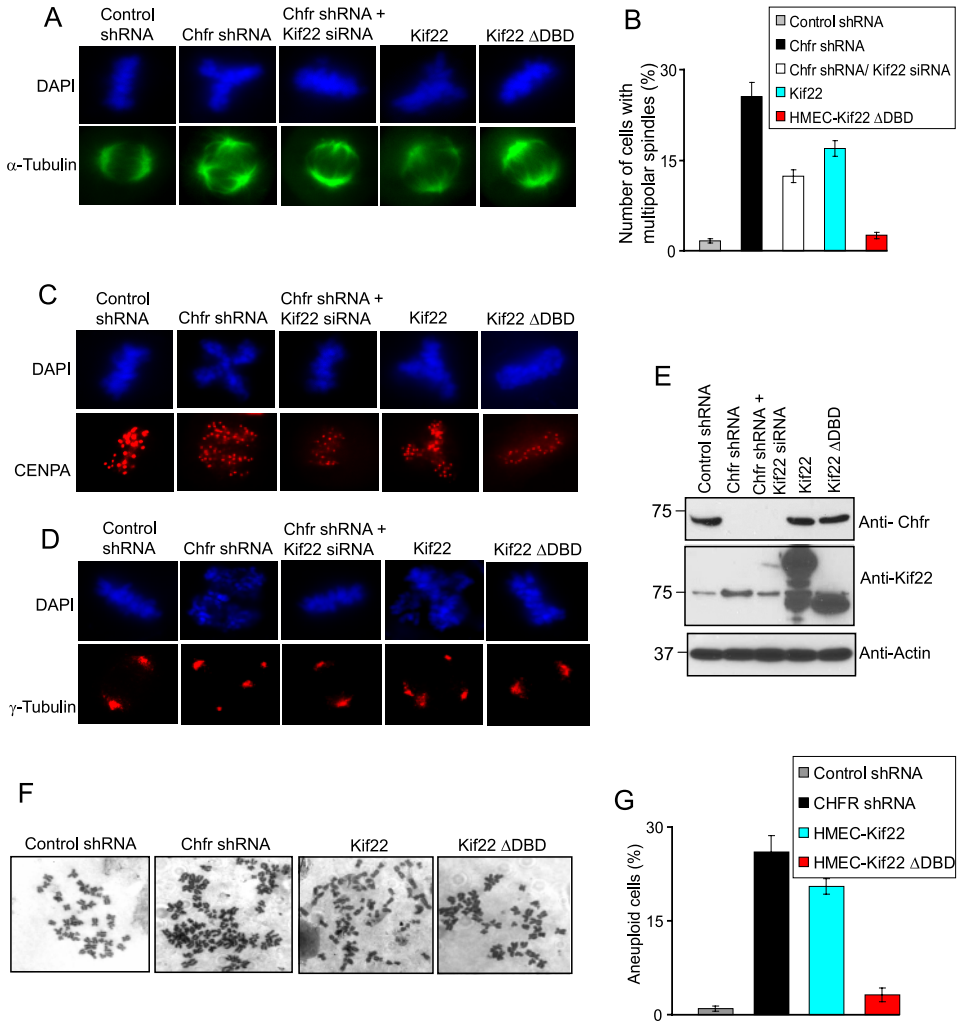

FIGURE 4. **Aberrant expression of Kif22 leads to genomic instability in primary cells.** *A*, human mammary epithelial cells transfected with control shRNA, Chfr shRNA alone or in combination with Kif22 siRNA, or plasmids encoding full-length Kif22 and Kif22 ΔDBD mutant were subjected to immunofluorescence staining using anti-α-tubulin antibody to visualize the integrity of mitotic spindle apparatus. *DAPI*, 4′6-diamidino-2-phenylindole. *B*, the frequency of multipolar mitotic spindles observed in cells expressing Chfr shRNA alone, in combination with Kif22 siRNA, or in cells with Kif22 and Kif22 ΔDBD overexpression was determined by quantification of the data from *A* after counting at least 200 mitotic spindles in each experiment (±S.D., $n = 3$). *C*, HMECs transfected as indicated in *A* were subjected to immunofluorescence staining using anti-CENPA antibody to visualize kinetochores. *D*, HMECs transfected as indicated in *A* were subjected to immunofluorescence staining using anti-γ tubulin antibody to visualize centrosomes. *E*, the protein levels of Chfr and Kif22 in HMECs used in *A* were evaluated by Western blotting using their respective antibodies as indicated. *F*, metaphase spreads were made using human mammary epithelial cells (HMEC) transfected with control shRNA, Chfr shRNA, Kif22 full-length, or Kif22 ΔDBD expression construct, and the examples from each case were presented. *G*, the frequency of aneuploid cells is determined by quantification of the data from *F* after counting 100 metaphase spreads in each experiment (±S.D., $n = 3$).

domain deletion mutants, indicating that Kif22 is a substrate of Chfr, and both the intact Chfr E3 ligase activity and its substrate recognition domain are required for efficient Chfr-mediated Kif22 ubiquitination (Fig. 3*A*). Conversely, full-length Kif22, a Kif22 mutant (Fig. 2*C*, *D2*) with intact N-terminal Chfr interaction region but devoid of the C-terminal Chfr-interacting region, and a Kif22 mutant (Fig. 2*C*, *D5*) with intact C-terminal Chfr interaction region but devoid of the N-terminal Chfr-interacting region were efficiently ubiquitinated by Chfr (Fig. 3*B*). Another Kif22 mutant (Fig. 2*C*, *D4*), which lacks both the N-terminal and the C-terminal Chfr-binding regions, could not be ubiquitinated by Chfr (Fig. 3*B*), again supporting the notion that a specific interaction of Chfr with Kif22 is essential for Chfr-dependent Kif22 polyubiquitination.

Polyubiquitination of Kif22 by the Chfr is likely to be required for Kif22 degradation as the stable knockdown of Chfr in T47D and MCF-7 cells results in up-regulation of Kif22 (Fig. 3*C*). In addition, the protein levels of Kif22 were down-regulated by stable expression of Myc-tagged Chfr in HeLa cells that lack endogenous Chfr expression. This difference in Kif22 protein levels in cells with or without Chfr expression may not be due to changes in cell cycle distribution in those cells because the levels of a control mitotic protein Aurora B were unaltered (Fig. 3*C*), and also, no significant differences in cell cycle distributions were observed in these cells (data not shown). These results indicate that Kif22 protein levels are tightly regulated by Chfr *in vivo*.

To further confirm the Chfr-mediated Kif22 down-regulation and its dependence on the proteasome pathway, we performed a co-transfection experiment with Chfr and Kif22 in the presence or absence of a proteasome inhibitor MG132. Co-transfection of Kif22 but not Chfr binding-deficient mutant of Kif22 (D4) along with Chfr reduced the steady-state levels of Kif22 protein (Fig. 3*D*). Pretreatment with MG132 prevents Chfr-mediated Kif22 down-regulation, suggesting the involvement of the proteasome-dependent pathway during Chfr-mediated Kif22 degradation. Taken together, these data suggest that Kif22 is a *bona fide in vivo* substrate of Chfr.

Aberrant Expression of Kif22 Results in Abnormal Mitotic Spindles and Promotes Genomic Instability—Kif22 is known to be required for proper mitotic spindle organization and normal chromosomal alignment on the metaphase spindle (17). In addition, our laboratory has previously reported that the loss of Chfr leads to multiple mitotic defects (9). Thus, we tested whether the Chfr-mediated Kif22 regulation would play a role in controlling mitotic progressions, especially during mitotic spindle assembly.

HMECs expressing control shRNA displayed normal bipolar mitotic spindles, whereas some of the cells with Chfr knockdown exhibited abnormal mitotic spindles with multiple poles and disorganized array of microtubules that failed to organize a proper metaphase plate (Fig. 4, *A* and *B*). Similar to Chfr

shRNA, transient overexpression of wild-type Kif22 but not DNA-binding domain-deleted (ΔDBD) Kif22 mutant (Fig. 4*E*) also resulted in cells with abnormal mitotic spindles (Fig. 4, *A* and *B*), suggesting that Chfr loss may lead to Kif22 overexpression and thus cause spindle disorganization. Upon knocking down of Chfr or Kif22 overexpression, we also observed aberrant arrangement of kinetochores (Fig. 4*C*) and the presence of abnormal number of centrosomes (Fig. 4*D*). A partial knock down of Kif22 (Fig. 4*E*) alleviated mitotic spindle defects observed in Chfr knockdown cells (Fig. 4, *A–D*).

Previously, our laboratory has also reported chromosomal instability in cells derived from Chfr knock-out mice (9). Similar to our previous findings using Chfr null mouse embryonic fibroblasts, the analysis of metaphase spreads revealed that Chfr down-regulation in HMECs results in abnormal chromosome numbers when compared with cells transfected with control shRNA (Fig. 4, *F* and *G*). Interestingly, Kif22 overexpression also results in chromosomal instability, analogous to cells with Chfr knockdown. These results suggest that at least one mechanism for Chfr functions in the maintenance of chromosomal stability and that tumor suppression could be through its regulation of Kif22 protein levels because both Chfr down-regulation and Kif22 overexpression result in chromosomal instability, which is a hallmark of tumorigenesis.

DISCUSSION

In this study, we have shown that Kif22 physically interacts with Chfr and is a newly identified Chfr substrate. Kif22 is a plus-end-directed microtubule-based motor protein that plays a role in bipolar organization of spindle microtubules and chromosome movement (11, 18), which are important for chromosome segregation during mitosis. We speculate that the spindle disorganization and abnormal metaphase chromosomal alignment observed in Chfr-deficient cells could be at least partially explained by the up-regulation of Kif22 in these cells. Importantly, analogous to Chfr expression, proper control of Kif22 expression is also important for the maintenance of chromosomal stability. Thus, we propose that in addition to previously identified Chfr substrates (Plk1 and Aurora A), Kif22 also plays a role in the maintenance of chromosomal stability. Moreover, chromosomal instability observed in primary cells with Kif22 overexpression may suggest a potential previously unidentified involvement of Kif22 in tumorigenesis that warrants further investigation.

Acknowledgments—We thank all members of the Chen laboratory for proving valuable suggestions and Zheng Fu (Mayo Clinic) for providing monoclonal anti-Chfr antibodies.

REFERENCES

1. Scolnick, D. M., and Halazonetis, T. D. (2000) *Nature* **406,** 430–435
2. Matsusaka, T., and Pines, J. (2004) *J. Cell Biol.* **166,** 507–516
3. Kang, D., Chen, J., Wong, J., and Fang, G. (2002) *J. Cell Biol.* **156,** 249–259
4. Bothos, J., Summers, M. K., Venere, M., Scolnick, D. M., and Halazonetis, T. D. (2003) *Oncogene* **22,** 7101–7107
5. Ahel, I., Ahel, D., Matsusaka, T., Clark, A. J., Pines, J., Boulton, S. J., and West, S. C. (2008) *Nature* **451,** 81–85
6. Summers, M. K., Bothos, J., and Halazonetis, T. D. (2005) *Oncogene* **24,** 2589–2598
7. Privette, L. M., and Petty, E. M. (2008) *Translational Oncol.* **1,** 57–64
8. Toyota, M., Sasaki, Y., Satoh, A., Ogi, K., Kikuchi, T., Suzuki, H., Mita, H., Tanaka, N., Itoh, F., Issa, J. P., Jair, K. W., Schuebel, K. E., Imai, K., and Tokino, T. (2003) *Proc. Natl. Acad. Sci. U. S. A.* **100,** 7818–7823
9. Yu, X., Minter-Dykhouse, K., Malureanu, L., Zhao, W. M., Zhang, D., Merkle, C. J., Ward, I. M., Saya, H., Fang, G., van Deursen, J., and Chen, J. (2005) *Nat. Genet.* **37,** 401–406
10. Tokai, N., Fujimoto-Nishiyama, A., Toyoshima, Y., Yonemura, S., Tsukita, S., Inoue, J., and Yamamota, T. (1996) *EMBO J.* **15,** 457–467
11. Tokai-Nishizumi, N., Ohsugi, M., Suzuki, E., and Yamamoto, T. (2005) *Mol. Biol. Cell* **16,** 5455–5463
12. Levesque, A. A., and Compton, D. A. (2001) *J. Cell Biol.* **154,** 1135–1146
13. Durocher, D., Henckel, J., Fersht, A. R., and Jackson, S. P. (1999) *Mol. Cell* **4,** 387–394
14. Daniels, M. J., Marson, A., and Venkitaraman, A. R. (2004) *Nat. Struct. Mol. Biol.* **11,** 1114–1121
15. Chaturvedi, P., Sudakin, V., Bobiak, M. L., Fisher, P. W., Mattern, M. R., Jablonski, S. A., Hurle, M. R., Zhu, Y., Yen, T. J., and Zhou, B. B. (2002) *Cancer Res.* **62,** 1797–1801
16. Yajima, J., Edamatsu, M., Watai-Nishii, J., Tokai-Nishizumi, N., Yamamoto, T., and Toyoshima, Y. Y. (2003) *EMBO J.* **22,** 1067–1074
17. Antonio, C., Ferby, I., Wilhelm, H., Jones, M., Karsenti, E., Nebreda, A. R., and Vernos, I. (2000) *Cell* **102,** 425–435
18. Funabiki, H., and Murray, A. W. (2000) *Cell* **102,** 411–424

PALB2 is an integral component of the BRCA complex required for homologous recombination repair

Shirley M. H. Sy, Michael S. Y. Huen, and Junjie Chen[1]

Department of Therapeutic Radiology, Yale University School of Medicine, New Haven, CT 06520

Edited by David M. Livingston, Dana–Farber Harvard Cancer Center, Boston, MA, and approved March 5, 2009 (received for review November 5, 2008)

Mutations in breast cancer susceptibility gene 1 and 2 (*BRCA1* and *BRCA2*) predispose individuals to breast and ovarian cancer development. We previously reported an in vivo interaction between BRCA1 and BRCA2. However, the biological significance of their association is thus far undefined. Here, we report that PALB2, the partner and localizer of BRCA2, binds directly to BRCA1, and serves as the molecular scaffold in the formation of the BRCA1-PALB2-BRCA2 complex. The association between BRCA1 and PALB2 is primarily mediated via apolar bonding between their respective coiled-coil domains. More importantly, BRCA1 mutations identified in cancer patients disrupted the specific interaction between BRCA1 and PALB2. Consistent with the converging functions of the BRCA proteins in DNA repair, cells harboring mutations with abrogated BRCA1-PALB2 interaction resulted in defective homologous recombination (HR) repair. We propose that, via its direct interaction with PALB2, BRCA1 fine-tunes recombinational repair partly through its modulatory role in the PALB2-dependent loading of BRCA2-RAD51 repair machinery at DNA breaks. Our findings uncover PALB2 as the molecular adaptor between the BRCA proteins, and suggest that impaired HR repair is one of the fundamental causes for genomic instability and tumorigenesis observed in patients carrying *BRCA1*, *BRCA2*, or *PALB2* mutations.

BRCA1 | BRCA2 | FANCN

Breast cancer and ovarian cancer is estimated to be responsible for more than one-fifth of cancer mortality (1). Because germ-line mutations in breast cancer susceptibility gene 1 and 2 (*BRCA1* and *BRCA2*) account for the development of a significant portion of hereditary breast and ovarian cancer, the understanding of their roles in tumor suppression is crucial to the improvement of therapeutic interventions. Because accumulation of genetic aberrations are often observed in cells derived from familial breast cancer patients with *BRCA1* or *BRCA2* mutations, the BRCA proteins have been considered as the caretakers of genomic integrity. Accordingly, tumor cells derived from these patients exhibit hypersensitivity to DNA damaging agents and display genomic instability (2–4).

Given the similar phenotypes in *BRCA1* and *BRCA2* patients, and the spectrum of deficits observed in cells deficient in these proteins, one would envision that the BRCA proteins might work in synchrony in certain cellular process(es) essential for tumor suppression. Consistent with this notion, interaction between the 2 BRCA proteins has been reported (5). However, exactly how their interaction is regulated and the biological significance for such interaction remains largely unexplored.

BRCA1 participates in numerous cellular processes (3, 6–8). In particular, BRCA1 has been proposed to have diverse roles to promote cell survival in response to genotoxic stress. Recent elucidation of multiple BRCA1 complexes in vivo suggests a multifactorial model by which BRCA1 mediates distinct processes that include checkpoint activation, damage signaling, and DNA repair (9, 10). However, BRCA2 has a pivotal role in the initiation of DNA repair, namely by loading of repair protein RAD51 onto single-stranded DNA for homologous recombination (HR) (11–13). More recently, Xia et al. (14) identified PALB2, the partner and localizer of BRCA2, as an essential component that is required for the loading of the BRCA2-RAD51 repair complex onto DNA. Similar to *BRCA1* and *BRCA2*, *PALB2* mutations have also been implicated in the predisposition of individuals to breast cancer development (15–20). That patients harbor *PALB2* mutation carries normal *BRCA1* and *BRCA2* suggests that these 3 proteins might be functionally linked.

In the current study, we provide direct evidence to support that PALB2 serves as the bridging molecule that connects BRCA1 and BRCA2. Our data suggest that PALB2 is an integral component of the BRCA1-BRCA2-RAD51 axis, which is critical for the maintenance of genomic stability via recombinational repair.

Results

BRCA1 Is a PALB2 Interacting Protein. To identify proteins that interact with PALB2, we adopted a tandem affinity purification (TAP) scheme using lysate derived from 293T cells stably expressing streptavidin binding peptide-Flag-S protein (SFB)-tagged PALB2. Mass spectrometry analyses of proteins that copurified with PALB2 revealed peptides that corresponded not only to BRCA2, but also BRCA1 (Fig. 1*A*). By employing insect SF9 cells and baculovirus expression system, we confirmed that PALB2 does indeed interact directly with BRCA1 (Fig. 1*B*; Fig. S1*b*). To examine whether endogenous PALB2 and BRCA1 interact in vivo, we performed coimmunoprecipitation (coIP) experiment using 293T cell lysate. Consistent with TAP results, both PALB2 and BRCA2 were found in BRCA1 precipitates (Fig. 1*C*). Conversely, BRCA1 and BRCA1-interacting proteins CtIP and BACH1 were also observed in PALB2 immunoprecipitates (Fig. 1*D*), suggesting that PALB2 is a component of BRCA1 complexes in vivo.

BRCA1 Exists in a Protein Complex with PALB2 and BRCA2. Because it has been reported that a significant portion of PALB2 associates with BRCA2 (14), and BRCA1 also interacts with BRCA2 (5), we asked whether BRCA1, PALB2, and BRCA2 coexist in a protein complex. We performed gel filtration chromatography using nuclease-treated 293T cell lysate to identify possible native protein complexes that contain BRCA1, PALB2, and BRCA2. All of the 3 proteins were found in overlapping fractions that corresponded to ≈2 MDa (Fig. 1*E*). These results indicated that BRCA1, BRCA2, and PALB2 possibly exist as a protein complex in vivo. Also, CtIP and BACH1, as well as RAD51 and RPA, were also concentrated in these fractions.

To further substantiate that PALB2 and the BRCA proteins form a single complex, serial immunodepletion experiment was

Author contributions: S.M.H.S., M.S.Y.H., and J.C. designed research; S.M.H.S. and M.S.Y.H. performed research; S.M.H.S., M.S.Y.H., and J.C. analyzed data; and S.M.H.S., M.S.Y.H., and J.C. wrote the paper.

The authors declare no conflict of interest.

This article is a PNAS Direct Submission.

[1]To whom correspondence should be addressed. E-mail: junjie.chen@yale.edu.

This article contains supporting information online at www.pnas.org/cgi/content/full/0811159106/DCSupplemental.

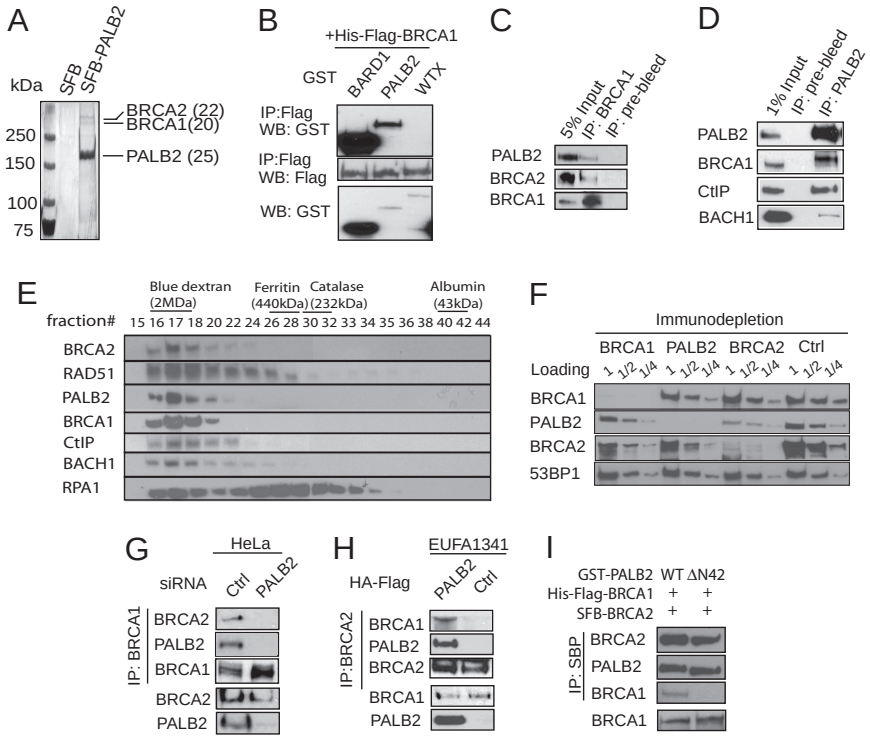

Fig. 1. Identification of PALB2 as an integral component of the BRCA protein complex. (*A*) Cell lysate prepared from 293T cells expressing SFB-PALB2 was subjected to TAP. PALB2-associated proteins were subsequently separated by SDS/PAGE and visualized by silver staining. Mass spectrometry analyses revealed the identities of the PALB2-associated proteins and their respective numbers of peptides obtained were shown in brackets. (*B*) SF9 cells were coinfected with baculoviruses expressing His-Flag-BRCA1 in addition to those expressing GST-PALB2, GST-BARD1, or GST-WTX. Cell lysates were subjected to IP by using anti-Flag (M2) beads. Immunoblotting was conducted as indicated. (*C*) CoIP of BRCA1 with PALB2 and BRCA2 was carried out using anti-BRCA1 antibody and immunoblotted with indicated antibodies. (*D*) Detection of PALB2-associated proteins; 293T cell lysates were subjected to IP using anti-PALB2 serum, and immunoblotting was carried out using antibodies as indicated. (*E*) Gel filtration chromatography analysis was performed using 293T cell lysate. Proteins eluted from the indicated fractions were separated by SDS/PAGE and analyzed by Western blotting using antibodies as indicated. (*F*) The 293T cell lysates were subjected to 3 rounds of immunodepletion using rabbit polyconal antibodies specifically raised against BRCA1, PALB2, or BRCA2. The resulting supernatants were examined for the presence of remaining BRCA1, PALB2, BRCA2, and 53BP1 content by immunoblotting using corresponding antibodies. (*G*) HeLa cells transfected with control or PALB2 siRNAs were subjected to IP using anti-BRCA1 antibody. Immunoblotting of whole-cell extracts or IPed samples was performed using antibodies as indicated. (*H*) Anti-BRCA2 IP was performed using lysates prepared from PALB2-deficient EUFA1341 cells or derivative cells reconstituted with HA-Flag-tagged PALB2. Immunoblotting of whole-cell extracts or IPed samples was performed using antibodies as indicated. (*I*) PALB2 bridges the BRCA1 and BRCA2 interaction in vitro. SF9 cells were infected with baculoviruses expressing His-Flag-BRCA1 and SFB-BRCA2, together with viruses expressing either GST-PALB2 or GST-PALB2 ΔN42. IP was carried out using streptavidin beads and immunoblotted with antibodies as indicated.

also performed. Consistent with previous observations (14), PALB2 depletion resulted in a significant reduction (≈50%) in the amount of BRCA2 (Fig. 1*F*). Also, PALB2 and BRCA2 protein levels were also reduced on BRCA1 depletion. Together, these results suggest that at least a fraction of BRCA1 associates with PALB2 and BRCA2 as a single protein complex.

One common feature of many DNA damage/repair proteins is their ability to localize and concentrate at sites of DNA breaks, forming discrete foci that colocalize with the double-stranded DNA break marker pH2AX. Because we found that BRCA1 associates with PALB2 and BRCA2 in vivo, we examined the extent of colocalization among these 3 proteins at DNA breaks in U2OS cells after ionizing radiation (IR). As shown in Fig. S1*c*, foci structures that contained BRCA1 and BRCA2, BRCA1 and PALB2, or BRCA1 and RAD51 were easily observed. Quantification analyses indicate that most of the PALB2, BRCA2, and RAD51 foci colocalize with that of BRCA1 (≈80%; Fig. S1*d*), which is similar to the extent of colocalization between PALB2 and RAD51 in PALB2-deficient EUFA1341 cell that has been reconstituted with flag-PALB2. These results suggest that the protein complex containing BRCA1, PALB2, and BRCA2 is concentrated at sites of DNA breaks, and may have a role in DNA damage signaling and/or DNA repair.

PALB2 Serves As the Molecular Scaffold for the Formation of BRCA Protein Complex. To study the functional significance of this complex formation, we first mapped the regions required for the BRCA1/PALB2 interaction. SFB-tagged wild-type PALB2 and a series of deletion mutants that span the entire PALB2 ORF (Fig. S2*a*) were subjected to coIP with full-length myc-BRCA1. Results showed that the PALB2 N terminus (P2F1; residues 1–319) is responsible for BRCA1 binding (Fig. S2*b*). Because a coiled-coil domain (residues 9–42) resides within this region, we tested whether it might be responsible for the association of PALB2 with BRCA1. Indeed, deletion mutant lacking the coiled-coil structure (P2ΔN42) was defective in BRCA1 binding (Fig. S2*c*), suggesting that BRCA1 binds directly to the very N terminus of PALB2.

Next, we sought to define the PALB2-binding region on BRCA1. We made use of a panel of myc-tagged deletion mutants that span the BRCA1 coding sequence (Fig. S3*a*). Pull-down assays indicated that full-length BRCA1 specifically associated with PALB2 in vitro (Fig. S3*b*). Further GST pull-down mapped the PALB2-binding region to residues 1314–1557 (Fig. S3 *a* and *b*). A more refined series of deletion mutants (Fig. S3*c*) narrowed down the binding region to residues 1364–1437 (Fig. S3*d*). Interestingly, this region (residues 1364–1437) of BRCA1 also harbors a putative coiled-coil domain. Internal deletion mutants of the predicted BRCA1 coiled-coil domains (B1ΔCC1 and B1ΔCC2) were generated (Fig. S3*c*). CoIP experiments demonstrated that although the wild-type and the B1ΔCC1 coIPed with PALB2, the B1ΔCC2 did not (Fig. S3*e*), indicating that the second coiled-coil domain (CC2) on BRCA1 is essential for its interaction with PALB2.

Intriguingly, the interaction domains between BRCA1 and PALB2 identified in this study (Fig. S2 and Fig. S3) overlap with the BRCA1-BRCA2 interaction domain identified previously (5). This observation prompted us to speculate that PALB2 may be the protein that links BRCA1 and BRCA2. To test this possibility, lysates prepared from HeLa cells transfected with control or PALB2 siRNA were subjected to IP by using anti-BRCA1 antibodies. Results showed that BRCA2 coIPed with BRCA1 only in the presence of PALB2 (Fig. 1*G*), suggesting that the interaction between BRCA1 and BRCA2 requires PALB2. Likewise, the BRCA1 and BRCA2 interaction was not observed in the PALB2 deficient EUFA1341 cells (Fig. 1*H*). However,

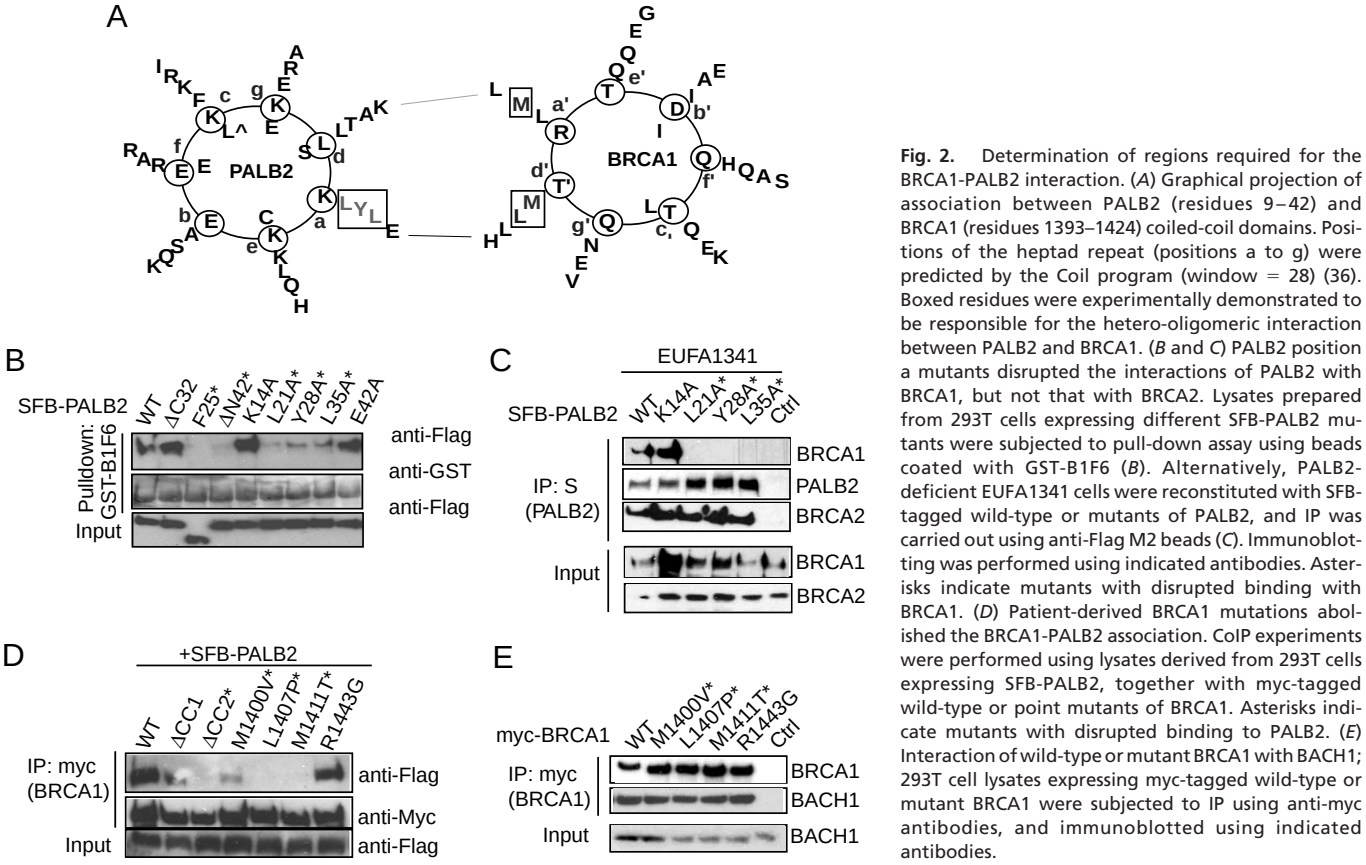

Fig. 2. Determination of regions required for the BRCA1-PALB2 interaction. (*A*) Graphical projection of association between PALB2 (residues 9–42) and BRCA1 (residues 1393–1424) coiled-coil domains. Positions of the heptad repeat (positions a to g) were predicted by the Coil program (window = 28) (36). Boxed residues were experimentally demonstrated to be responsible for the hetero-oligomeric interaction between PALB2 and BRCA1. (*B* and *C*) PALB2 position a mutants disrupted the interactions of PALB2 with BRCA1, but not that with BRCA2. Lysates prepared from 293T cells expressing different SFB-PALB2 mutants were subjected to pull-down assay using beads coated with GST-B1F6 (*B*). Alternatively, PALB2-deficient EUFA1341 cells were reconstituted with SFB-tagged wild-type or mutants of PALB2, and IP was carried out using anti-Flag M2 beads (*C*). Immunoblotting was performed using indicated antibodies. Asterisks indicate mutants with disrupted binding with BRCA1. (*D*) Patient-derived BRCA1 mutations abolished the BRCA1-PALB2 association. CoIP experiments were performed using lysates derived from 293T cells expressing SFB-PALB2, together with myc-tagged wild-type or point mutants of BRCA1. Asterisks indicate mutants with disrupted binding to PALB2. (*E*) Interaction of wild-type or mutant BRCA1 with BACH1; 293T cell lysates expressing myc-tagged wild-type or mutant BRCA1 were subjected to IP using anti-myc antibodies, and immunoblotted using indicated antibodies.

when these cells were reconstituted with wild-type PALB2, the BRCA1/BRCA2 interaction was readily detected (Fig. 1*H*).

To further substantiate the notion that PALB2 bridges the interaction between BRCA proteins, coIP experiments were performed using recombinant His-Flag-BRCA1 and SFB-BRCA2 together with GST-PALB2 or GST-PALB2 ΔN42 expressed in insect cells. As shown in Fig. 1*I*, in the presence of wild-type PALB2, BRCA2 associated with both PALB2 and BRCA1. In contrast, BRCA1 failed to interact with BRCA2 in cells expressing the PALB2 ΔN42 mutant, which has compromised association with BRCA1 (Fig. S2*c*), although it exhibits intact interaction with BRCA2 (Fig. 1*I*). These data firmly established PALB2 as the bridging protein that mediates BRCA1/BRCA2 interaction.

Structural Requirements for the BRCA1-PALB2 Interaction. Coiled-coil domains are known to mediate protein–protein interactions. Based on the results shown in Fig. S2 and Fig. S3, we suspected that the BRCA1-PALB2 interaction might be mediated by intermolecular interaction between their respective coiled-coil motifs. Therefore, we further studied this interaction, and generated alanine substitution mutations for residues at position "a" in the heptad-helical coiled-coil arrangement on PALB2 (K14A, L21A, Y28A, L35A, and E42A) (Fig. 2*A*). Pull-down experiments using GST-BRCA1 showed that the interactions between BRCA1 and the PALB2 L21A, Y28A, or L35A mutants were largely abolished (Fig. 2*B*), indicating that these residues are likely to be the contacting sites at the PALB2-BRCA1 interface. Reconstitution of these PALB2 mutants into PALB2-deficient EUFA1341 cells confirmed their compromised binding to BRCA1, whereas these mutants interacted normally with BRCA2 (Fig. 2*C*).

Within the coiled-coil domain of BRCA1 required for PALB2-binding (residues 1364–1437), we identified 3 BRCA1 missense mutations found among cancer patients (the Breast cancer information core database and the Human mutation database). Strikingly, all of these patient mutations (M1400V, L1407P, and M1411T) coincided with position a or "d" in the heptad coiled-coil (CC2) on BRCA1 (Fig. 2*A*). CoIP experiments revealed that, unlike the control mutation R1443G, all of the 3 point mutations within the BRCA1 CC2 region resulted in attenuated PALB2 interactions (Fig. 2*D*), although they have negligible effect on their interactions with BACH1 (Fig. 2*E*). These results imply that the interaction between BRCA1 and PALB2 may have a role in the tumor suppression functions of these proteins.

Independent Requirements for PALB2 and BRCA1 Focal Accumulation at DNA Double-Strand Breaks (DSBs). We next examined whether the physical interaction between BRCA1 and PALB2 might be important for their localization at sites of DNA breaks. IR-induced BRCA1 foci were observed for wild-type BRCA1, as well as all of the BRCA1 mutants within the CC2 region, regardless of their PALB2-binding activity (Fig. S4 *a* and *c*). Similarly, discrete foci were also detected for the BRCA1-binding defective mutants of PALB2 (Fig. S4*b*), although a reduction in the percentage of foci positive cells was observed for some of these mutants when compared with wild-type PALB2 (Fig. S4*d*). However, the PALB2 ΔF mutation (lacking residues 71–561), which retains BRCA1-binding motif, showed a drastic reduction in its foci formation capability (Fig. S4 *b* and *d*). Therefore, the foci forming abilities of these PALB2 mutants do not strictly correlate with their BRCA1-binding activities.

Exogenous PALB2 foci were also readily observed in HCC1937 cells (Fig. 3 *A* and *B*), which express only a truncated BRCA1 that lacks BRCT domain, and could not be recruited to

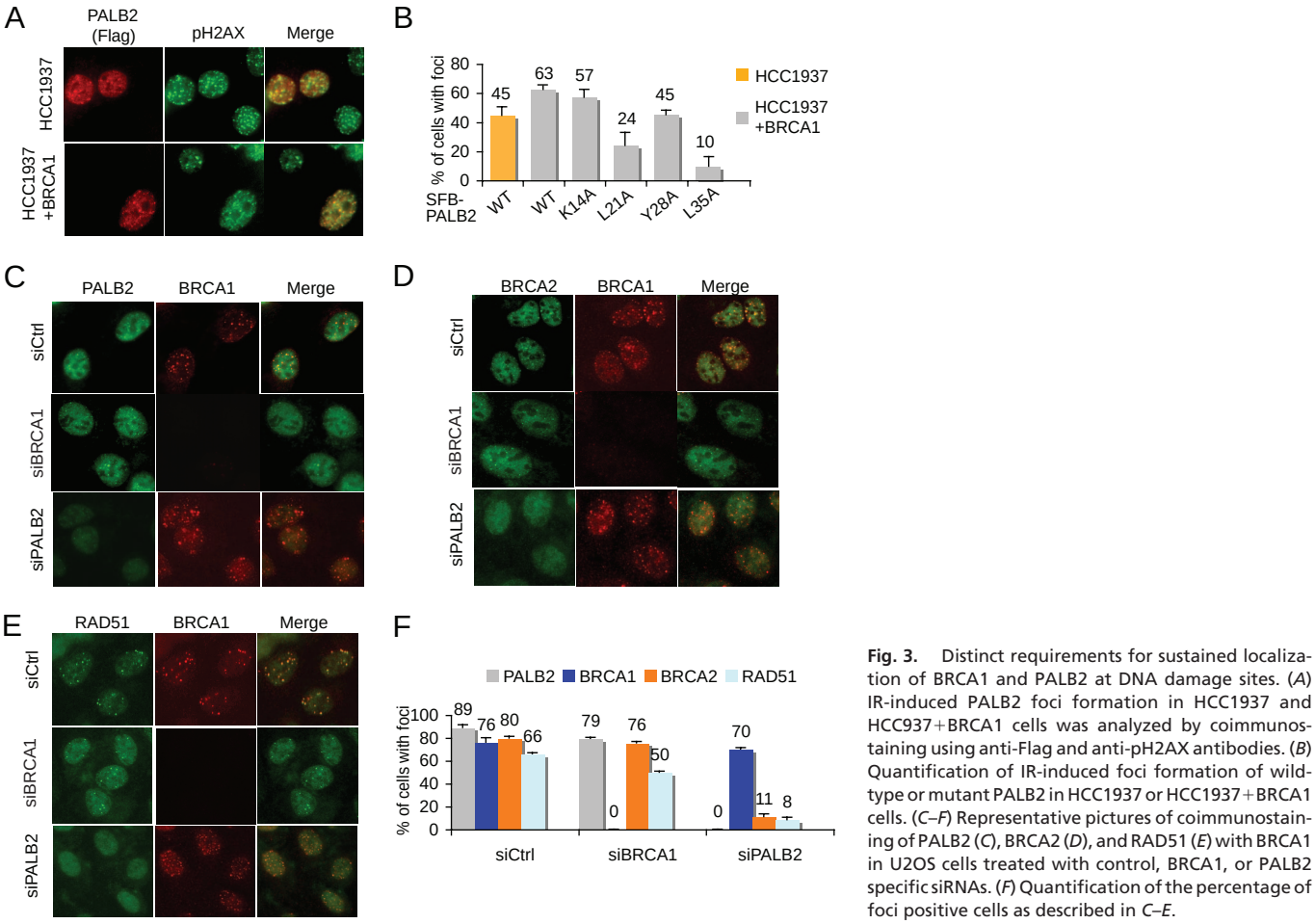

Fig. 3. Distinct requirements for sustained localization of BRCA1 and PALB2 at DNA damage sites. (*A*) IR-induced PALB2 foci formation in HCC1937 and HCC937+BRCA1 cells was analyzed by coimmunostaining using anti-Flag and anti-pH2AX antibodies. (*B*) Quantification of IR-induced foci formation of wild-type or mutant PALB2 in HCC1937 or HCC1937+BRCA1 cells. (*C–F*) Representative pictures of coimmunostaining of PALB2 (*C*), BRCA2 (*D*), and RAD51 (*E*) with BRCA1 in U2OS cells treated with control, BRCA1, or PALB2 specific siRNAs. (*F*) Quantification of the percentage of foci positive cells as described in *C–E*.

site of DSB (Fig. S4*e*). This result indicates that sustained localization of PALB2 at DNA breaks does not require prior focal accumulation of BRCA1. It is noteworthy to mention that PALB2 foci forming ability, although not entirely BRCA1-dependent, as observed in and Fig. 3 *A–C* and Fig. S4, is modestly elevated in HCC1937 cells reconstituted with wild-type BRCA1 (HCC1937+BRCA1) (Fig. 3*B*), suggesting that BRCA1 may help stabilize PALB2 at DNA damage sites.

Previous report implicated an essential role of PALB2 in the loading of BRCA2-RAD51 at DNA breaks (Fig. S5 *a* and *b*) (14, 21). In agreement with the proposed accessory role of BRCA1 in stabilizing PALB2 at DNA breaks, RAD51 foci were modestly reduced (≈2-fold) in HCC1937 cells, when compared with the same cells reconstituted with wild-type BRCA1 (Fig. S5 *c* and *d*) (22). To further explore whether BRCA1 might be essential for focal accumulation of PALB2, BRCA2, and RAD51 after DNA damage, we examined the localization of these proteins in U2OS cells with siRNA-mediated depletion of BRCA1. BRCA1 depletion led to a modest reduction in the foci forming ability of PALB2, BRCA2, and RAD51 (Fig. 3 *C–F*). However, in consistent with those observed in PALB2 deficient patient cells (Fig. S5 *a* and *b*), PALB2 depletion in U2OS cells resulted in a significant decrease in the number of cells containing damage-induced BRCA2 or RAD51 foci (Fig. 3 *C–F*), confirming that PALB2 is required for the stable accumulation of both BRCA2 and RAD51 at DNA damage sites. However, PALB2-depleted cells still displayed apparent normal BRCA1 foci formation after DNA damage (Fig. 3 *C–F*). Together, these results suggest that BRCA1 and PALB2 are recruited to DNA lesions via independent mechanisms.

The BRCA1-PALB2 Interaction Is Involved in HR Repair. Because PALB2 has a critical role in HR repair through its ability to recruit BRCA2 and RAD51 to DNA breaks, we tested whether the interaction between BRCA1 and PALB2 may be involved in HR. Using U2OS cells with a single integration of the DR-GFP reporter, we found that gene conversion efficiency was reduced by ≈3- or 4-fold in PALB2 or BRCA1-depleted cells (Fig. 4*A*). To examine whether the direct interaction between PALB2 and BRCA1 has a role in the documented BRCA1-mediated HR repair, we introduced siRNA-resistant constructs of wild-type or mutant BRCA1 into cells after the depletion of endogenous BRCA1 by siRNA. FACS analyses indicated that reintroduction of wild-type BRCA1 successfully restored gene conversion to levels comparable with that of control cells (Fig. 4*B*; Fig. S6*b*). By contrast, BRCA1 mutants defective in PALB2-binding failed to fully rescue the gene conversion defect associated with BRCA1 depletion. Also, the ability of BRCA1 in promoting gene conversion closely correlates with its ability to interact with PALB2. Although the introduction of L1407P and M1411T failed to restore gene conversion in BRCA1-depleted cells, the M1400V mutant, which has some residual PALB2-binding activity (Fig. 2*D*), partially restored gene conversion activity (Fig. 4*B*; Fig. S6 *b* and *c*).

To further corroborate the importance of the BRCA1-PALB2 complex formation in HR repair, we also assessed rates of gene conversion in PALB2-depleted U2OS cells reconstituted with either wild-type PALB2 or its BRCA1-binding defective mutants. Reintroduction of wild-type PALB2 restored efficient gene conversion, whereas the L21A, Y28A, and L35A mutants did not (Fig. 4*C*). As an extension to further validate the

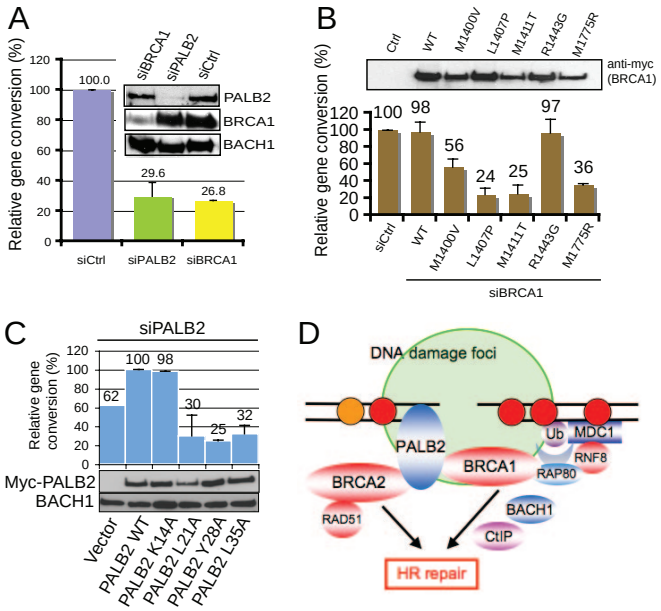

Fig. 4. The BRCA1-PALB2 interaction is required for homologous recombination repair. (*A*) Gene conversion was assessed in U2OS DR-GFP cells treated with control, PALB2, or BRCA1-specific siRNAs. Percentage of GFP positive cells was determined by FACS analyses 48 h posttransfection. Relative gene conversion efficiency was normalized using control siRNA transfected cells, which was set as 100%. (*B*) Relative gene conversion was determined in BRCA1-depleted U2OS cells reconstituted with siRNA-resistant wild-type or mutant BRCA1. (*C*) Gene conversion was determined in PALB2-depleted cells transfected with empty vector, or reconstituted with siRNA-resistant wild-type or mutant PALB2. Relative gene conversion efficiency was normalized using cells reconstituted with wild-type PALB2, which was set as 100%. (*D*) A working model of the BRCA1/BRCA2/PALB2 complex in the DNA damage response.

significance of the BRCA1-PALB2 interaction, mitomycin C (MMC) sensitivity assay was performed using PALB2-deficient EUFA1341 cells that have been reconstituted with wild-type or mutants PALB2. EUFA1341 cells reconstituted with PALB2 ΔN42, L21A, Y28A, or L35A mutants were hypersensitive toward MMC treatments, whereas the reintroduction of wild-type PALB2 or its control K14A mutant rescued the MMC hypersensitive phenotype (Fig. S6*d*). Together, these data suggest that the physical interaction between BRCA1 and PALB2 has an instrumental role essential for HR repair and cell survival.

Discussion

In this study, we have uncovered PALB2 as an integral component of the BRCA complex in vivo. Importantly, we found that PALB2 directly associates with BRCA1. We also provided biochemical evidences to demonstrate the existence of the trimeric BRCA complex containing BRCA1, PALB2, and BRCA2. We demonstrated that the specific interaction between BRCA1 and PALB2 is mediated by the coiled-coil motifs where mutations on the coiled-coil domains, including cancer patient derived BRCA1 mutations, would disrupt their complex formation. Functional analyses suggested that HR repair would be compromised when the PALB2-BRCA1 interaction is disrupted. These findings extend our earlier study (5), underscore the importance of the BRCA1-PALB2-BRCA2 complex in HR repair, and support the idea that distinct BRCA1 macromolecular complexes participate in various aspect in the DNA damage response.

BRCA1 has multiple roles in the cellular response to DNA damage (3, 6–10). Besides its functions in DNA damage checkpoint control, BRCA1 can also promotes cell survival via DNA repair (23, 24). Our findings that abrogation of the BRCA1-PALB2 interaction resulted in HR repair defects and compromised cell survival on DNA damage suggest that BRCA1 contributes to HR repair, at least in part, via the PALB2-BRCA2-RAD51 axis. That BRCA1, and its interaction with PALB2, is required for optimal formation of RAD51-ssDNA nucleoprotein filament (Fig. S7 *a* and *b*) is entirely consistent with this hypothesis. Given that BRCA1 also interacts with CtIP and BACH1, both of which have documented nonoverlapping roles at various steps of HR repair (25–29), it will be interesting to examine how each of these BRCA1 macrocomplexes work in concert in the maintenance of genome stability.

Domain mapping studies revealed that the BRCA1-PALB2 interaction is mediated via their respective coiled-coil motifs, and is independent from the BRCA1 BRCT domain (Fig. 2; Fig. S3). This observation is striking, considering that distinct BRCA1 macrocomplexes, including those that contains CtIP, BACH1, and the CCDC98/RAP80 complex, respectively, are selectively formed via the BRCA1 BRCT domain. This result suggests that PALB2 might be present among the various BRCA1 macrocomplexes. Indeed, both CtIP and BACH1 were found in PALB2 precipitates (Fig. 1*D*). Thus, the existence of BRCA1-PALB2 complex that contains CtIP or BACH1 highlights the possibility that BRCA1 may coordinate and fine-tune DNA repair via its ability to monitor processes including DNA resection and RAD51 loading simultaneously. Indeed, besides its interaction with PALB2, a requirement of the BRCA1 BRCT domain for efficient RAD51 foci formation (Fig. S5 and Fig. S6*a*), and optimal HR repair (Fig. 4*B*; Fig. S6 *b* and *c*), was also observed, and parallels the repair deficits in CtIP and BACH1-depleted cells (Fig. S7). Also, codepletion of PALB2 and CtIP or BACH1 demonstrated further reductions in gene conversion rates, as compared with PALB2-depleted cells (Fig. S7*e*). All these results, together, imply that BRCA1 may have accessory functions at multiple steps during HR repair via its associations with several of these proteins directly involved in HR processes.

Notably, disruption of the BRCA1-PALB2 interaction, although resulted in profound effects in HR repair and MMC hypersensitivity, did not noticeably affect the intra-S-phase checkpoint (Fig. S8 *a* and *b*), revealing the function specificity for the complex formation. We now know that through its phosphorylation-dependent interaction with the CCDC98/RAP80 complex, the BRCA1 BRCT domain is required for its damage-induced focal accumulation at sites of DNA damage (30–34). Intriguingly, our data demonstrated that BRCA1 only has an accessory role in the focal concentration of PALB2 and RAD51 at DSBs (Fig. 3; Fig. S4, Fig. S5, Fig. S6*a*, and Fig. S8*c*). This observation suggests that other factors or activities might be more important for the sustained localization of PALB2 at DNA lesions. We speculate that, although BRCA1 is not essential for sustained localization of PALB2 at DNA breaks, BRCA1 may stabilize PALB2 at the sites of DNA damage by serving as an additional anchor point for PALB2 at DSBs (Fig. 4*D*).

Mutations in BRCA1 predispose individuals to early development of breast and ovarian cancers. Given the prominent role of BRCA1 in protecting genome integrity, one would speculate that clinical mutations found among BRCA1 patients might provide mechanistic insights into its tumor suppressing function in vivo. Accordingly, our study exploited the patient derived BRCA1 missense mutations residing within its PALB2-interacting coiled-coil motif. The altered BRCA1-PALB2 interaction (Fig. 2; Fig. S2 and Fig. S3) and, thus, the BRCA1-PALB2-BRCA2 complex formation, together with DNA repair deficits observed with these patient-derived BRCA1 mutations, strongly suggest that in vivo assembly of the BRCA complex through PALB2 likely constitutes an important event required for their tumor suppressor functions. These results may also explain the similar phenotype observed in patients harboring mutations in each of these 3 proteins. Together with the observation that the BRCA1 BRCT mutant M1775R also displays significant DNA repair deficits (Fig. 4*B*; Fig. S6 *b* and *c*), our data support the idea that various BRCA1 functions converge

and contribute to its role in HR repair and its tumor suppressor activity.

Materials and Methods

Antibodies. Monoclonal antibody against the FLAG epitope (M2) and Myc epitope (9E10) were purchased from Sigma and Covance, respectively. Mouse monoclonal anti-RPA1, RPA2 and BRCA1 (SD118) antibodies were purchased from Calbiochem. Anti-GST-HRP was purchased from Santa Cruz. Rabbit polyclonal anti-RAD51, anti-BRCA2, and anti-BRCA1 antibodies were generous gifts from David Livingston. Rabbit polyclonal anti-pH2AX, BACH1, CtIP, and 53BP1 antibodies used were described previously (9, 27, 35). Rabbit polyclonal anti-PALB2 antibodies were generated by immunizing rabbits with recombinant GST-PALB2 fragments (containing residues 463–814 and 611–764 of PALB2), which were expressed and purified from *Escherichia coli*.

Purification of PALB2-Associated Protein Complex. 293T cells expressing SFB-PALB2 were lysed with NETN (20 mM Tris·HCl, pH 8/100 mM NaCl/1 mM EDTA/0.5% Nonidet P-40) on ice for 20 min, followed by centrifugation at 13,000 × *g* for 20 min at 4 °C. Supernatant was incubated with streptavidin beads for 2 h at 4 °C. Bound complex was eluted with 2 mg/mL biotin diluted in NETN. Supernatant was further incubated with S protein conjugated agarose beads for 2 h at 4 °C. Beads were washed 3 times with NETN buffer, and proteins bound to the beads were eluted by boiling with SDS sample buffer. Proteins were resolved by SDS/PAGE, stained with silver. Visible bands were excised for mass spectrometry protein identification (Taplin biological mass spectrometry facility, Harvard University, Cambridge, MA).

Serial Immunodepletion Experiments. Cell lysate was subjected to immunodepletion using indicated antibodies coupled to protein A beads for 2 h. Supernatant was saved and immunodepleted for 2 additional rounds. Thereafter, cell lysates were boiled in SDS loading buffer and analyzed by immunoblotting.

Protein Production in Insect Cells. Baculoviruses expressing His-Flag-BRCA1 or GST-BARD1 were gifts from Richard Baer. The coding sequences of full-length PALB2, BRCA2, WTX, and PALB2 N42 were transferred to pDEST20 vector for the expression of GST-fusion proteins in insect cells. Transposition occurred in DH10Bac competent cells and correct bacmids confirmed by PCR were transfected into SF9 cells for baculovirus production. Protein expression was confirmed by SDS/PAGE, Coomassie blue staining, and Western blotting. For coIP experiments, SF9 cells infected with corresponding baculoviruses were lysed in NETN for 20 min on ice, and the crude lysate was clarified by centrifugation (13,000 × *g*, 10 min). Supernatant was saved, and pellet was digested with Benzoase for 1 h at 4 °C and clarified again by centrifugation. Pooled supernatant was used for coIP.

Immunostaining. Cells were treated with 10 Gy of gamma radiation. After recovery, cells were washed with PBS, fixed at room temperature with 3% paraformaldehyde for 12 min, permeabilized with 0.5% triton for 3 min, and then immunostained with appropriate antibodies for 30 min. Whenever transfection was needed, cells were transfected with indicated constructs using Lipofectamine 2000 (Invitrogen), and irradiated 24 h posttransfection. For detection of RPA foci, cells grown on coverslips were first permeabilized with 0.5% triton for 2.5 min, washed twice with PBS, and fixed with 3% paraformaldehyde for 15 min at room temperature before incubation with primary anti-RPA antibodies. After incubation with primary antibodies, cells were washed twice with PBS and immunostained with Rhodamine-conjugated goat anti-mouse and/or FITC-conjugated goat anti-rabbit antibodies for 30 min. Nuclei were counterstained with DAPI. Images were visualized and captured (Nikon Eclipse 800 microscope). For foci quantification, all of images were captured at identical exposure time, and 100 cells were counted for duplicated experiments.

Gene Conversion Assay. U2OS cells (3×10^6) stably expressing DR-GFP substrate and pCBASce plasmid were electroporated with 8 μg pCBASce plasmid at 250V, 975 μF by using a Bio-Rad genepulsar II. For the reintroduction of BRCA1 or PALB2 after siRNA-mediated depletion, constructs containing either BRCA1 or PALB2 were electroporated together with the pCBASce construct into the cell. Cells were then plated onto 10-cm dishes and incubated in culture media for 48 h before FACS analyses. Cells were analyzed in a Becton-Dickinson FACScan on a green (FL1) versus orange (FL2) fluorescence plot. Results represent average of 2 to 3 independent experiments (mean ± SEM).

For more details, see *SI Materials and Methods*.

ACKNOWLEDGMENTS. We thank Prof. David Livingston (Dana-Farber Harvard Cancer Institute, Boston) for providing the pOZC-PALB2 construct and the various antibodies used in this study; Prof. Maria Jasin (Memorial Sloan-Kettering Cancer Center, New York) for the U2OS cells with DR-GFP integration, DR-GFP, and pCBASce plasmids; Prof. Johan P. de Winter (Vrije Universiteit Medical Center, Amsterdam) for EUFA1341 cells; Prof. Richard Baer (Columbia University, New York) for the BRCA1 and BARD1 baculoviruses; Drs. Gargi Ghosal, Xiaohua Xu, and Zihua Gong for their assistance in gel filtration chromatography; and Drs. Jingsong Yuan and Jun Huang for insightful discussion. S.M.H.S. is supported by a Postdoctoral fellowship from the Croucher Foundation; M.S.Y.H. by an Anna Fuller Fund fellowship; and J.C. by grants from the National Institutes of Health and an Era of Hope Scholar award from the Department of Defense. J.C. is a member of the Mayo Clinic Breast Specialized Programs of Research Excellence program.

1. Jemal A, et al. (2008) Cancer statistics, 2008. *CA Cancer J Clin* 58:71–96.
2. Zhang H, Tombline G, Weber BL (1998) BRCA1, BRCA2, and DNA damage response: Collision or collusion? *Cell* 92:433–436.
3. Wang W (2007) Emergence of a DNA-damage response network consisting of Fanconi anaemia and BRCA proteins. *Nat Rev Genet* 8:735–748.
4. Gudmundsdottir K, Ashworth A (2006) The roles of BRCA1 and BRCA2 and associated proteins in the maintenance of genomic stability. *Oncogene* 25:5864–5874.
5. Chen J, et al. (1998) Stable interaction between the products of the BRCA1 and BRCA2 tumor suppressor genes in mitotic and meiotic cells. *Mol Cell* 2:317–328.
6. Mullan PB, Quinn JE, Harkin DP (2006) The role of BRCA1 in transcriptional regulation and cell cycle control. *Oncogene* 25:5854–5863.
7. Venkitaraman AR (2001) Functions of BRCA1 and BRCA2 in the biological response to DNA damage. *J Cell Sci* 114:3591–3598.
8. Kerr P, Ashworth A (2001) New complexities for BRCA1 and BRCA2. *Curr Biol* 11:R668–R676.
9. Yu X, Chen J (2004) DNA damage-induced cell cycle checkpoint control requires CtIP, a phosphorylation-dependent binding partner of BRCA1 C-terminal domains. *Mol Cell Biol* 24:9478–9486.
10. Greenberg RA, et al. (2006) Multifactorial contributions to an acute DNA damage response by BRCA1/BARD1-containing complexes. *Genes Dev* 20:34–46.
11. Lord CJ, Ashworth A (2007) RAD51, BRCA2 and DNA repair: A partial resolution. *Nat Struct Mol Biol* 14:461–462.
12. Pellegrini L, Venkitaraman A (2004) Emerging functions of BRCA2 in DNA recombination. *Trends Biochem Sci* 29:310–316.
13. Thorslund T, West SC (2007) BRCA2: A universal recombinase regulator. *Oncogene* 26:7720–7730.
14. Xia B, et al. (2006) Control of BRCA2 cellular and clinical functions by a nuclear partner, PALB2. *Mol Cell* 22:719–729.
15. Rahman N, et al. (2007) PALB2, which encodes a BRCA2-interacting protein, is a breast cancer susceptibility gene. *Nat Genet* 39:165–167.
16. Simpson S (2007) PALB2-new breast-cancer susceptibility gene. *Lancet Oncol* 8:105.
17. Reid S, et al. (2007) Biallelic mutations in PALB2 cause Fanconi anemia subtype FA-N and predispose to childhood cancer. *Nat Genet* 39:162–164.
18. Foulkes WD, et al. (2007) Identification of a novel truncating PALB2 mutation and analysis of its contribution to early-onset breast cancer in French-Canadian women. *Breast Cancer Res* 9:R83.
19. Erkko H, et al. (2007) A recurrent mutation in PALB2 in Finnish cancer families. *Nature* 446:316–319.
20. Tischkowitz M, et al. (2007) Analysis of PALB2/FANCN-associated breast cancer families. *Proc Natl Acad Sci USA* 104:6788–6793.
21. Xia B, et al. (2007) Fanconi anemia is associated with a defect in the BRCA2 partner PALB2. *Nat Genet* 39:159–161.
22. Zhang J, et al. (2004) Chk2 phosphorylation of BRCA1 regulates DNA double-strand break repair. *Mol Cell Biol* 24:708–718.
23. Moynahan ME, Cui TY, Jasin M (2001) Homology-directed dna repair, mitomycin-c resistance, and chromosome stability is restored with correction of a Brca1 mutation. *Cancer Res* 61:4842–4850.
24. Moynahan ME, Chiu JW, Koller BH, Jasin M (1999) Brca1 controls homology-directed DNA repair. *Mol Cell* 4:511–518.
25. Takeda S, Nakamura K, Taniguchi Y, Paull TT (2007) Ctp1/CtIP and the MRN complex collaborate in the initial steps of homologous recombination. *Mol Cell* 28:351–352.
26. Yu X, Wu LC, Bowcock AM, Aronheim A, Baer R (1998) The C-terminal (BRCT) domains of BRCA1 interact in vivo with CtIP, a protein implicated in the CtBP pathway of transcriptional repression. *J Biol Chem* 273:25388–25392.
27. Yu X, Chini CC, He M, Mer G, Chen J (2003) The BRCT domain is a phospho-protein binding domain. *Science* 302:639–642.
28. Gupta R, et al. (2007) FANCJ (BACH1) helicase forms DNA damage inducible foci with replication protein A and interacts physically and functionally with the single-stranded DNA-binding protein. *Blood* 110:2390–2398.
29. Cantor SB, et al. (2001) BACH1, a novel helicase-like protein, interacts directly with BRCA1 and contributes to its DNA repair function. *Cell* 105:149–160.
30. Kim H, Huang J, Chen J (2007) CCDC98 is a BRCA1-BRCT domain-binding protein involved in the DNA damage response. *Nat Struct Mol Biol* 14:710–715.
31. Liu Z, Wu J, Yu X (2007) CCDC98 targets BRCA1 to DNA damage sites. *Nat Struct Mol Biol* 14:716–720.
32. Sobhian B, et al. (2007) RAP80 targets BRCA1 to specific ubiquitin structures at DNA damage sites. *Science* 316:1198–1202.
33. Kim H, Chen J, Yu X (2007) Ubiquitin-binding protein RAP80 mediates BRCA1-dependent DNA damage response. *Science* 316:1202–1205.
34. Wang B, et al. (2007) Abraxas and RAP80 form a BRCA1 protein complex required for the DNA damage response. *Science* 316:1194–1198.
35. Lou Z, et al. (2004) MDC1 regulates DNA-PK autophosphorylation in response to DNA damage. *J Biol Chem* 279:46359–46362.
36. Lupas A, Van Dyke M, Stock J (1991) Predicting coiled coils from protein sequences. *Science* 252:1162–1164.

nature cell biology

RAD18 transmits DNA damage signalling to elicit homologous recombination repair

Jun Huang[1], Michael S. Y. Huen[1], Hongtae Kim[1,3], Charles Chung Yun Leung[2], J N Mark Glover[2], Xiaochun Yu[4] and Junjie Chen[1,5]

To maintain genome stability, cells respond to DNA damage by activating signalling pathways that govern cell-cycle checkpoints and initiate DNA repair. Cell-cycle checkpoint controls should connect with DNA repair processes, however, exactly how such coordination occurs *in vivo* is largely unknown. Here we describe a new role for the E3 ligase RAD18 as the integral component in translating the damage response signal to orchestrate homologous recombination repair (HRR). We show that RAD18 promotes homologous recombination in a manner strictly dependent on its ability to be recruited to sites of DNA breaks and that this recruitment relies on a well-defined DNA damage signalling pathway mediated by another E3 ligase, RNF8. We further demonstrate that RAD18 functions as an adaptor to facilitate homologous recombination through direct interaction with the recombinase RAD51C. Together, our data uncovers RAD18 as a key factor that orchestrates HRR through surveillance of the DNA damage signal.

DNA double-strand breaks (DSBs) are highly cytotoxic lesions that can cause cell death, mutations and chromosomal instability, which eventually lead to tumorigensis[1–5]. Cells respond to DSBs by rapidly recruiting a host of proteins to chromatin regions surrounding these sites. The concentration of DNA damage and/or repair proteins at or near DSBs allows for the visualization of these proteins as ionizing radiation-induced foci (IRIF)[6]. Increasing evidence suggests that ATM kinase (ataxia-telangiectasia mutated)-dependent phosphorylation of the histone variant H2AX is the initial signal for subsequent accumulation of various checkpoint and repair proteins at the sites of DNA breaks[7,8]. Phosphorylated H2AX binds directly to the BRCT domains of MDC1 (mediator of DNA damage checkpoint 1), which allows for RNF8 recruitment. RNF8, together with an E2 ubiquitin conjugase UBC13 promotes protein ubiquitylation at DNA damage sites, bringing about a local increase in several other mediator proteins such as BRCA1 and 53BP1, which culminates in proper checkpoint activation[9–14].

Similarly to the advances in elucidation of checkpoint mechanisms, research in the past decade has provided much detail on how damaged DNA is repaired in cells. There are at least two main repair pathways, the non-homologous end-joining (NHEJ) pathway and the homologous recombination pathway[1,2,15–17]. DNA repair through homologous recombination requires the recombinase RAD51, and for vertebrates five RAD51 paralogues[18,19]. These RAD51 paralogues form two distinct protein complexes *in vivo*, a RAD51C/XRCC3 heterodimer and a RAD51B/ RAD51C/ RAD51D/XRCC2 heterotetramer[20,21]. Mutation of any of these five paralogues reduces their subnuclear assembly and renders cells hypersensitive to DSBs, highlighting the importance of these RAD51 paralogues in HRR.

An emerging concept in the field is that there is continuous cross-talk between DNA repair and DNA damage checkpoint pathways, however, little is known about how such coordination is achieved in the cell. Here we provide evidence suggesting that RAD18 relays the DNA damage signal from a well-defined pathway, involving ATM, MDC1 and RNF8, to orchestrate DSB repair by homologous recombination through direct interaction with RAD51C. These data suggest a crucial role of RAD18 in coordinating DNA damage checkpoint response with DNA repair.

RESULTS

RAD18 localizes to sites of DNA DSBs

RAD18 is well-known for its function in DNA damage bypass and post-replication repair in yeast and vertebrates, where it promotes monoubiquitylation of proliferating cell nuclear antigen (PCNA) at stalled replication forks[22–25]. Although RAD18 has also been implicated in HRR[26,27], exactly how RAD18 participates in this process remains elusive. Many proteins involved in DSB-induced checkpoint control and DNA repair physically localize to DNA damage sites. RAD18 IRIF were readily detected after ionizing radiation (IR) or camptothecin (CPT) treatment (Fig. 1a), indicating a possible role of RAD18 in the DSB response.

[1]Department of Therapeutic Radiology, Yale University School of Medicine, P.O. Box 208040, New Haven, CT 06520, USA. [2]Department of Biochemistry, University of Alberta, Edmonton, Alberta, Canada. [3]Current address: Department of Biological Science, Sungkyunkwan University, 300 Chunchundong, Suwon 440–746, Korea. [4]Current address: Division of Molecular Medicine and Genetics, Department of Internal Medicine, University of Michigan Medical School, 109 Zina Pitcher Place, BSRB 1520, Ann Arbor, MI 48109, USA.
[5]Correspondence should be addressed to J.C. (e-mail: Junjie.chen@yale.edu)

Received 21 November 2008; accepted 9 January 2009; published online 26 April 2009; DOI: 10.1038/ncb1865

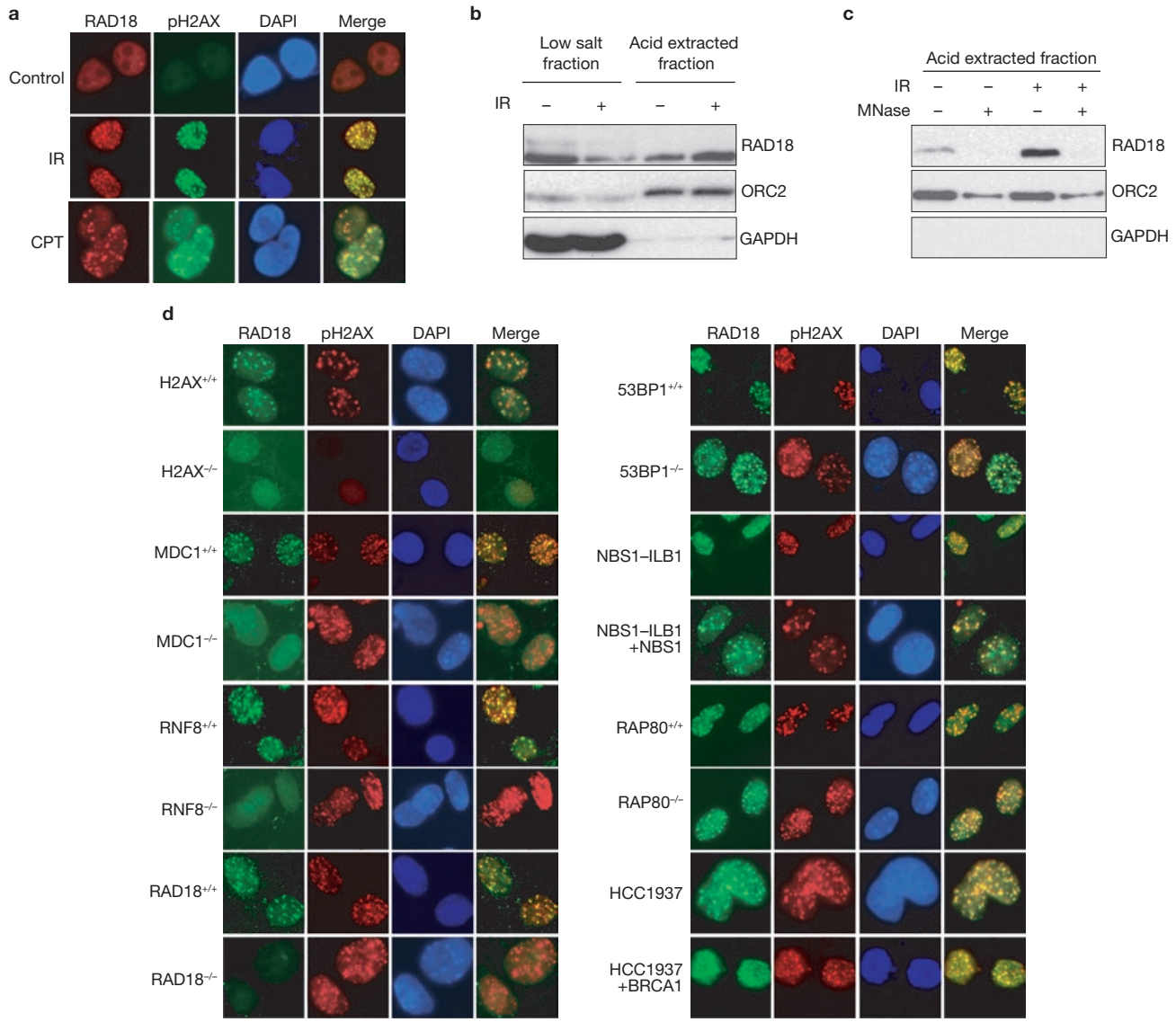

Figure 1 RAD18 forms DNA DSB-induced foci. (**a**) Localization of RAD18 in response to IR or CPT. HeLa cells were treated with of IR (10 Gy; left) or CPT (1 μM; right), fixed and immunostained with anti-RAD18 and anti-pH2AX antibodies. (**b**, **c**) RAD18 relocalizes to the chromatin (acid extracted) fraction after IR treatment (**b**). This is reversible after micrococcal nuclease treatment (**c**). Experiments were carried out as described in the Methods section and immunoblotting experiments were performed using indicated antibodies. ORC2 and GAPDH represent loading controls for chromatin and the soluble fraction, respectively. (**d**) Genetic dependence of RAD18 relocalization after IR treatment. DNA damage response protein deficient cells and their respective wild-type counterparts were irradiated, fixed and immunostained with anti-RAD18 and anti-pH2AX antibodies. Uncropped images of blots are shown in Supplementary Information, Fig. S9.

Generally, the binding of damage response proteins to chromatin in the vicinity of DNA breaks results in damage-induced foci. In biochemical fractionation experiments, a significant portion of RAD18 shifted from the low salt-extracted fraction (soluble fraction) to the acid-extracted fraction (chromatin fraction) after IR treatment (Fig. 1b). Moreover, the chromatin fraction of RAD18 can be easily released after nuclease treatment (Fig. 1c). These data suggest that RAD18 accumulates on chromatin after DNA damage.

Damage-induced RAD18 foci formation requires the ubiquitin ligase RNF8 E3

To determine where RAD18 fits in the established DNA damage signalling cascade, we examined its assembly into IRIFs formation in an exhaustive panel of cell lines with known genetic defects in DNA damage checkpoint components. In contrast to their respective wild-type counterparts, we failed to detect IR-induced RAD18 foci formation in H2AX-, MDC1- or RNF8-deficient cells (Fig. 1d). However, RAD18 relocalization to γ-H2AX containing foci was not noticeably affected in cells with BRCA1, 53BP1, NBS1 or RAP80 deficiency (Fig. 1d). These data suggest that RAD18 functions downstream of H2AX, MDC1 and RNF8 in the known DNA damage signal transduction pathway.

To further explore the role of RNF8 in targeting RAD18 to IRIF, we established RNF8$^{-/-}$ mouse embryonic fibroblasts (MEFs) stably expressing wild-type, forkhead-associated (FHA)- or RING-domain deletion mutants of human RNF8. Our results, and results from other laboratories, demonstrated that although the FHA domain of RNF8

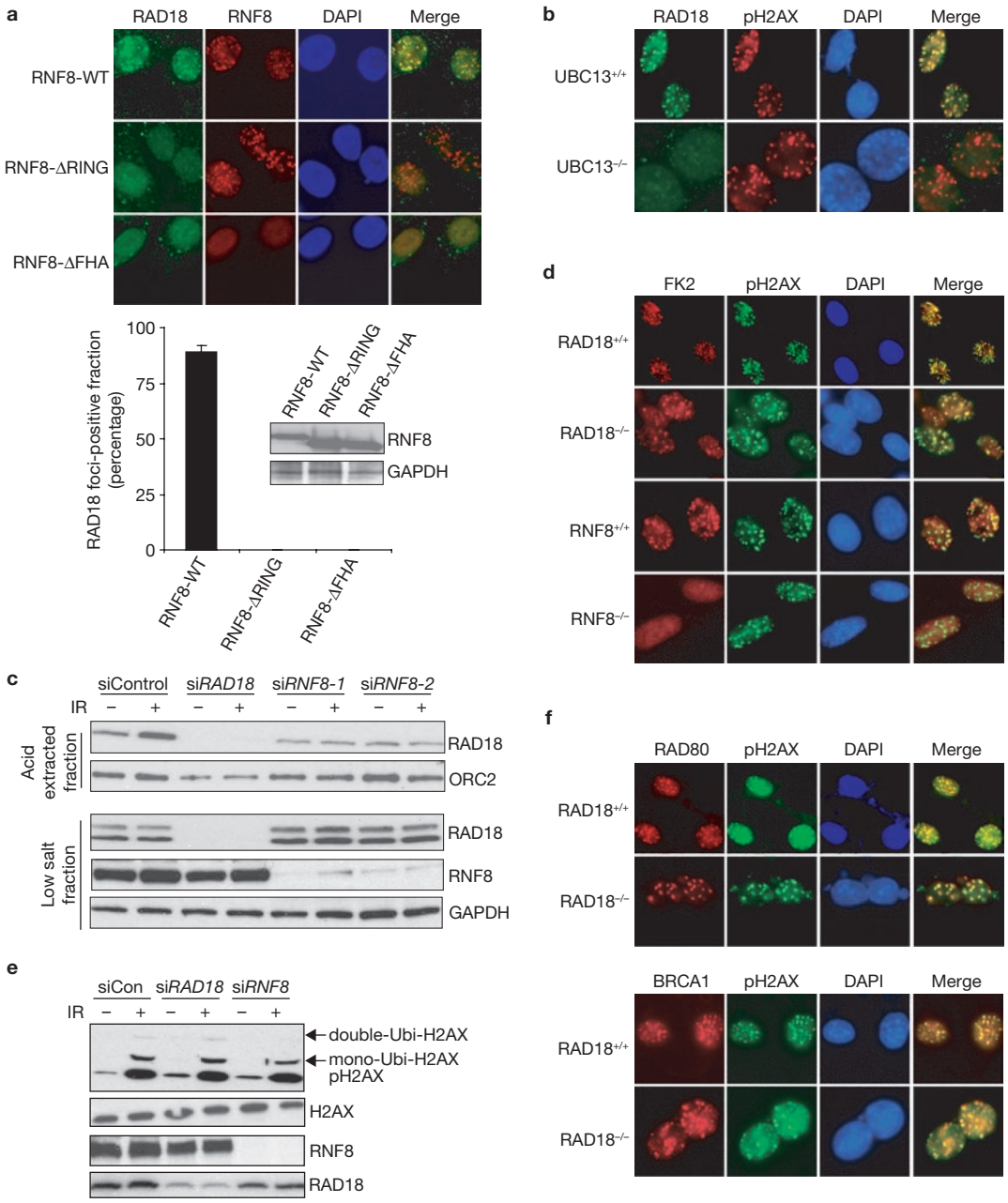

Figure 2 RNF8/UBC13 is required for DSB-induced RAD18 recruitment. (**a**) Both the FHA and RING domain of RNF8 are required for RAD18 relocalization. RNF8-deficient cells were reconstituted with Flag-tagged wild-type (WT) RNF8 or various internal-deletion mutants of RNF8. The expression of wild-type and mutant RNF8 was confirmed by western blotting (bottom). Data were mean ± s.e.m. of three independent experiments, > 100 cells were counted in each experiment. After irradiation, cells were fixed and immunostained using anti-RAD18 and anti-Flag antibodies (representative RAD18 foci are shown, top). (**b**) UBC13 is required for RAD18 relocalization. Wild-type or UBC13-deficient cells were irradiated, fixed and immunostained with anti-RAD18 and anti-pH2AX antibodies. (**c**) RNF8 is required for IR-induced RAD18 chromatin localization. HeLa cells cells transfected with control siRNA, *RAD18* siRNA, *RNF8* siRNA1 or *RNF8* siRNA2 were treated with IR (10 Gy) or left untreated. After 6 h, cells were collected and chromatin fractions were isolated (see Methods). Immunoblotting experiments were performed using the indicated antibodies. (**d**) RAD18 is not required for IR-induced ubiquitin conjugate formation. Wild-type, RAD18- or RNF8-deficient cells were irradiated, fixed and immunostained with anti-FK2 and pH2AX antibodies. (**e**) RAD18 is not required for H2AX ubiquitylation after DNA damage. HeLa cells transfected with control siRNA, *RAD18* siRNA or *RNF8* siRNA were treated with IR (10 Gy) or left untreated. Cells were collected 1 h post-irradiation and cell lysates were immunoblotted with the indicated antibodies (Ubi, ubiquitylated). (**f**) RAD18 is not required for RAP80 and BRCA1 foci formation after IR treatment. Wild-type or RAD18-deficient cells were irradiated, fixed and immunostained with anti-RAP80 or BRCA1 antibodies. Uncropped images of blots are shown in Supplementary Information, Fig. S9.

is required for its recruitment to damage sites through its interaction with MDC1, its E3 ligase activity is required for the targeting of downstream checkpoint and repair proteins to DSBs[10,12,13]. Indeed, only reconstitution with wild-type RNF8 restored RAD18 IRIF (Fig. 2a), suggesting that RAD18 requires RNF8 E3 ligase activity for recruitment to DSB sites. Similarly, UBC13, an E2 ubiquitin conjugating

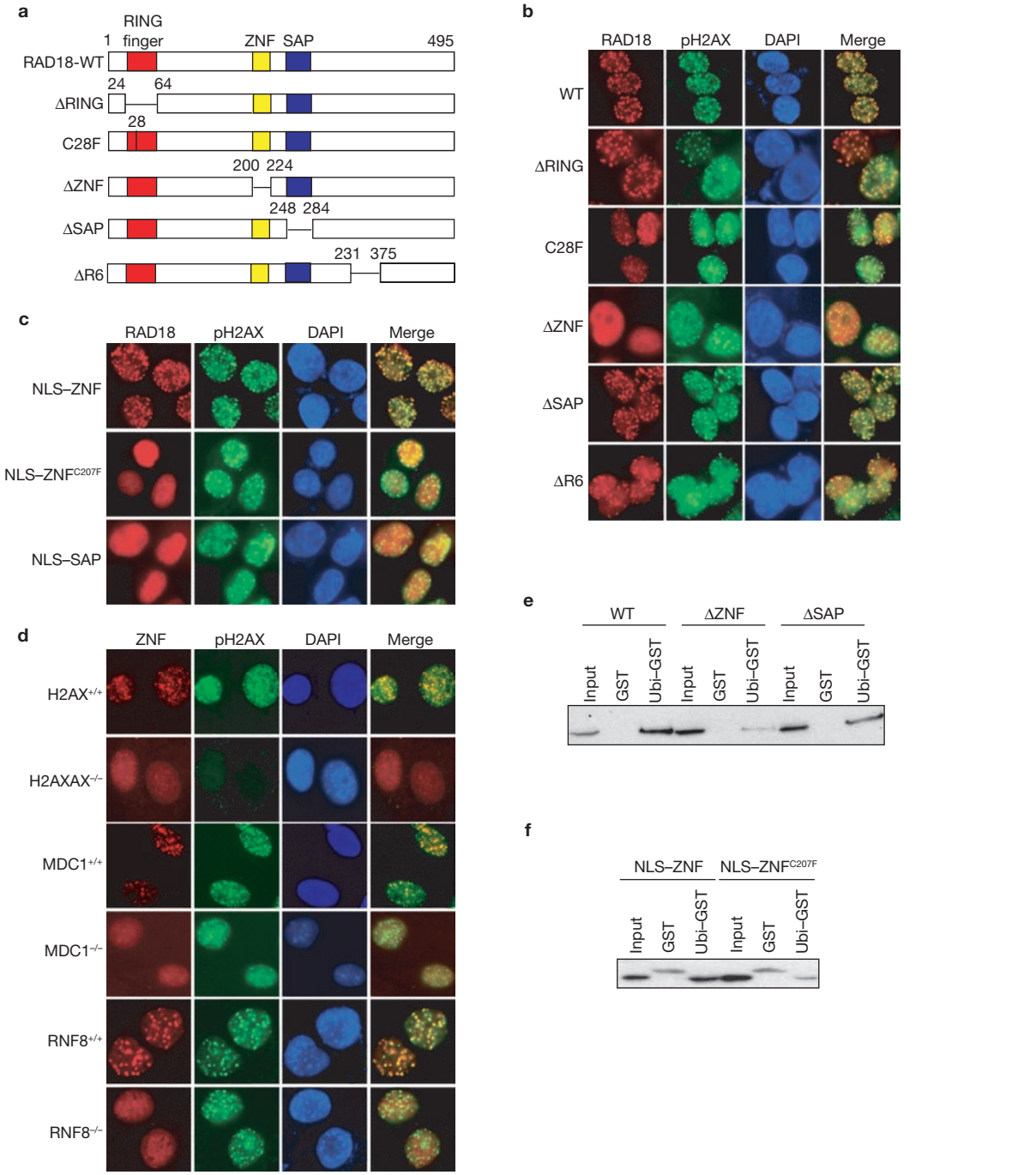

Figure 3 The ZNF domain of RAD18 is required for RAD18 localization to the sites of DNA damage. (**a**) Schematic representation of human RAD18 and its deletion/point mutants used in this study. (**b**) The ZNF domain of RAD18 targets it to IR-induced foci. 293T cells expressing Flag-tagged wild-type or mutants of RAD18 were irradiated, fixed and immunostained with anti-Flag and anti-pH2AX antibodies. (**c**) The ZNF domain alone is sufficient for RAD18 IRIF formation. 293T cells expressing indicated Flag-tagged proteins were irradiated and immunostained as described in **b**. (**d**) Genetic dependence of the ZNF domain relocalization after IR treatment. Immunostaining experiments were performed as described in Fig. 1d. (**e**, **f**) The ZNF domain of RAD18 is essential and sufficient for binding to ubiquitin *in vitro*. GST or Ubiquitin–GST (Ubi-GST) was incubated with cell lysates exogenously expressing Flag-tagged wild-type or various internal-deletion mutants of RAD18 (**e**), NLS–ZNF or NLS–ZNF^{C207F} (**f**). After extensive washing, bound RAD18 fragments or fusion proteins were analysed by immunoblotting with an anti-Flag antibody. Uncropped images of blots are shown in Supplementary Information, Fig. S9.

enzyme that works with RNF8, was also crucial for RAD18 foci formation (Fig. 2b). Consistent with its role in targeting RAD18 to DNA damage-induced foci, in fractionation experiments RNF8 depletion significantly reduced accumulation of RAD18 in the chromatin fraction after IR treatment (Fig. 2c).

RNF8 is crucial for the formation of IR-induced ubiquitin conjugates at DSBs[10–14,28], which can be detected by use of the anti-ubiquitin antibody FK2 (refs 29, 30). These FK2 foci can be impaired by the depletion of free nuclear ubiquitin, achieved by a short treatment with the proteasome inhibitor MG132 before irradiation. Consistently, the accumulation of RAD18 at

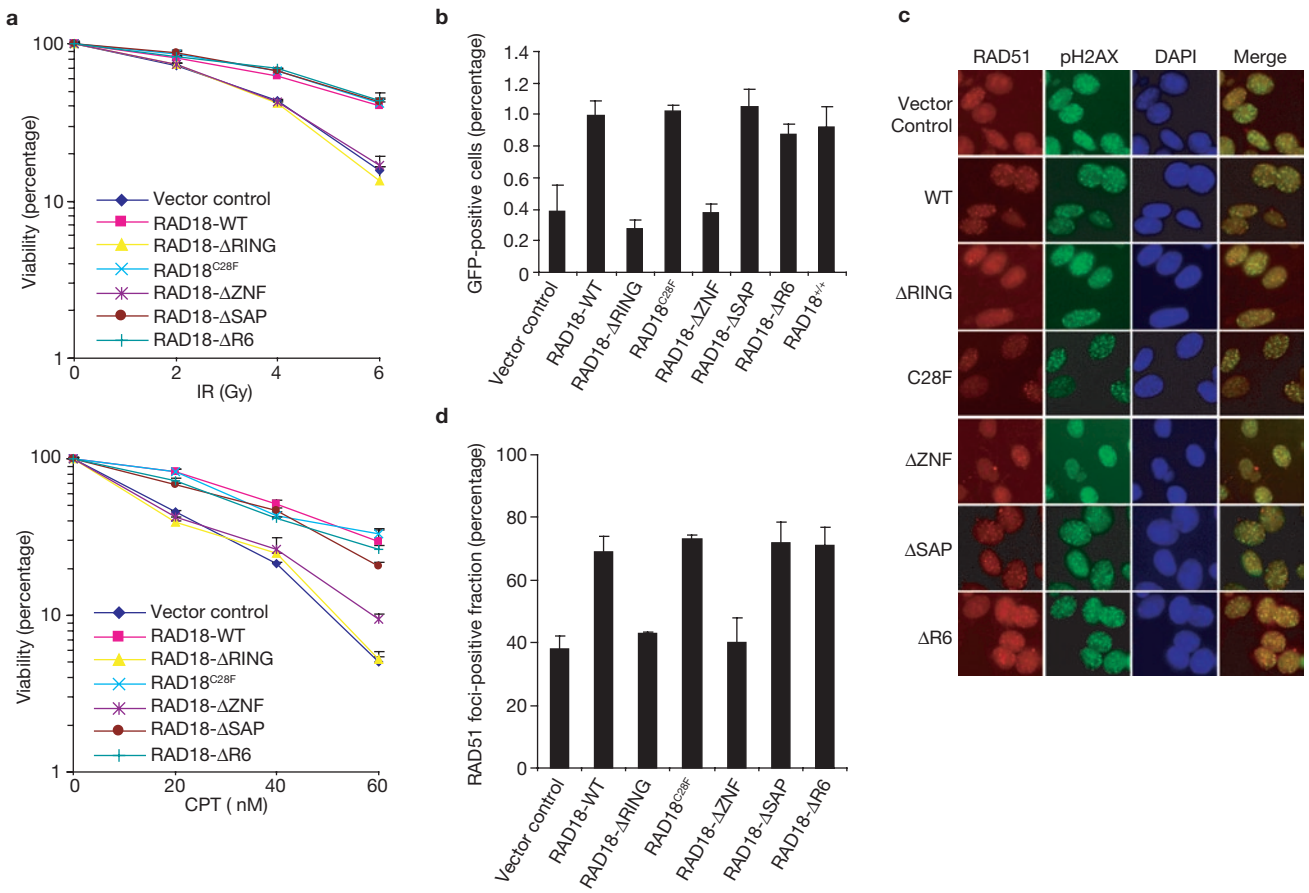

Figure 4 RAD18 promotes homologous recombination. (**a**) The ZNF and RING domains of RAD18, but not its E3 ligase activity, are required for restoring cellular resistance to DSBs. Colony formation assays were performed (see Methods). Data are mean ± s.e.m. of three independent experiments. (**b**) RAD18 promotes homologous recombination. RAD18-deficient cells were reconstituted with wild-type or various RAD18 mutants as indicated. Gene conversion assays were performed (see Methods). Data are mean ± s.e.m. of three independent experiments. (**c**, **d**) RAD18 is required for efficient RAD51 foci formation. RAD18-deficient or reconstituted cells were irradiated, fixed and immunostained with anti-RAD51 and anti-pH2AX antibodies. Representative RAD51 foci are shown (**c**). Data are mean ± s.e.m. of three independent experiments, > 100 cells were counted in each experiment (**d**).

DNA damage sites was abrogated when cell were pretreated with MG132 (Supplementary Information, Fig. S1). As RAD18 also shows ubiquitin ligase activity, we tested whether RAD18 itself would contribute to FK2 foci formation. In contrast to RNF8, RAD18 was not required for IR-induced FK2 foci formation and H2AX ubiquitylation (Fig. 2d, e). Furthermore, RAD18 was not required for RAP80 or BRCA1 foci formation (Fig. 2f).

The zinc-finger domain of RAD18 targets it to sites of DSBs

Next, we sought to identify the region(s) within RAD18 that is important for its translocation to IRIF. As shown in Fig. 3a, b, only the zinc-finger (ZNF) domain deletion mutant (ΔZNF) of RAD18 totally lost its foci forming ability, whereas wild-type, the RING domain point mutant (C28F, mutation of Cys 28 to Phe), the RING domain deletion mutant (ΔRING), the SAP (SAF-A/B, Acinus and PIAS) domain deletion mutant (ΔSAP) and the RAD6 binding-domain deletion mutant (ΔR6; ref. 25) could all form IRIF. These observations suggest the RAD18 ZNF domain, but not its E3 ligase activity (ΔRING, C28F and ΔR6 are E3 ligase-inactivating mutants), is essential for targeting RAD18 to IRIF.

To further clarify whether the ZNF domain alone is sufficient to target RAD18 to sites of DNA damage, we used a RAD18 ZNF domain (residues 186–240) that harboured an amino-terminal nuclear localization signal (NLS–ZNF) and a RAD18 ZNF domain with a ZNF domain-disrupting point-mutation (NLS–ZNF^{C207F}; mutation of Cys 207 to Phe). Whereas the NLS–ZNF fusion protein could form foci, the NLS–ZNF^{C207F} mutant and the SAP domain of RAD18 that also harboured an N-terminal NLS (NLS–SAP; residues 241–290) failed to do so (Fig. 3c), suggesting that the ZNF domain alone fulfills the role of targeting RAD18 to DSBs. Moreover, as with the full-length protein, foci formation of the NLS–ZNF fusion protein also depends on RNF8, MDC1 and H2AX (Fig. 3d).

The ZNF domain of RAD18 binds directly to ubiquitin *in vitro*

RNF8 and UBC13 are known to generate polyubiquitin chains that recruit other ubiquitin-binding proteins to DNA damage sites[31–34]. Recent studies have showed that some ZNF domains are capable of binding to ubiquitin; these have been renamed as ubiquitin-binding ZNF domains. We examined whether the ZNF domain of RAD18 would bind to ubiquitin *in vitro*. A ubiquitin-glutathione S-transferase fusion protein (Ubi–GST) specifically bound to wildtype and ΔSAP RAD18, but not to ΔZNF RAD18 (Fig. 3e). In addition, Ubi–GST pulled down NLS–ZNF, but not the NLS–ZNF^{C207F} mutant, *in vitro* (Fig. 3f). This ubiquitin-binding activity of RAD18 *in vitro* is consistent with its ability to localize to damage-induced foci *in vivo*, suggesting that RAD18,

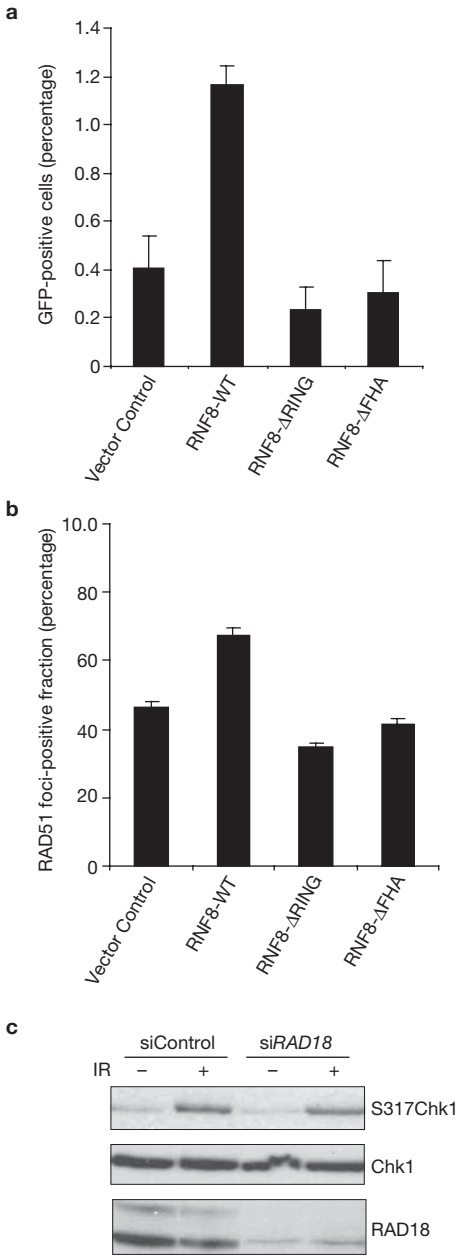

Figure 5 RNF8 participates in homologous recombination. (**a**) RNF8 promotes homologous recombination. RNF8-deficient cells were reconstituted with wild-type or various mutants of RNF8 as indicated in Fig. 2a. Gene conversion assays were performed, similar to those described in Fig. 4b. (**b**) RNF8 is required for efficient RAD51 foci formation. Data are are mean ± s.e.m. of three independent experiments in **a** and **b**. (**c**) RAD18 is not required for Chk1 activation after DNA damage. Control or *RAD18* siRNA-transfected HeLa cells were mock treated or exposed to of IR (10 Gy). Cells were collected 2 h later and lysates were immunoblotted with indicated antibodies. Uncropped images of blots are shown in Supplementary Information, Fig. S9.

similarly to RAP80, may associate with certain RNF8/UBC13-catalysed ubiquitylated protein(s) at DSBs.

Notably, the RAD18 ZNF domain, but not the RAP80 ZNF domain, has an affinity for different polyubiquitin chains *in vitro* (Supplementary Information, Fig. S2a), implying that the ability to bind ubiquitin is specific to the RAD18 ZNF domain. Moreover, the GST–RAD18 ZNF domain binds to Lys 48 and Lys 63-linked ubiquitin chains with similar affinities (36 ± 10 nM and 17 ± 4 nM, respectively; Supplementary Information, Fig. S2b, c). The significance of this finding is not yet clear.

RAD18 promotes homologous recombination in an RNF8-dependent manner

As RAD18 localization seems to be regulated in response to DSBs, we determined whether RAD18 is required for cell survival after this type of DNA damage. We obtained mouse RAD18$^{-/-}$ MEFs[23] and established derivative cell lines stably expressing either wild-type RAD18 or various deletion/point mutants of human RAD18. Cells deficient in RAD18 were sensitive to IR or CPT treatment (Fig. 4a). Furthermore, cells reconstituted with wild-type or ΔSAP RAD18, but not those reconstituted with ΔZNF or ΔRING RAD18 mutants, had their cellular resistance to DNA breaks restored (Fig. 4a). Unexpectedly, the E3 ligase-inactivating mutants C28F and ΔR6 retained the ability to restore cell survival after IR or CPT treatment (Fig. 4a). These results suggest that RAD18 is required for cell survival after DNA DSBs and that both its ZNF and RING domain, but not its E3 ligase activity, are crucial for this role.

As CPT-induced replication-associated DSBs are usually repaired by HRR[35], the observed requirement of RAD18 in DSB repair may suggest that RAD18 is involved in HRR. Indeed, this possibility was raised by previous studies using chicken DT40 cells[26,27,36,37]. To confirm the role of RAD18 in HRR, we performed a gene conversion assay to examine homologous recombination efficiency using the DR–GFP reporter system[38]. Notably, re-introduction of wild-type or ΔSAP RAD18 restored HRR in RAD18$^{-/-}$ cells, whereas ΔZFN and ΔRING RAD18 were defective in this assay (Fig. 4b; Supplementary Information, Fig. S3a). The mutants C28F and ΔR6 could also restore HRR (Fig. 4b; Supplementary Information, Fig. S3a), indicating that the E3 ligase activity of RAD18 is not required for its homologous recombination function. Consistently, depletion of RAD6A has no effect on gene conversion (Supplementary Information, Fig. S4).

RAD18-deficient chicken DT40 cells are hypersensitive to CPT and this hypersensitivity can be reversed by further inactivation of NHEJ[27], indicating that RAD18 in chicken cells may regulate the NHEJ pathway and thus influence CPT sensitivity. To address whether this is the case in mammalian cells, we performed clonogenic survival assays using RAD18$^{+/+}$ and RAD18$^{-/-}$ cells exposed to IR or camptothecin alone or in combination with the NHEJ inhibitor NU7441. Treatment with NU7441 increased CPT sensitivity in both RAD18 wild-type and deficient MEFs (Supplementary Information, Fig. S5a), suggesting that in mammalian cells, unlike in chicken cells, RAD18 does not seem to participate in NHEJ and may directly facilitate HRR. As a control, we showed that RAD18 wild-type and deficient cells have comparable cell-cycle profiles (Supplementary Information, Fig. S6a). The fact that RAD18 expression increases in the S and G2/M phases (Supplementary Information, Fig. S6b) is also consistent with its role in HRR, as the homologous recombination pathway mainly operates in the S and G2 phases of the cell cycle.

The recombination protein RAD51 is the key component of the HRR machinery and the formation of Rad51 foci can be used as an indicator of HRR. Indeed, IR-induced RAD51 foci formation was reduced in RAD18$^{-/-}$ MEFs (Fig. 4c, d; Supplementary Information, Fig. S3b). We also obtained similar data using human HCT116 and HCT116–RAD18$^{-/-}$ cell lines (data not shown). In agreement with the results from our clonogenic and gene conversion assays, RAD51 foci formation can be restored by reconstitution of RAD18$^{-/-}$ cells with wild-type, ΔSAP, or

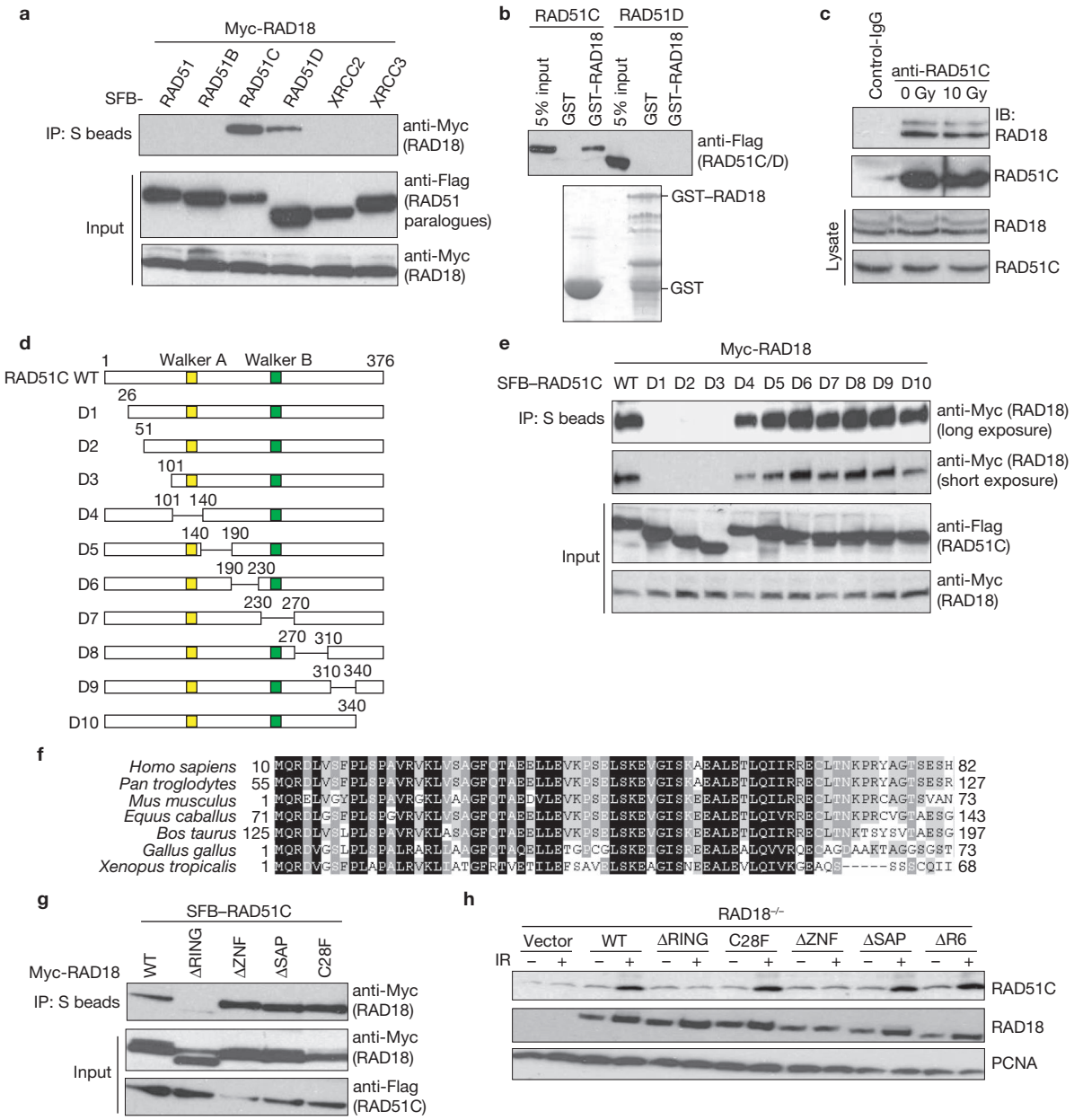

Figure 6 RAD18 interacts with RAD51C. (a) Ectopically expressed RAD18 interacts with RAD51C. Cells (293T) were transfected with plasmids encoding Myc-tagged RAD18 together with plasmids encoding SFB-tagged RAD51 or RAD51 paralogues. Cells were collected 24 h after transfection. Immunoprecipitation (IP) reactions were performed using S beads and cells were then subjected to immunoblotting using the antibodies as indicated. (**b**) RAD18 directly interacts with RAD51C. GST or GST–RAD18 immobilized on sepharose beads were incubated with cell lysates containing exogenously expressed Flag-tagged RAD51C or RAD51D. Bound RAD51C was analysed by anti-Flag immunoblotting. (**c**) Endogenous RAD18 and RAD51C form a complex *in vivo*. Cells (293T) were mock treated or treated with IR (10 Gy). Control or anti-RAD51C immunoprecipitates were immunoblotted with anti-RAD18 and anti-RAD51C antibodies (top). The expression levels of the endogenous proteins were detected by immunoblotting using anti-RAD18 and anti-RAD51C antibodies (bottom; IB, immunoblot). (**d**) Schematic representation of human RAD51C and its deletion mutants (D) used in this study. (**e**, **g**) Mapping of the corresponding regions required for RAD18/RAD51C interaction. Immunoprecipitation reactions were performed using S beads and then cells were subjected to immunoblotting using antibodies as indicated (WT, wild type). (**f**) Alignment of RAD51C N-terminal sequences from different species. (**h**) RAD18 is required for IR-induced RAD51C chromatin localization. RAD18-deficient cells were reconstituted with wild-type or various RAD18 mutants as indicated. Cells were irradiated and chromatin fractions were isolated as shown in the Methods. Immunoblotting experiments were performed using the indicated antibodies. Uncropped images of blots are shown in Supplementary Information, Fig. S9.

the E3 ligase-inactivating mutants C28F and ΔR6 RAD18, but not with ΔZNF or ΔRING RAD18 (Fig. 4c, d).

The striking correlation between the requirements of the RAD18 ZNF domain for RAD18 recruitment to DSBs and for HRR led us to postulate that RNF8 may be the upstream signalling molecule mediating RAD18 function in homologous recombination. As expected, HRR and IR-induced Rad51 foci formation were noticeably impaired in RNF8$^{-/-}$ MEFs (Fig. 5a, b; Supplementary Information, Fig. S3c). Furthermore, whereas wild-type RNF8 could restore this homologous recombination deficiency, FHA or RING domain

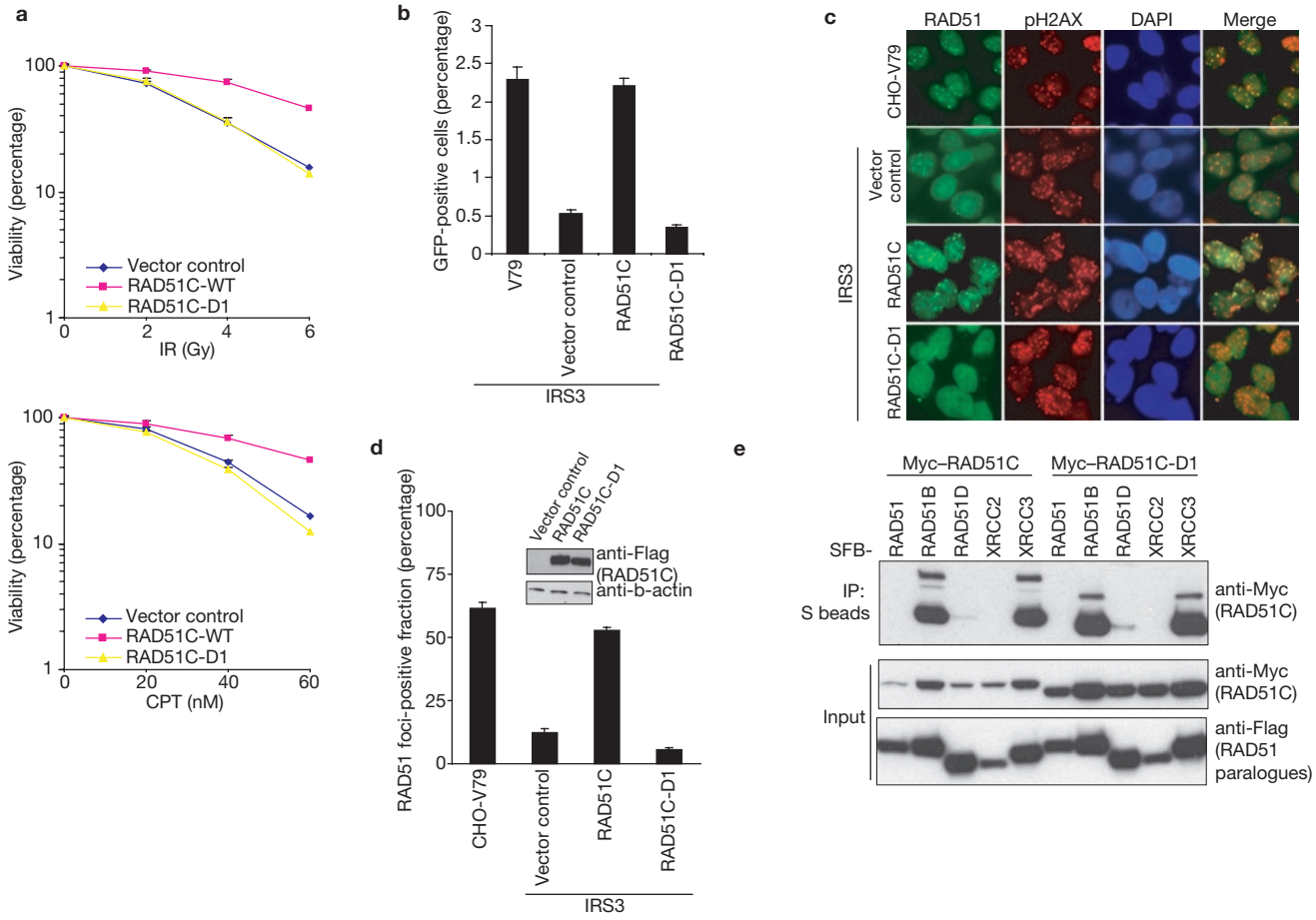

Figure 7 RAD18-binding is critical for RAD51C function in homologous recombination. (**a**) The D1 mutant of RAD51C is defective in restoring cell survival after IR or CPT treatment. RAD51C-deficient IRS3 cells were transduced with a control virus or a virus expressing HA–Flag-tagged wild-type RAD51C (WT) or an N-terminal deletion mutant (D1), which does not bind to RAD18. Wild-type or RAD51C-D1 expression was confirmed by immunoblotting as shown in **d**. Clonogenic assays were performed (see Methods). Data are mean ± s.e.m. of three independent experiments. (**b**) RAD18-binding is required for RAD51C function in homologous recombination. RAD51C-deficient IRS3 cells were reconstituted with wild-type or D1 mutant of RAD51C. Gene conversion assays were performed (see Methods). Data are mean ± s.e.m. of three independent experiments. (**c**, **d**) Interaction with RAD18 is important for RAD51C function in promoting RAD51 foci formation. IRS3 cells, expressing RAD51C or RAD51C-D1, and CHO-V79 cells were irradiated, fixed and immunostained with anti-RAD51 and anti-pH2AX antibodies. Representative RAD51 foci are shown in **c**. Data are mean ± s.e.m. of three independent experiments, > 100 cells were counted in each experiment (**d**). (**e**) The N-terminal region of RAD51C is not required for complex formation by RAD51 paralogues. Cells (293T) were transfected with plasmids encoding Myc-tagged RAD51C or RAD51C-D1 together with plasmids encoding SFB-tagged RAD51 or RAD51 paralogues. Immunoprecipitation (IP) reactions were performed using S beads and cells were then subjected to immunoblotting using the indicated antibodies. Uncropped images of blots are shown in Supplementary Information, Fig. S9.

deletion mutants of RNF8 failed to do so (Fig. 5a; Supplementary Information, Fig. S3c).

A previous report suggests that checkpoint kinase 1 (Chk1) promotes HRR through directly interacting with and phosphorylating RAD51 (ref. 39), raising the possibility that RAD18 may regulate HRR by influencing Chk1 activation. However, we found that RAD18 was not required for Chk1 activation after IR treatment (Fig. 5c), thus indicating that RAD18 may control HRR through a different mechanism.

RAD18 interacts with RAD51C

To explore how RAD18 participates in HRR, we generated a human HEK-293T-derivative cell line stably expressing a triple-tagged RAD18 for the identification of potential RAD18-interacting proteins. After a tandem affinity purification (TAP) scheme, proteins associated with RAD18 were identified by mass spectrometry analysis (Supplementary Information Table S1). Results showed several known RAD18-associated proteins, including PCNA, ubiquitin and RAD6A/UBE2A. Interestingly, one of these RAD18-associated proteins was RAD51C, a key component of both Rad51 paralogue complexes in human cells[20,21,40–44].

We first confirmed the interaction between RAD18 and RAD51C. As shown in Fig. 6a, RAD18 interacted with RAD51C and weakly with RAD51D. In addition, RAD51C specifically interacted with GST–RAD18 but not GST alone (Fig. 6b). This interaction was also detected *in vivo* between endogenous proteins before and after irradiation (Fig. 6c).

Next we sought to identify the region on RAD51C responsible for its interaction with RAD18 (Fig. 6d). Whereas neither the ATPase Walker A/Walker B motifs nor the Linker domain in between was required for this interaction, we found that the N terminus of RAD51C was necessary for its binding to RAD18 (Fig. 6e). Interestingly, the N terminus of RAD51C has been highly conserved throughout evolution (Fig. 6f), suggesting that it may carry out an important function of RAD51C.

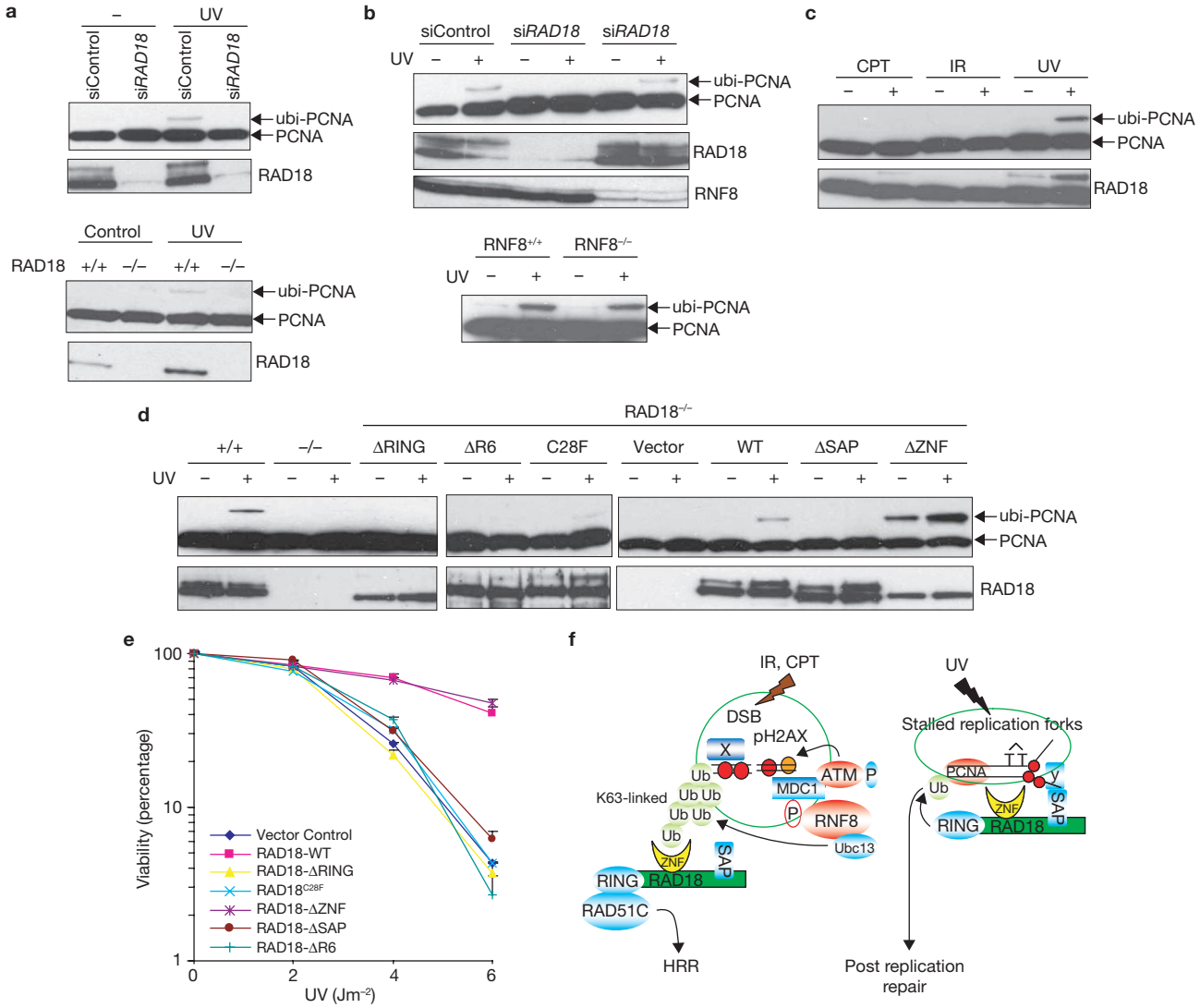

Figure 8 RAD18 participates in two distinct DNA repair pathways. (**a**) RAD18 is required for PCNA monoubiquitylation after UV damage. Control cells (HeLa cells depleted of endogenous RAD18; left) or RAD18-deficient MEFs (right) were treated with of UV radiation (60 J per m^2) or left untreated. Chromatin fractions were isolated (see Methods) and immunoblotted with the indicated antibodies. (**b**) RNF8 is not required for UV-induced PCNA monoubiquitylation (ubi). Experiments were carried out similarly to those described in **a**. (**c**) Monoubiquitylation of PCNA in cells after UV, X-ray or CPT treatment. HeLa cells were irradiated with UV light (60 J per m^2), X-rays (10 Gy) or treated with CPT (50 nM) and were allowed to recover for 4, 6 and 16 h, respectively. Chromatin fractions were isolated (see Methods) and immunoblotted with the indicated antibodies. (**d**) Both the SAP domain and E3 ligase activity of RAD18 are required for PCNA monoubiquitylation. UV-induced PCNA monoubiquitylation was analysed using western blotting in control or $RAD18^{-/-}$ cells reconstituted with wild-type or various deletion/point mutants of RAD18. The experiments were carried out similarly to those described in **a**. (**e**) The ZNF domain of RAD18 is not required for cell survival after UV treatment. Clonogenic assays were performed (see Methods). Data are mean ± s.e.m. of three independent experiments. (**f**) A model showing the role of RAD18 in mediating the PRR and HRR pathways (see Discussion).

We analysed a series of internal deletion/point mutations of RAD18 and found that the RING domain is critical for its interaction with RAD51C (Fig. 6g). Moreover, although the interaction between RAD51C and RAD18 depends on this RING domain, the conserved RAD18 cysteine mutants C28F, C25F and C46F retained the ability to interact with RAD51C, indicating that RAD18 E3 ligase activity and the intact structure of its RING domain may not be required for this interaction (Fig. 6g; Supplementary Information, Fig. S7). More importantly, the requirement for the RAD18 RING domain, but not its E3 ligase activity, for the retention of RAD51C to damaged chromatin (Fig. 6h) further indicates that RAD18 facilitates the accumulation of RAD51C through direct protein–protein interaction. Together, these data suggest that a physical interaction between RAD18 and RAD51C may have an important role in regulating HRR and they explain why the RAD18 RING domain, but not its E3 ligase activity, is required for its function in HRR and cell survival after DSBs.

The ability of RAD51C to function in homologous recombination correlates with its association with RAD18

RAD51C-deficient cells show homologous recombination defects and hypersensitivity to agents that induce DNA double-strand breaks[45–47]. Previous studies have also reported a significant reduction of RAD51 foci formation in RAD51C-deficient or depleted cells[48,49]. To explore the physiological relevance of the highly conserved N terminus of RAD51C,

which is required for its binding to RAD18, we used the RAD51C-D1 mutant that lacks this conserved region. Clonogenic assays in RAD51C-deficient CHO-IRS3 cells indicated that reconstitution with wild-type RAD51C, but not with the RAD51C-D1 mutant, restored cell survival after DSBs (Fig. 7a). In addition, re-introduction of wild-type RAD51C restored HRR efficiency to a level comparable with that observed in wild-type Chinese hamster ovary CHO-V79 cells, whereas the RAD51C-D1 mutant was defective in this assay (Fig. 7b, Supplementary Information, Fig. S3d). Moreover, we also observed a significant reduction of RAD51 foci formation in RAD51C-D1 reconstituted IRS3 cells when compared with cells reconstituted with wild-type RAD51C (Fig. 7c, d).

To rule out the possibility that the phenotypes observed in RAD51C-D1 reconstituted IRS3 cells may be due to a failure in forming RAD51 paralogue complexes, we performed co-immunoprecipitation experiments. As shown in Fig. 7e, the interaction between RAD51B or XRCC3 with RAD51C-D1 is similar to that with wild-type RAD51C. These results suggest that the specific interaction between RAD18 and the N terminus of RAD51C is probably important for RAD51C function in HRR.

RAD18 participates in two independent DNA damage repair pathways

The known function of RAD18 *in vivo* is to facilitate PCNA monoubiquitylation after DNA damage, especially in response to UV (ultraviolet)-induced lesions. We first confirmed the role of RAD18 in promoting UV-induced PCNA monoubiquitylation (Fig. 8a). As RNF8 is required for RAD18 relocalization after DSBs, we tested whether RNF8 would also be required for RAD18 function after UV damage. Interestingly, UV-induced PCNA monoubiquitylation was readily detected in RNF8-depleted HeLa cells or RNF8-deficient MEFs (Fig. 8b), indicating that RNF8 is exclusively involved in RAD18 function after DNA DSB induction. Indeed, whereas PCNA monoubiquitylation was readily detected after UV irradiation, it was either absent or very weak in cells treated with CPT or IR (Fig. 8c). These results indicate that RAD18 may participate in two independent repair processes. We further examined which domains of RAD18 would be required for its function in promoting PCNA monoubiquitylation. Intriguingly, although UV-induced PCNA monoubiquitylation was largely abrogated in RAD18-deficient cells ectopically expressing either the RAD18 E3 ligase-inactivating mutants (including ΔRING, C28F and ΔR6) or ΔSAP, PCNA monoubiquitylation was readily observed in cells expressing wild-type or ΔZNF RAD18(Fig. 8d). These results suggest that both the SAP domain and functional E3 ligase activity, but not the ZNF domain, of RAD18 are required for PCNA monoubiquitylation. Consistent with the notion that tolerance to UV-induced DNA damage involves damage-induced PCNA monoubiquitylation, the UV sensitivity of RAD18–/– cells stably expressing ΔZNF RAD18 was similar to that of cells expressing wild-type RAD18. In contrast, RAD18$^{-/-}$ cells expressing the E3 ligase-inactivating mutants or ΔSAP were more sensitive to UV damage (Fig. 8e). Thus, different domains of RAD18 are required for cell survival after UV damage and DNA DSBs, indicating that RAD18 participates in these repair pathways through distinct mechanisms (Fig. 8f).

DISCUSSION

Protein ubiquitylation is emerging as an important form of covalent modification that regulates various biological processes including DNA damage signalling and repair pathways. In this study, we demonstrate that RAD18 can be recruited to damaged chromatin through its ZNF domain in a RNF8/UBC13-dependent manner. Because the RAD18 ZNF domain directly binds to ubiquitin *in vitro*, we speculate that one or several ubiquitylated proteins on chromatin may interact with RAD18, recruiting it to sites of DNA breaks. So far, the nature of these ubiquitylated proteins remains unknown, although chromatin components such as H2A/H2B or H2AX are likely candidates[10,12,13,28]. This hypothesis is reminiscent of the damage-induced recruitment of RAP80, a recently identified ubiquitin-interacting domain (UIM)-containing protein that serves as an adaptor for BRCA1 accumulation at sites of DNA breaks[31–33]. Its ability to bind to ubiquitin (through its UIM domains) means RAP80 can be tethered to certain FK2-reacting ubiquitylated proteins in a similar manner to that of the ZNF domain of RAD18. Together, these data support a model whereby RNF8-dependent ubiquitin chains formed at DNA damage sites are used as docking sites for specific downstream complexes. Should this be a general phenomenon, RAD18 and RAP80 may represent a new class of DNA damage repair proteins that use ubiquitin-interacting domains as part of their recruitment to DSBs.

To achieve maximal efficiency for DNA damage response, cells need to synchronize the activation of DNA damage checkpoints with DNA repair processes. However, the precise mechanisms for this coordination are not well understood. In this study, we describe one example of such a mechanism in which RAD18 functions as a molecular linker between checkpoint signalling and DNA damage repair. We show that the function of RAD18 in DNA repair is strictly congruent with its recruitment to damaged chromatin. Deletion of the RAD18 zinc finger domain abolished the loading of RAD18 to DSB sites, therefore its role in homologous recombination is eliminated. Moreover, that double knockdown of *RNF8* and *RAD18* did not lead to increased IR or CPT sensitivity when compared with *RNF8* single knockdown further supports the idea that RAD18 activates HRR downstream of RNF8 (Supplementary Information, Fig. S5b). UBC13 works together with RNF8 in the assembly of checkpoint proteins at the damage site[10,12,13]. Interestingly, UBC13 has also been shown to have a role in HRR[28]. Together, these data support cross-talk between cell-cycle checkpoint regulation and DNA repair through a functional link between RNF8/UBC13 and RAD18.

We do not yet know exactly how RAD18 controls HRR. One possibility is that RAD18 participates in homologous recombination by facilitating the accumulation of RAD51C at damaged chromatin (Fig. 6h). As mammalian RAD51C is required for both the early and the late stages of HRR, through mediating the loading of RAD51 to DNA damage sites and the dissolution of Holliday junctions[41,44,49], respectively, it is not surprising that in gene conversion assays with RAD18-deficient cells, we observed a severe reduction in HRR, but only a moderate effect on RAD51 foci formation (Fig. 4).

We believe that RAD18 carries out distinct functions in response to DSBs and UV lesions (Fig. 8f). Whereas the main function of RAD18 in UV repair seems to be in promoting PCNA monoubiquitylation, increasing evidence suggests that monoubiquitylated PCNA is not necessary for RAD18 function in HRR: (1) RAD18 promotes PCNA monoubiquitylation and HRR using separate domains; (2) the E3 ligase activity of RAD18 is not required for RAD18-mediated HRR; (3) DSBs cannot efficiently induce PCNA monoubiquitylation; (4) RNF8 is required for RAD18 loading to DSB sites but not for UV-induced PCNA monoubiquitylation; (5) RAD51 foci are induced after IR treatment in PCNA^{K164R} mutant DT40 cells[28] and (6) DT40 cells carrying the PCNA^{K164R} mutation showed only

a modest increase in sensitivity to CPT[27]. Similarly to RAD18, UBC13 also functions in both DSB repair and UV-induced post-replication repair (PRR) in higher eukaryotes[28]. The dual roles of RAD18 and UBC13 are in marked contrast to their assigned functions in PRR in yeast: however, it is possible that the PPR-functions of these regulatory molecules may have changed during metazoan evolution to help cope with the more complex tasks of ensuring genome stability in vertebrate cells. □

METHODS

Antibodies. RAD18 monoclonal and polyclonal antibodies were obtained from Novus and Bethyl respectively. Antibodies against the Myc epitope, H2AX, γ-H2AX, ubiquitin, RNF8, RAP80, BRCA1 and RAD51 were described previously[10,50]. The anti-FK2 and anti-ORC2 antibodies were from Upstate Cell Signalling. Anti-Chk1 and anti-PCNA antibodies were obtained from Santa Cruz. Anti-Flag (M2), anti-RAD51C, anti-GAPDH and anti-p-Chk1 S317 antibodies were from Sigma, Novus, Calbiochem and Cell Signaling, respectively.

Constructs. The full-length and deletion/point mutants of human RAD18, RAD51 and RAD51 paralogues were generated by PCR and subcloned into the pDONR201 vector using Gateway Technology (Invitrogen). For transient expression, the corresponding fragments in entry vectors were transferred into a Gateway-compatible destination vector, which harboured an N terminal triple-epitope tag (SFB; S protein tag, Flag epitope tag and Streptavidin-binding peptide tag) or Myc epitope tag. DNA fragments corresponding to residues 495–585 of RAP80 and residues 186–240 of RAD18 were also subcloned into the pDONR201 vector, which was transferred into a Gateway-compatible destination vector to generate constructs for the expression of GST–RAP80-ZNF or GST–RAD18-ZNF in *Escherichia coli*. Generation of constructs containing full-length or deletion mutants of human RNF8 was as described previously[10]. The GST–Ubi construct was provided by B. Horazdovsky (Mayo Clinic, MN).

Cell Cultures. For the generation of RAP80$^{-/-}$ MEFs, an embryonic stem (ES) cell line RRN158 was used (Bay Genomics). The *RAP80* gene was disrupted by a neo gene selection cassette inserted between exon 1 (with ATG in it) and exon 2. Similarly, an ES cell line RRR260 (Bay Genomics) was used for the generation of RNF8-deficient MEFs. The RNF8 gene was disrupted by a neo gene selection cassette inserted between transcripted exon 4 and exon 5. The exact insertion sites were mapped by genomic PCR and DNA sequencing. These ES cells were injected into C57BL/6 blastocysts to generate chimaeric mice, which were crossed back with C57BL/6 mice to obtain RAP80^{+} or RNF8^{+} mice. The heterozygotes were intercrossed to generate RAP80$^{-/-}$ or RNF8$^{-/-}$ mice. RAP80- or RNF8-deficient MEFs were generated from their corresponding embryonic day13.5 embryos. The full description of these mice will be published in separate manuscripts.

H2AX$^{-/-}$, MDC1$^{-/-}$, 53BP1$^{-/-}$ and wild-type MEFs, NBS-deficient fibroblast cells (NBS-ILB1) and cells reconstituted with wild-type NBS1, HCC1937 and HCC1937–BRCA1 were generated as described previously[10,51]. HCT116 Rad18$^{-/-}$ cells, RAD18$^{-/-}$ MEFs, UBC13-deficient cells, IRS3 cells and V79 cells were gifts from T. Shiomi (National Institute of Radiological Sciences, Japan), M Yamaizumi (Kumamoto University, Japan), S. Akira (Osaka University, Japan) and H. Nagasawa (Colorado state university), respectively. U2OS cells with DR–GFP integration were from M. Jasin (Memorial Sloan-Kettering Cancer Center, NY).

GST pull-down assay. The GST fusion proteins were expressed in *E. coli* and purified as described previously[52]. GST-fusion protein (2 μg) or GST alone was immobilized on glutathione-Sepharose 4B beads and incubated with lysates prepared from cells that were transiently transfected with plasmids encoding indicated proteins.

The establishment of stable cell lines and affinity purification of SFB-tagged protein complexes. 293T cells were transfected with plasmids encoding SFB-tagged proteins. Cell lines stably expressing the tagged proteins were selected by culturing in a medium containing puromycin (2 μg ml^{-1}) and expression was confirmed by immunoblotting and immunostaining. For affinity purification, 293T cells stably expressing tagged proteins were lysed with NETN buffer (20 mM Tris-HCL, 100 mM NaCl, 1 mM EDTA and 0.5% Nonidet P-40) for 20 min. Crude lysates were cleared by centrifugation at 12,000g at 4 °C for 10 min, and supernatants were incubated with streptavidin-conjugated beads (300 μl; Amersham). The immunocomplexes were washed three times with NETN buffer and then bead-bound proteins were eluted with NETN buffer (1 ml) containing biotin (1 mg ml^{-1}; Sigma). The eluted supernatant was incubated with S-protein agarose beads (80 μl Novagen). The immunocomplexes were washed three times with NETN buffer and subjected to SDS–PAGE. Protein bands were excised, digested and the peptides were analysed by mass spectrometry.

Gene conversion assay. Cells (1×10^6) were electroporated with DR-GFP plasmid (12 μg) together with pCBASce plasmid (12 μg) at 270V, 975μF using a Gene Pulsar II (BioRad). Cells were plated onto 10-cm dishes and incubated in culture media for 48 h before FACS analyses.

Immuofluorescence staining. To visualize IRIF, cells cultured on coverslips were treated with gamma irradiation (10 Gy) or CPT (1 μM) for 6 h or 2 h, respectively, before recovery. Cells were then pre-extracted with buffer containing 0.5% triton X-100 for 5 min and fixed using 3% paraformaldehyde solution for 10 min at room temperature. Samples were blocked with 5% goat serum and incubated with primary antibodies anti-RAD18 (1:500), anti-pH2AX (1:1000), anti-RAD51 (1:1000), anti-RAP80 (1:500) and anti-BRCA1 (1:500) for 30 min. Next, samples were washed and incubated with secondary antibodies for 30 min. Cells were then stained with DAPI (4′,6-diamidino-2-phenylindole) to visualize nuclear DNA.

siRNA. All short interfering RNA (siRNA) duplexes were from Dharmacon Research. The sequences of *RAD18* siRNA, *RNF8* siRNA1 and siRNA2 were 5'-ACUCAGUGUCCAACUUGCUdTdT-3', 5'-GAGAAGCUUACAGAUGUUU-3' and 5'-AGAAUGAGCUCCAAUGUAUUU-3', respectively. The sequence of control siRNA was 5'-UUCAAUAAAUUCUUGAGGUUU-3'.

Retrovirus production and infection. pDONR201 derivative constructs containing full-length or mutant RAD18 or RAD51C were transferred into a Gateway-compatible pEF1A-HA–Flag retroviral vector. Virus supernatant was collected 48 h after the co-transfection of pEF1A vectors and pcl-ampho into BOSC23 human embryonic kidney cells. MEFs or IRS3 cells were infected with viral supernatant in the presence of polybrene (8 μg ml^{-1}) and were then selected in growth media containing 2 μg ml^{-1} or 5 μg ml^{-1} puromycin, respectively.

Cell survival assays. Cells (1×10^3) were seeded onto 60-mm dish in triplicates. At 24 h after seeding, cells were treated with CPT or irradiated with IR or UV. The medium was replaced 24 h later and cells were then incubated for 14 days. Resulting colonies were fixed and stained with Coomassie blue. Numbers of colonies were counted using a GelDoc with Quantity One software (BioRad).

Chromatin fractionation. Preparation of chromatin fractions was as described previously[10,53] with modifications. Briefly, 6 h after treatment with 10 Gy of ionizing radiation, 4 h after treatment with UV (60 J per m^2) or 16 h after treatment with of CPT (50 nM) cells were collected and washed once with PBS. Cell pellets were subsequently resuspended in low salt permeabilization buffer (10 mM HEPES at pH 7.4, 10 mM KCl, 0.05% NP-40 and protease inhibitors) and incubated on ice for 20 min., Nuclei were then recovered and resuspended in HCl (0.2 M). The soluble fraction was neutralized with Tris-HCl (1 M at pH 8.0) for further analysis. For micrococcal nuclease (MNase) treatment, nuclei recovered after low salt extraction were washed and resuspended in nuclease reaction buffer (10 mM HEPES at pH 7.4, 10 mM KCl, 0.5 mM $MgCl_2$ and 2 mM $CaCl_2$). Nuclease (20 U) was added and nuclei were incubated for 30 min on ice. The insoluble fraction was essential for isolating the chromatin-bound proteins.

Note: Supplementary Information is available on the Nature Cell Biology website.

ACKNOWLEDGEMENTS

We thank T. Shiomi for HCT116 RAD18$^{-/-}$ cells, M. Yamaizumi for RAD18$^{-/-}$ MEFs, S. Akira for UBC13-deficient cells, H.Nagasawa for IRS3 and V79 cells, M. Jasin for U2OS cells with DR–GFP integration and pCBASce plasmids, B. P. Chen for NU7441 and J. Groenendyk for helping with the BIAcore system. J.C would like to thank all colleagues for discussions and technical assistance, and J. Wood for proofreading. This work was supported by grants from the National Institutes of Health to J.C., M.S.Y.H. is supported by the Anna Fuller Fund Fellowship and J.C. is a recipient of an Era of Hope Scholar award from the Department of Defense (a member of the Mayo Clinic Breast SPORE program).

AUTHOR CONTRIBUTIONS

J.H. performed most of the experiments; J.H. and J.C. designed the experiments, analysed the data and wrote the manuscript; M.S.Y.H. performed the experiments shown in Fig. 2e; H.K. performed the experiments shown in Fig. S2a; C.C.Y.L. and J.N.M.G. performed the experiments shown in Fig. S2b, c and X.Y. generated the RNF8 and RAP80 knockout mice.

COMPETING FINANCIAL INTERESTS

The authors declare no competing financial interests.

Published online at http://www.nature.com/naturecellbiology/
Reprints and permissions information is available online at http://npg.nature.com/reprintsandpermissions/.

1. Hoeijmakers, J. H. Genome maintenance mechanisms for preventing cancer. *Nature* **411,** 366–374 (2001).
2. Friedberg, E. C. DNA damage and repair. *Nature* **421,** 436–440 (2003).
3. Bartkova, J. *et al.* DNA damage response as a candidate anti-cancer barrier in early human tumorigenesis. *Nature* **434,** 864–870 (2005).
4. Gorgoulis, V. G. *et al.* Activation of the DNA damage checkpoint and genomic instability in human precancerous lesions. *Nature* **434,** 907–913 (2005).
5. Bartek, J. & Lukas, J. DNA damage checkpoints: from initiation to recovery or adaptation. *Curr. Opin. Cell Biol.* **19,** 238–245 (2007).
6. Fernandez-Capetillo, O., Lee, A., Nussenzweig, M. & Nussenzweig, A. H2AX: the histone guardian of the genome. *DNA Repair (Amst.)* **3,** 959–967 (2004).
7. Bassing, C. H. *et al.* Histone H2AX: a dosage-dependent suppressor of oncogenic translocations and tumors. *Cell* **114,** 359–370 (2003).
8. Celeste, A. *et al.* H2AX haploinsufficiency modifies genomic stability and tumor susceptibility. *Cell* **114,** 371–383 (2003).
9. Kim, H., Huang, J. & Chen, J. CCDC98 is a BRCA1-BRCT domain-binding protein involved in the DNA damage response. *Nature Struct. Mol. Biol.* **14,** 710–715 (2007).
10. Huen, M. S. *et al.* RNF8 transduces the DNA-damage signal via histone ubiquitylation and checkpoint protein assembly. *Cell* **131,** 901–914 (2007).
11. Wang, B. & Elledge, S. J. Ubc13/Rnf8 ubiquitin ligases control foci formation of the Rap80/Abraxas/Brca1/Brcc36 complex in response to DNA damage. *Proc. Natl Acad. Sci. USA* **104,** 20759–20763 (2007).
12. Mailand, N. *et al.* RNF8 ubiquitylates histones at DNA double-strand breaks and promotes assembly of repair proteins. *Cell* **131,** 887–900 (2007).
13. Kolas, N. K. *et al.* Orchestration of the DNA-damage response by the RNF8 ubiquitin ligase. *Science* **318,** 1637–1640 (2007).
14. Plans, V. *et al.* The RING finger protein RNF8 recruits UBC13 for lysine 63-based self polyubiquitylation. *J. Cell. Biochem* **97,** 572–582 (2006).
15. Weinstock, D. M., Richardson, C. A., Elliott, B. & Jasin, M. Modeling oncogenic translocations: distinct roles for double-strand break repair pathways in translocation formation in mammalian cells. *DNA Repair (Amst.)* **5,** 1065–1074 (2006).
16. Lukas, J. & Bartek, J. Watching the DNA repair ensemble dance. *Cell* **118,** 666–668 (2004).
17. Kennedy, R. D. & D'Andrea, A. D. DNA repair pathways in clinical practice: lessons from pediatric cancer susceptibility syndromes. *J. Clin. Oncol.* 24, 3799–3808 (2006).
18. West, S. C. Molecular views of recombination proteins and their control. *Nature Rev. Mol. Cell Biol.* **4,** 435–445 (2003).
19. Thacker, J. The RAD51 gene family, genetic instability and cancer. *Cancer Lett.* **219,** 125–135 (2005).
20. Masson, J. Y. *et al.* Identification and purification of two distinct complexes containing the five RAD51 paralogs. *Genes Dev.* **15,** 3296–3307 (2001).
21. Sigurdsson, S. *et al.* Mediator function of the human Rad51B-Rad51C complex in Rad51/RPA-catalyzed DNA strand exchange. *Genes Dev.* **15,** 3308–3318 (2001).
22. Tateishi, S., Sakuraba, Y., Masuyama, S., Inoue, H. & Yamaizumi, M. Dysfunction of human Rad18 results in defective postreplication repair and hypersensitivity to multiple mutagens. *Proc. Natl Acad. Sci. USA* **97,** 7927–7932 (2000).
23. Tateishi, S. *et al.* Enhanced genomic instability and defective postreplication repair in RAD18 knockout mouse embryonic stem cells. *Mol. Cell. Biol.* **23,** 474–481 (2003).
24. Hoege, C., Pfander, B., Moldovan, G. L., Pyrowolakis, G. & Jentsch, S. RAD6-dependent DNA repair is linked to modification of PCNA by ubiquitin and SUMO. *Nature* **419,** 135–141 (2002).
25. Watanabe, K. *et al.* Rad18 guides poleta to replication stalling sites through physical interaction and PCNA monoubiquitination. *EMBO J.* **23,** 3886–3896 (2004).
26. Szuts, D., Simpson, L. J., Kabani, S., Yamazoe, M. & Sale, J. E. Role for RAD18 in homologous recombination in DT40 cells. *Mol. Cell. Biol.* **26,** 8032–8041 (2006).
27. Saberi, A. *et al.* RAD18 and poly(ADP-ribose) polymerase independently suppress the access of nonhomologous end joining to double-strand breaks and facilitate homologous recombination-mediated repair. *Mol. Cell. Biol.* **27,** 2562–2571 (2007).
28. Zhao, G. Y. *et al.* A critical role for the ubiquitin-conjugating enzyme Ubc13 in initiating homologous recombination. *Mol. Cell* **25,** 663–675 (2007).
29. Morris, J. R. & Solomon, E. BRCA1 : BARD1 induces the formation of conjugated ubiquitin structures, dependent on K6 of ubiquitin, in cells during DNA replication and repair. *Hum. Mol. Genet.* **13,** 807–817 (2004).
30. Polanowska, J., Martin, J. S., Garcia-Muse, T., Petalcorin, M. I. & Boulton, S. J. A conserved pathway to activate BRCA1-dependent ubiquitylation at DNA damage sites. *EMBO J.* **25,** 2178–2188 (2006).
31. Kim, H., Chen, J. & Yu, X. Ubiquitin-binding protein RAP80 mediates BRCA1-dependent DNA damage response. *Science* **316,** 1202–1205 (2007).
32. Sobhian, B. *et al.* RAP80 targets BRCA1 to specific ubiquitin structures at DNA damage sites. *Science* **316,** 1198–1202 (2007).
33. Wang, B. *et al.* Abraxas and RAP80 form a BRCA1 protein complex required for the DNA damage response. *Science* **316,** 1194–1198 (2007).
34. Petrini, J. H. Cell signaling. A touching response to damage. *Science* **316,** 1138–1139 (2007).
35. Sartori, A. A. *et al.* Human CtIP promotes DNA end resection. *Nature* **450,** 509–514 (2007).
36. Yamashita, Y. M. *et al.* RAD18 and RAD54 cooperatively contribute to maintenance of genomic stability in vertebrate cells. *EMBO J.* **21,** 5558–5566 (2002).
37. Yoshimura, A. *et al.* A novel Rad18 function involved in protection of the vertebrate genome after exposure to camptothecin. *DNA Repair (Amst.)* **5,** 1307–1316 (2006).
38. Weinstock, D. M., Nakanishi, K., Helgadottir, H. R. & Jasin, M. Assaying double-strand break repair pathway choice in mammalian cells using a targeted endonuclease or the RAG recombinase. *Methods Enzymol.* **409,** 524–540 (2006).
39. Sorensen, C. S. *et al.* The cell-cycle checkpoint kinase Chk1 is required for mammalian homologous recombination repair. *Nature Cell Biol.* **7,** 195–201 (2005).
40. French, C. A., Tambini, C. E. & Thacker, J. Identification of functional domains in the RAD51L2 (RAD51C) protein and its requirement for gene conversion. *J. Biol. Chem.* **278,** 45445–45450 (2003).
41. Kuznetsov, S. *et al.* RAD51C deficiency in mice results in early prophase I arrest in males and sister chromatid separation at metaphase II in females. *J. Cell Biol.* **176,** 581–592 (2007).
42. Liu, Y., Tarsounas, M., O'Regan, P. & West, S. C. Role of RAD51C and XRCC3 in genetic recombination and DNA repair. *J. Biol. Chem.* **282,** 1973–1979 (2007).
43. Reynolds, J. Resolving a Holliday romance. *Nature Cell Biol.* **6,** 184 (2004).
44. Liu, Y., Masson, J. Y., Shah, R., O'Regan, P. & West, S. C. RAD51C is required for Holliday junction processing in mammalian cells. *Science* **303,** 243–246 (2004).
45. French, C. A. *et al.* Role of mammalian RAD51L2 (RAD51C) in recombination and genetic stability. *J. Biol. Chem.* **277,** 19322–19330 (2002).
46. Godthelp, B. C. *et al.* Mammalian Rad51C contributes to DNA cross-link resistance, sister chromatid cohesion and genomic stability. *Nucleic Acids Res.* **30,** 2172–2182 (2002).
47. Hinz, J. M., Helleday, T. & Meuth, M. Reduced apoptotic response to camptothecin in CHO cells deficient in XRCC3. *Carcinogenesis* **24,** 249–253 (2003).
48. Takata, M. *et al.* Chromosome instability and defective recombinational repair in knockout mutants of the five Rad51 paralogs. *Mol. Cell. Biol.* **21,** 2858–2866 (2001).
49. Rodrigue, A. *et al.* Interplay between human DNA repair proteins at a unique double-strand break in vivo. *EMBO J.* **25,** 222–231 (2006).
50. Chen, J. *et al.* Stable interaction between the products of the *BRCA1* and *BRCA2* tumor suppressor genes in mitotic and meiotic cells. *Mol. Cell* **2,** 317–328 (1998).
51. Maser, R. S., Zinkel, R. & Petrini, J. H. An alternative mode of translation permits production of a variant NBS1 protein from the common Nijmegen breakage syndrome allele. *Nature Genet* **27,** 417–421 (2001).
52. Hofer, B., Backhaus, S. & Timmis, K. N. The biphenyl/polychlorinated biphenyl-degradation locus (bph) of Pseudomonas sp. LB400 encodes four additional metabolic enzymes. *Gene* **144,** 9–16 (1994).
53. Yu, X., Fu, S., Lai, M., Baer, R. & Chen, J. BRCA1 ubiquitinates its phosphorylation-dependent binding partner CtIP. *Genes Dev.* **20,** 1721–1726 (2006).

nature cell biology

DOI: 10.1038/ncb1865

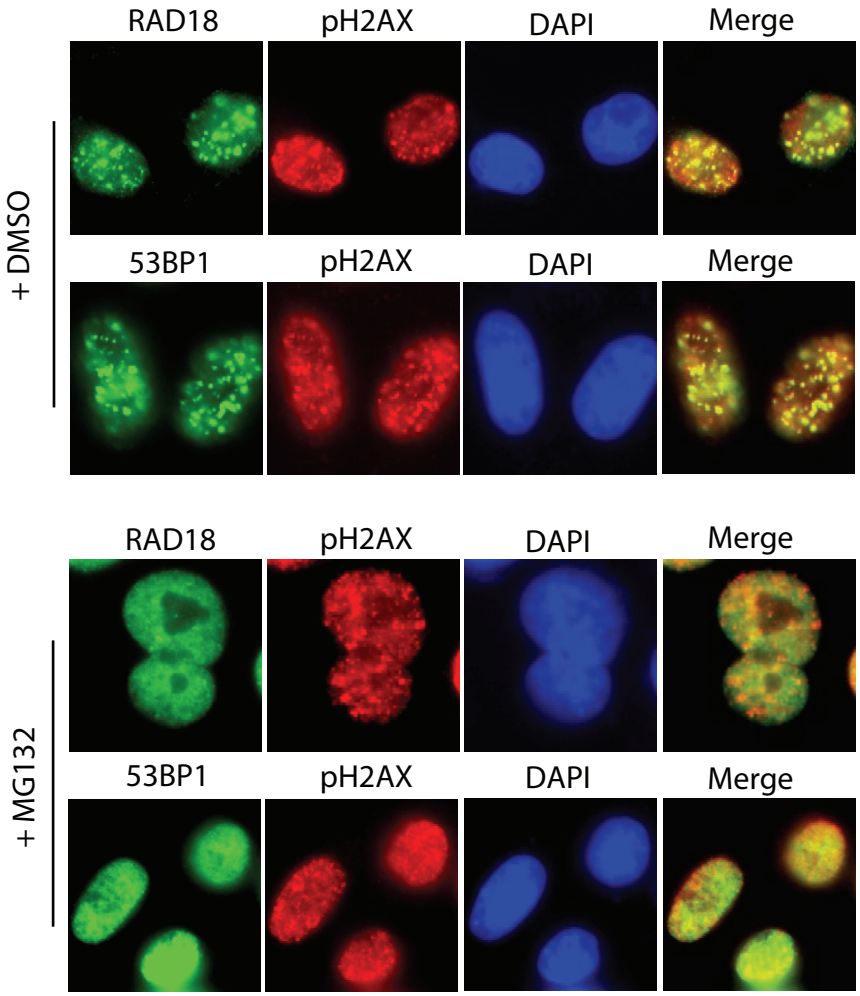

Figure S1 RAD18 focus formation is suppressed by proteasome inhibitor MG132. HeLa cells were treated with MG132 (20 μM) or DMSO for 2 hours before irradiation (10 Gy). Cells were fixed six hours later and immunostained with anti-p-H2AX, anti-RAD18 or anti-53BP1 antibodies.

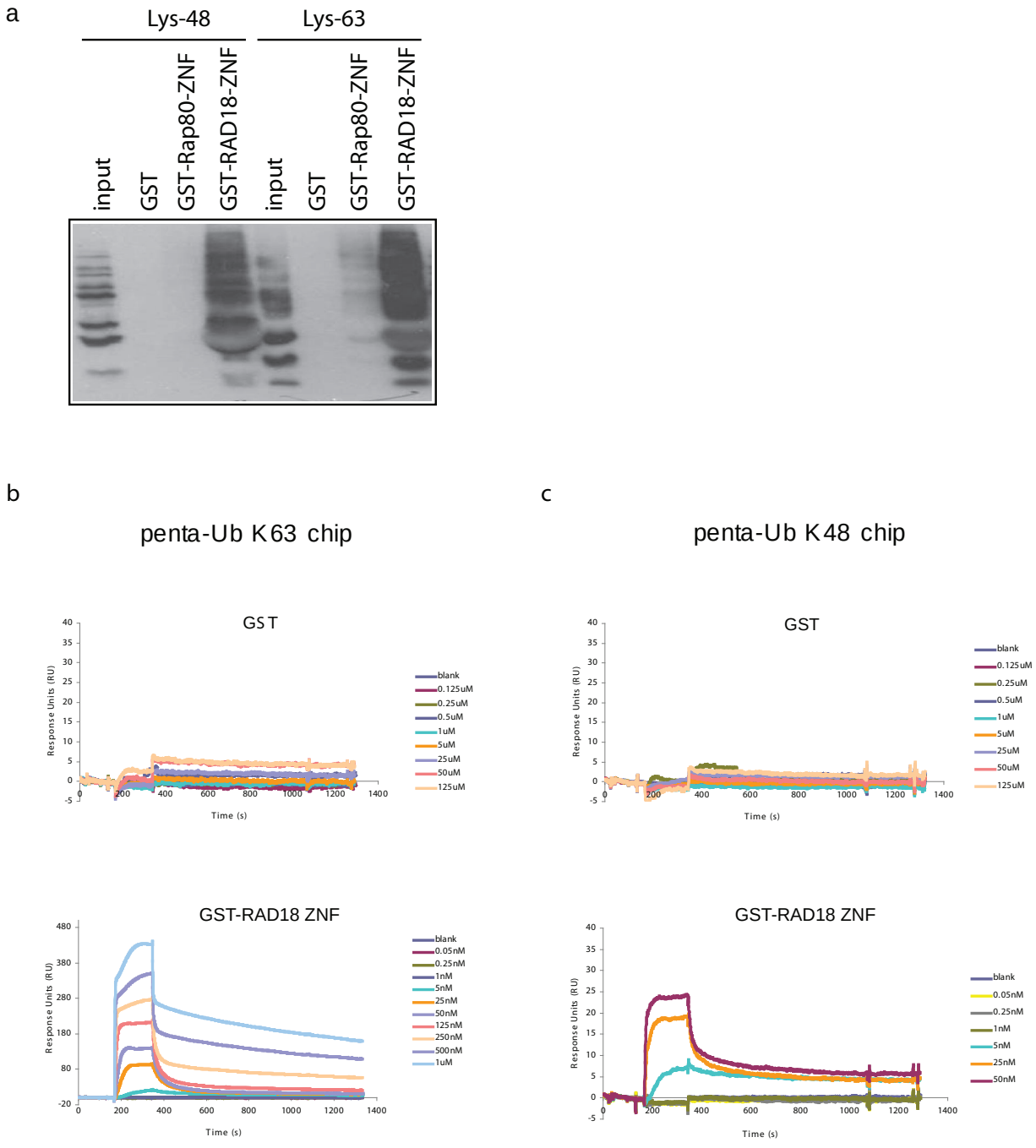

Figure S2 Direct binding of RAD18 ZNF domain to polyubiquitin chains *in vitro*. (a) GST, GST-RAD18 ZNF domain or GST-Rap80 ZNF domain were incubated with lysine 48-linked polyubiquitin chains (Lys-48 Ubs) or lysine 63-linked polyubiquitin chains (Lys-63 Ubs). After extensive washing, bound polyubiquitin chains were analyzed by immunoblotting with monoclonal antibody to ubiquitin. (b, c) SPR sensorgrams for GST and GST-RAD18 ZNF with immobilized penta-ubiquitin linked K63 (b) and K48 (c) chains. The experiments were performed according to the Experimental Procedures.

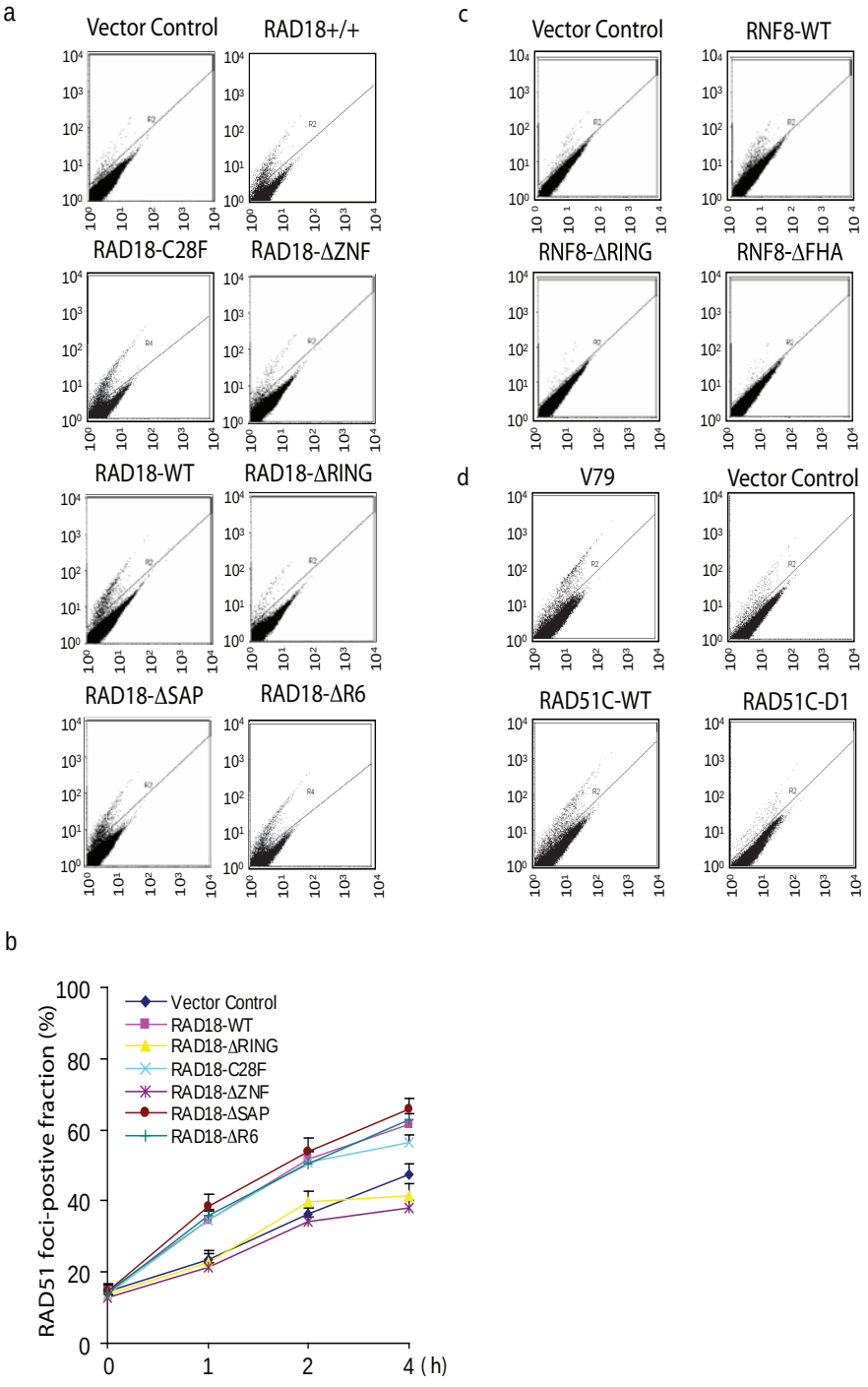

Figure S3 (a) RAD18-deficient cells were reconstituted with wild-type or different RAD18 mutants as indicated. Cells were electroporated with 12 μg of DR-GFP and 12 μg of pCBASce plasmids. Forty-eight hours later, GFP-positive cells were quantified by flow cytometry analysis. (b) RAD18 is required for efficient RAD51 foci formation. RAD18-deficient cells were reconstituted with wild-type or different RAD18 mutants as indicated. Different timepoints after treatment with 4 Gy of ionizing radiation, cells were fixed and immunostained using anti-RAD51 and pH2AX antibodies. Results were the average of three independent experiments and were presented as mean±SEM. (c) RNF8 participates in homologous recombination. (d) RAD18-binding is required for RAD51C function in homologous recombination. RAD51C-deficient IRS3 cells were reconstituted with wild-type or D1 mutant of RAD51C. Cells were electroporated with DR-GFP and pCBASce plasmids. Forty-eight hours later, GFP-positive cells were quantified by flow cytometry analysis.

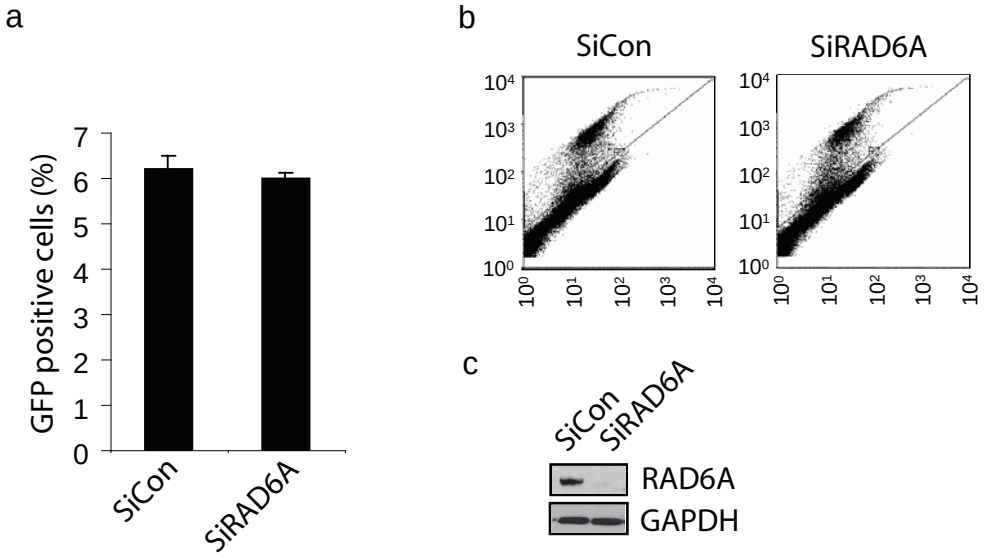

Figure S4 RAD6A is not required for RAD18-mediated HR repair. (a, b) Depletion of RAD6A in U2OS cells has no effect on gene conversion. U2OS DR-GFP cells transfected with control or RAD6A siRNAs were electroporated with 12 μg pCBASce construct and subjected to FACS analyses 48 hours later (b). Results (mean±SEM) were the average of three independent experiments (a). (c) Expression of RAD6A following siRNA transfection was confirmed by immunoblotting.

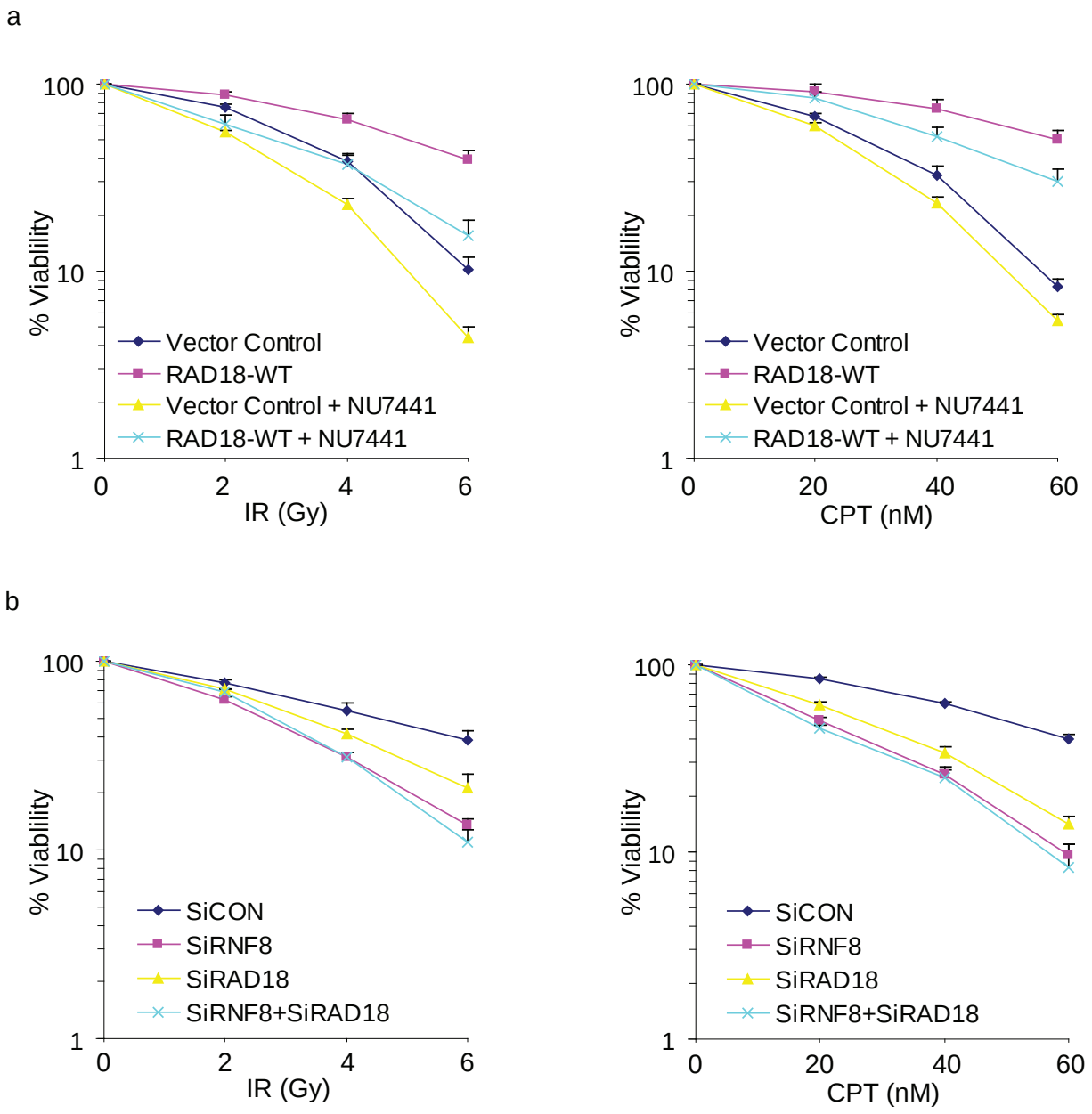

Figure S5 (a) RAD18 promotes HR repair independent of NHEJ pathway. Clonogenic survival assays were performed using RAD18+/+ and RAD18-/- cells exposed to IR or CPT alone or in combination with NU7441 (0.5 μM). For NU7441 treatment, cells were exposed to NU7441 for 16 hours before seeding for colony formation. (b) RAD18 acts downstream of RNF8. Colony formation assays were performed according to the Experimental Procedures. Results were averages of three independent experiments and were presented as mean±SEM.

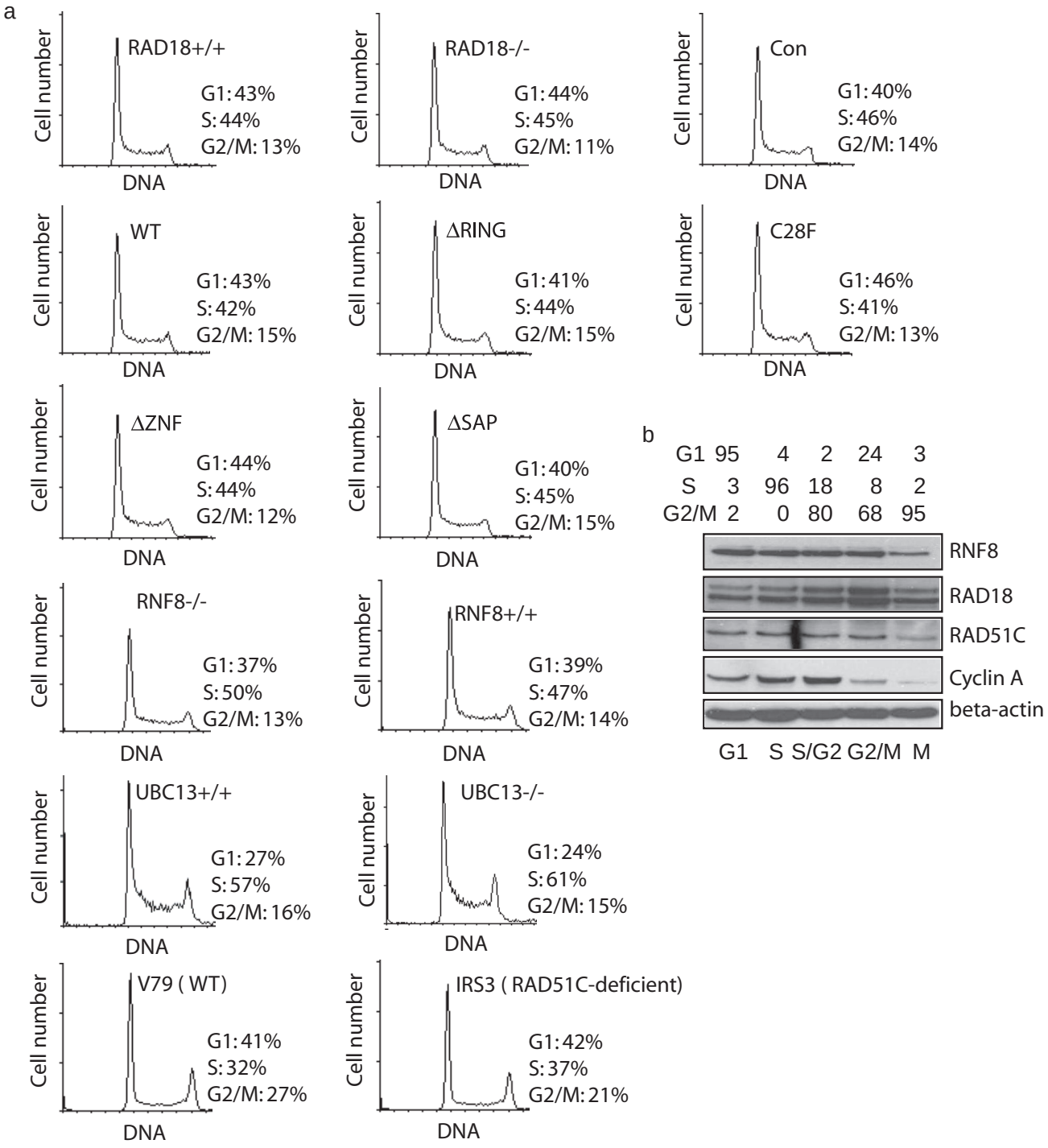

Figure S6 (a) Cell cycle distribution of RNF8-/-, UBC13-/-, RAD18-/-, RAD51C-deficient IRS3 and their corresponding wild-type cells. Cells were collected and treated as described in the Experimental Procedures. Flow cytometric analysis was performed using a FACSCalibur flow cytometer. (b) HeLa cells were synchronized as described in the Experimental Procedures. Cell lysates were analyzed by immunblotting using antibodies as indicated.

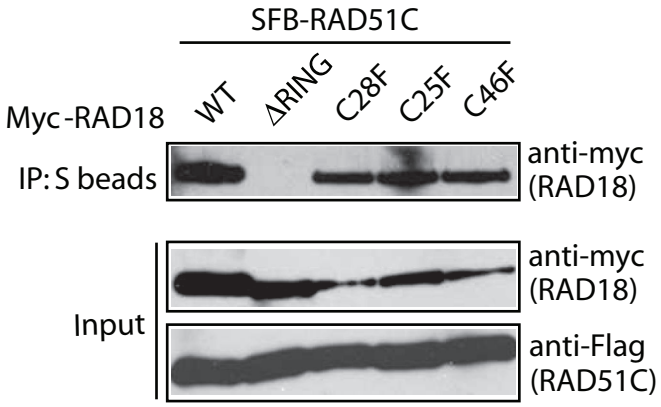

Figure S7 The E3 ligase activity and the intact RING domain structure are not required for RAD18 and RAD51C interaction. 293T cells were transfected with plasmids encoding SFB-tagged RAD51C together with plasmids encoding Myc-tagged RAD18 or various mutants. Cells were collected 24 hour after transfection. Immunoprecipitation (IP) reactions were performed using S beads and then subjected to immunoblotting using indicated antibodies.

Figure 1a

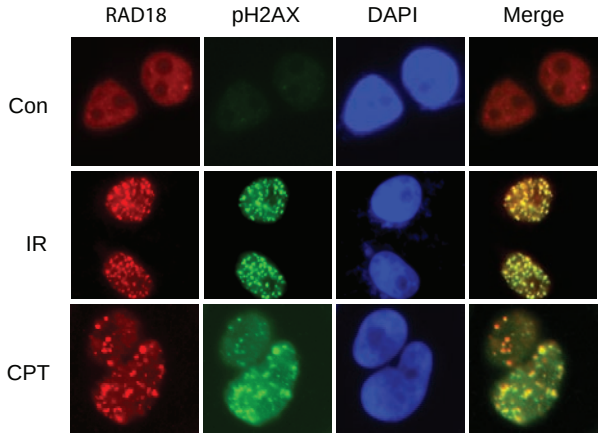

Figure 1d left

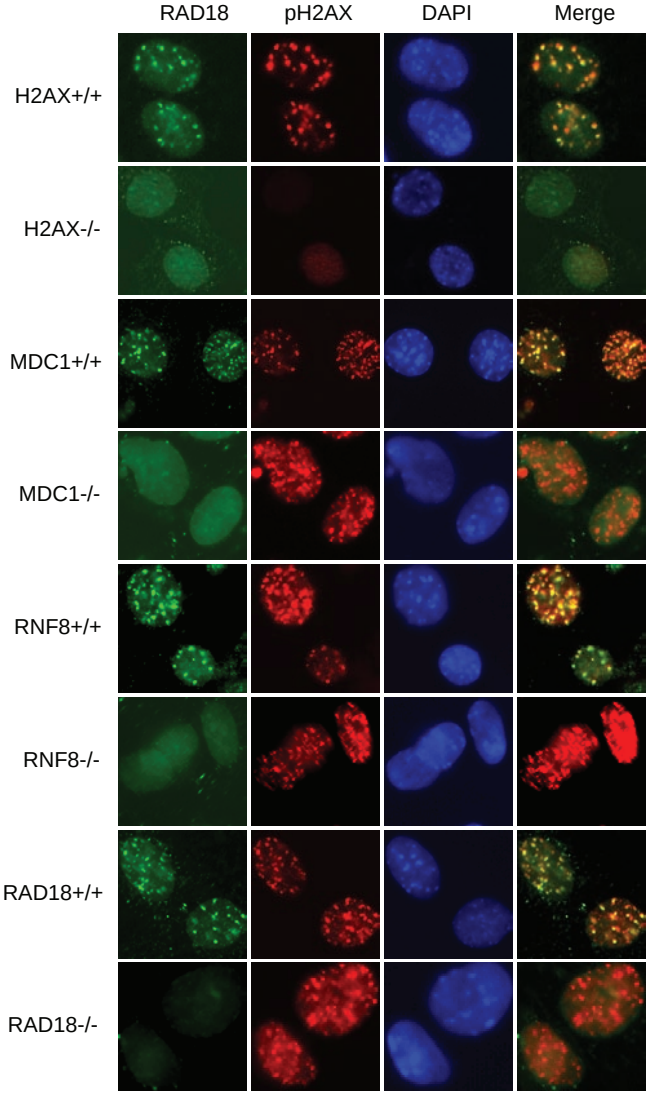

Figure S8 Enlarged key immunostaining images shown in the manuscript.

Figure 1d right

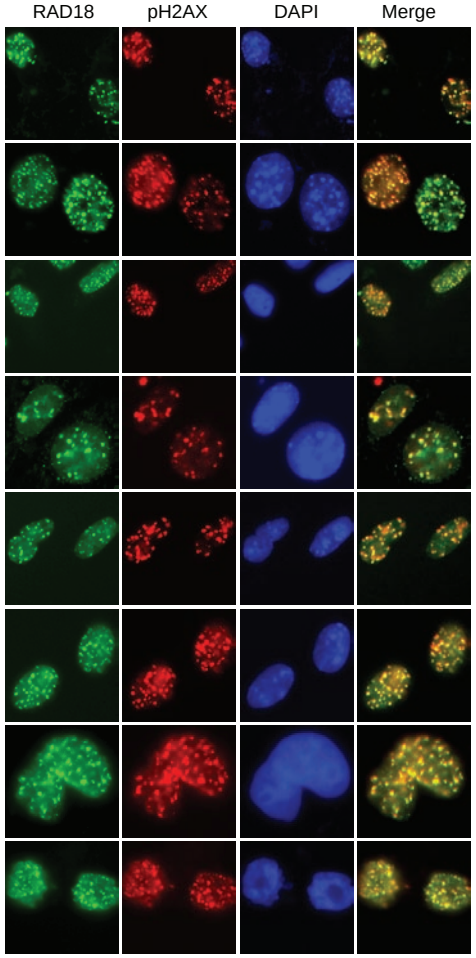

Figure 2a, b

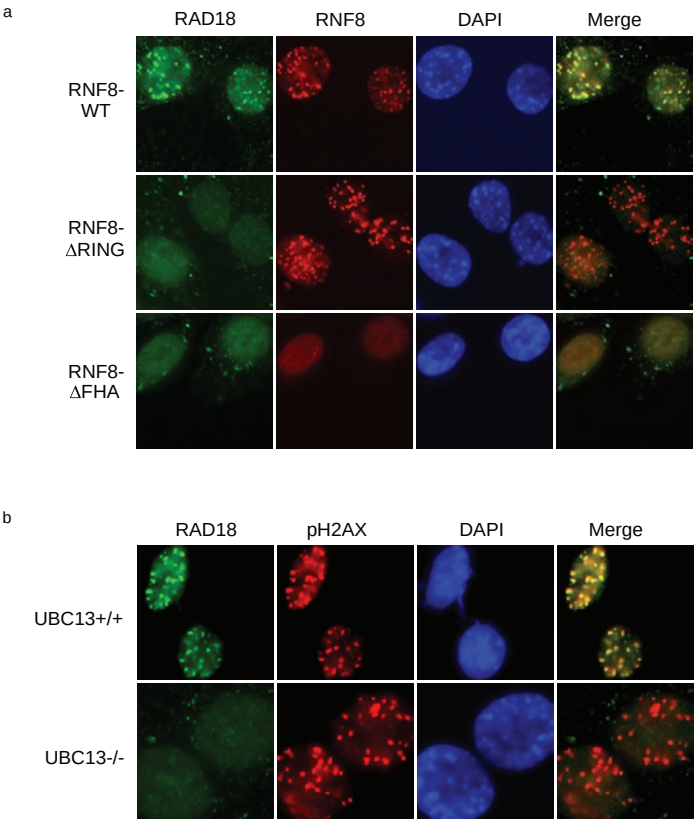

Figure S8 continued

Figure 3b

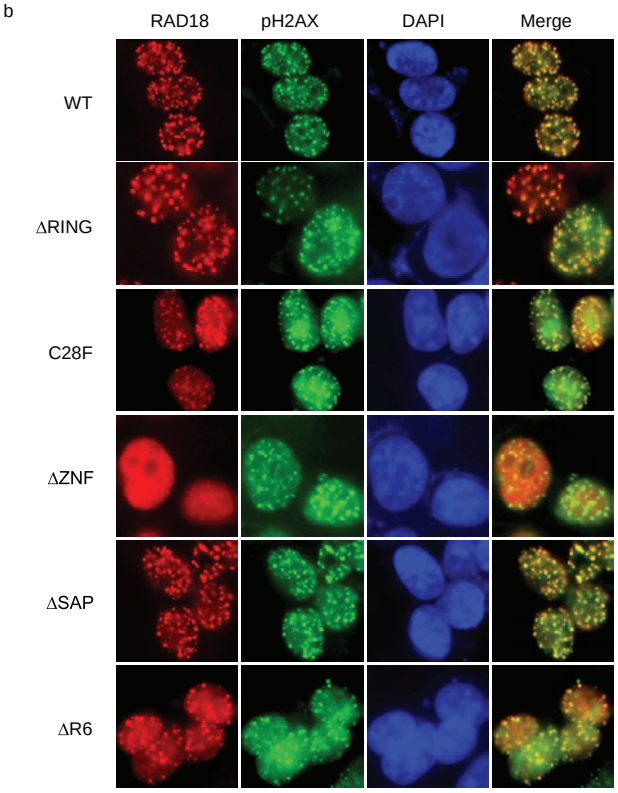

Figure 2d

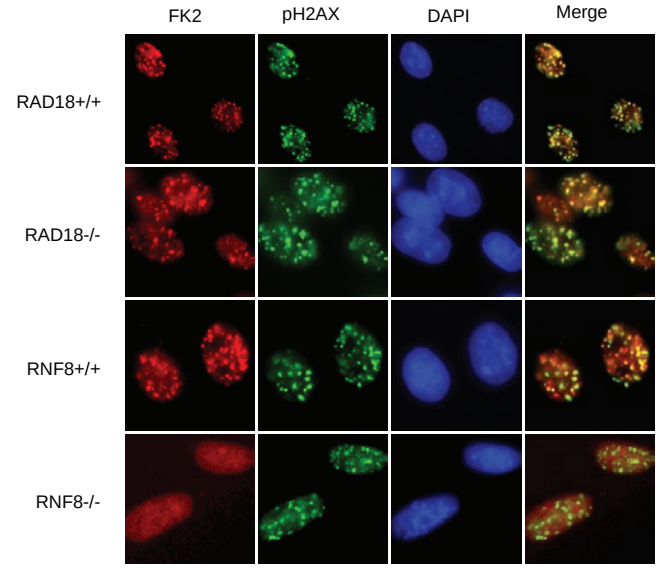

Figure 2F

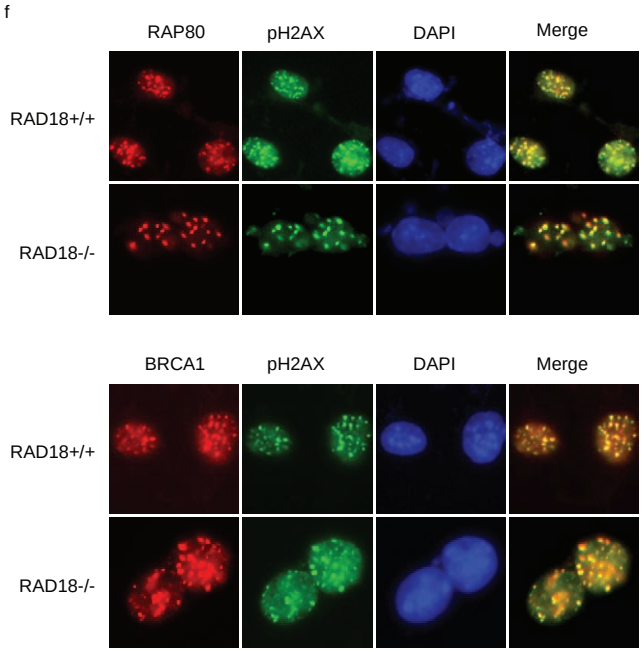

Figure S8 continued

Figure 3c

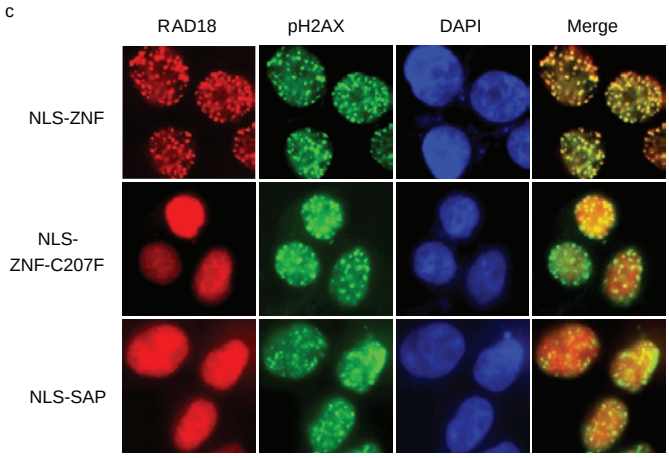

Figure 3d

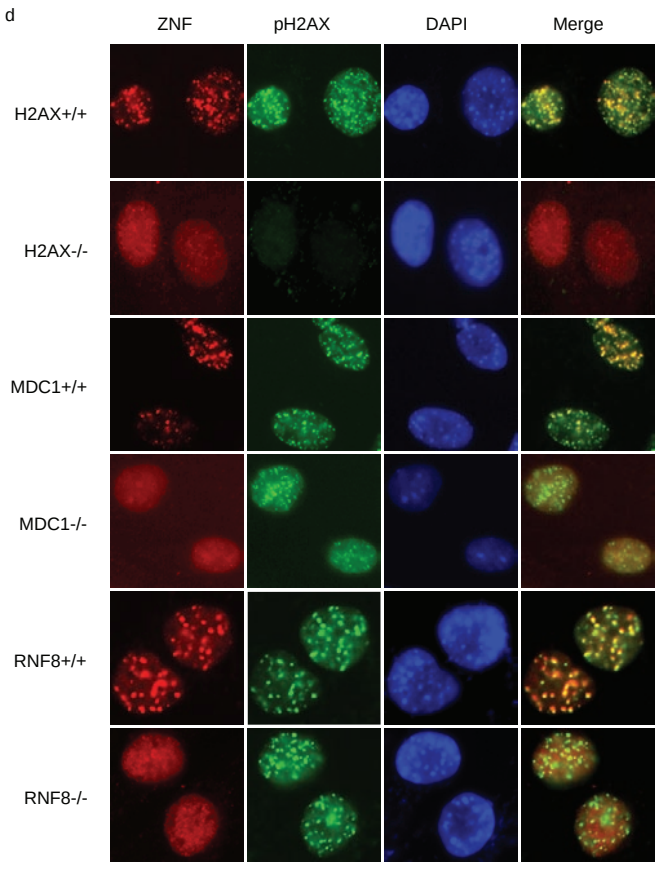

Figure S8 continued

Figure 4c

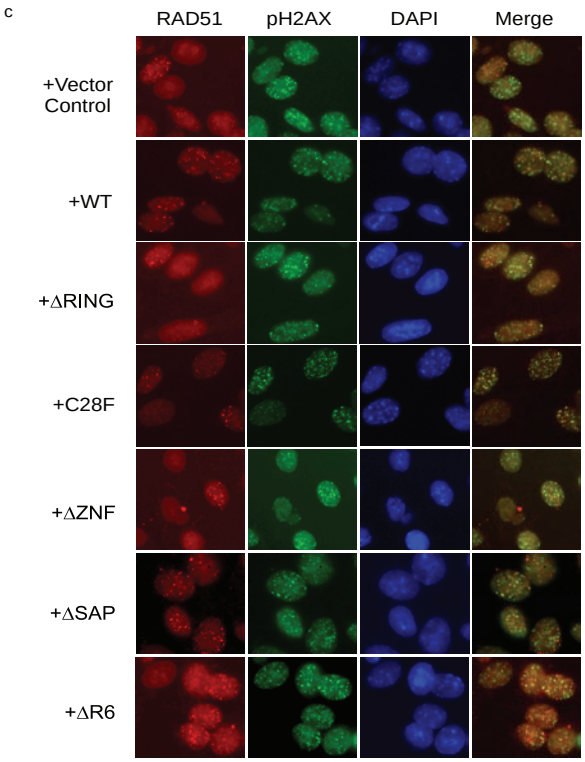

Figure 7c

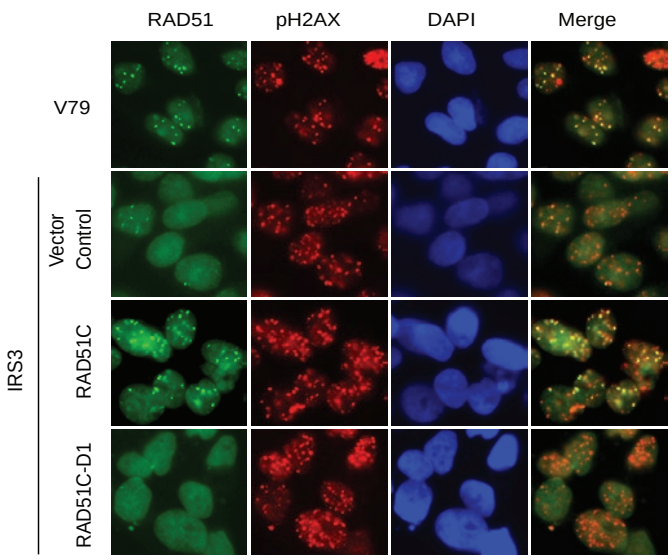

Figure S8 continued

Fig 1b

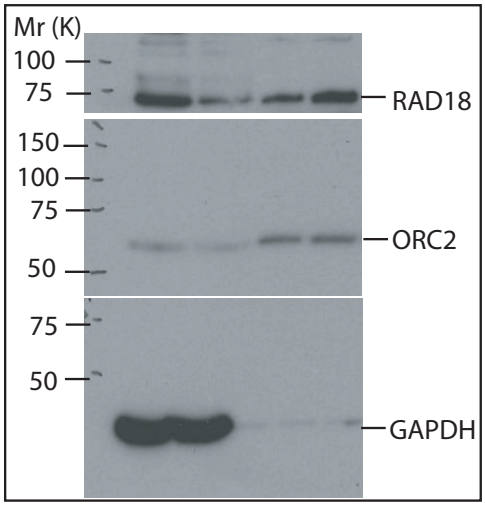

Fig 1c

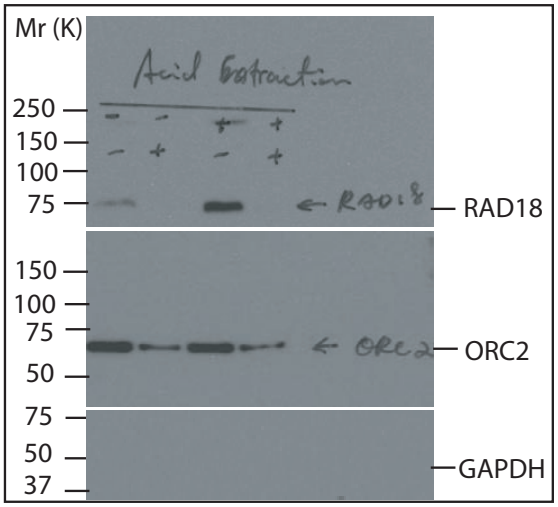

Fig 2c

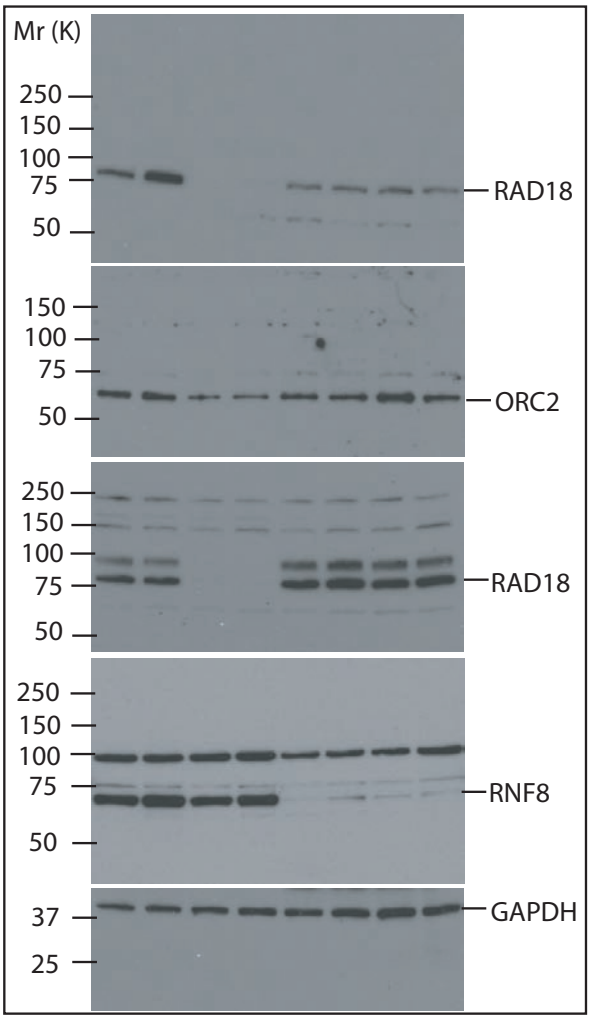

Fig 2e

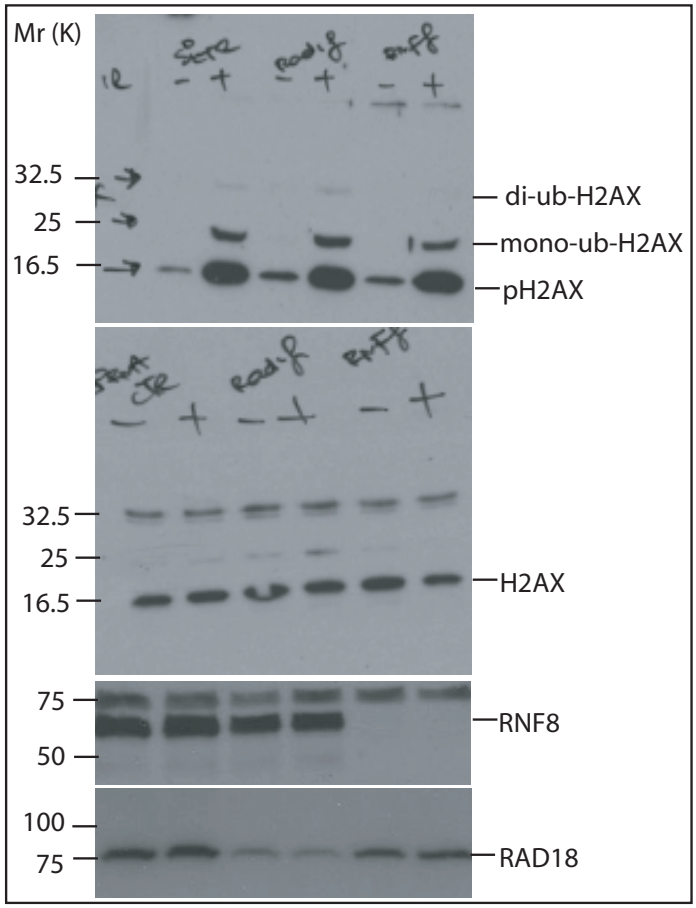

Figure S9 Full scans of key immunoblots shown in the manuscript.

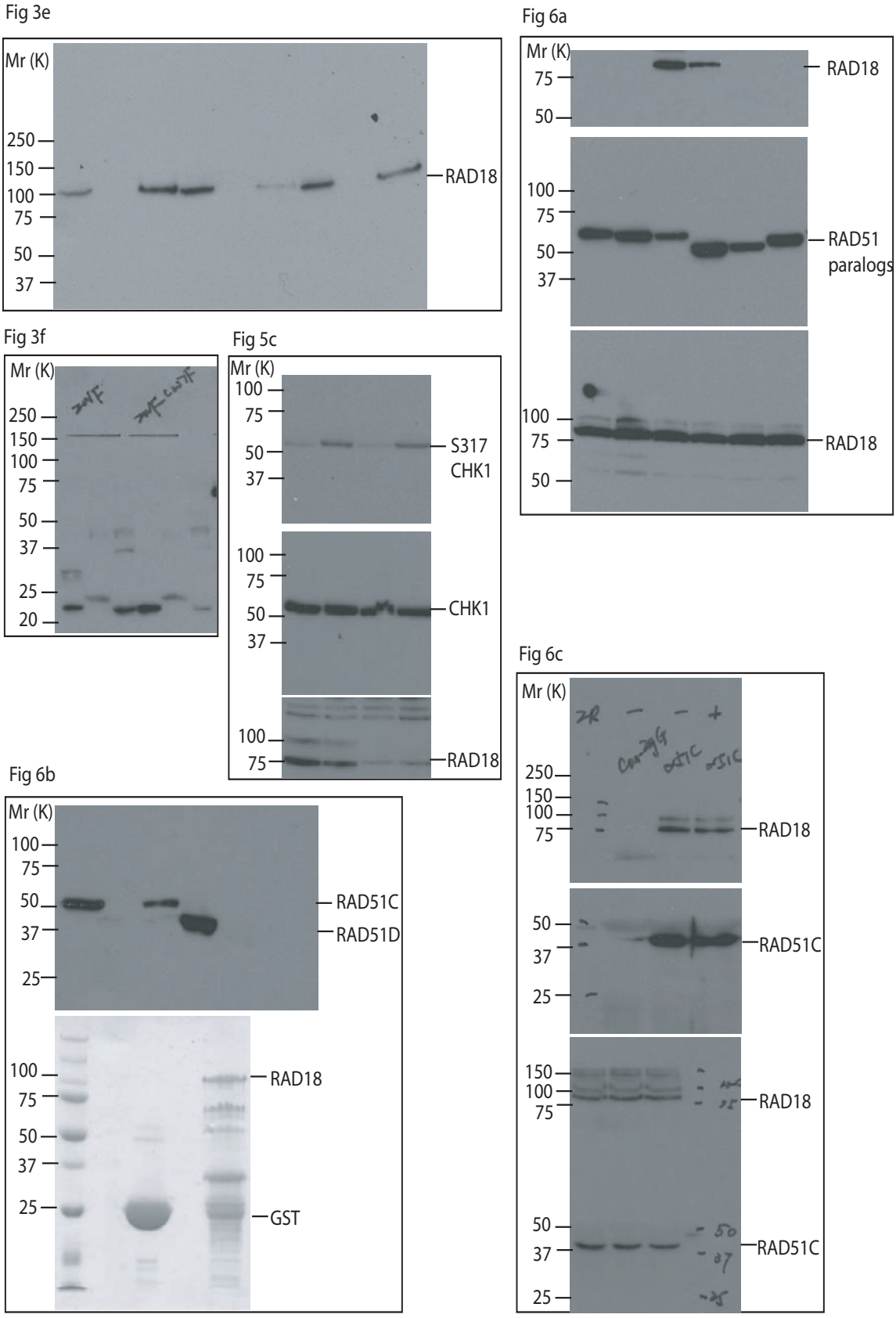

Figure S9 continued

Fig 6e

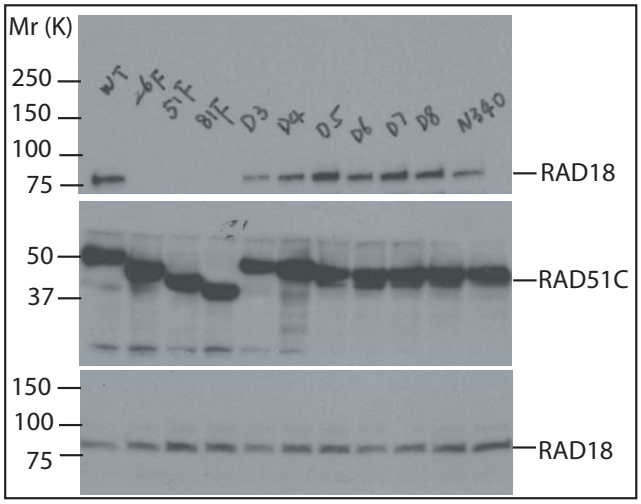

Fig 6g

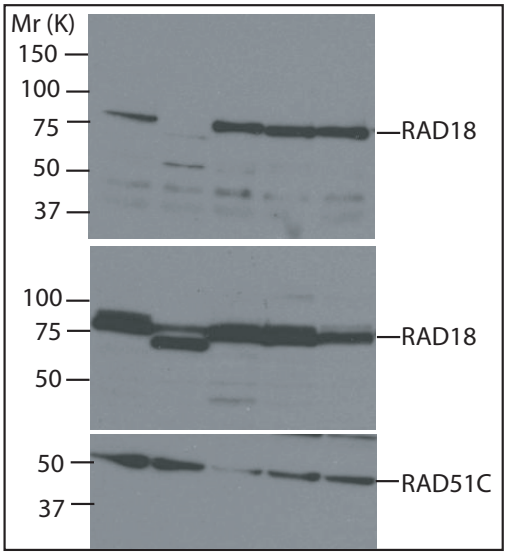

Fig 6h

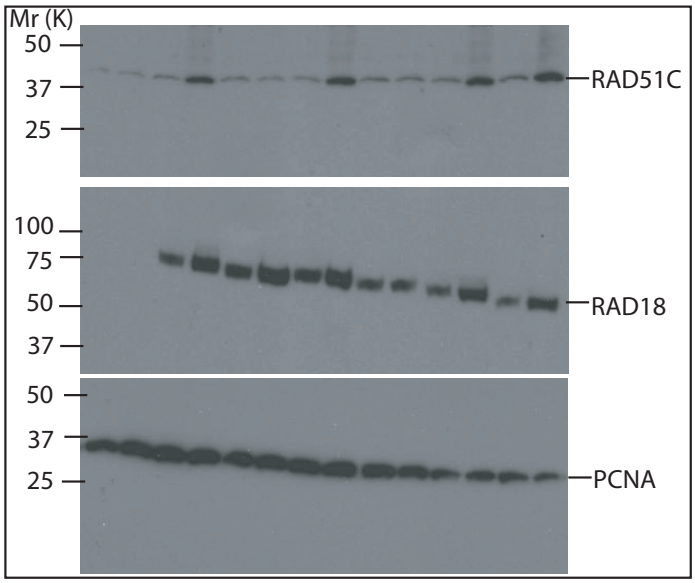

Fig 7e

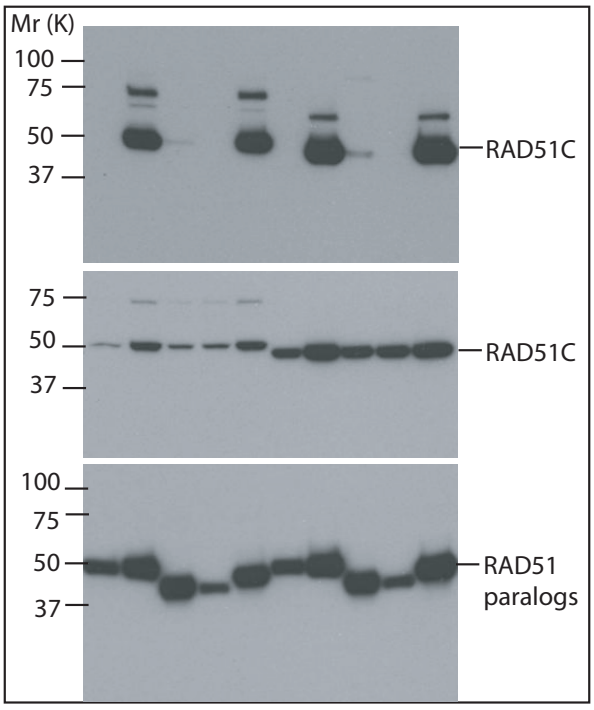

Figure S9 continued

Fig 8a

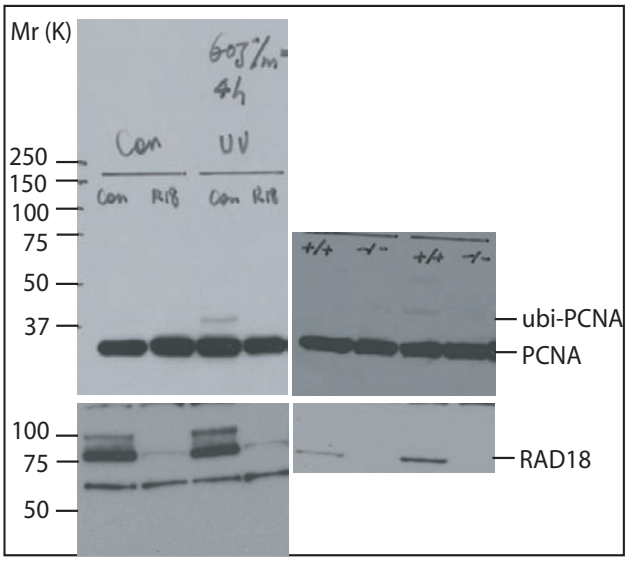

Fig 8b

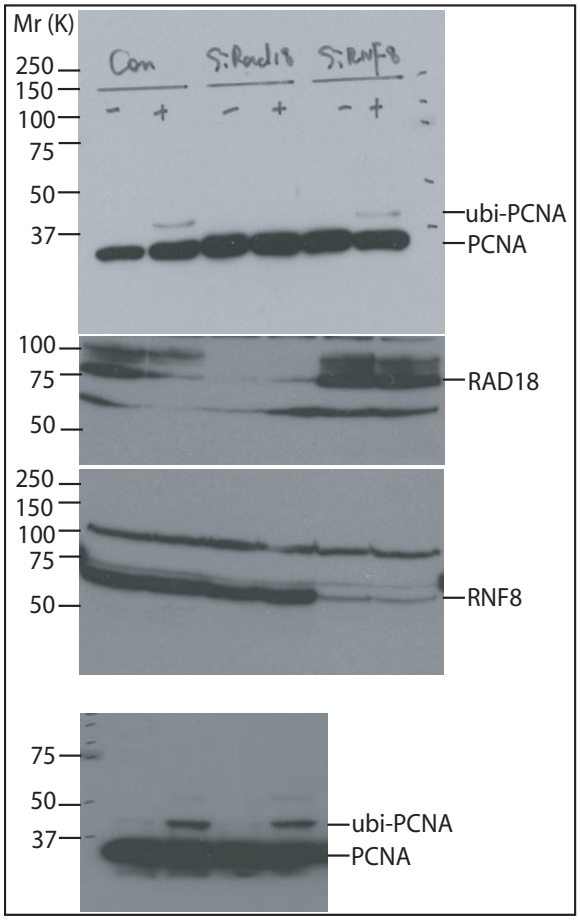

Fig 8c

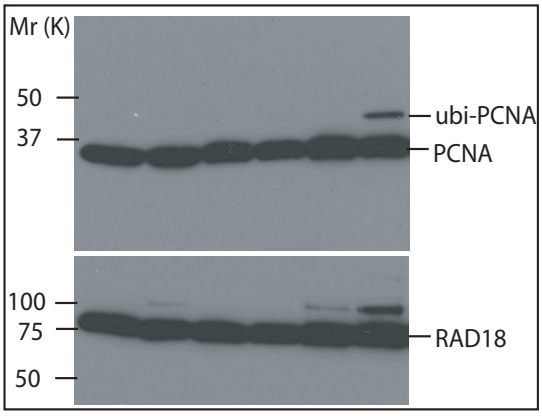

Fig 8d

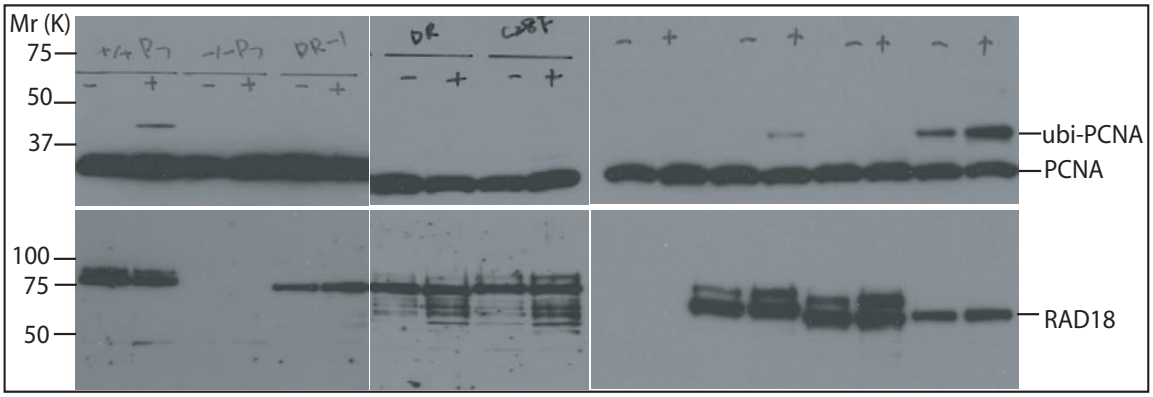

Figure S9 continued

Supporting Online Material for

RAD18 transmits DNA damage signaling to elicit homologous recombination repair

Jun Huang[1], Michael S. Y. Huen[1], Hongtae Kim[1, 2], Charles Chung Yun Leung[3], J N Mark Glover[3], Xiaochun Yu[4] and Junjie Chen[1]*

[1]Department of Therapeutic Radiology, Yale University School of Medicine, P. O. Box 208040, New Haven, Connecticut 06520, USA

[2]Current address: Department of Biological Science, Sungkyunkwan University, 300 Chunchundong, Suwon 440-746, Republic of Korea

[3] Department of Biochemistry, University of Alberta, Edmonton, Alberta, Canada

[4] Current address: Division of Molecular Medicine and Genetics, Department of Internal Medicine, University of Michigan Medical School, 109 Zina Pitcher Place, BSRB 1520, Ann Arbor, Michigan 48109, USA

*To whom correspondence should be addressed.

Tel: 1-203-785-3758 Fax: 1-203-785-7482

E-mail: Junjie.chen@yale.edu

This file contains Supplemental Experimental Procedures, Supplementary Table 1 and Supplementary Figures S1-S9.

Supplemental Experimental Procedures

Antibodies RAD6A polyclonal antibody was obtained form Bethyl.

SiRNA SiRNA Pool targeting RAD6A was purchased from Dharmacon. SiRNA transfection was performed according to the manufacturer's protocol. The sequences of RAD6A SiRNAs are: CUAUGCAGAUGGUAGUAUA, GCGUGUUUCUGCAAU AGUA, GGACAUACUUCAGAACCGU and GAACAAACGGGAAUAUGAA.

Fluorescence Activated Cell Sorting (FACS) For cell cycle analysis, cells were washed with PBS, resuspended in 300 μl of PBS and then fixed with the addition of 700 μl of 100% ethanol. After stored at -20°C overnight, fixed cells were washed and incubated in RNAse A in sodium citrate buffer for 30 minutes, and then stained with propidium idodide (50 μg/ml) for 30 minutes. Flow cytometric analysis was performed using a FACSCalibur flow cytometer. A total of 100,000 events were analyzed for each sample and the experiment was repeated at least twice.

Cell synchronization HeLa cells were treated with 2 mM thymidine for 19 hours and then released in fresh medium for 9 hours. 2 mM Thymidine was added again and cells were allowed to incubate for another 16 hours before releasing into fresh medium. After release, cells were collected at the G1/S border (0 h), S phase (4 h), G2 phase (8 h), and G2/M phase (12 h). For the collection of mitotic cells, cells were treated with 0.5 mg/ml nocodazole for 18 hours. Mitotic arrested cells were collected by the "mitotic shake-off" method. Cell cycle distributions were determined by FACS analysis.

***In vitro* ubiquitin binding** 2 μg of GST-fusion protein or GST alone was immobilized on the glutathione-Sepharose 4B beads and incubated with 1 μg lysine 48-linked polyubiquitin chains (Lys-48) or 1 μg lysine 63-linked polyubiquitin chains (Lys-63) for two hours at 4°C. After washing with NETN buffer, the samples were analyzed by Western blotting analysis.

Surface Plasmon Resonance Binding experiments were carried out on the BIAcore 3000 system. Penta-ubiquitin linked K48 and K63 chains were immobilized using the Amine Coupling Kit (BIAcore). Specifically, two lanes on a CM5 chip were activated using 1:1 N-hydroxysuccinimide (NHS)/1-ethyl-3-(3-dimethylaminopropyl)carbodiimide (EDC) at a flow rate of 5 μl/min for 7 min. Penta-ubiquitin linked K48 chains (1 μM) or K63 chains (1 μM) in 10 mM sodium acetate buffer (pH 4) were then immobilized at a flow rate of 5 μl/min, followed by blocking with 1 M ethanolamine (pH 8.5) for 7 min at a flow rate of 5 μl/min. A total of 70 response units of penta-ubiquitin linked K63 and 400 response units of penta-ubiquitin linked K48 chains were immobilized. A control lane was made by activation and blocking, but without any immobilization of protein. Binding of GST and GST-RAD18 ZNF to either penta-ubiquitin linked K48 or K63 chains were carried out at 4°C at 30 μL/min in 10 mM HEPES (pH 7.4), 150 mM NaCl, 0.05% NP-40 and 1 mM DTT. The amount of specific analyte protein bound was monitored by subtracting the response units from the control lane from the penta-ubiquitin immobilized lane. All sensorgram data was averaged from duplicate runs. Assuming a 1:1 stiochiometry for GST-RAD18 ZNF interactions with either K48 and

K63-linked chains, equilibrium dissociation constants (KD) were fit from the titration data using the equation,

$$R_{eq} = \frac{R_{\max}[RAD18]}{K_D + [RAD18]}$$

where [RAD18] is the concentration of GST-RAD18 ZNF analyte, Req is the peak response level observed at [RAD18], and Rmax is the maximum SPR response level. Fitting of KD and Rmax against the experimental data was performed with SigmaPlot software.

Supplementary Table 1:

Complete list of RAD18 associated proteins identified by Mass spectrometric analysis:

Protein	No. of Peptides
Rad18	**57**
Hsp7C	35
Hsp71	26
Hsp70L	23
GRP78	18
COA1	12
Hsp72	8
GRP75	8
UBE2A/RAD6A	**6**
Ubiquitin	**6**
Myosin-9	6
TBA2	4
Hsp76	4
40s ribosomal protein s17	4
Ribosomal protein s3	3
Rps3	3
40s ribosomal protein s2	3
Acetyl-coenzyme a carboxylase alpha isoform 2 variant	3
Heat shock 70 kda protein 4	2
Serum albumin precursor	2
Signal recognition particle 14 kda protein	2
3-methylcrotonyl-coa carboxylase 2	2
Rps16 protein	2
Ribosomal protein l11	2
Ankyrin repeat domain-containing protein 32	2
Ribosomal protein l11	2
RAD51C	**1**
PCNA	**1**
Ribosomal protein s5 variant	1
Rig homolog	1
Tubulin alpha-6 chain	1
Proteasome activator 28-gamma subunit	1
ODB2	1
40s ribosomal protein s23	1
Signal recognition particle 9 kda protein	1
Tubulin beta-6 chain	1
Tubulin alpha-6 chain	1
Kiaa1529 protein	1
Myosin regulatory light chain 2	1

THE JOURNAL OF BIOLOGICAL CHEMISTRY VOL. 284, NO. 27, pp. 18302–18310, July 3, 2009

PALB2 Regulates Recombinational Repair through Chromatin Association and Oligomerization*

Received for publication, March 23, 2009, and in revised form, May 4, 2009 Published, JBC Papers in Press, May 7, 2009, DOI 10.1074/jbc.M109.016717

Shirley M.-H. Sy[1], **Michael S. Y. Huen**[2], **Yongyou Zhu, and Junjie Chen**[3]

From the Department of Therapeutic Radiology, Yale University School of Medicine, New Haven, Connecticut 06520

Maintenance of genomic stability ensures faithful transmission of genetic information and helps suppress neoplastic transformation and tumorigenesis. Although recent progress has advanced our understanding of DNA damage checkpoint regulations, little is known as to how DNA repair, especially the RAD51-dependent homologous recombination repair pathway, is executed *in vivo*. Here, we reveal novel properties of the BRCA2-associated protein PALB2 in the assembly of the recombinational DNA repair machinery at DNA damage sites. Although the chromatin association of PALB2 is a prerequisite for subsequent BRCA2 and RAD51 loading, the focal accumulation of the PALB2·BRCA2·RAD51 complex at DSBs occurs independently of known DNA damage checkpoint and repair proteins. We provide evidence to support that PALB2 exists as homo-oligomers and that PALB2 oligomerization is essential for its focal accumulation at DNA breaks *in vivo*. We propose that both PALB2 chromatin association and its oligomerization serve to secure the BRCA2·RAD51 repair machinery at the sites of DNA damage. These attributes of PALB2 are likely instrumental for proficient homologous recombination DNA repair in the cell.

Fanconi anemia is a rare disease in which patients are prone to the development of childhood aplastic anemia and cancer as well as other congenital defects. Cellular phenotypes of FA[4] patients are also characterized by their hypersensitivity toward DNA-cross-linking agents, such as mitomycin C (MMC) or cisplatin. Accordingly, MMC treatment greatly induces aberrant chromosomal structures in cells derived from FA patients, including chromosome breakage and chromatin interchanges. Thus, genomic instability is considered as one of the fundamental causes responsible for the clinical and cellular phenotypes observed among FA patients.

In human cells two major repair pathways are employed to repair DSBs, namely the homologous recombination (HR) and the non-homologous end-joining pathways. The use of the sister chromatid as information donor during repair renders HR a largely faithful mechanism (1), whereas non-homologous end-joining often leads to genetic mutations because of the gain or loss of genetic information (2).

Mounting evidence suggests a functional connection between the 13 FA-complementation group genes (FA-A, B/FAAP95, C, D1/BRCA2, D2, E, F, G/XRCC9, I, J/BACH1, L/PHF9/FAAP43, M/Hef/FAAP250, and N/PALB2) and the DNA repair pathway (3). Recent studies revealed that eight of the FA proteins form a complex to facilitate the ubiquitylation of FANCD2 and FANCI; however, mechanistically how they affect DNA repair remains elusive. Importantly, the identification of the FANCJ/BACH1, FANCD1/BRCA2, and FANCN/PALB2 proteins as components of the HR machinery further support the notion that FA mutations result in DNA repair defects (3–7).

Genetics and biochemical studies have shown that the FANCD1 product, BRCA2, facilitates the assembly of RAD51 onto ssDNA substrates, forming a nucleoprotein filament (8–10) that catalyzes DNA strand invasion and D-loop formation. Accordingly, abrogation of FANCD1/BRCA2 function abolishes focal accumulation of RAD51 at DNA breaks. The recent identification of FANCN/PALB2 as the Partner and Localizer of BRCA2 (11) indicated that, much like the damage-signaling pathway, a hierarchical relationship exist for the HR pathway. PALB2 is essential for the focal accumulation of BRCA2 and RAD51 at DSBs. Moreover, PALB2 depletion compromised HR repair and cell survival in response to genotoxic stress (11). Similarly, HR defects and hypersensitivity to cross-linking agents are restored in FANCN/PALB2 patient cells by reconstitution or spontaneous reversion of PALB2, indicating that PALB2 dysfunction is responsible for this FA subtype (12). Moreover, inactivation of PALB2 has also been implicated in breast cancer predisposition, as truncation mutations of *PALB2* are found in familial breast cancer cases with intact *BRCA1* and *BRCA2* (13–15). *PALB2* mutations are also associated with an elevated frequency of prostate and colorectal cancers, although the role of PALB2 in the suppression of these cancer types requires further exploration (14, 16). Nevertheless, these human genetic studies provide strong evidence to support that PALB2 plays a critical role in HR repair and is important for the maintenance of genomic integrity and tumor suppression.

Given the intimate relationship between PALB2 and HR repair, we decided to examine mechanistically how PALB2 regulates the BRCA2-RAD51-dependent DNA repair events. Interestingly, we found an oligomerization domain on

* This work was supported, in whole or in part, by National Institutes of Health Grant CA089239 (to J. C.).

[1] Recipient of a postdoctoral fellowship from the Croucher Foundation.

[2] Supported by the Anna Fuller Postdoctoral Fellowship.

[3] Recipient of an Era of Hope Scholar award from the Dept. of Defense and a member of the Mayo Clinic Breast SPORE program and to whom correspondence should be addressed: Hunter Bldg. Rm. 213C, Dept. of Therapeutic Radiology, Yale University School of Medicine, 333 Cedar St., P. O. Box 208040, New Haven, CT 06520-8040. Tel.: 203-785-3758; Fax: 203-785-7482; E-mail: Junjie.Chen@yale.edu.

[4] The abbreviations used are: FA, Fanconi anemia; ssDNA, single strand DNA; DSBs, double strand breaks; HR, homologous recombination; IRIF, ionizing radiation-induced focus formation; MMC, Mitomycin C; SFB, S-tag, FLAG epitope, and streptavidin-binding peptide-tag; siRNA, small interfering RNA; Gy, gray; GST, glutathione *S*-transferase; CHO, Chinese hamster ovary; DBD, DNA binding domain; RPA, replication protein A; ATR, atoxia telangiectaia mutated and Rad3-related; ATRIP, ATR-interacting protein.

PALB2 and provide evidence to support that PALB2 focal accumulation at the site of DNA damage requires its oligomerization property. Together with its chromatin associating ability, PALB2 initiates recombinational repair at DSBs via the coordination of BRCA2 and RAD51 association with chromatin and the concentration of the repair complex at sites of DNA breaks.

EXPERIMENTAL PROCEDURES

Antibodies—Monoclonal antibodies against the FLAG epitope (M2) were purchased from Sigma. Rabbit polyclonal anti-RAD51 (D51), anti-BRCA2 (C25), and anti-phopsho-H2AX antibodies were described previously (17). Rabbit polyclonal anti-PALB2 antibodies were generated by immunizing rabbits with GST-PALB2 F6 (residues 611–764) recombinant protein expressed and purified from *Escherichia coli*. Goat anti-ATR antibody (C-17) and mouse anti-CHK1 were purchased from Santa Cruz, and rabbit anti-p-CHK1 S317 antibody was purchased from Upstate. Both β-actin and β-tubulin antibodies were purchased from Sigma.

Cell Cultures—Cell lines of human origin were maintained in RPMI supplemented with 10% fetal bovine serum and 1% penicillin and streptomycin. Mouse embryonic fibroblasts deficient of ATM, 53BP1, H2AX, MDC1, and RNF8 were maintained in Dulbecco's modified Eagle's medium supplemented with 15% fetal bovine serum and 1% penicillin and streptomycin (18–21). Cell lines were maintained in 37 °C incubator with 5% CO_2.

Constructs—pOZC-PALB2 (a gift from Dr. David Livingston (Dana-Farber Cancer Institute)) was subcloned into the entry vector pDONR201 (Invitrogen). Mutations or deletions of PALB2 were generated using site-directed mutagenesis (QuikChange, Stratagene). All plasmid transfection into mammalian cells were performed using Lipofectamine 2000.

Retrovirus Production and Infection—pDONR201-PALB2 constructs were transferred into a gateway-compatible pEF1A-HA-FLAG retroviral vector. Virus supernatant was collected 48 h after the co-transfection of pEF1A vectors and pcl-ampho into BOSC23 cells. EUFA1341 cells were infected with viral supernatant in the presence of Polybrene. Cells were selected in growth media containing 2 μg/ml puromycin. Protein expression in transduced cells was confirmed by Western blot and immunofluoresence staining using anti-FLAG antibodies.

RNA Interference—SmartPool siRNA targeting human ATR and CHK1 were purchased from Dharmacon. A non-targeting siRNA was used as the control. U2OS cells were seeded at 30% confluency for 24 h before double siRNA transfection using Oligofectamine (Invitrogen). Forty-eight hours after the second siRNA transfection, cells were subjected to ionizing radiation (10 Gy) and collected for further analysis.

Chromatin Fractionation, Immunoprecipitation, and Pulldown Experiments—Cells were lysed in NETN (20 mM Tris-HCl, pH 8, 100 mM NaCl, 1 mM EDTA, 0.5% Nonidet P-40) buffer. After centrifugation, the pellets were washed extensively with NETN and boiled in 2× Laemmli buffer to extract chromatin-associated proteins.

For immunoprecipitation or pulldown experiments, cell extracts prepared using NETN buffer were incubated with either S-agarose (EMD Biosciences) or GST fusion proteins immobilized on glutathione beads for 2 h at 4 °C. Beads were washed with NETN buffer, and proteins were eluted by boiling in 2× Laemmli buffer. Samples were resolved by SDS-PAGE and transferred to polyvinylidene difluoride membrane. Immunoblotting was subsequently performed with the antibodies as indicated.

Immunofluoresence Staining—Cells grown on coverslips were mock-treated or treated with 10 Gy of γ-irradiation. Cells were then pre-extracted with buffer containing 0.5% Triton X and fixed using 3% paraformaldehyde solution. Immunostaining experiments were performed using anti-FLAG (M2), anti-γH2AX, BRCA2, RAD51, and PALB2 antibodies. Cells were mounted onto glass slides in 4′,6-diamidino-2-phenylindole-containing antifade. Immunofluorescent analyses and image capturing were performed on a Nikon Eclipse 800 microscope.

MMC Sensitivity Assay—1×10^3 cells were seeded onto a 60-mm dish in triplicate. Different concentrations of MMC were added 24 h after cell seeding. Cells were incubated for 14 days, and the resulting colonies were fixed and stained with Coomassie Blue. Number of colonies was counted using a Gel-Doc with Quantity One software (Bio-Rad). Results were the averages of data obtained from three independent experiments.

Gene Conversion Assay—1×10^6 cells were electroporated with 15 μg of pDR-GFP plasmid together with 5 μg of pCBASce plasmid at 270 V, 975 microfarads using a Bio-Rad Gene Pulsar II. Cells were plated onto 60-mm dishes and incubated in culture media for 48 h before fluorescence-activated cell sorter analyses. Cells were analyzed in a BD Biosciences FACScan on a green (FL1) *versus* orange (FL2) fluorescence plot. Results were the averages of data obtained from three independent experiments.

RESULTS

Role of PALB2 in HR Repair Complex Assembly—PALB2 was previously ascribed a role as a scaffold protein and is essential for BRCA2 relocalization in response to DNA damage (11). Given that BRCA2 is required for RAD51 accumulation at DNA breaks, we asked whether the three proteins might function in a linear and hierarchical pathway. Discernible foci that colocalized with those of γH2AX were observed for PALB2, BRCA2, and RAD51 in U2OS and MCF7 cells after ionizing radiation treatment (IR) (Fig. 1, *A* and *B*). In contrast, both BRCA2 and RAD51 foci were absent in the PALB2-deficient fibroblast EUFA1341, indicating that PALB2 function is required for the focal accumulation of both repair proteins at DSBs. To further test whether PALB2 is indeed responsible for the DSB recruitment of BRCA2 and RAD51, we reconstituted EUFA1341 cells with PALB2 (EUFA1341+PALB2) and examined BRCA2 and RAD51 IR-induced foci formation (IRIF). Results indicated that BRCA2 and RAD51 IRIF was restored and can be readily observed in EUFA1341+PALB2 cells. On the other hand, the retention of PALB2 at DNA breaks was unaffected by the BRCA2 status, as PALB2 foci persisted in both BRCA2-deficient VC8 Chinese hamster ovary (CHO) cells and a derivative that has been reconstituted with wild-type BRCA2 (Fig. 1*A*). This is in contrast to

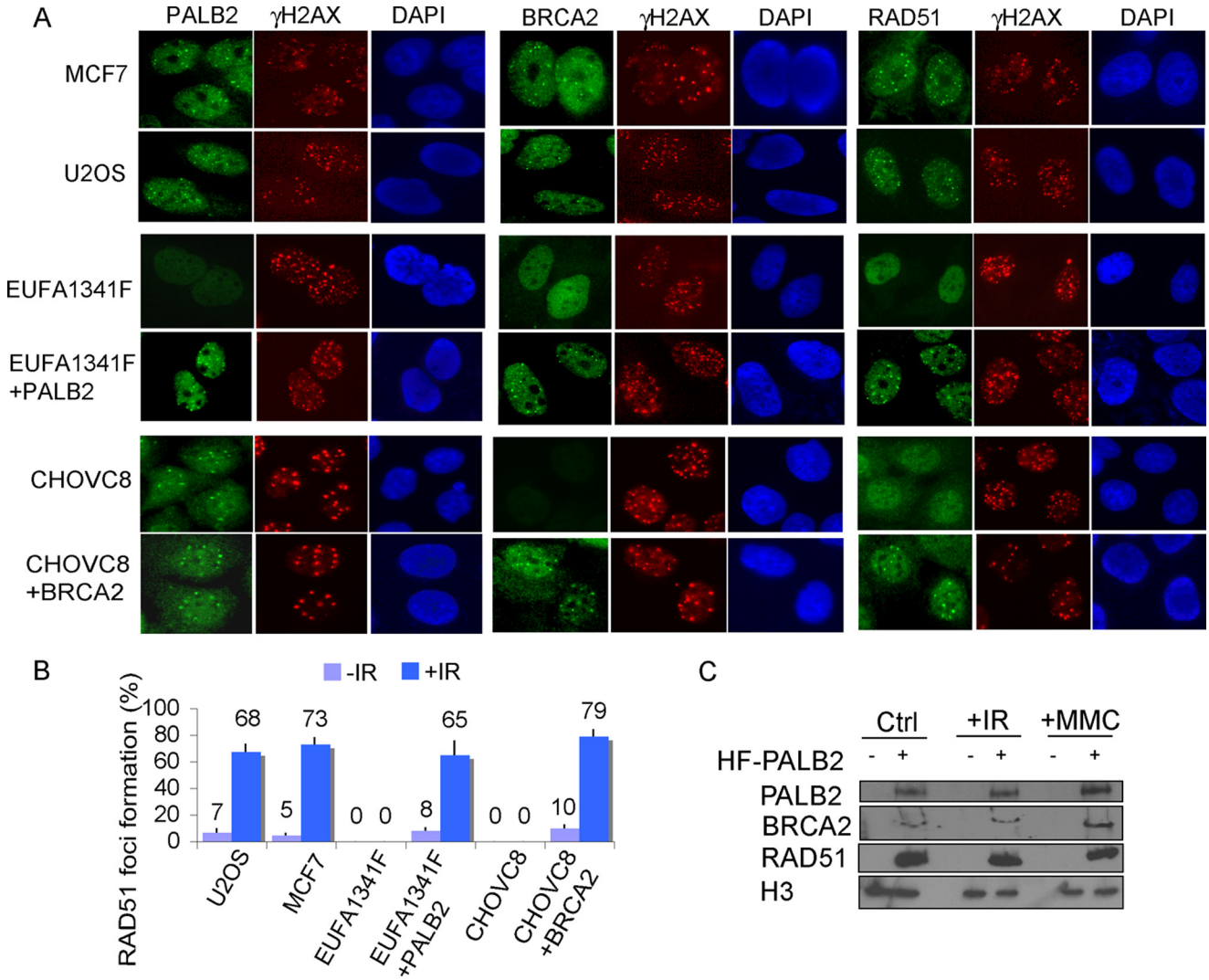

FIGURE 1. **PALB2 controls focal accumulation of BRCA2 and RAD51 at DNA damage site.** *A*, cells were irradiated with 10 Gy of ionizing radiation and recovered for 5 h. Immunofluorescence staining was performed using antibodies as indicated. *C*, PALB2-deficient EUFA1341 cells and its derivative (*EUFA1341+PALB2*) were treated with 10 Gy of ionizing radiation and recovered for 5 h or 1 mM MMC for 24 h. Cell lysates were separated by fractionation to retrieve both nuclear and chromatin-associated proteins. The presence of PALB2, BRCA2, and RAD51 was examined by Western blot analyses as indicated. *B*, RAD51 foci formation was examined in indicated cell lines using anti-RAD51 antibody. *DAPI*, 4′,6-diamidino-2-phenylindole.

RAD51, whose foci were observed only in CHO VC8 cells reconstituted with BRCA2 (Fig. 1*B*). These data suggest that PALB2 facilitates the accumulation of RAD51 at DNA lesions by targeting BRCA2 to chromatin.

The above cytological observations suggest a linear relationship between PALB2, BRCA2, and RAD51 in response to DNA damage. To biochemically test if the PALB2 is responsible for the recruitment of BRCA2·RAD51 complex to chromatin, EUFA1341 or EUFA1341+PALB2 were treated with either IR or DNA cross-linking agent MMC. Chromatin fractionation indicated that only in the presence of PALB2, a significant portion of BRCA2 and RAD51 associated with chromatin after DNA damage (Fig. 1*C*). Together, these results indicate that PALB2 is crucial for the recruitment of BRCA2 and RAD51 to chromatin and is important for their focal accumulation at sites of DNA breaks.

Recruitment of the PALB2·BRCA2·RAD51 Repair Complex to DSBs Can Occur Independently of Several Known DNA Damage Repair or Checkpoint Pathways—In an attempt to identify possible upstream signaling molecules that facilitate the accumulation of the PALB2·BRCA2·RAD51 complex at DNA damage sites, we examined its DNA damage-induced focus formation in cells deficient for various components in DNA damage repair or checkpoint pathways (Fig. 2). Because of the limited sensitivity of our PALB2 and BRCA2 antibodies, RAD51 focus formation was exploited as a marker to assess the focal accumulation of the PALB2·BRCA2·RAD51 complex in response to DNA damage.

We first investigated cell lines deficient for various DNA repair components. These included the FANCA-deficient (PD220), FANCG-deficient (PD352), and FANCD2-deficient (PD733) cells. As shown in Fig. 2*A*, RAD51 IRIF was not drastically changed by deficiencies in these FA genes. Examination of FANCD2 deficient (PD20) and its derivative cell line that has been reconstituted with FANCD2 (PD20+FANCD2) further confirmed that RAD51 IRIF could form in FANCD2-deficient

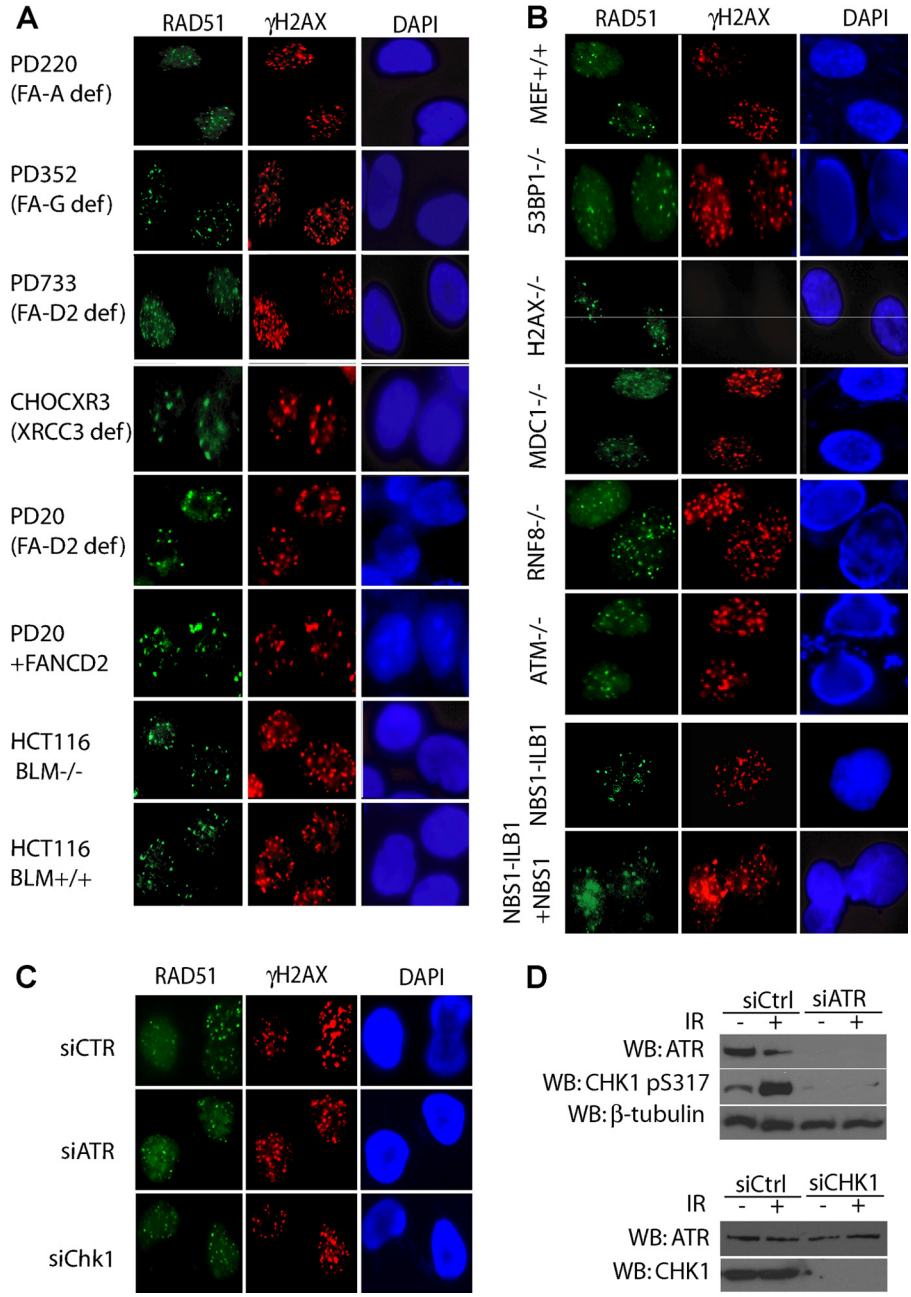

FIGURE 2. **RAD51 focus formation is not dependent on major DNA repair and DNA damage checkpoint pathway components.** Cells deficient in various components in DNA repair (*A*) or DNA damage signaling and checkpoint pathways (*B* and *C*) were examined for the formation of ionizing radiation induced RAD51 foci. Cells were all collected 5 h after radiation (10 Gy), and immunostaining experiments were performed with anti-RAD51 and anti-γH2AX antibodies. *D*, expression levels of ATR and CHK1 after siRNA knockdown were monitored by Western blot (*WB*) analyses. *DAPI*, 4′,6-diamidino-2-phenylindole. *siCTR*, control siRNA.

cells (Fig. 2*A*). Likewise, cells deficient in the BLM helicase (HCT116 BLM$^{-/-}$) also did not reveal any exceedingly large change in RAD51 focal accumulation as compared with its normal counterpart (Fig. 2*A*).

Next we tested whether the localization of PALB2·BRCA2·RAD51 complex might be regulated by any of the known DNA damage checkpoint pathway components (Fig. 2*B*). In a series of mouse embryonic fibroblasts generated from different knock-out mice, we observed that RAD51 was able to localize to γH2AX-containing foci in ATM$^{-/-}$, 53BP1$^{-/-}$, H2AX$^{-/-}$, MDC1$^{-/-}$, and $^{-/-}$ mouse embryonic fibroblasts and their respective wild-type counterparts after ionizing radiation. RAD51 foci formation was also detected in cells deficient for NBS1 (Fig. 2*B*). Similarly, RAD51 IRIF was observed after depletion of ATR or CHK1 in U2OS cells (Fig. 2, *C* and *D*).

We noted that there were changes in the percentages of cells displaying RAD51 foci in some of the deficient cells examined (data not shown); however, none of these deficiencies led to complete loss of RAD51 foci as observed in PALB2- and BRCA2-deficient cells. Although it is likely that RAD51 focus formation may be altered in some of these cell lines and, therefore, suggest that some of these DNA damage repair or checkpoint proteins may regulate RAD51 focal formation, our results indicated that none of them is essential for the formation of RAD51 foci after DNA damage.

PALB2 Focal Accumulation to DSBs Requires Its Oligomerization—To elucidate how PALB2 is recruited to damaged chromatin, HEK293T was transiently transfected with plasmids encoding wild type and a series of overlapping S-tag, FLAG epitope, and streptavidin-binding peptide tripe-tagged (dubbed as SFB-tag)-PALB2 deletion mutants spanning the entire coding sequence of PALB2 (Fig. 3*A*). Cells were exposed to IR, and indirect immunofluorescence staining was used to visualize PALB2 localization. Like endogenous PALB2, SFB-tagged PALB2 became concentrated at foci that colocalized with γH2AX (Fig. 3, *A* and *B*). Interestingly, such co-localization with γH2AX was observed only in PALB2 deletion mutants that retained the N terminus (F12, F13, and F14), indicating that the PALB2 N terminus mediates PALB2 accumulation at DNA lesions. Further deletions of flanking residues from either side of the F12 fragment affected PALB2 foci formation. Note that F12-2 demonstrated a reduction in the percentage of cells with damage-induced foci, indicating a possible foci formation domain within residues 1–160 of PALB2 (Fig. 3*A*). A domain search identified a coiled-coil domain runs from residues 9 to 42 of PALB2. Notably, deletion of the coiled-coil domain (ΔN42) resulted in severely diminished IRIF resembling the phenotype of mutant F12-2, indicating that the PALB2 N ter-

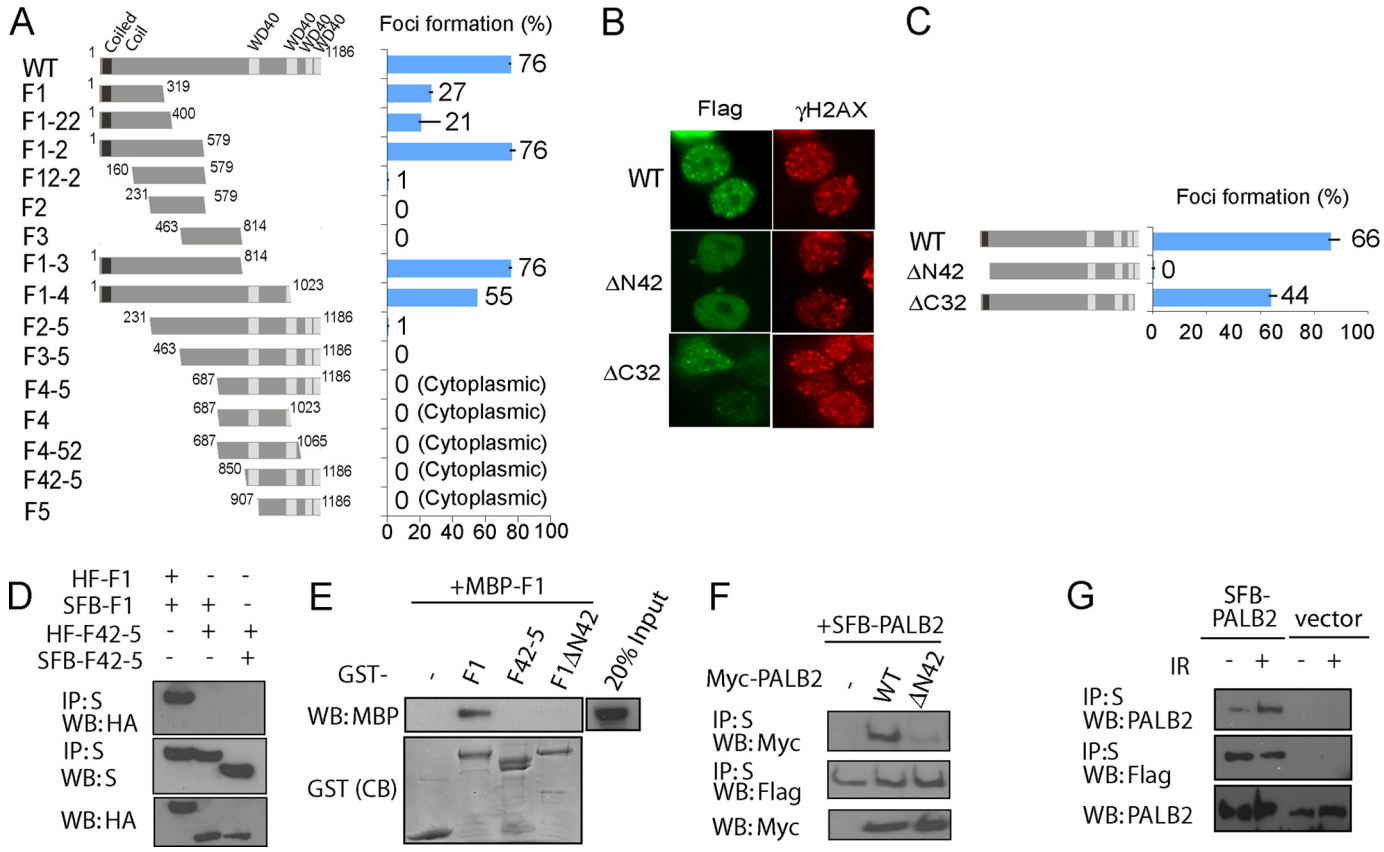

FIGURE 3. **PALB2 focus formation at DSBs requires its N terminus.** *A*, HEK293T cells transfected with plasmids encoding SFB-tagged wild type (*WT*) or deletion mutants of PALB2 were exposed to 10 Gy of ionizing radiation. Cells were fixed, and immunostaining was performed with anti-FLAG and anti-pH2AX antibodies. The percentage of cells showing foci overlapping with γH2AX was plotted. *B*, foci accumulation of wild type and PALB2 internal deletion mutants. The percentage of foci positive cells was plotted in *C*. *D*, co-immunoprecipitation (*IP*) experiments using hemagglutinin (*HA*)-FLAG-tagged and SFB-tagged PALB2 F1 and F42–5 fragments were performed (5% input was showed). *WB*, Western blot. *E*, recombinant GST and MBP-tagged PALB2 fragments were subjected to pulldown assays. *CB*, Coomassie Blue staining. *F*, Myc-tagged wild-type and ΔN42 PALB2 mutant were subjected to co-immunoprecipitation experiments along with wild-type SFB-tagged PALB2 (5% input was showed). *G*, 293T cells stably expressing SFB-PALB2 or vector alone were mock-treated or irradiated. Cell lysates were subjected to S beads pulldown (5% input was showed). The amounts of SFB-tagged and endogenous PALB2 presented in the precipitates were determined by Western blotting analyses using anti-FLAG or anti-PALB2 antibodies.

minus plays an important role in mediating its retention at DNA damage sites (Fig. 3, *B* and *C*).

Because coiled-coil domain is often involved in protein oligomerization, we tested whether PALB2 has intrinsic oligomerization property. The SFB-PALB2 N terminus specifically immunoprecipitated HA-PALB2 F1 fragment but not the C-terminal F42–5 fragment (Fig. 3*D*). In addition, the C-terminal F42–5 fragments did not form oligomers (Fig. 3*D*). These data suggest that PALB2 oligomerizes via its N terminus. Next we tested if the deletion of the coiled-coil domain could abolish the PALB2 oligomerization. Bacterially expressed and purified GST- or MBP-tagged PALB2 fragments were used in pulldown experiments. Although the GST-PALB2 F1 fragment successfully pulled down MBP-PALB2 F1 *in vitro*, deletion of the coiled-coil domain (F1ΔN42) abolished this interaction (Fig. 3*E*). Accordingly, the Myc-ΔN42 deletion mutant also failed to interact with wild-type SFB-PALB2, whereas oligomerization occurred between SFB- and Myc-tagged wild-type PALB2 *in vivo* (Fig. 3*F*). Interestingly, we observed an enhanced oligomerization between SFB-PALB2 and endogenous PALB2 after DNA damage (Fig. 3*G*), implying that the oligomerization status of PALB2 may be modulated and, thus, account for its focal localization after DNA damage. Taken together, our data suggest that PALB2 N terminus, which harbors a coiled-coil domain required for its oligomerization, is important for its focal concentration at DNA damage sites.

PALB2 C Terminus WD40 Repeats Mediate Its Interaction with BRCA2—Results from a previous report (Xia *et al.* (11)) indicated that the interaction between PALB2 and BRCA2 is critical for HR. The PALB2 binding domain has been mapped to the very N terminus of BRCA2 (residues 10–40) (11). To further understand how PALB2 facilitates the BRCA2-dependent HR function *in vivo*, we sought to identify the region on PALB2 responsible for its interaction with BRCA2. A series of SFB-tagged PALB2 deletion mutants were tested for their ability to interact with Myc-BRCA2 N terminus that harbors the PALB2 binding domain (Ref. 11; B2N, residues 1–305 of BRCA2). Results indicated that the PALB2-BRCA2 interaction required a region of PALB2 which encompasses four WD40 domains (*i.e.* residues 850–1186, Fig. 4, *A* and *B*). The same results were obtained in pulldown experiments (Fig. 4*C*) when bacterially expressed GST-B2N and control GST fusion protein encoding the BRCA2 C terminus (B2C, residue 3120–3418) were used. These data indicate that PALB2 C-terminal WD40 domains are required for BRCA2 interaction.

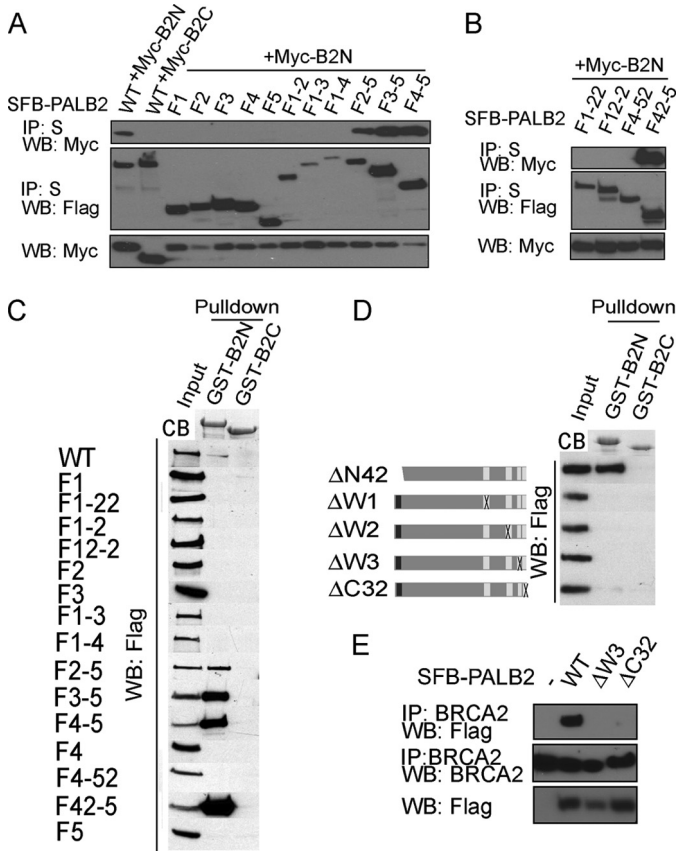

FIGURE 4. **PALB2 interacts with BRCA2 via its C-terminal WD40 repeats.** *A* and *B*, SFB-tagged wild type and deletion mutants of PALB2 were expressed in HEK293T and subjected to co-immunoprecipitation (*IP*) with Myc-B2N or Myc-B2C. *C*, pulldown assays using GST-B2N or control GST-B2C purified from *E. coli*. Western blotting (*WB*) using anti-FLAG antibody was performed to verify the interaction between wild type or mutants of PALB2 with BRCA2. *D*, internal deletion mutants lacking each of the four WD40 domains at the C terminus of PALB2 and the N-terminal mutant of PALB2 with deletion of the coiled-coil domain were subjected to pulldown assays similar to that described in *C*. *E*, extracts prepared from 293T cells expressing SFB-tagged wild-type, ΔW3, or ΔC32 mutants of PALB2 were subjected to immunoprecipitation using anti-BRCA2 antibody. Western blotting experiments were conducted with anti-BRCA2 or anti-FLAG antibodies. *B2N*, BRCA2 N terminus; *B2C*, BRCA2 C terminus; *CB*, Coomassie Blue stain.

To ask whether all four of the WD40 domains are needed for the observed PALB2/BRCA2 interaction, deletion mutants lacking each of the WD40 domains (ΔW1, ΔW2, ΔW3, and ΔC32-deleted C-terminal 32 residues containing the 4th WD40 domain) or ΔN42 were examined. Results showed that the interaction between PALB2 and BRCA2 was abolished by deletion in any of the four PALB2 WD40 domains, whereas the deletion of the N-terminal coil-coiled domain had no effect on the protein complex formation (Fig. 4, *D* and *E*). Our results suggest that the physical interaction between PALB2 and BRCA2 requires the PALB2 C terminus and that all four WD40 domains therein are indispensable in this regard.

The HR Function of PALB2 Requires Its Oligomerization Domain and Its BRCA2-interacting Motif—Cells deficient in PALB2 exhibit hypersensitivity to DNA cross-linking agents and display HR defects. To explore the physiological relevance of the PALB2 domains that mediate DNA damage-induced focus formation and BRCA2 complex formation, we first set out to determine whether mutants that lack the above domains, namely ΔC32 and ΔN42, can restore the DNA damage hypersensitivity phenotype of PALB2-deficient cells. EUFA1341 cells transduced with wild-type PALB2, the ΔC32 or the ΔN42 mutant (Fig. 5*A*), or vector alone were treated with different doses of the DNA cross-linking agent MMC (Fig. 5*B*). A clonogenic assay indicated that only cells reconstituted with wild-type PALB2, but not those with the ΔC32 or ΔN42 mutant, restored MMC resistance (Fig. 5*B*), suggesting that PALB2 function requires both oligomerization and BRCA2 interacting domains.

We also performed a gene conversion assay to examine HR efficiency in these cell lines. In accordance with results from MMC sensitivity (Fig. 5*B*), re-introduction of wild-type PALB2 restored HR, whereas the ΔC32 or ΔN42 variants are defective in this regard (Fig. 5, *C* and *D*). From these results, we concluded that PALB2 function in HR is contingent upon its oligomerization property and its association with BRCA2.

DISCUSSION

PALB2 was previously implicated in the recruitment of BRCA2 to DNA breaks (11). Dysregulation of PALB2 function resulted in the failure of DNA damage-induced BRCA2 relocalization to DSBs and impaired HR repair (11). However, mechanistically how PALB2 is recruited to DNA breaks and how it mediates recombinational repair remain largely unexplored. In this study we have examined how PALB2 orchestrates DNA repair in response to DNA damage. PALB2 localizes to chromatin and assembled as oligomers at the site of DNA damage, which then serves as an anchor for the loading of BRCA2 and RAD51 to allow the activation of the error-free HR repair. Accordingly, disruption of either the PALB2 oligomerization domain or the BRCA2 binding motif resulted in defective HR and increased cellular sensitivity to DNA-damaging agents.

Previous studies have shown that PALB2 affects the stability and association of BRCA2 with certain nuclear structure in the cell and is essential for BRCA2 focal accumulation upon DNA damage (11). Here we provide evidence to support that PALB2 not only stabilizes the association of BRCA2 at the chromatin but is also a prerequisite for BRCA2 binding to chromatin structure (Fig. 1*C*). Indeed, we found that PALB2 associate with chromatin constitutively irrespective of treatments with DNA damaging reagent, as does BRCA2 and RAD51 (Fig. 1*C*).

Our observation underscores a possible intrinsic DNA binding activity of PALB2 in HR functioning. Notably, identification of DNA binding activity among the PALB2·BRCA2·RAD51 complex is not unprecedented, as RAD51 was previously shown to display single and double strand DNA binding activities (22). Likewise, a ssDNA binding domain (DBD) on BRCA2 has also been identified (23). It has been proposed that the BRCA2 DBD helps mediate the assembly of the RAD51-ssDNA nucleoprotein filament via the displacement of the single-strand DNA-binding protein RPA from the HR substrate (24). However, a recent report has provided evidence that the BRCA2 DBD might be dispensable for HR repair. Specifically, BRCA2 mutants lacking the DBD were shown to restore HR repair capacity and resistance to a PARP1 inhibitor to BRCA2-deficient cells (25). This observation is congruent with the hypothesis that PALB2 might possess DNA binding activity that could

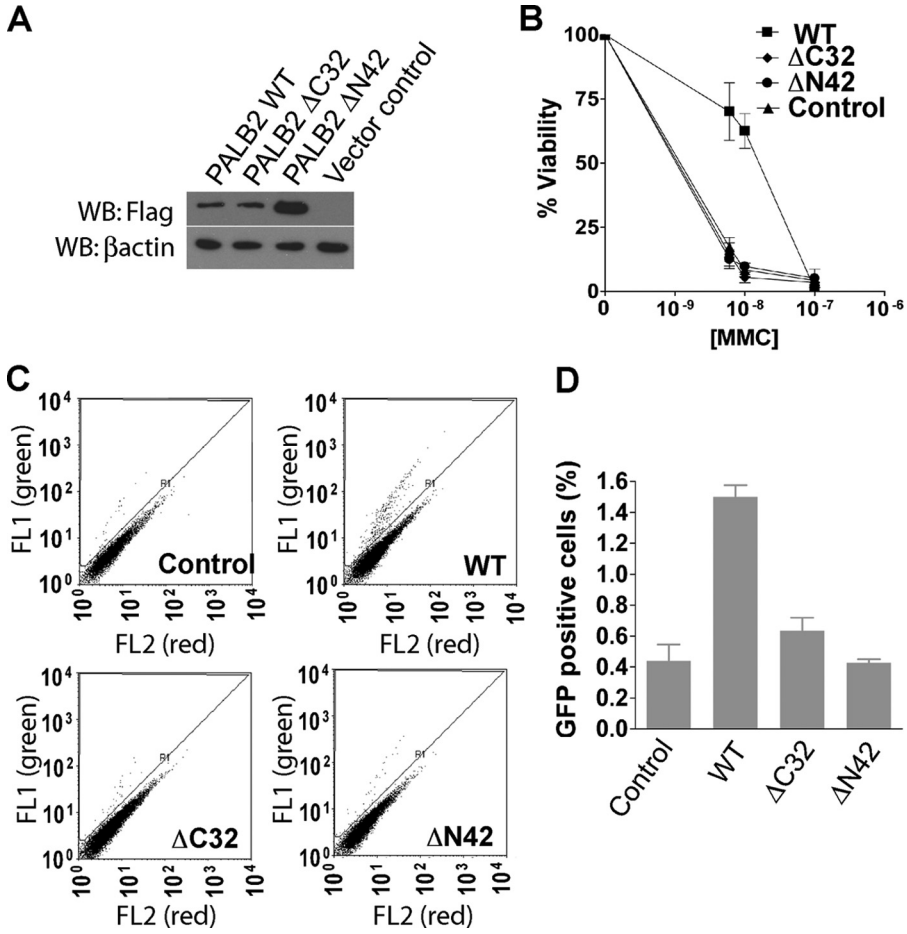

FIGURE 5. **PALB2 elevates cell survival following DNA damage by restoring homologous recombination repair.** *A*, EUFA1341 cells were transduced with vector control or HA-FLAG-tagged wild-type PALB2 (*WT*), the C-terminal deletion mutant (*ΔC32*), and the N-terminal deletion mutant (*ΔN42*). PALB2 expression was confirmed by Western blot (*WB*) as indicated. *B*, clonogenic assay after MMC treatment indicated that both the N-terminal and C-terminal regions of PALB2 are required for cell survival after MMC treatment. Results are the averages of three independent experiments. *C* and *D*, gene conversion in EUFA1341 reconstituted with wild-type or mutant PALB2. GFP-positive cells indicative of gene conversion (R1) were quantified by flow cytometry analysis. Results are the average of three independent experiments and were presented as mean ± S.E.

substitute BRCA2 DBD activity. In this study we observed a linear hierarchical relationship in the recruitment of the three HR repair proteins to DNA damage-induced foci in the sequence of 1) PALB2, 2) BRCA2, and 3) RAD51 (Fig. 1, *A* and *B*). Being the upstream co-factor, PALB2 might serve as the initial recognition module that in turn facilitates the loading and accumulation of the BRCA2·RAD51 complex at DSBs. Once the PALB2·BRCA2·RAD51 repair complex is loaded onto the damaged DNA, additional DNA binding activities of BRCA2, RAD51, and others then play important roles in mediating subsequent steps during HR repair processes.

We note that the deletion of the PALB2 N-terminal coiled-coil domain alone disrupted its focus forming ability *in vivo* (Fig. 3). Coiled-coil domains are modules that promote protein-protein interaction or protein oligomerization (26). We found that PALB2 exists as a dimeric or multimeric structure via its coiled-coil domain (Fig. 3, *D–G*). We proposed that upon DNA damage, the constitutively chromatin-associated PALB2 oligomerize so as to facilitate its accumulation at sites of DSBs to initiate HR repair by recruiting the BRCA2·RAD51 repair complex. Indeed, the PALB2 deletion mutant lacking the oligomerization domain not only is defective in foci formation at DSBs, but it also demonstrated deficits in homologous recombination and MMC sensitivity (Fig. 5). Interestingly, we and others have also found that PALB2 interacts with BRCA1 via its coiled-coil domain, forming a three-way complex with BRCA2 to allow optimal HR repair (27, 44). Given that PALB2 foci formation does not require BRCA1, our observation that the PALB2 coiled-coil motif mediates its oligomerization suggests that this particular property might regulate sustained localization of PALB2 at DSBs *in vivo*. We are currently testing this hypothesis.

It has been illustrated that protein oligomerization stabilizes protein-DNA association in DNA damage signaling, where oligomerization of Rad9 is required for sustain checkpoint signaling (28). Indeed, many of the DNA repair protein have been shown to exist as dimer or oligomers. Oligomerization of RAD51 to form the nucleofilament has been demonstrated by electronic microscopy (29). Structural studies also implicated a dimerization property for BRCA2 (23). Together with the PALB2 oligomerization property revealed in the current study and also its association with BRCA1, we proposed that the DNA repair complex exists as arrays of protein homo- and hetero-oligomers at site of DSBs upon DNA damage, where the quaternary structural configurations of the oligomers mediate the stabilization of the complex at the DSBs to facilitate subsequent repair processes.

Although our study shows that oligomerization of PALB2 is required for its focal accumulation at DSBs and, thus, the subsequent recruitment of the BRCA2·RAD51 complex to DNA lesions, mechanistically how PALB2 locates DNA breaks has yet to be clarified. It was previously shown that ATR-ATRIP senses DNA damage via recognition of RPA-coated ssDNA (30). The PALB2·BRCA2·RAD51 repair complex may utilize a similar system to recognize DSBs, as the replacement of RPA from ssDNA by RAD51 nucleofilament is the first step for DNA repair (8–10). Another possibility is that structural changes of the chromatin surrounding DNA breaks may signal for the recruitment of PALB2. A number of chromatin remodeling enzymes have been found to play an early role in response to DNA damage to facilitate the recruitment of signaling molecules as well as DNA repair proteins (31). The remodeled chromatin structure might enhance PALB2 access to DNA lesions. This may occur in parallel to the

known role of chromatin remodeling in the DNA damage signaling cascade (32, 33).

Alignment of PALB2 homologues (data not shown) shows that both the coiled-coil domain and the WD40 repeats are highly conserved among species. This suggests that both domains are significant for PALB2 function. Indeed, apart from the oligomerization property mediated by the coiled-coil motif, we have also refined the BRCA2 binding motif on PALB2 to its WD40 repeats (Fig. 4). WD40 repeats are known to mediate multiprotein complex assemblies as well as protein-DNA association. WD repeats are thought to organize as circularized β-propeller structure and serves as a rigid scaffold for protein interactions. The fact that deletion of any of the four WD40 domains on the PALB2 C terminus disrupted its interaction with BRCA2 indicated that the tertiary structure of the β-propeller is required for their interaction. We observed that disruption in the PALB2/BRCA2 interaction led to HR deficiency as observed in PALB2 FA patient cells (Fig. 5). It suggests that the essential role of PALB2 in HR is primarily via its ability in recruiting the BRCA2·RAD51 complex to DSBs. Because both coiled-coil and WD40 motifs are structural scaffolds and are both required for PALB2 function in HR, the PALB2 structure should provide insightful information to explain how PALB2 organizes the repair complex at DSBs.

DNA damage checkpoints play key roles in ensuring genomic stability by delaying cell cycle progression to allow sufficient time for DNA repair (34, 35). One would expect that cross-talk between the DNA repair machinery and cell cycle checkpoint pathways might enable an elaborate and precise coordination of cellular events essential for cell survival and proliferation. It remains largely elusive as to what the connections between DNA repair processes and DNA damage checkpoints are.

Recent studies demonstrated that human CtBP-interacting protein and its orthologues are involved in the generation of ssDNAs through resection of DSBs (36–41). The formation of RPA-ssDNA complexes could then lead to the recruitment and activation of ATR-ATRIP, which in turns control the intra-S checkpoint (30). Similarly RPA-ssDNA complexes may also be required for HR repair. Thus, RPA-coated ssDNA might represent a common signal for DNA repair and cell cycle checkpoint control. ATR and CHK1 depletion was reported to dramatically reduce RAD51 IRIF and HR repair (42, 43). However, we still detected RAD51 IRIF after depletion of ATR or CHK1 by siRNA in our study. The discrepancies in these observations might largely be because of the very different cell types used in these studies. Nevertheless, these differences point out that the relationship between cell cycle checkpoints and DNA repair is multifactorial and may involve many feedback loops and converging/diverging points. In agreement with this idea, PALB2 depletion also resulted in compromised intra-S checkpoint defect (11), suggesting an intimate relationship between checkpoint control and HR repair.

We believe that cross-talk between the DNA repair machinery and cell cycle checkpoint control not only couples the initiation of DNA repair and checkpoint activation but also serves as means to coordinate between the resumption of cell cycle progression upon completion of DNA repair. Future studies will reveal mechanistically how this coordination is achieved in the cell.

Acknowledgments—We thank Prof. David Livingston for the pOZC-PALB2, Prof. Maria Jasin for the pDR-GFP and pCBASce plasmids, and Prof. Johan P de Winter for EUFA1341 cell. S. M. Sy thanks all colleagues in the Chen laboratory for insightful discussion and technical assistance, especially Dr. Jun Huang.

REFERENCES

1. Bartek, J., Lukas, C., and Lukas, J. (2004) *Nat. Rev. Mol. Cell Biol.* **5,** 792–804
2. Kennedy, R. D., and D'Andrea, A. D. (2006) *J. Clin. Oncol.* **24,** 3799–3808
3. Wang, W. (2007) *Nat. Rev. Genet.* **8,** 735–748
4. Zhang, H., Tombline, G., and Weber, B. L. (1998) *Cell* **92,** 433–436
5. Gudmundsdottir, K., and Ashworth, A. (2006) *Oncogene* **25,** 5864–5874
6. Cantor, S. B., Bell, D. W., Ganesan, S., Kass, E. M., Drapkin, R., Grossman, S., Wahrer, D. C., Sgroi, D. C., Lane, W. S., Haber, D. A., and Livingston, D. M. (2001) *Cell* **105,** 149–160
7. Litman, R., Peng, M., Jin, Z., Zhang, F., Zhang, J., Powell, S., Andreassen, P. R., and Cantor, S. B. (2005) *Cancer Cell* **8,** 255–265
8. Pellegrini, L., and Venkitaraman, A. (2004) *Trends Biochem. Sci.* **29,** 310–316
9. Lord, C. J., and Ashworth, A. (2007) *Nat. Struct. Mol. Biol.* **14,** 461–462
10. Thorslund, T., and West, S. C. (2007) *Oncogene* **26,** 7720–7730
11. Xia, B., Sheng, Q., Nakanishi, K., Ohashi, A., Wu, J., Christ, N., Liu, X., Jasin, M., Couch, F. J., and Livingston, D. M. (2006) *Mol. Cell* **22,** 719–729
12. Xia, B., Dorsman, J. C., Ameziane, N., de Vries, Y., Rooimans, M. A., Sheng, Q., Pals, G., Errami, A., Gluckman, E., Llera, J., Wang, W., Livingston, D. M., Joenje, H., and de Winter, J. P. (2007) *Nat. Genet.* **39,** 159–161
13. Rahman, N., Seal, S., Thompson, D., Kelly, P., Renwick, A., Elliott, A., Reid, S., Spanova, K., Barfoot, R., Chagtai, T., Jayatilake, H., McGuffog, L., Hanks, S., Evans, D. G., Eccles, D., Easton, D. F., and Stratton, M. R. (2007) *Nat. Genet.* **39,** 165–167
14. Erkko, H., Xia, B., Nikkilä, J., Schleutker, J., Syrjäkoski, K., Mannermaa, A., Kallioniemi, A., Pylkäs, K., Karppinen, S. M., Rapakko, K., Miron, A., Sheng, Q., Li, G., Mattila, H., Bell, D. W., Haber, D. A., Grip, M., Reiman, M., Jukkola-Vuorinen, A., Mustonen, A., Kere, J., Aaltonen, L. A., Kosma, V. M., Kataja, V., Soini, Y., Drapkin, R. I., Livingston, D. M., and Winqvist, R. (2007) *Nature* **446,** 316–319
15. Tischkowitz, M., Xia, B., Sabbaghian, N., Reis-Filho, J. S., Hamel, N., Li, G., van Beers, E. H., Li, L., Khalil, T., Quenneville, L. A., Omeroglu, A., Poll, A., Lepage, P., Wong, N., Nederlof, P. M., Ashworth, A., Tonin, P. N., Narod, S. A., Livingston, D. M., and Foulkes, W. D. (2007) *Proc. Natl. Acad. Sci. U.S.A.* **104,** 6788–6793
16. Foulkes, W. D., Ghadirian, P., Akbari, M. R., Hamel, N., Giroux, S., Sabbaghian, N., Darnel, A., Royer, R., Poll, A., Fafard, E., Robidoux, A., Martin, G., Bismar, T. A., Tischkowitz, M., Rousseau, F., and Narod, S. A. (2007) *Breast Cancer Res.* **9,** R83
17. Chen, J., Silver, D. P., Walpita, D., Cantor, S. B., Gazdar, A. F., Tomlinson, G., Couch, F. J., Weber, B. L., Ashley, T., Livingston, D. M., and Scully, R. (1998) *Mol. Cell* **2,** 317–328
18. Ward, I. M., Minn, K., van Deursen, J., and Chen, J. (2003) *Mol. Cell. Biol.* **23,** 2556–2563
19. Celeste, A., Difilippantonio, S., Difilippantonio, M. J., Fernandez-Capetillo, O., Pilch, D. R., Sedelnikova, O. A., Eckhaus, M., Ried, T., Bonner, W. M., and Nussenzweig, A. (2003) *Cell* **114,** 371–383
20. Lou, Z., Minter-Dykhouse, K., Franco, S., Gostissa, M., Rivera, M. A., Celeste, A., Manis, J. P., van Deursen, J., Nussenzweig, A., Paull, T. T., Alt, F. W., and Chen, J. (2006) *Mol. Cell* **21,** 187–200
21. Huen, M. S., Huang, J., Yuan, J., Yamamoto, M., Akira, S., Ashley, C., Xiao, W., and Chen, J. (2008) *Mol. Cell. Biol.* **28,** 6104–6112
22. Shinohara, A., Ogawa, H., and Ogawa, T. (1992) *Cell* **69,** 457–470
23. Yang, H., Jeffrey, P. D., Miller, J., Kinnucan, E., Sun, Y., Thoma, N. H., Zheng, N., Chen, P. L., Lee, W. H., and Pavletich, N. P. (2002) *Science* **297,**

1837–1848
24. Shin, D. S., Chahwan, C., Huffman, J. L., and Tainer, J. A. (2004) *DNA Repair* **3,** 863–873
25. Edwards, S. L., Brough, R., Lord, C. J., Natrajan, R., Vatcheva, R., Levine, D. A., Boyd, J., Reis-Filho, J. S., and Ashworth, A. (2008) *Nature* **451,** 1111–1115
26. Burkhard, P., Stetefeld, J., and Strelkov, S. V. (2001) *Trends Cell Biol.* **11,** 82–88
27. Zhang, F., Ma, J., Wu, J., Ye, L., Cai, H., Xia, B., and Yu, X. (2009) *Curr. Biol.* **19,** 524–529
28. Usui, T., Foster, S. S., and Petrini, J. H. (2009) *Mol. Cell* **33,** 147–159
29. Sung, P., and Robberson, D. L. (1995) *Cell* **82,** 453–461
30. Zou, L., and Elledge, S. J. (2003) *Science* **300,** 1542–1548
31. Murr, R., Loizou, J. I., Yang, Y. G., Cuenin, C., Li, H., Wang, Z. Q., and Herceg, Z. (2006) *Nat. Cell Biol.* **8,** 91–99
32. Harper, J. W., and Elledge, S. J. (2007) *Mol. Cell* **28,** 739–745
33. Huen, M. S., and Chen, J. (2008) *Cell Res.* **18,** 8–16
34. Motoyama, N., and Naka, K. (2004) *Curr. Opin. Genet. Dev.* **14,** 11–16
35. Myung, K., Datta, A., and Kolodner, R. D. (2001) *Cell* **104,** 397–408
36. Uanschou, C., Siwiec, T., Pedrosa-Harand, A., Kerzendorfer, C., Sanchez-Moran, E., Novatchkova, M., Akimcheva, S., Woglar, A., Klein, F., and Schlögelhofer, P. (2007) *EMBO J.* **26,** 5061–5070
37. Takeda, S., Nakamura, K., Taniguchi, Y., and Paull, T. T. (2007) *Mol. Cell* **28,** 351–352
38. Sartori, A. A., Lukas, C., Coates, J., Mistrik, M., Fu, S., Bartek, J., Baer, R., Lukas, J., and Jackson, S. P. (2007) *Nature* **450,** 509–514
39. Penkner, A., Portik-Dobos, Z., Tang, L., Schnabel, R., Novatchkova, M., Jantsch, V., and Loidl, J. (2007) *EMBO J.* **26,** 5071–5082
40. Limbo, O., Chahwan, C., Yamada, Y., de Bruin, R. A., Wittenberg, C., and Russell, P. (2007) *Mol. Cell* **28,** 134–146
41. Chen, L., Nievera, C. J., Lee, A. Y., and Wu, X. (2008) *J. Biol. Chem.* **283,** 7713–7720
42. Sørensen, C. S., Hansen, L. T., Dziegielewski, J., Syljuåsen, R. G., Lundin, C., Bartek, J., and Helleday, T. (2005) *Nat. Cell Biol.* **7,** 195–201
43. Collis, S. J., Barber, L. J., Clark, A. J., Martin, J. S., Ward, J. D., and Boulton, S. J. (2007) *Nat. Cell Biol.* **9,** 391–401
44. Sy, S. M., Huen, M. S., and Chen, J. (2009) *Proc. Natl. Acad. Sci. U. S. A.* **106,** 7155–7160

ACCELERATED PUBLICATION

This paper is available online at www.jbc.org

THE JOURNAL OF BIOLOGICAL CHEMISTRY VOL. 284, NO. 32, pp. 21127–21131, August 7, 2009

MRG15 Is a Novel PALB2-interacting Factor Involved in Homologous Recombination*[S]

Received for publication, May 21, 2009, and in revised form, June 23, 2009
Published, JBC Papers in Press, June 24, 2009, DOI 10.1074/jbc.C109.023937

Shirley M.-H. Sy[1], Michael S. Y. Huen[2], and Junjie Chen[3]

From the Department of Therapeutic Radiology, Yale University School of Medicine, New Haven, Connecticut 06520

PALB2 is an integral component of the BRCA complex important for recombinational DNA repair. However, exactly how this activity is regulated *in vivo* remains unexplored. Here we provide evidence to show that MRG15 is a novel PALB2-associated protein that ensures regulated recombination events. We found that the direct interaction between MRG15 and PALB2 is mediated by an evolutionarily conserved region on PALB2. Intriguingly, although damage-induced RAD51 foci formation and mitomycin C sensitivity appeared normal in MRG15-binding defective PALB2 mutants, these cells exhibited a significant increase in gene conversion rates. Consistently, we found that abrogation of the PALB2-MRG15 interaction resulted in elevated sister chromatid exchange frequencies. Our results suggest that loss of the PALB2-MRG15 interaction relieved the cells with the suppression of sister chromatid exchange and therefore led to a hyper-recombination phenotype in the gene conversion assay. Together, our study indicated that although PALB2 is required for proficient homologous recombination, it could also govern the choice of templates used in homologous recombination repair.

The tumor suppressor protein PALB2 plays a crucial role in homologous recombinational repair. Previous studies indicated that PALB2 functions upstream of the BRCA2-RAD51 axis, where it is essential for the loading of the repair machinery to the damaged chromatin to facilitate DNA repair (1, 2). We and others have recently demonstrated that PALB2 is the link between the BRCA1 and BRCA2 tumor suppressors and orchestrates DNA repair in response to DNA damage (3, 4). Sequence alignment of PALB2 homologues revealed several conserved regions (see Fig. 1*A*). Although the BRCA2-interacting domain was mapped to the conserved C terminus, which contains the WD40 repeats (see Fig. 1*A*, *region C*) (2), the BRCA1-binding motif was mapped to the N-terminal conserved coiled-coil domain (see Fig. 1*A*, *region A*). Interestingly, the same region was found to be responsible for PALB2 oligomerization and foci formation (2). Accordingly, disruption of either the N-terminal or the C-terminal leads to impaired DNA repair *in vivo*, suggesting that these highly conserved regions are important for PALB2 function in homologous recombination.

Apart from the N and C termini of PALB2, bioinformatic analysis revealed another highly conserved region in the middle of the PALB2 coding sequence (see Fig. 1*A*, *region B*). Although no function has been ascribed to this region of the PALB2 protein, we found that this conserved region (*i.e.* region B), missing from the PALB2-deficient Fanconi anemia (FA) patient cells (EUFA1341F) that express a truncated PALB2 mutant (residues 1–500), was restored during spontaneous reversion (5). Notably, this particular revertant supported normal levels of RAD51 foci formation and restored mitomycin C (MMC)[4] resistance in the patient cells. Sequencing analysis indicated that this revertant, containing an internal deletion (residues 71–561), harbors all of the three conserved regions (*i.e.* regions A–C). From these observations, we speculated that apart from its ability to interact with BRCA1 and BRCA2, the conserved region B might also play an important role in the regulation of PALB2 function *in vivo*.

MRG15 belongs to a highly conserved protein family that contains the MRG domain responsible for transcriptional regulation via chromatin remodeling by histone acetylation (6). Its yeast homologue Eaf3 has been demonstrated to be a component of both the NuA4 histone acetyltransferase and the Rpd3 histone deacetylase complexes and affects global acetylation (7–9). MRG15 has been demonstrated to bind directly to methylated lysine 36 on histone H3 peptide and was functionally correlated to the acetylation of lysine 16 on histone H4 (10–12). It was demonstrated that Eaf3, via its chromo domain-mediated binding to methylated lysine 36 on histone H3, allows specific recruitment of the Rpd3S histone deacetylase complex (13).

In the current study, we have identified MRG15 as a novel interacting partner of PALB2 that binds to a previously uncharacterized conserved region on PALB2 (see Fig. 1*A*, *region B*). In keeping with the importance of the conservation of functional protein motifs, we demonstrated that the PALB2-MRG15 interaction is important for the suppression of sister chromatid-mediated homologous recombination.

EXPERIMENTAL PROCEDURES

Antibodies—Monoclonal antibodies against the FLAG epitope (M2) were purchased from Sigma. Rabbit polyclonal anti-RAD51 (D51), anti-PALB2, anti-BRCA2 (C25), and anti-pH2AX antibodies were described previously (4, 14). Mouse

* This work was supported, in whole or in part, by National Institutes of Health Grants CA089239, CA092312 and CA100109 (to J. C.).
[S] The on-line version of this article (available at http://www.jbc.org) contains supplemental Figs. S1 and S2.
[1] A recipient of postdoctoral fellowship from the Croucher Foundation.
[2] Supported by the Ann Fuller Postdoctoral Fellowship.
[3] A recipient of an Era of Hope Scholar award from the Dept. of Defense and a member of the Mayo Clinic Breast SPORE program. To whom correspondence should be addressed: Dept. of Experimental Radiation Oncology, the University of Texas M. D. Anderson Cancer Center, 1515 Holcombe Blvd. – Unit 66 (Rm. Y3.6006), Houston, TX 77030. Tel.: 713-792-4863; Fax: 713-794-5369; E-mail: jchen8@mdanderson.org.

[4] The abbreviations used are: MMC, mitomycin C; DSBs, double strand breaks; FA, Fanconi anemia; SFB, S-tag, FLAG epitope, and streptavidin-binding peptide tag; SCE, sister chromatid exchange; TAP, tandem affinity purification; GST, glutathione *S*-transferase; siRNA, small interfering RNA; DAPI, 4′,6-diamidino-2-phenylindole; BrdUrd, bromodeoxyuridine; hyper-rec, hyper-recombination; GFP, green fluorescent protein.

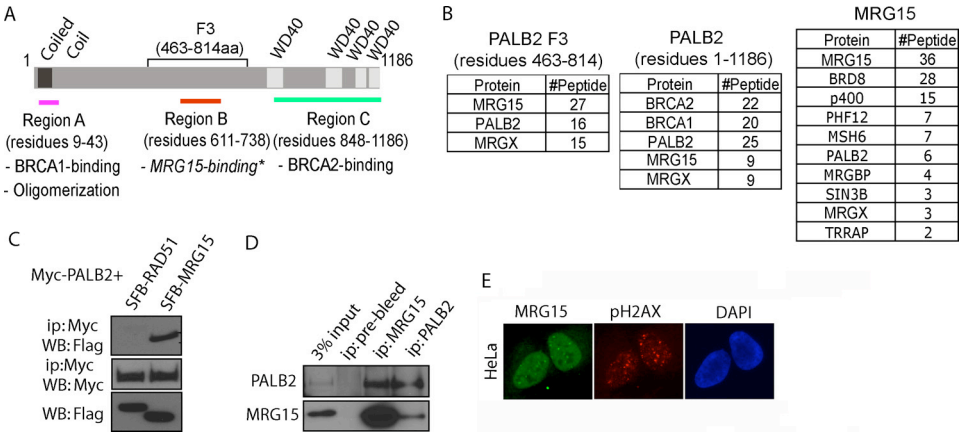

FIGURE 1. **MRG15 is a PALB2-binding protein.** *A*, schematic presentation of PALB2. Three conserved regions A, B, and C are identified in the alignment of PALB2 homologues. *, identified in this study. *B*, the identification of PALB2- or MRG15-interacting protein(s) by TAP. Proteins identified by mass spectrometry analysis and the numbers of peptide hits are listed. *C*, MRG15 interacts with PALB2. 293T cells were transfected with plasmids encoding Myc-PALB2 together with plasmids encoding SFB-RAD51 or SFB-MRG15. Lysates were subjected to immunoprecipitation (*ip*) using anti-Myc antibodies and immunoblotted (*WB*) with antibodies as indicated. *D*, co-immunoprecipitation of endogenous proteins was conducted using HeLa lysates and anti-MRG15, anti-PALB2 antibodies, or prebleed serum. Immunoblotting was performed using indicated antibodies. *E*, HeLa or U2OS cells were irradiated with 10 grays of ionizing radiation and recovered for 5 h. Immunofluorescence staining was performed using the antibodies as indicated.

anti β-actin antibody was purchased from Sigma. To facilitate the study of endogenous MRG15 protein, we generated a rabbit polyclonal antibody raised against recombination GST-MRG15 purified from *Escherichia coli*.

Cell Cultures—Cells were maintained in RPMI supplemented with 10% fetal bovine serum and 1% penicillin and streptomycin and kept in a 37 °C incubator with 5% CO_2.

Constructs—pOZC-PALB2 (a gift from Dr. David Livingston (Dana-Farber Cancer Institute)) was subcloned into the entry vector pDONR201 (Invitrogen). Mutations or deletions of PALB2 were generated using site-directed mutagenesis (QuikChange, Stratagene).

Tandem Affinity Purification (TAP)—293T cells expressing SFB-PALB2 F3 or SFB-MRG15 were used for the purification of protein complex(es). TAP procedures were described in Ref. 4.

RNA Interference—A non-targeting siRNA and siRNA specifically targeting human MRG15, MRGX, PALB2, and BRCA2 were purchased from Dharmacon. Cells were seeded at 30% confluency for 24 h before double siRNA transfection using Oligofectamine (Invitrogen). Cells were harvested 48 h after the second siRNA transfection.

Immunoprecipitation and Pulldown Experiments—Cells were lysed in NETN (20 mM Tris-HCl, pH 8, 100 mM NaCl, 1 mM EDTA, 0.5% Nonidet P-40, 1 mM $MgCl_2$) buffer containing Benzonase (Novagen). For immunoprecipitation or pulldown experiments, cell extracts were incubated with either S-agarose (EMD Biosciences) or GST fusion proteins immobilized on glutathione-beads for 2 h at 4 °C. Beads were washed with NETN buffer, and proteins were eluted by boiling in 2× Laemmli buffer. Samples were resolved by SDS-PAGE and transferred to polyvinylidene difluoride membrane. Immunoblottings were subsequently performed with antibodies as indicated.

Immuofluoresence Staining—Cells grown on coverslips were pre-extracted with buffer containing 0.5% Triton X-100 and fixed using 3% paraformaldehyde solution. Immunostaining experiments were performed using MRG15, RAD51, and pH2AX antibody. Cells were mounted onto glass slides in DAPI-containing antifade. Immunofluorescent analyses and image capturing were performed on a Nikon Eclipse 800 microscope.

MMC Sensitivity Assay—Cells were seeded at a density of 1×10^3 cells in triplicate onto 96-well plates. A different concentration of MMC was added 24 h after cell seeding. Cells were incubated for another 5 days. MMC sensitivity was monitored by the Alamar blue assay (Biosource). Absorbances at 570/600 nm were measured using the TECAN SAFIRE plate reader. Results were the averages of data from three independent experiments.

Gene Conversion Assay—1×10^6 cells were electroporated with 10 μg of pCBASce plasmid at 270 V, 975 microfarads using a Bio-Rad gene pulser II (15). Cells were plated and incubated in culture media for 48 h prior to fluorescence-activated cell sorter analyses. Cells were analyzed in a BD Biosciences FACScan on a green (FL1) *versus* orange (FL2) fluorescence plot. Results were the average of data obtained from two independent experiments.

Sister Chromatin Exchange Assay—Cells were incubated with 10 μM BrdUrd for 48 h and then chased for 24 h. Cells were treated with Colcemid for 8 h and harvested for the preparation of metaphase spread. For MMC treatment, 10 μM MMC was added to the media 6 h before harvest. Metaphases were spread onto slides and aged for 5 days. Prior to the incubation with mouse anti-BrdUrd antibody, slides were denatured with 70% formamide/4× SSC and dried with an ethanol series. Rhodamine-conjugated anti-mouse antibody was used to visualize chromatids labeled with BrdUrd. Chromosomes were counterstained with DAPI.

RESULTS AND DISCUSSION

To identify proteins that interact with PALB2 through its conserved region B, we used 293T cells stably expressing an SFB-tagged PALB2 fragment (F3) (Fig. 1*A*) for tandem affinity purification. Mass spectrometry analysis identified MRG15 as a major binding partner of PALB2 F3, along with its close homologue MRGX (Fig. 1*B* and supplemental Fig. 1*A*). In addition, MRG15 was also co-purified with full-length PALB2 when we performed TAP using 293T cells expressing SFB-tagged full-length PALB2. To confirm the interaction between PALB2 and MRG15, we performed reverse TAP using 293T cells expressing SFB-tagged MRG15. Consistently, PALB2 was co-purified with MRG15 along with other known MRG15-binding partners including p400 and BRD8 (Fig. 1*B*). Reciprocal co-immunoprecipitation experiments also verified a specific interaction between PALB2 and MRG15 (Fig. 1, *C* and *D*). MRG15 chromo

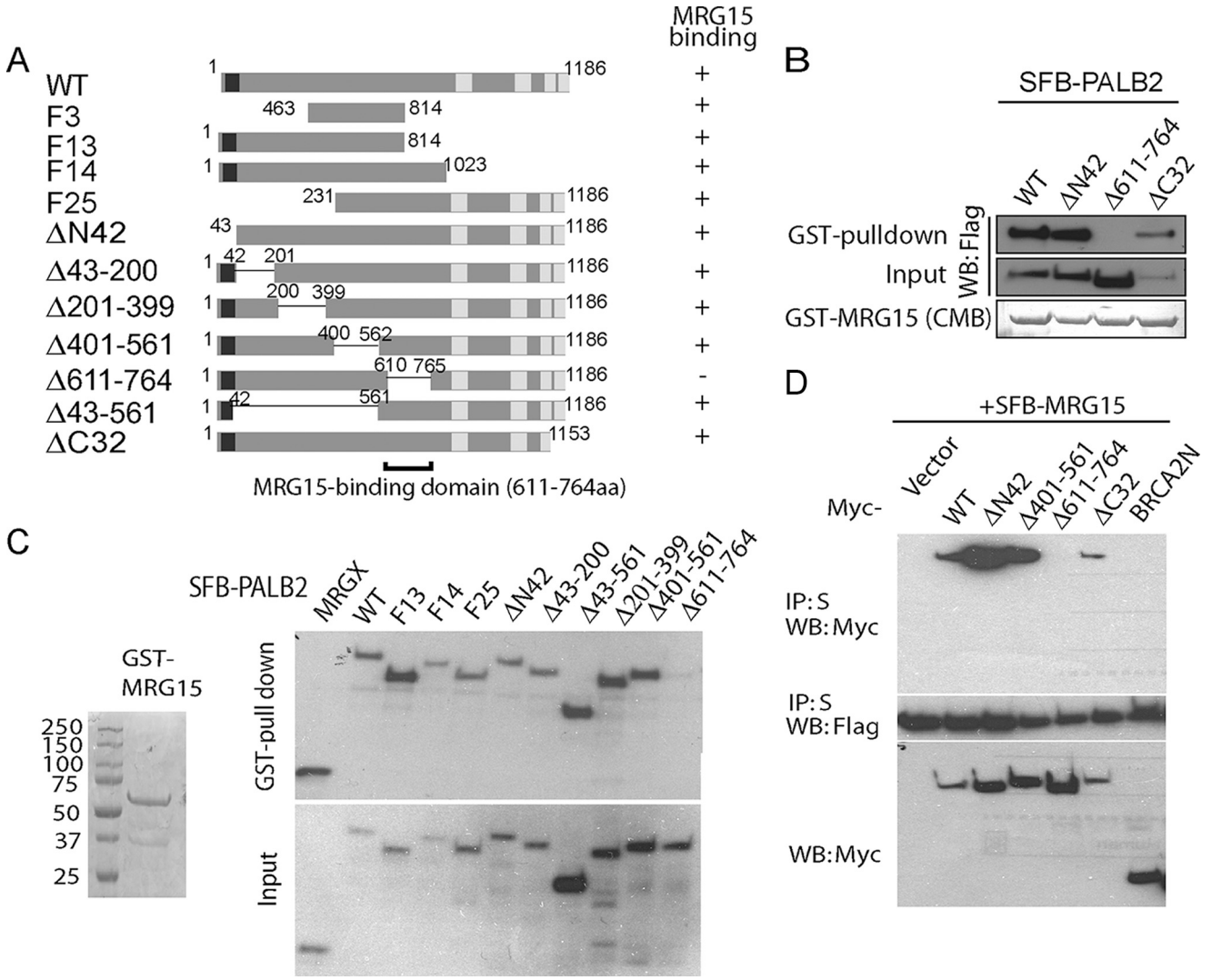

FIGURE 2. **PALB2 interacts with MRG15 via its conserved domain C, which contains residues 611–764.** *A*, schematic presentation of PALB2 deletion mutants used in the study. The MRG15 binding property of these PALB2 mutants is summarized. *WT*, wild type. *B* and *C*, lysates prepared from 293T cells expressing various SFB-PALB2 mutants were subjected to a pulldown assay using beads coated with GST-MRG15. *CMB*, Coomassie Blue. *D*, co-immunoprecipitation (*IP*) experiments were performed using lysates prepared from 293T cells expressing Myc-tagged wild-type or mutant PALB2 together with SFB-MRG15. *WB*, immunoblot.

domain fragment (F1) and MRG domain fragment (F2) were generated, and a co-immunoprecipitation experiment indicated that MRG15 interacts with PALB2 via its MRG domain (supplemental Fig. 1, *B* and *C*).

MRG15 belongs to the MRG domain-containing protein family, which is highly conserved among organisms including yeast, *Caenorhabditis elegans*, and *Drosophila* (6). Although the MRG domain is highly conserved, MRG15 is the only member in the family that harbors a chromo domain on its N-terminal, which has been shown to be capable to bind methylated H3K36 lysine 36 (10, 12). Intriguingly, MRG15 knock-out mice manifested DNA repair defects in which the recruitment of repair proteins including 53BP1 to sites of DNA damage was delayed (11). It is not clear what is the MRG15 function in DNA repair. The interaction between MRG15 and PALB2 prompted us to investigate whether MRG15 serves as a cofactor in the PALB2-dependent DNA repair.

Because PALB2 localizes at sites of DNA breaks upon DNA damage, we next asked whether MRG15 might similarly be recruited to DSBs. Immunofluorescent staining revealed that following ionizing radiation, endogenous MRG15 localized to sites of DNA breaks that are marked by pH2AX (Fig. 1*E*). These results indicated that PALB2 and MRG15 may function together in response to DNA damage.

To further understand exactly how PALB2 interacts with MRG15, we used a series of SFB-tagged PALB2 mutants to map the MRG15-binding region (Fig. 2*A*). Pulldown experiments using GST-MRG15 fusion protein suggested that the PALB2 and MRG15 interaction requires the conserved region B of PALB2 (residues 611–764; Fig. 2*B*). Further experiments using a series of PALB2 deletion mutants reassured us that this region B of PALB2 is the only region that mediates its interaction with MRG15 (Fig. 2*C*). In addition, co-immunoprecipitation experiments showed that although wild-type PALB2 associated readily with an MRG15, PALB2 deletion mutant that lacks residues 611–764 did not (Fig. 2*C*). Furthermore, disruption of either the oligomerization and BRCA1-interacting motif (ΔN42) or the BRCA2-binding domain (ΔC32) of PALB2 has no obvious impact on the PALB2-MRG15 interaction (Fig. 2, *B* and *D*). The fact that the MRG15-binding

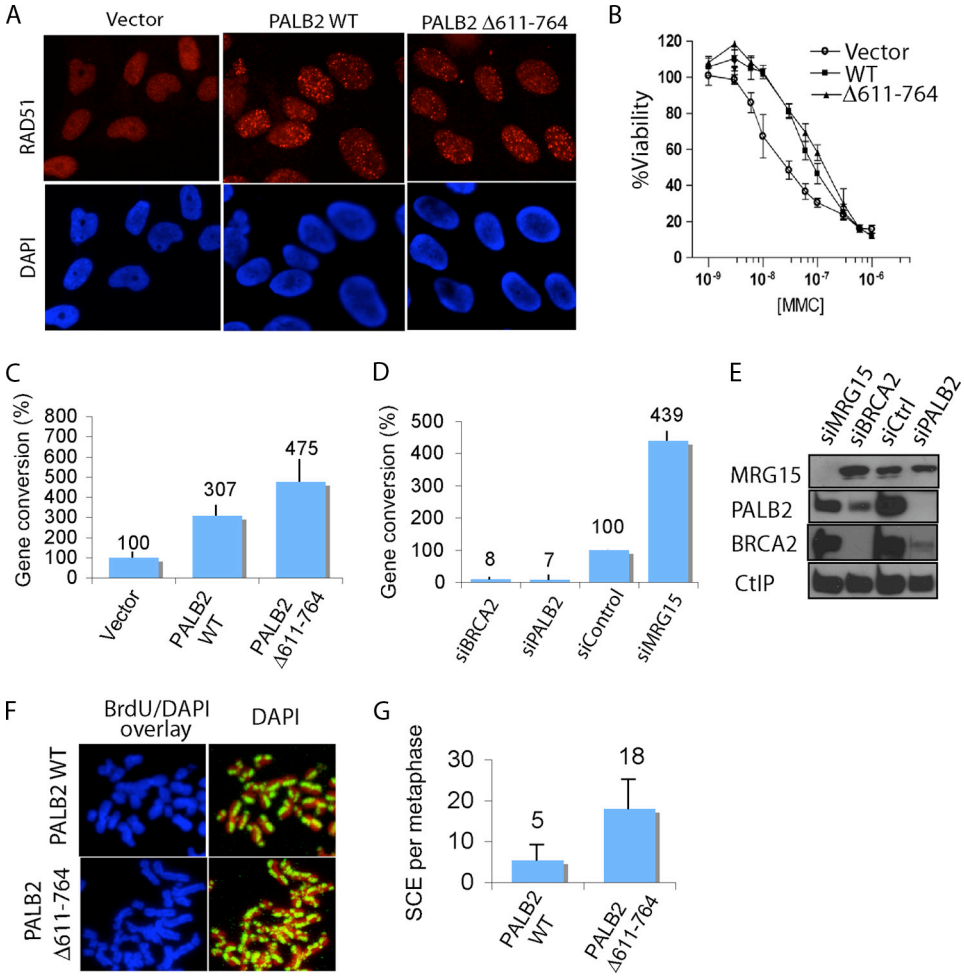

FIGURE 3. **PALB2 suppresses sister chromatid exchange.** *A*, EUFA1341F cells reconstituted with empty vector or constructs encoding wild-type (*WT*) or Δ611–764 mutant of PALB2 were examined for the formation of ionizing radiation induced RAD51 foci. Cells were collected 5 h after radiation (10 grays), and immunostaining experiments were performed using anti-RAD51 antibodies. *B*, MMC sensitivity assays were performed in EUFA1341F+vector cells and EUFA1341F cells reconstituted with wild-type or the Δ611–764 mutant of PALB2. Cells were treated with indicated concentration of MMC for 24 h and recovered for 5 days. *C*, gene conversion efficiency was measured in EUFA1341F, and its derivative cells were reconstituted with wild-type or the Δ611–764 mutant of PALB2. The percentage of GFP-positive cells was determined by fluorescence-activated cell sorter analyses 48 h after transfection. Relative gene conversion efficiency was normalized using vector-reconstituted cells, which was set as 100%. *D* and *E*, gene conversion efficiency was assessed in U2OS DR-GFP cells treated with control, PALB2-, BRCA2-, or MRG15-specific siRNAs. Relative gene conversion efficiency was normalized using control siRNA-transfected cells, which was set as 100% (*D*). The expression of PALB2, BRCA2, and MRG15 was examined using Western blotting using the indicated antibodies (*E*). *F*, representative images of BrdUrd (*Brdu*)-labeled metaphases prepared using EUFA1341F cells reconstituted with wild-type or the Δ611–764 mutant of PALB2. BrdUrd labeled metaphase images were overlaid with DAPI to aid visualization. *G*, the average number of SCE events per metaphase was plotted.

resistance *in vivo* (1–5), we further examined whether the reconstitution of PALB2-deficient cells with PALB2 Δ611–764 mutant could restore these PALB2-dependent functions. Surprisingly, we found that EUFA1341F cells reconstituted with either wild-type PALB2 or PALB2 Δ611–764 mutant fully restored RAD51 foci formation, whereas cells reconstituted with empty vector alone did not (Fig. 3*A*). The same is observed in 293T cells reconstituted with wild type or PALB2 Δ611–764 mutant after the depletion of endogenous PALB2 (supplemental Fig. 2*A*). In addition, the MMC sensitivity assay indicated that similar to wild-type PALB2, Δ611–764 mutant of PALB2 was also able to restore cell survival following MMC treatment (Fig. 3*B*).

We further performed a gene conversion assay to directly measure the efficiency of homologous recombination in cells reconstituted with either wild type or Δ611–764 mutant of PALB2. Intriguingly, cells reconstituted with PALB2 Δ611–764 mutant consistently displayed higher homologous recombination efficiency than cells reconstituted with wild-type PALB2 (Fig. 3*C*), suggesting that loss of the PALB2-MRG15 interaction results in a hyper-rec phenotype. Likewise, a hyper-rec phenotype was also observed in U2OS cells with depletion of endogenous PALB2 and the reintroduction of PALB2 Δ611–764 mutant when compared with the wild-type PALB2 reconstituted cells (supplemental Fig. 2*B*). Consistently, siRNA-mediated MRG15 knockdown significantly enhanced gene conversion efficiency (Fig. 3*D*), suggesting that MRG15 and its interaction with PALB2 may be responsible for the hyper-recombination phenotype we observed here. As a control, we examined the expression levels of PALB2, BRCA2, and MRG15 in these siRNA-transfected cells (Fig. 3*E*). Results indicated that although PALB2 or BRCA2 knockdown led to the destabilization of each other (1), knockdown of MRG15 did not affect the expression levels of either PALB2 or BRCA2, and thus, this rules out the possibility that the hyper-recombination phenotype observed in MRG15-depleted cells was due to an indirect effect on PALB2 or BRCA2 expression.

In mammalian cells, the major repair pathways exploited to repair DSBs are the homologous recombination pathway and

motif on PALB2 is well separated from its other interaction domains suggests that MRG15 possibly serves as an additional factor to modulate the PALB2-dependent DNA repair process.

To assess whether the interaction with MRG15 is critical for the PALB2-dependent DNA repair, we reconstituted the EUF1341F PALB2-deficient cell with constructs encoding wild-type PALB2, PALB2 Δ611–764, or empty vector. Both wild-type PALB2 and the Δ611–764 deletion of PALB2 displayed discrete ionizing radiation-induced DNA damage foci that co-localized with pH2AX (data not shown), which agrees with our earlier study that suggests that only the N terminus of PALB2 is required for its focus localization following DNA damage (2). Because PALB2 is known to be required for RAD51 foci formation, homologous recombination, and MMC

the non-homologues end-joining pathway. Homologous recombination allows accurate repair of DSBs with the use of homologous templates (16). During the cell cycle, cells employ homologous chromosomes as templates for recombinational repair in S and G_2 phases. The use of sister chromatids during homologous recombination may also occur under some circumstance in mitotic cells for repairing DSBs, especially when the recombination between homologues might lead to loss of heterozygosity in mitotic cells, which could result in inactivation of both alleles of tumor suppressors.

The hyper-recombination phenotype observed in cells reconstituted with PALB2 Δ611–764 mutant raised the possibility that PALB2 may be normally responsible for the suppression of recombination or the sister chromatid exchange (SCE). We thus performed the SCE assay using EUFA1341F cells reconstituted with either wild-type PALB2 or Δ611–764 mutant of PALB2. Analyses of metaphase chromosomes clearly indicated that cells expressing only PALB2 Δ611–764 mutant have a significantly higher rate of SCE than that observed in cells expressing wild-type PALB2 (Fig. 3, *F* and *G*), although both of these cells are fully capable of restoring RAD51 foci formation and MMC resistance (Fig. 3, *A* and *B*). Therefore, we proposed that PALB2 suppresses SCE events during homologous recombination to assure error-free DNA repair. Deletion of the MRG15-binding motif on PALB2 would lead to the loss of such suppression, and thus, result in hyper-recombination and genomic instability.

The exact role of MRG15 in chromatin remodeling involved in DNA damage or repair remains unknown. However, MRG15-deficient mouse embryonic fibroblasts demonstrated DNA repair deficits, and 53BP1 and pH2AX foci formation was delayed in these cells upon DNA damage (11). There are a number of possibilities. MRG15 and its homologue Eaf3 have been identified as component of the Tip60-NuA4 histone acetylase complex in human and yeast, respectively (9, 17). It has been demonstrated that the Tip60 complex acetylates nucleosomal phospho-H2Av at Lys-5 in a DSB-dependent manner and catalyzes H2AX variant exchange upon DNA damage (18). It is possible that MRG15 is required for such a function given that dMRG15 mutant embryos demonstrated defects in the acetylation of nucleosomal phospho-H2Av similar to the dTip60 mutant embryos (18). On the other hand, Tip60 histone acetyltransferase was shown to bind to chromatin surrounding sites of DSBs *in vivo*. Tip60-Trrap deficiency impaired damage-induced histone H4 hyperacetylation, impeded chromatin accessibility to repair proteins, and resulted in defective homologous recombination (19). As such, there is a possibility that MRG15 functions in regulating chromatin structure and accessibility and therefore affects the frequency of recombination. Interestingly, MRG15 and its homologue MRGX exist in similar protein complexes involving chromatin remodeling. Because MRGX was also identified as a component of the PALB2 complex, we further checked whether MRGX shares a similar function of MRG15 in the PALB2-dependent repair pathway. A gene conversion assay performed in U2OS cells transfected with control siRNA- or MRGX-specific siRNA showed that depletion of MRGX led to a hyper-rec phenotype when compared with control cells (supplemental Fig. 1*D*). This observation suggests that like MRG15, MRGX may also regulate sister chromatin exchange frequency in the cell. The exact mechanism as to how MRG15 and also MRGX participate in DNA repair and recombination requires further investigations.

In conclusion, our findings here highlight that PALB2 not only regulates the efficiency of homologous recombination but also dictates the specific homologous recombination pathway in which it participates. These attributes are likely critical for the maintenance of genomic stability in the cell. Further studies into the underlying mechanism as to how PALB2 dictates the repair mechanisms should warrant a more comprehensive understanding on the role of PALB2 in tumor suppression.

Acknowledgments—We thank Prof. David Livingston for the pOZC-PALB2, Prof. Maria Jasin for the DR-GFP and pCBASce plasmids, Prof. Johan P. de Winter for EUFA1341 cell, and Prof. Ben Turk for the TECAN SAFIRE plate reader.

REFERENCES

1. Xia, B., Sheng, Q., Nakanishi, K., Ohashi, A., Wu, J., Christ, N., Liu, X., Jasin, M., Couch, F. J., and Livingston, D. M. (2006) *Mol. Cell* **22,** 719–729
2. Sy, S. M., Huen, M. S., Zhu, Y., and Chen, J. (2009) *J. Biol. Chem.* **284,** 18302–18310
3. Zhang, F., Ma, J., Wu, J., Ye, L., Cai, H., Xia, B., and Yu, X. (2009) *Curr. Biol.* **19,** 524–529
4. Sy, S. M., Huen, M. S., and Chen, J. (2009) *Proc. Natl. Acad. Sci. U.S.A.* **106,** 7155–7160
5. Xia, B., Dorsman, J. C., Ameziane, N., de Vries, Y., Rooimans, M. A., Sheng, Q., Pals, G., Errami, A., Gluckman, E., Llera, J., Wang, W., Livingston, D. M., Joenje, H., and de Winter, J. P. (2007) *Nat. Genet.* **39,** 159–161
6. Bertram, M. J., and Pereira-Smith, O. M. (2001) *Gene* **266,** 111–121
7. Reid, J. L., Moqtaderi, Z., and Struhl, K. (2004) *Mol. Cell Biol.* **24,** 757–764
8. Carrozza, M. J., Li, B., Florens, L., Suganuma, T., Swanson, S. K., Lee, K. K., Shia, W. J., Anderson, S., Yates, J., Washburn, M. P., and Workman, J. L. (2005) *Cell* **123,** 581–592
9. Doyon, Y., Selleck, W., Lane, W. S., Tan, S., and Côté, J. (2004) *Mol. Cell Biol.* **24,** 1884–1896
10. Zhang, P., Du, J., Sun, B., Dong, X., Xu, G., Zhou, J., Huang, Q., Liu, Q., Hao, Q., and Ding, J. (2006) *Nucleic Acids Res.* **34,** 6621–6628
11. Garcia, S. N., Kirtane, B. M., Podlutsky, A. J., Pereira-Smith, O. M., and Tominaga, K. (2007) *FEBS Lett.* **581,** 5275–5281
12. Sun, B., Hong, J., Zhang, P., Dong, X., Shen, X., Lin, D., and Ding, J. (2008) *J. Biol. Chem.* **283,** 36504–36512
13. Li, B., Gogol, M., Carey, M., Lee, D., Seidel, C., and Workman, J. L. (2007) *Science* **316,** 1050–1054
14. Chen, J., Silver, D. P., Walpita, D., Cantor, S. B., Gazdar, A. F., Tomlinson, G., Couch, F. J., Weber, B. L., Ashley, T., Livingston, D. M., and Scully, R. (1998) *Mol. Cell* **2,** 317–328
15. Moynahan, M. E., Pierce, A. J., and Jasin, M. (2001) *Mol. Cell* **7,** 263–272
16. Bartek, J., Lukas, C., and Lukas, J. (2004) *Nat. Rev. Mol. Cell Biol.* **5,** 792–804
17. Kusch, T., Florens, L., Macdonald, W. H., Swanson, S. K., Glaser, R. L., Yates, J. R., 3rd, Abmayr, S. M., Washburn, M. P., and Workman, J. L. (2004) *Science* **306,** 2084–2087
18. Squatrito, M., Gorrini, C., and Amati, B. (2006) *Trends Cell Biol.* **16,** 433–442
19. Murr, R., Loizou, J. I., Yang, Y. G., Cuenin, C., Li, H., Wang, Z. Q., and Herceg, Z. (2006) *Nat. Cell Biol.* **8,** 91–99

Molecular Cell
Short Article

SOSS Complexes Participate in the Maintenance of Genomic Stability

Jun Huang,[1,2] Zihua Gong,[1,2] Gargi Ghosal,[1] and Junjie Chen[1,3,*]
[1]Department of Therapeutic Radiology, Yale University School of Medicine, New Haven, CT 06520, USA
[2]These authors contributed equally to this work
[3]Present address: Department of Experimental Radiation Oncology, The University of Texas M.D. Anderson Cancer Center, 1515 Holcombe Boulevard, Houston, TX 77030 USA
*Correspondence: junjie.chen@yale.edu
DOI 10.1016/j.molcel.2009.06.011

SUMMARY

Proteins that bind to single-stranded DNA (ssDNA) are essential for DNA replication, recombinational repair, and maintenance of genomic stability. Here, we describe the characterization of an ssDNA-binding heterotrimeric complex, SOSS (sensor of ssDNA) in human, which consists of human SSB homologs hSSB1/2 (SOSS-B1/2) and INTS3 (SOSS-A) and a previously uncharacterized protein C9orf80 (SOSS-C). We have shown that SOSS-A serves as a central adaptor required not only for SOSS complex assembly and stability, but also for facilitating the accumulation of SOSS complex to DNA ends. Moreover, SOSS-depleted cells display increased ionizing radiation sensitivity, defective G2/M checkpoint, and impaired homologous recombination repair. Thus, our study defines a pathway involving the sensing of ssDNA by SOSS complex and suggests that this SOSS complex is likely involved in the maintenance of genome stability.

INTRODUCTION

DNA double-strand breaks (DSBs) are highly cytotoxic lesions that, if unrepaired or repaired incorrectly, can cause genome instability and promote tumorigenesis (Bartek and Lukas, 2007; Bartkova et al., 2005; Friedberg, 2003; Hoeijmakers, 2001). Cells possess two main DSB repair mechanisms: nonhomologous end joining (NHEJ) and homologous recombination (HR) (Kennedy and D'Andrea, 2006; Lukas and Bartek, 2004; Weinstock et al., 2006b). In vertebrates, NHEJ and HR differentially contribute to DSB repair, depending on the nature of the DSB and the phase of the cell cycle (Bartek et al., 2004; Sonoda et al., 2006). HR pathway is critical for the maintenance of genome stability through its involvement in the precise repair of DNA DSBs and restarting stalled or collapsed DNA replication forks. It is believed that one of the initial steps during HR is the resection of DSBs to generate single-stranded DNA (ssDNA), which is bound by ssDNA-binding proteins (SSBs) that play essential roles in DNA replication, recombination, and repair in bacteria, archaea, and eukarya (Borde, 2007; Buis et al., 2008; Clerici et al., 2005; Hopkins and Paull, 2008; Lavin, 2004; Lengsfeld et al., 2007; Petrini and Stracker, 2003; Sartori et al., 2007; Takeda et al., 2007; West, 2003; Williams et al., 2008; Wold, 1997).

The human SSB, known as human replication protein A (RPA), is a heterotrimer composed of subunits of 70, 32, and 14 kDa, each of which is conserved not only in mammals but also in all other eukaryotic species (Wold, 1997). RPA is generally believed to be the major SSB protein in eukaryotic cells given that it not only is critically important for DNA replication but also participates in various DNA repair or other cellular processes that involve DNA transaction.

This view was challenged by the recent identification of two additional human SSB homologs, hSSB1 and hSSB2 (Richard et al., 2008). Cells deficient in hSSB1 exhibit defective checkpoint activation, increased radiation sensitivity, and defective HR repair, indicating that hSSB1 plays an important role in the cellular response to DNA damage (Richard et al., 2008). Unlike RPA, which exists as heterotrimeric complex, hSSB1 and hSSB2 were believed to be more similar to *E. coli* SSB, which exists as a monomeric form or homo-oligomers (Richard et al., 2008). However, exactly how hSSB1 (or hSSB2) would specifically sense ssDNA regions during DNA damage repair but not be involved in normal DNA replication is still unknown. In this study, we used an affinity purification approach to isolate the hSSB1/2-containing complex. Interestingly, we identified a heterotrimeric complex, which we refer to as SOSS (sensor of ssDNA) complex that contains not only hSSB1/2, but also INTS3 and a previously uncharacterized protein, C9orf80. We demonstrated that both SOSS complexes and CtIP/RPA act downstream of the MRE11/RAD50/NBS1 (MRN) complex and function in DNA damage repair.

RESULTS AND DISCUSSION

INTS3, hSSB1/2, and C9orf80 Form a Heterotrimeric Protein Complex

In an attempt to understand what determines the specialized role of hSSBs in DNA repair, we performed tandem affinity purification using HEK293T cells stably expressing streptavidin-flag-S protein (SFB)-tagged wild-type hSSB1/2 for the identification of hSSB1/2-associated proteins. We repeatedly found INTS3 and a previously uncharacterized protein, C9orf80, as major hSSB1/2-associated proteins (Figure 1A). To further confirm that INTS3 and C9orf80 exist in the same complex with hSSB1 or hSSB2, we generated stable cells expressing triple-tagged

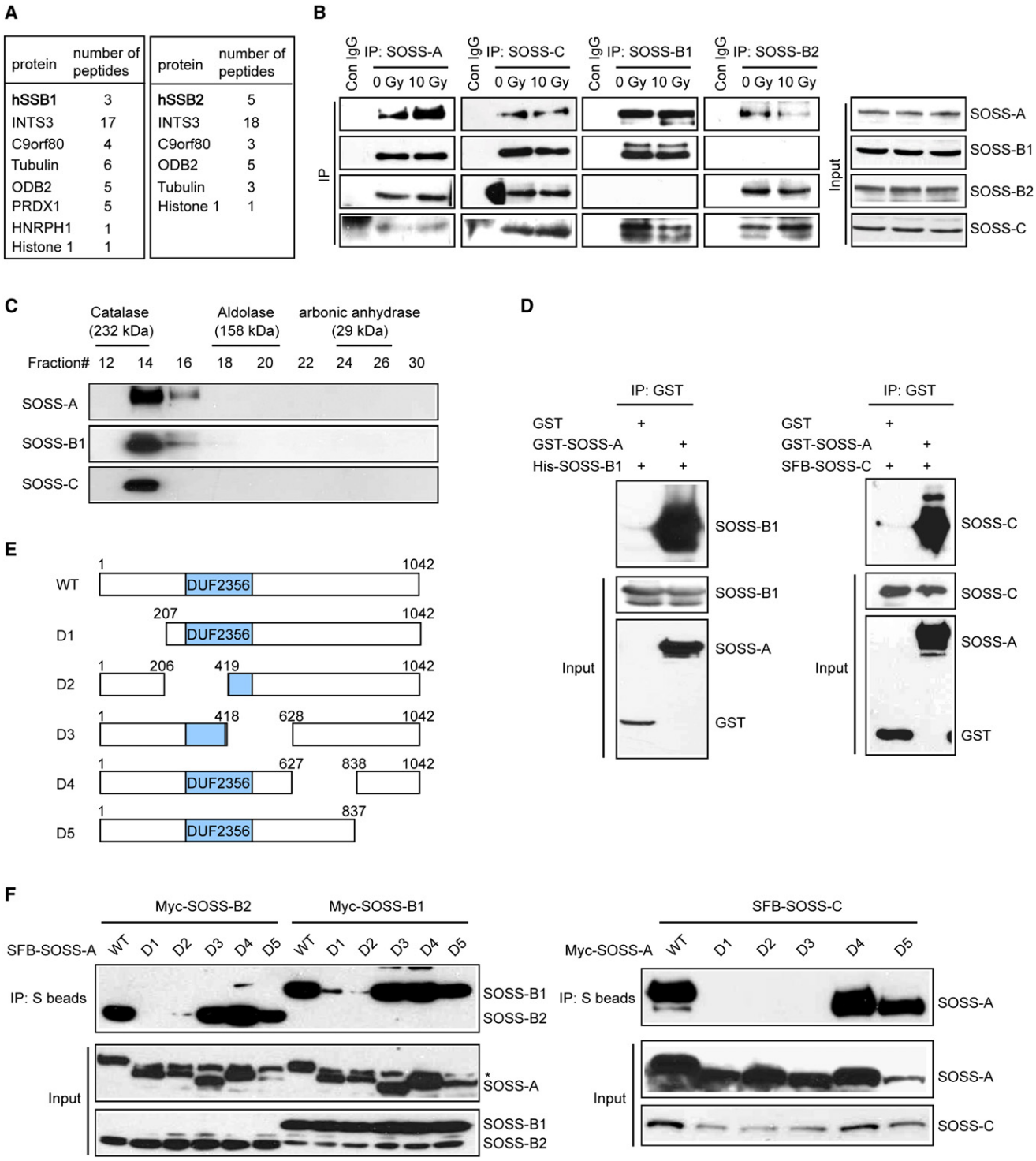

Figure 1. Formation of an SOSS Complex Containing INTS3 (SOSS-A), hSSB1/2 (SOSS-B1/2), and C9orf80 (SOSS-C)

(A) 293T cells stably expressing SFB-tagged (S tag, Flag epitope tag, and streptavidin-binding peptide tag) hSSB1 or hSSB2 were used for tandem affinity purification of protein complexes specifically from chromatin fractions isolated from irradiated cells. Tables are summaries of proteins identified by mass spectrometry analysis. Letters in bold indicate the bait proteins.

(B) HeLa cells were treated with IR (10 Gy) or left untreated and then incubated for 2 hr before collection. Immunoprecipitations were performed using preimmune serum or anti-SOSS antibodies. Interactions among endogenous components of SOSS complex were assessed by immunoblotting using antibodies as indicated.

INTS3 and C9orf80, respectively. Notably, mass spectrometry analyses of INTS3 or C9orf80-associated protein complexes revealed peptides that corresponded to hSSB1 and hSSB2 (data not shown), suggesting that these proteins likely form a stable complex in vivo. INTS3 (integrator complex subunit 3) was originally identified as a subunit of Integrator (Baillat et al., 2005); however, there was no further characterization of this protein concerning its domain structure, activity, or biological function. C9orf80 is a hypothetical protein with no known function. Although INTS3 and C9orf80 were present in both hSSB1 and hSSB2 purification, we did not detect the presence of hSSB1 from several independent hSSB2 large-scale affinity purifications and vice versa (Figure 1A and data not shown), indicating that hSSB1 and hSSB2 might exist in two complementary complexes that contain the common subunits INTS3 and C9orf80. Therefore, in this study, we named the complex containing INTS3/hSSB1/C9orf80 or INTS3/hSSB2/C9orf80 as SOSS1/2 (SOSS DNA complex 1/2), respectively. Accordingly, we designated INTS3, hSSB1/2, and C9orf80 as SOSS subunit A, B1/2, and C, respectively.

To verify the association among SOSS-A, SOSS-B1, SOSS-B2, and SOSS-C, we performed coimmunoprecipitation experiments. When immunoprecipitation experiments were conducted with anti-SOSS-A or anti-SOSS-C antibodies, all of the SOSS subunits could be detected (Figure 1B). However, while antibodies specifically recognizing SOSS-B1 or SOSS-B2 coimmunoprecipitated the common subunits SOSS-A and SOSS-C, no SOSS-B1 or 2 were present in each other's immunocomplex (Figure 1B). These data agree with the data obtained from SOSS-B1/2 large-scale affinity purifications and support our hypothesis that SOSS-A, SOSS-B1/2, and SOSS-C might form two complementary heterotrimeric complexes: SOSS1 (SOSS-A/B1/C) or SOSS2 (SOSS-A/B2/C) in vivo. Interestingly, neither RPA nor CTIP could interact with SOSS-A (see Figure S1 available online). Furthermore, the SOSS complex formation was DNA damage independent and these pre-existing complexes could be detected in HeLa cells as well as in other cell lines including HEK293T cells (Figure 1B and data not shown). Formation of the heterotrimeric complex was further ascertained by gel filtration analysis. Insect cells were coinfected with baculovirus expressing GST-SOSS-A, His-SOSS-B, and SOSS-C and complex formation was studied by FPLC. As shown in Figure 1C, SOSS-A, SOSS-B, and SOSS-C coeluted as a heterotrimeric complex with a molecular mass of approximately 190 kDa. A previous study has already established that recombinant SOSS-B1/hSSB1 binds specifically to ssDNA substrates (Richard et al., 2008). As shown in Figure S2, recombinant SOSS heterotrimeric complex also specifically binds to ssDNA but not to dsDNA.

To find out exactly how the SOSS complex is assembled, we examined the association among SOSS-A, SOSS-B1, and SOSS-C in insect cells. As shown in Figure 1D, SOSS-A interacted strongly with SOSS-B or SOSS-C, whereas no direct binding was detected between SOSS-B and SOSS-C (data not shown), suggesting that SOSS-A likely serves as a central assembly factor that mediates the formation of this complex. Therefore we focused on this key subunit SOSS-A in this study.

We first sought to identify the regions on SOSS-A responsible for its interaction with SOSS-B or SOSS-C. Myc-tagged wild-type SOSS-A and a series of deletion mutants that span the entire SOSS-A open reading frame were subjected to coimmunoprecipitation with full-length SFB-tagged SOSS-B or SOSS-C. Results showed that while the SOSS-A N terminus (residues 1–419) is responsible for SOSS-B binding, a larger N-terminal region (residues 1–628) is necessary for its binding to SOSS-C (Figures 1E and 1F). These data indicate that SOSS-B and SOSS-C share overlapping binding regions on SOSS-A.

SOSS-A Is Required for the Proper Localization and Stability of SOSS-B1/2 In Vivo

The absence of a critical subunit of a multicomponent protein complex often destabilizes the complex (Yin et al., 2005). Therefore, we depleted either SOSS-A or SOSS-B1/2 and examined the stability of the other subunits. As shown in Figure 2A, depletion of SOSS-B1 or SOSS-B2 did not result in any significant change in SOSS-A protein level; however, depletion of SOSS-A by siRNA led to a dramatic decrease in SOSS-B1 and SOSS-B2 protein levels. This implies that SOSS-A may help to stabilize SOSS-B1 and SOSS-B2 in the cell. Interestingly, we noticed that the protein levels of SOSS-B1 and SOSS-B2 seem to have an inverse relationship, as depletion of one protein appears to increase the level of the other (Figure 2A), again indicating that SOSS-B1 and SOSS-B2 might play complementary roles in the DNA damage response pathway.

Like many DNA damage/repair proteins, SOSS-B1 was able to localize at sites of DNA breaks and form discrete foci that colocalize with the DNA DSB marker γ-H2AX (Richard et al., 2008). Given that SOSS-A and SOSS-C exist in a complex with SOSS-B1 or SOSS-B2, we would like to examine whether SOSS-A and SOSS-C could also form foci following DNA damage. Immunostaining experiments showed SOSS-A, SOSS-B2, and SOSS-C to be evenly distributed in the nucleoplasm in normal cells (data not shown). However, after exposure of cells to ionizing radiation (IR), SOSS-A, SOSS-B2, and SOSS-C relocalized to foci that costained with γ-H2AX (Figure 2B), indicating that the localization of SOSS-A, SOSS-B2, and SOSS-C, like that of SOSS-B1, is regulated in response to DNA damage. Since all the components of SOSS complexes form IR-induced foci (IRIF), we next examined how they would influence each other's foci formation ability. As shown in Figures 2C and 2D, IRIF of SOSS-B1 and SOSS-B2 were dramatically decreased in

(C) Heterotrimeric complex formation was studied by gel filtration chromatography as described in Experimental Procedures. Aliquots from peak fractions were analyzed on 12.5% SDS-PAGE and confirmed by western blot analysis.
(D) Specific binding of SOSS-A to SOSS-B1 or SOSS-C. SF9 cells were coinfected with baculoviruses expressing GST or GST-tagged SOSS-A together with those expressing His-SOSS-B1 or SFB-SOSS-C. Immunoprecipitation and immunoblotting were carried out as indicated.
(E) Schematic presentation of SOSS-A constructs used in this study.
(F) Mapping of the corresponding regions required for SOSS-A/SOSS-B or SOSS-A/SOSS-C interaction. Immunoprecipitation reactions were performed using S protein beads and then subjected to western blot analyses using antibodies as indicated. Asterisk shows nonspecific band.

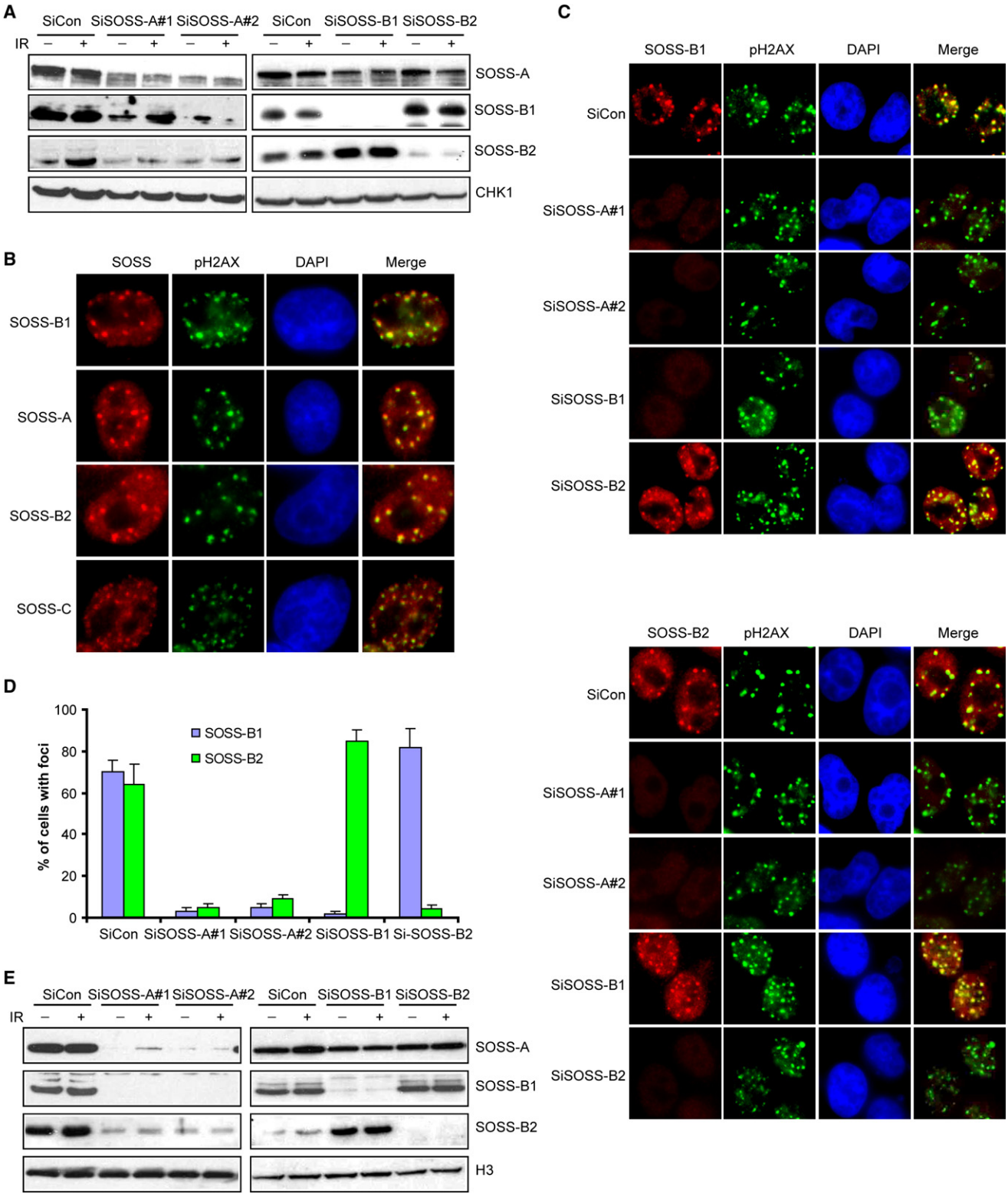

Figure 2. SOSS-A Regulates SOSS Complex Stability and Focus Formation

(A) Immunoblots showing levels of SOSS-A, SOSS-B1, and SOSS-B2 in lysates prepared from HeLa cells transfected with the indicated siRNAs. Two hours after mock treatment or IR (10 Gy), cells were harvested and cell lysates were blotted with indicated antibodies.

SOSS-A-depleted cells. However, depletion of SOSS-B1 or SOSS-B2 did not lead to any significant change in SOSS-A IRIF formation (Figures 4B and S6A), implying that SOSS-A may act upstream of SOSS-B1/2 and be required for SOSS-B1/2 focus formation. In agreement with our previous hypothesis that SOSS-B1 and SOSS-B2 might play a complementary role in the DNA damage response, depletion of SOSS-B1 led to a modest increase of SOSS-B2 foci formation and vice verse (Figure 2D).

Generally, the DNA damage-induced focus formation reflects the assembly of proteins at the vicinity of DNA breaks. These proteins are recruited physically to the damaged DNA and become chromatin bound. Since SOSS-A is required for SOSS-B foci formation, we hypothesized that SOSS-A should also be required for the localization of SOSS-B to chromatin. Indeed, SOSS-A depletion results in abrogation of chromatin targeting of both SOSS-B1 and SOSS-B2 (Figure 2E). Together, these data suggest that SOSS-A not only is required for the assembly of this trimeric protein complex, but also plays an important role in stabilizing this protein complex at DNA damage sites.

SOSS Complex Participates in Cellular Response to DSBs

Cells deficient in hSSB1 display enhanced genomic instability including defective G2/M checkpoint activation, increased IR sensitivity, and deficient HR repair (Richard et al., 2008). We examined whether the loss of the SOSS-A would result in similar defects in the DNA damage response. Using a previously established G2/M checkpoint assay (Xu et al., 2001), we showed defective G2/M checkpoint control in SOSS-A-depleted cells (Figure 3A). SOSS-A-depleted cells were also more sensitive to radiation than control cells (Figure 3B). Moreover, we performed a gene conversion assay to examine HR efficiency using the DR-GFP reporter system (Weinstock et al., 2006a). Indeed, HR repair efficiency was reduced by ~2- to 2.5-fold in SOSS-A-depleted cells (Figures 3C and 3D). The recombination protein RAD51 is the key component of the HR repair machinery and the formation of Rad51 foci can be used as another indicator of HR repair. In agreement with the results from gene conversion assay, DNA damage-induced Rad51 foci formation was also impaired in SOSS-A-depleted cells (Figures 3E, 3F, and S3). Together, these data indicated that SOSS complexes play an important role in DNA damage response.

MRN Is Required for Efficient SOSS Foci Formation in S/G2 Cells

It has been shown that the MRN complex promotes DNA end resection and the generation of ssDNA, which is critically important for recruitment of RPA and HR repair (Borde, 2007; Buis et al., 2008; Hopkins and Paull, 2008; Lavin, 2004; Petrini and Stracker, 2003; Williams et al., 2008). Given that the SOSS complex bound to ssDNA, we expected that MRN might be required for SOSS complex foci formation. Strikingly, like RPA2, SOSS complex foci formation was significantly reduced upon MRN depletion, indicating that MRN complexes are involved in the generation of not only RPA but also SOSS-coated ssDNAs (Figures 4A and S4A–S4C). This requirement of MRN complex for the formation of SOSS foci appears to be restricted to S or G2 cells, since the damage-induced SOSS focus formation in G1-arrested cells could still occur independent of the MRN complex (Figures S4D and S4E).

Because SOSS-A was absolutely required for SOSS complex chromatin targeting and focus formation, we tested the possibility that the MRN complex might bring the SOSS complex to ssDNAs via a direct interaction with SOSS-A. Indeed, we found that SOSS-A specifically interacted with NBS1, but not with Mre11 or RAD50 (Figure S5A). Moreover, SOSS-A interacted with NBS1 in insect cells (Figure S5B). This interaction between SOSS-A and NBS1 suggests that SOSS and MRN complexes may at least in part act together and participate in DNA damage response.

Both SOSS Complex and CTIP Function in DNA Damage Repair

More recently, the proposed mammalian Sae2 homolog CTIP was also shown to interact with MRN complex and be required for the generation of RPA-coated ssDNAs (Clerici et al., 2005; Lengsfeld et al., 2007; Mimitou and Symington, 2008; Sartori et al., 2007; Takeda et al., 2007). We thus examined whether CTIP, like the MRN complex, would also be involved in SOSS complex focus formation. When cells were treated with CTIP siRNA, only RPA focus formation, but not the focus formation of SOSS complex, was disrupted (Figures 4B and S6A–6D). Conversely, in SOSS-depleted cells, CTIP or RPA2 foci formation was not obviously altered (Figures 4B, S6A–6D, and data not shown), indicating that the foci formation of RPA and SOSS can arise independently of each other.

It is now apparent that there are at least two sets of heterotrimeric ssDNA-binding complexes, RPA and SOSS, involved in DNA damage response. The observation that the association of SOSS or CtIP/RPA with ssDNA occurs independently of each other raises the possibility that these two different complexes may each be responsible for a part of this DNA damage repair process. To test this possibility, we compared their relative contributions to HR repair through siRNA-mediated deletion of these proteins either individually or in combination. As shown

(B) Localization of SOSS components in response to IR in HeLa cells. Cells were irradiated and immunostained as described in Experimental Procedures with anti-SOSS and pH2AX antibodies.

(C and D) SOSS-A is required for the accumulation of SOSS-B1/2 at DNA damage sites. HeLa cells were transfected twice with either SOSS-A siRNA or a non-targeting control siRNA. Forty-eight hours after the second transfection, cells were irradiated and immunostaining experiments were performed. Representative SOSS-B1/2 foci were shown (C). Quantification results were the average of three independent experiments and were presented as mean ± SEM (D). More than one hundred cells were counted in each experiment.

(E) SOSS-A is required for SOSS-B1/2 chromatin localization. HeLa cells depleted of endogenous SOSS-A were treated with 10 Gy IR or left untreated. Two hours later, cells were collected and chromatin fractions were isolated as described in Experimental Procedures. Immunoblotting experiments were performed using indicated antibodies.

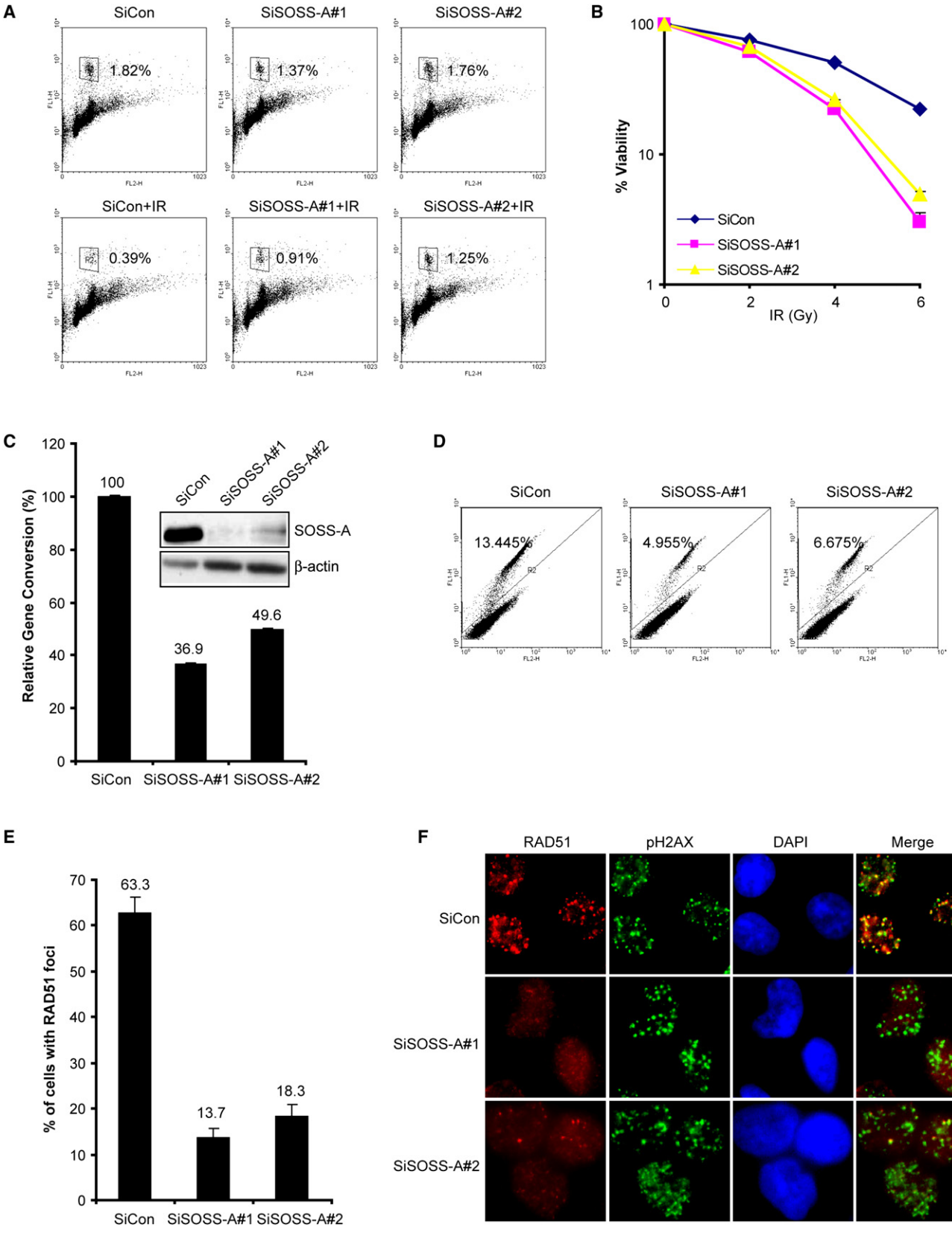
A
SiCon
SiSOSS-A#1
SiSOSS-A#2
1.82%
1.37%
1.76%
SiCon+IR
SiSOSS-A#1+IR
SiSOSS-A#2+IR
0.39%
0.91%
1.25%
B
% Viability
IR (Gy)
SiCon
SiSOSS-A#1
SiSOSS-A#2
C
Relative Gene Conversion (%)
SOSS-A
β-actin
100
36.9
49.6
SiCon
SiSOSS-A#1
SiSOSS-A#2
D
13.445%
4.955%
6.675%
E
% of cells with RAD51 foci
63.3
13.7
18.3
F
RAD51
pH2AX
DAPI
Merge

in Figures 4C and S6E, although HR repair efficiency is impaired in the absence of SOSS-A or CTIP, we noticed that codepletion of SOSS-A and CTIP decreased HR efficiency further than that achieved by SOSS-A or CTIP depletion alone. Consistently, simultaneous ablation of SOSS-A and CTIP by siRNA resulted in a further increase of cellular sensitivity to IR (Figure 4D). Together, these results indicate that SOSS and CtIP/RPA likely represent two independent subpathways, which act at least in part downstream of the MRN complex and function in DNA damage repair (Figure 4E).

In summary, we identified a trimeric complex, which we refer to as SOSS complex in this study. The existence of two independent ssDNA-binding complexes, RPA and SOSS, in mammalian cells underscores the importance of this process in DNA repair. We believe that further study of this second human ssDNA-binding heterotrimeric complex will provide insight in the repair of DNA DSBs, especially the poorly understood HR repair process.

EXPERIMENTAL PROCEDURES

Antibodies

Rabbit polyclonal anti-SOSS-B1, SOSS-B2, and SOSS-C antibodies were generated by immunizing rabbits with MBP-SOSS-B1, MBP-SOSS-B2, and MBP-SOSS-C recombinant protein expressed and purified from *E. Coli*, respectively. These antibodies were further affinity purified using columns containing corresponding GST fusion proteins. Antibodies against the myc epitope, γ-H2AX, and RAD51 were previously described (Chen et al., 1998; Huen et al., 2007). The anti-SOSS-A and anti-H3 antibodies were purchased from Bethyl and Millipore, respectively. Anti-CHK1 and GST antibodies were obtained from Santa Cruz Biotechnology Inc. Anti-Flag (M2) and anti-β-actin antibodies were purchased from Sigma. Anti-MRE11, RAD50, and NBS1 antibodies were purchased from Novus Biologicals, Abcam, and Calbiochem, respectively.

Cell Cultures and Transfection

293T and HeLa Cells were maintained in RPMI supplemented with 10% fetal bovine serum and 1% penicillin and streptomycin. SF9 insect cells were maintained in Grace's medium supplemented with 10% fetal bovine serum. Cell lines of human origin were maintained in 37°C incubator with 5% CO2, whereas insect cells were maintained at 27°C. U2OS cells with DR-GFP integration were kindly provided by Maria Jasin at Memorial Sloan-Kettering Cancer Center (NY, New York). Cell transfection was performed using Lipofectamine 2000 (Invitrogen) following the manufacturer's protocol.

Constructs

The full-length and deletion/point mutants of human SOSS-A, SOSS-B, SOSS-C, and NBS1 were generated by PCR and subcloned into the pDONR201 vector using Gateway Technology (Invitrogen). The corresponding fragments in entry vectors were transferred into a Gateway compatible destination vector, which harbors an N-terminal triple-epitope tag (S protein tag, flag epitope tag, and streptavidin-binding peptide tag) or a Myc epitope tag for expression in mammalian cells.

Baculoviruses and Protein Purification from Insect Cells

DNA fragment containing full-length SOSS-A, SOSS-B1, SOSS-C, or NBS1 in pDONR201 vector were transferred to pDEST20, pDEST10, pDEST8, and SFB-tagged vectors for the expression of GST-SOSS-A, His-SOSS-B1, SOSS-C, and SFB fusion proteins in insect cells, respectively. Transposition occurred in DH10Bac-competent cells and correct bacmids confirmed by PCR were transfected into SF9 cells for baculovirus production. After viral amplification, SF9 cells were infected with the desired baculovirus and cell lysates were collected 48 hr later.

Gel Filtration Chromatography

Sf9 cells were coinfected with baculovirus stocks expressing GST-SOSS-A, His-SOSS-B1, and untagged SOSS-C. Forty-eight hours later, cells were harvested, washed with 1 × PBS, and resuspended in 10 ml lysis buffer (10% [v/v] glycerol, 20 mM HEPES [pH 7.6], 0.3 M KCl, 0.01% NP-40, 1 mM DTT, 0.2 mM PMSF, and 1 μg/ml each of leupeptin, aprotinin, and pepstatin). Cells were homogenized with ten strokes with Dounce homogenizer on ice. The lysate was centrifuged for 15 min at 10,000 rpm. The supernatant was incubated at 4°C with 300 μl of glutathione Sepharose 4B for 4 hr. The resin was washed with wash buffer (lysis buffer containing 0.5 M KCl). Protein was eluted with elution buffer (lysis buffer containing 20 mM glutathione). Eluted protein was dialyzed in buffer B (10% [v/v] glycerol, 20 mM sodium phosphate [pH 7.6], 0.3 M KCl, 0.01% NP-40, and 1 mM DTT) and incubated with 200 μl Ni-NTA beads at 4°C for 4 hr. Ni-NTA beads were washed with wash buffer (buffer B containing 20 mM imidazole) and eluted with elution buffer (buffer B containing 300 mM imidazole). The eluted protein was resolved on Superdex 200 gel filtration column against buffer C (10% [v/v] glycerol, 20 mM HEPES [pH 7.6], 0.3 M KCl, 0.01% NP-40, and 1 mM DTT). Indicated fractions were analyzed on 12.5% SDS-PAGE.

Electrophoretic Mobility Shift Assay

Reaction mixtures (20 μl) contained 20 mM Tris-HCl (pH 7.5), 50 mM NaCl, 1 mM $MgCl_2$, 0.5 mM EDTA, 0.2 mM DTT, and 100 pmol ^{32}P-labeled ssDNA (d60T) or dsDNA (d60A-T; d60T annealed to its complimentary d60A) and were incubated with increasing concentrations of SOSS-B1 (0, 0.5, 1, 2, 4, and 6 μM) or SOSS complex (0, 0.5, 1, 2, 4, 6, 8, and 10 μM) for 60 min at 37°C. Reaction was terminated by the addition of 2 μl of gel loading dye (0.1% [w/v] bromophenol blue and 0.1% [w/w] xylene cyanol in 20% glycerol) and transferred on ice. Samples were separated by PAGE in an 8% gel at 10V/cm for 6 hr at 4°C using 45 mM Tris-borate (pH 8.3) and 1 mM EDTA as the running buffer. The gels were visualized by phosphorimaging.

RNA Interference

All siRNA duplexes were purchased from Dharmacon Research (Lafayette, CO). The following sequences were used in HeLa Cells: SOSS-A#1: GAUGA GAGUUGCUAUGA CAdTdT; SOSS-A#2: CCAAGCGAGCUGUGACGAA dTdT; SOSS-B1: CGACGGA GACCUUUGUGAAdTdT; SOSS-B2: CGUG CAAAGUAGCAGAUAAdTdT; MRE11: GGA GGUACGUCGUUUCAGAdTdT;

Figure 3. SOSS-A Is Required for IR-Induced G2/M Checkpoint, Cell Survival, and Efficient DNA Repair

(A) G2/M checkpoint defect was observed in SOSS-A-depleted cells. HeLa cells transfected with control or SOSS-A siRNAs were exposed to 0 or 2 Gy of IR. Cells were incubated for 1 hr before fixation and subjected to staining with antibody to phosphorylated histone H3 (pH3) and propidium iodide. The percentages of mitotic cells were determined by fluorescence-activated cell sorting analysis. The boxed area in the upper-left panel indicates mitotic cells.

(B) Radiation sensitivity of cells lacking SOSS-A. HeLa cells were transfected with control or SOSS-A siRNAs and then irradiated with indicated doses of IR. Percentages of surviving colonies were determined 2 weeks later. These experiments were performed in triplicate, and the results represent the average of three independent experiments and were presented as mean ± SEM.

(C and D) SOSS-A promotes HR. U2OS cells with a single integration of DR-GFP were transfected twice with either SOSS-A siRNA or a nontargeting control siRNA. Twenty-four hours after the second transfection, cells were electroporated with pCBASce construct and were subjected to FACS analyses 48 hr later (D). Results (mean ± SEM) were the average of three independent experiments (C).

(E and F) SOSS-A is required for efficient RAD51 foci formation. SOSS-A-depleted HeLa cells were treated with 10 Gy IR and recovery for 6 hr before fixation. Immunostaining experiments were performed as described in the Experimental Procedures. Representative RAD51 foci were shown (F). Quantification results were the average of three independent experiments and were presented as mean ± SEM (E). More than one hundred cells were counted in each experiment.

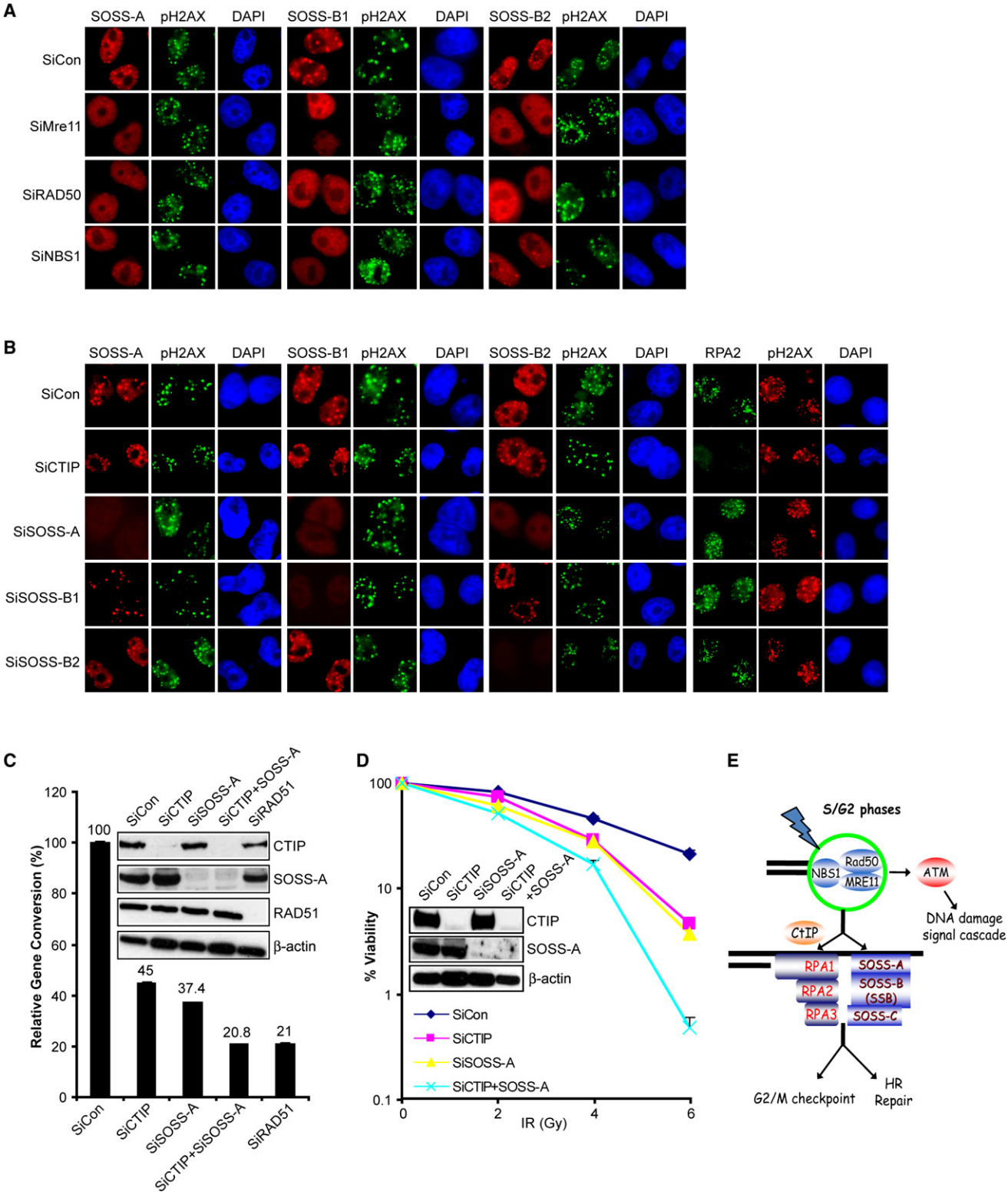

Figure 4. Both SOSS and CTIP/RPA Promote Optimal DNA Damage Response

(A) MRN complex is required for efficient SOSS complex foci formation. MRN-depleted HeLa cells were treated with 10 Gy IR and allowed to recover for 6 hr before fixation. Immunostaining experiments were performed as described in the Experimental Procedures. Representative SOSS foci were shown.

RAD50: ACAAGGAUCUGGAUAUUUAUU; and NBS1: CCAACUAAAUUGC CAAGUAUU. The following sequences were used in U2OS cells: SOSS-A#1: CGUGAUGGCAUGAAUAUUGdTdT; SOSS-A#2: GUAG UCCACCCUUCUAA UGdTdT; and RAD51: CUAAUCAGGUGGUAGCUCAUU. The siRNA for CtIP was previously described (Yu and Chen, 2004). The siRNAs transfection was performed using Oligofectamine (Invitrogen) following the manufacturer's instruction.

The Establishment of Stable Cell Lines and Affinity Purification of S-Flag-SBP(SFB)-Tagged Protein Complexes

293T cells were transfected with plasmids encoding SFB-tagged proteins. Cell lines stably expressing tagged proteins were selected by culturing in the medium containing puromycin (2 μg/ml) and confirmed by immunoblotting and immunostaining. For affinity purification, 293T cells stably expressing tagged proteins were lysed with NETN buffer for 20 min. Crude lysates were removed by centrifugation at 14,000 rpm at 4°C for 10 min, and pellet was sonicated for 40 s in high-salt solution (20 mM HEPES [pH 7.8], 0.4 M NaCl, 1 mM EDTA, 1 mM EGTA, and protease inhibitor) to extract chromatin-bound proteins fractions. The supernatants were cleared at 14,000 rpm to remove debris and then incubated with streptavidin-conjugated beads (Amersham) for 2 hr at 4°C. The immunocomplexes were washed three times with NETN buffer and then bead-bound proteins were eluted with NETN buffer containing 1 mg/ml biotin (Sigma). The elutes were incubated with S protein beads (Novagen). The immunocomplexes were again washed three times with NETN buffer and subjected to SDS-PAGE. Protein bands were excised and digested, and the peptides were analyzed by mass spectrometry.

Immunofluorescence Staining Procedure

To visualize IRIF, cells cultured on coverslips were treated with 10 Gy of gamma irradiation (1 Gy = 100 Rads) followed by recovery for 6 hr. Cells were then fixed using 3% paraformaldehyde solution for 10 min at room temperature and then extracted with buffer containing 0.5% Triton X-100 for 5 min. Samples were blocked with 5% goat serum and incubated with primary antibody for 30 min. Samples were washed and incubated with secondary antibody for 30 min. Cells were then counterstained with DAPI to visualize nuclear DNA.

Cell Synchronization

HeLa cells were treated with 2 mM thymidine for 19 hr and then released in fresh medium for 9 hr. Two micromoles of thymidine were added again and cells were incubated for another 16 hr to arrest cells in G1 phase. Cell cycle distributions were confirmed by FACS analysis.

Chromatin Fractionation

Preparation of chromatin fractions were described previously with some modifications (Yu et al., 2006). Briefly, cells were collected 2 hr after treatment with 10 Gy of IR and washed once with PBS. Cell pellets were subsequently resuspended in NETN buffer (10 mM HEPES [pH 7.4], 10 mM KCl, 0.05% NP-40, and protease inhibitors) and incubated on ice for 20 min. Crude lysates were removed by centrifugation at 14,000 rpm at 4°C for 10 min, and pellet was recovered and resuspended in 0.2 M HCl for 20 min. The soluble fraction was then neutralized with 1 M Tris-HCl (pH 8.0) for further analysis.

G2/M Checkpoint Assay

G2/M checkpoint assay was performed as described previously (Lou et al., 2003). Briefly, cells were treated with 2 Gy IR. One hour later, cells were fixed with 70% (v/v) ethanol overnight, and then stained with anti-phospho-histone H3 (Ser10) antibody and propidium iodide. Samples were analyzed by flow cytometry to determine the percentages of cells in mitosis.

Cell Survival Assays

Cells (1×10^3) were seeded onto 60 mm dish in triplicates. Twenty-four hours after seeding, cells were irradiated with IR and then incubated for 14 days. Resulting colonies were fixed and stained with Coomassie blue. Numbers of colonies were counted using a GelDoc with Quantity One software (Bio-Rad). Results were the averages of data obtained from three independent experiments.

Gene Conversion Assay

A U2OS cell clone stably expressing HR reporter DR-GFP was described previously (Weinstock et al., 2006a). U2OS-DR-GFP cells (1×10^6) were electroporated with 12 μg of pCBASce plasmid at 270 V and 975 uF, using a Bio-Rad genepulsar II. Cells were plated onto 10 cm dishes and incubated for 48 hr prior to FACS analyses using a Becton Dickinson FACScan on a green (FL1) versus orange (FL2) fluorescence plot. Results were the averages of data obtained from three independent experiments.

SUPPLEMENTAL DATA

Supplemental Data include six figures and can be found with this article online at http://www.cell.com/molecular-cell/supplemental/S1097-2765(09)00402-X.

ACKNOWLEDGMENTS

We thank all colleagues in Chen's laboratory for insightful discussion and technical assistance, especially Dr. Jingsong Yuan and Michael S.Y. Huen. This work was supported in part by grants from the National Institutes of Health to J.C. (CA089239, CA092312, and CA100109). J.C is a recipient of an Era of Hope Scholar award from the Department of Defense and a member of the Mayo Clinic Breast SPORE program.

Received: April 8, 2009
Revised: May 21, 2009
Accepted: June 8, 2009
Published: August 13, 2009

REFERENCES

Baillat, D., Hakimi, M.A., Naar, A.M., Shilatifard, A., Cooch, N., and Shiekhattar, R. (2005). Integrator, a multiprotein mediator of small nuclear RNA processing, associates with the C-terminal repeat of RNA polymerase II. Cell *123*, 265–276.

Bartek, J., and Lukas, J. (2007). DNA damage checkpoints: from initiation to recovery or adaptation. Curr. Opin. Cell Biol. *19*, 238–245.

Bartek, J., Lukas, C., and Lukas, J. (2004). Checking on DNA damage in S phase. Nat. Rev. Mol. Cell Biol. *5*, 792–804.

Bartkova, J., Horejsi, Z., Koed, K., Kramer, A., Tort, F., Zieger, K., Guldberg, P., Sehested, M., Nesland, J.M., Lukas, C., et al. (2005). DNA damage response as a candidate anti-cancer barrier in early human tumorigenesis. Nature *434*, 864–870.

Borde, V. (2007). The multiple roles of the Mre11 complex for meiotic recombination. Chromosome Res. *15*, 551–563.

(B) Foci formation of SOSS and RPA occurs independently. HeLa cells transfected with indicated siRNAs were treated with 10 Gy IR and allowed to recover for 6 hr before fixation. Immunostaining experiments were performed as described in the Experimental Procedures and representative SOSS and RPA2 foci were shown.

(C) Simultaneous ablation of SOSS-A and CTIP resulted in further defect in HR. Experiments were carried out similar to that described in Figure 3C. Results (mean ± SEM) were the average of three independent experiments.

(D) Simultaneous depletion of SOSS-A and CTIP resulted in added IR sensitivity. Colony formation assays were performed as described in the Experimental Procedures, and results (mean ± SEM) are averages of three independent experiments.

(E) A proposed model for the DNA damage-responsive pathway involving SOSS complex.

Buis, J., Wu, Y., Deng, Y., Leddon, J., Westfield, G., Eckersdorff, M., Sekiguchi, J.M., Chang, S., and Ferguson, D.O. (2008). Mre11 nuclease activity has essential roles in DNA repair and genomic stability distinct from ATM activation. Cell *135*, 85–96.

Chen, J., Silver, D.P., Walpita, D., Cantor, S.B., Gazdar, A.F., Tomlinson, G., Couch, F.J., Weber, B.L., Ashley, T., Livingston, D.M., and Scully, R. (1998). Stable interaction between the products of the BRCA1 and BRCA2 tumor suppressor genes in mitotic and meiotic cells. Mol. Cell *2*, 317–328.

Clerici, M., Mantiero, D., Lucchini, G., and Longhese, M.P. (2005). The *Saccharomyces cerevisiae* Sae2 protein promotes resection and bridging of double strand break ends. J. Biol. Chem. *280*, 38631–38638.

Friedberg, E.C. (2003). DNA damage and repair. Nature *421*, 436–440.

Hoeijmakers, J.H. (2001). Genome maintenance mechanisms for preventing cancer. Nature *411*, 366–374.

Hopkins, B.B., and Paull, T.T. (2008). The *P. furiosus* mre11/rad50 complex promotes 5′ strand resection at a DNA double-strand break. Cell *135*, 250–260.

Huen, M.S., Grant, R., Manke, I., Minn, K., Yu, X., Yaffe, M.B., and Chen, J. (2007). RNF8 transduces the DNA-damage signal via histone ubiquitylation and checkpoint protein assembly. Cell *131*, 901–914.

Kennedy, R.D., and D'Andrea, A.D. (2006). DNA repair pathways in clinical practice: lessons from pediatric cancer susceptibility syndromes. J. Clin. Oncol. *24*, 3799–3808.

Lavin, M.F. (2004). The Mre11 complex and ATM: a two-way functional interaction in recognising and signaling DNA double strand breaks. DNA Repair (Amst.) *3*, 1515–1520.

Lengsfeld, B.M., Rattray, A.J., Bhaskara, V., Ghirlando, R., and Paull, T.T. (2007). Sae2 is an endonuclease that processes hairpin DNA cooperatively with the Mre11/Rad50/Xrs2 complex. Mol. Cell *28*, 638–651.

Lou, Z., Chini, C.C., Minter-Dykhouse, K., and Chen, J. (2003). Mediator of DNA damage checkpoint protein 1 regulates BRCA1 localization and phosphorylation in DNA damage checkpoint control. J. Biol. Chem. *278*, 13599–13602.

Lukas, J., and Bartek, J. (2004). Watching the DNA repair ensemble dance. Cell *118*, 666–668.

Mimitou, E.P., and Symington, L.S. (2008). Sae2, Exo1 and Sgs1 collaborate in DNA double-strand break processing. Nature *455*, 770–774.

Petrini, J.H., and Stracker, T.H. (2003). The cellular response to DNA double-strand breaks: defining the sensors and mediators. Trends Cell Biol. *13*, 458–462.

Richard, D.J., Bolderson, E., Cubeddu, L., Wadsworth, R.I., Savage, K., Sharma, G.G., Nicolette, M.L., Tsvetanov, S., McIlwraith, M.J., Pandita, R.K., et al. (2008). Single-stranded DNA-binding protein hSSB1 is critical for genomic stability. Nature *453*, 677–681.

Sartori, A.A., Lukas, C., Coates, J., Mistrik, M., Fu, S., Bartek, J., Baer, R., Lukas, J., and Jackson, S.P. (2007). Human CtIP promotes DNA end resection. Nature *450*, 509–514.

Sonoda, E., Hochegger, H., Saberi, A., Taniguchi, Y., and Takeda, S. (2006). Differential usage of non-homologous end-joining and homologous recombination in double strand break repair. DNA Repair (Amst.) *5*, 1021–1029.

Takeda, S., Nakamura, K., Taniguchi, Y., and Paull, T.T. (2007). Ctp1/CtIP and the MRN complex collaborate in the initial steps of homologous recombination. Mol. Cell *28*, 351–352.

Weinstock, D.M., Nakanishi, K., Helgadottir, H.R., and Jasin, M. (2006a). Assaying double-strand break repair pathway choice in mammalian cells using a targeted endonuclease or the RAG recombinase. Methods Enzymol. *409*, 524–540.

Weinstock, D.M., Richardson, C.A., Elliott, B., and Jasin, M. (2006b). Modeling oncogenic translocations: distinct roles for double-strand break repair pathways in translocation formation in mammalian cells. DNA Repair (Amst.) *5*, 1065–1074.

West, S.C. (2003). Molecular views of recombination proteins and their control. Nat. Rev. Mol. Cell Biol. *4*, 435–445.

Williams, R.S., Moncalian, G., Williams, J.S., Yamada, Y., Limbo, O., Shin, D.S., Groocock, L.M., Cahill, D., Hitomi, C., Guenther, G., et al. (2008). Mre11 dimers coordinate DNA end bridging and nuclease processing in double-strand-break repair. Cell *135*, 97–109.

Wold, M.S. (1997). Replication protein A: a heterotrimeric, single-stranded DNA-binding protein required for eukaryotic DNA metabolism. Annu. Rev. Biochem. *66*, 61–92.

Xu, B., Kim, S., and Kastan, M.B. (2001). Involvement of Brca1 in S-phase and G(2)-phase checkpoints after ionizing irradiation. Mol. Cell. Biol. *21*, 3445–3450.

Yin, J., Sobeck, A., Xu, C., Meetei, A.R., Hoatlin, M., Li, L., and Wang, W. (2005). BLAP75, an essential component of Bloom's syndrome protein complexes that maintain genome integrity. EMBO J. *24*, 1465–1476.

Yu, X., and Chen, J. (2004). DNA damage-induced cell cycle checkpoint control requires CtIP, a phosphorylation-dependent binding partner of BRCA1 C-terminal domains. Mol. Cell. Biol. *24*, 9478–9486.

Yu, X., Fu, S., Lai, M., Baer, R., and Chen, J. (2006). BRCA1 ubiquitinates its phosphorylation-dependent binding partner CtIP. Genes Dev. *20*, 1721–1726.